Yan Baglo

Preclinical Studies of Photodynamic Therapy and Photochemical Internalization in Bladder Cancer

Thesis for the degree of Philosophiae Doctor

Trondheim, June 2014

Norwegian University of Science and Technology
Faculty of Medicine
Department of Cancer Research and Molecular Medicine

NTNU – Trondheim
Norwegian University of
Science and Technology

NTNU
Norwegian University of Science and Technology

Thesis for the degree of Philosophiae Doctor

Faculty of Medicine
Department of Cancer Research and Molecular Medicine

© Yan Baglo

ISBN 978-82-326-0026-7 (printed ver.)
ISBN 978-82-326-0027-4 (electronic ver.)
ISSN 1503-8181

Doctoral theses at NTNU, 2014:50

Printed by NTNU-trykk

Prekliniske studier av fotodynamisk terapi og fotokjemisk internalisering ved urinblærekreft

Urinblærekreft er en av de hyppigste kreftformene i verden med høy frekvens av tilbakefall og progresjon. Omtrent 70-80 % av diagnostiserte tilfeller av urinblærekreft er ikke-muskel-invasiv blærekreft (NMIBC). Denne kreftformen er potensielt godt egnet for behandlingsformer som fotodynamisk terapi (PDT) eller fotokjemisk internalisering (PCI). Denne avhandlingen beskriver bruken av både PDT og PCI i fire prekliniske studier på urinblærekreft.

I studien av PDT-effekt på proteinuttrykk og post-translasjonelle modifikasjoner (PTM) ble hexyl 5-aminolevulinate (HAL) brukt til å mediere PDT i en kreftcellelinje fra rotteblære (AY-27). Målet var å utvide vår forståelse av PDT-mekanismen. Ved å kombinere todimensjonal gel-elektroforese (2D-DIGE), immunopresipitering og massepektrometri identifiserte vi 40 proteiner som ble kartlagt for endringer knyttet til PDT, og identifiserte dessuten 10 proteiner med endret karbonylering. Det ble vist at PDT påvirket proteinuttrykk og induserte proteinmodifikasjoner. Dette tyder på at PDT utløser en kompleks cellulær respons som involverer flere biologiske prosesser, slik som transport, stressrespons, DNA-reparasjon, overlevelse og celledød.

I den neste studien så vi på transportmekanismer for 5-aminolevulinate (ALA) og metyl aminolevulinate (MAL) via GABA-transportør (GAT) i forbindelse med PDT. Vi modellerte fire humane GAT-er ved molekylmodellering (ICM). Etter kvalitetssikring av modellene ble GABA, ALA og MAL dokket til bindingssetet i hver modell, og elektrostatiske potensialer (ESPs) i porene for translokasjon i modellene ble beregnet. Resultatene tyder på at ALA kan være substrat for alle GAT-ene, mens MAL er substrat for GAT-2, GAT-3 og BGT-1. I tillegg kan forskjeller i ESP mellom transportørene bli utnyttet i utviklingen av selektive inhibitorer, for eksempel for å redusere smerte i PDT ved bruk av ALA eller MAL.

For å forbedre effekten av bleomycin som cytostatika ved blærekreft ble PCI kombinert med bleomycin i tre cellelinjer (T24, AY-27, A431), ved hjelp av en ny amfifil fotosensitizer tetrafenyl klorin disulfonat ($TPCS_{2a}$). To nye strategier for å forsterke PCI-bleomycin effekten ble studert; et nytt peptid-basert medikament ATX -101, som kan svekke DNA- reparasjon, og en proteaseinhibitor E-64, som kan inaktivere bleomycin hydrolase. Våre resultater viser at PCI øker bleomycin-effekten, og at denne effekten blir ytterligere forsterket av ATX-101. Vi viser også at PCI øker DNA-skadenivået (studert med comet assay), noe som tyder på at den observerte effekten skyldes økt cellulær internalisering av bleomycin.

For å etablere en protokoll for PCI-bleomycin i dyreforsøk med $TPCS_2a$ fotosensitizer ble kinetikk og lokaliseringen av $TPCS_{2a}$ studert i en etablert dyremodell for blærekreft i rotte, ved bruk av histologi og *ex vivo* fluorescensmålinger. Dette viser at $TPCS_{2a}$ har et overfladisk distribusjonsmønster i tumorvevet i rotteblæren, og at det er nesten fullstendig eliminert fra tumorvevet etter 72 timer. En optimal protokoll for $TPCS_{2a}$ ble utviklet for dyremodellen, inkludert et 24 timers $TPCS_{2a}$-til-lys-intervall med en dose på 3 mg/ml $TPCS_{2a}$.

Kandidat: Yan Baglo
Institutt for kreftforskning og molekylær medisin
Veileder: Odrun Arna Gederaas
Biveiledere: Finn Drabløs, Ingebrigt Sylte, og Anders Høgset
Finansiering: Samarbeidsorganet HMN-NTNU og PCI Biotech AS

Ovennevnte avhandling er funnet verdig til å forsvares offentlig for graden PhD
Disputas finner sted i Auditoriet, Medisinsk Teknisk Forskningssenter
Fredag 04. juli 2014, kl. 12.15

Contents

Acknowledgments

The work for this thesis was performed at the Department of Cancer Research and Molecular Medicine, Faculty of Medicine, Norwegian University of Science and Technology. I am grateful for the financial support from the Liaison Committee between the Central Norway Regional Health Authority (RHA) and the Norwegian University of Science and Technology (NTNU) during 2011-2014. I am grateful for the salary received from PCI Biotech AS (Norway) and the Research Council of Norway (NFR) for performing some of the animal experiments during 2009-2010.

I would like to express my deepest appreciation to my vice supervisor Prof. Finn Drabløs, who has acted as my principle supervisor towards the end of my PhD project since 2013. Without his excellent professional guidance in science and research, and essential contribution in particular on scientific writing, this thesis would not have been possible. His intelligence, kindness, and leadership will never be forgotten. I want to send my special thanks to my vice supervisor Prof. Ingebrigt Sylte and collaborator Dr. Mari Gabrielsen in Tromsø, who took me back to the world of computer science and played with docking in three computers with laughs; and to my vice supervisor Dr. Anders Høgset (PCI Biotech ASA) who gave me great help when applying for the position and writing the manuscripts, and valuable discussion of the results.

I would like to express my sincere gratitude to Prof. Geir Slapphaug, Prof. Marit Otterlei, Prof. Hans Krokan, Dr. Lars Hagen and colleagues of their groups who offered me fruitful discussion, insightful comments, and advanced technique training. I am deeply grateful to associate Prof. Anna Bofin and Prof. Qian Peng (Department of Pathology, the Norwegian Radium Hospital, Oslo) for their education and training in histology.

I would like to send my warmest thanks to my co-authors and department engineers for their invaluable and thoughtful contribution to this work and for their rigorous scientific comments, discussion, and personal charisma which have deeply impressed me. My special thanks go to my partner Linda Helander for always having time to go through my experiments, results, presentations and writings, for benefits from her invaluable critical comments, literature searching and physical knowledge, and for the time we were in the same boat and cooperated for the same aim. Out of science, I am always attracted by the lovely stories of her two kids.

I would like to thank researcher Odrun Arna Gederaas, the project leader and the main supervisor, who introduced me to the research field of photo-treatment in cancers, to the research environment and provided the opportunity to do this project. I am particularly grateful for her help and guidance, and the time we were together with joys and sorrows. Furthermore, I want to thank Prof. Kristian Berg and senior researcher Pål Kristian

Selbo (Department of Radiation Biology, the Norwegian Radium Hospital, Oslo) for their help and guidance in my PCI work. My thanks also go to the girls from their research group for preparing ESP examination together at Bressanone and talking at ESP congress.

I am deeply grateful to the administrative colleagues and leaders for all kinds of timely advices and helps; to the animal laboratory and the core facilities at the faculty for experiment supports and training; to European Society of Photobiology (ESP) and BioStruct PhD School (Tromsø, Norway) for the courses and meetings.

Finally, I want to thank my family and friends in China, Canada and Norway for their constant encouragement and various supports, especially to my dear husband and daughter who are experienced architect and future petroleum geologist, but always understand what I do in the lab.

Stjørdal, April 2014

List of papers

Paper 1:

Photodynamic therapy with hexyl aminolevulinate induces carbonylation, posttranslational modifications and changed expression of proteins in cell survival and cell death pathways

Yan Baglo, Mirta M. L. Sousa, Geir Slupphaug, Lars Hagen, Sissel Håvåg, Linda Helander, Kamila A. Zub, Hans E. Krokan and Odrun A. Gederaas*

Photochem Photobiol Sci. 2011 Jul; 10(7):1137-45.
doi: 10.1039/c0pp00369g.

Paper 2:

Homology modeling of human γ-butyric acid transporters and the binding of pro-drugs 5-aminolevulinic acid and methyl aminolevulinic acid used in photodynamic therapy

Yan Baglo[ŧ], Mari Gabrielsen[ŧ], Ingebrigt Sylte and Odrun A. Gederaas*

[ŧ] These authors contributed equally to this work.

PLOS One. 2013 Jun 7; 8(6):e65200.
doi: 10.1371/journal.pone.0065200

Paper 3:

Enhanced efficacy of bleomycin in bladder cancer cells by photochemical internalization

Yan Baglo*, Lars Hagen, Anders Høgset, Finn Drabløs, Marit Otterlei and Odrun A. Gederaas

BioMed Research International. Submitted, March 2014, manuscript ID: 921296,

Paper 4:

Studies of the photosensitizer disulfonated meso-tetraphenyl chlorin in an orthotopic rat bladder tumor model

Yan Baglo*, Qian Peng, Lars Hagen, Kristian Berg, Anders Høgset, Finn Drabløs, and Odrun A. Gederaas

Manuscript, ready for submission

Abbreviations

2D-DIGE	two dimensional difference gel electrophoresis
2D-GE	two dimensional gel electrophoresis
AJCC	American Joint Committee on Cancer
AK	actinic keratosis
ALA	5-aminolevulinic acid
ALAD	5-aminolevulinic acid deaminase
AlPcS	aluminum phthalocyanin sulfonates
$AlPcS_{2a}$	disulfonated aluminium phthalocyanine
AMD	age-related macular degeneration
BCC	basal cell carcinoma
BCG	bacillus Calmette- Guérin
BLM	bleomycin
BLMH	bleomycin hydrolase
CIS	carcinoma *in situ*
COPRO	coproporphyrinogen
DMSO	dimethyl sulfoxide
DNPH	2,4-dinitrophenyl hydrazine
ECM	extracellular matrix
EGF	epidermal growth factor
EGFR	epidermal growth factor receptor
EMDA	electromotive administration
ER	endoplasmic reticulum
ERK	extracellular signal-regulated kinase
ESP	electrostatic potential
GABA	γ-aminobutyric acid
GAT	γ-aminobutyric acid transporter, GABA transporter
H&E	haematoxilin and eosin
HAL	hexyl 5-aminolevulinic acid
Hb	hemoglobin
HbO_2	oxyhemoglobin
HER2	epidermal growth factor receptor 2
HES	haematoxylin erythrosine saffron
Hp	haematoporphyrin
HpD	haematoporphyrin derivative
HPPH	hexylether derivative of pyroheophorbide

HRP	horseradish peroxidase
HSP	heat shock protein
IPL	intense pulsed light
JNK	c-Jun NH2 terminal kinase
LDL	low-density lipoprotein
LED	light-emitting diode
LeuT	leucine transporter
MAL	methyl 5-aminolevulinic acid
MMC	mitomycin C
MS	mass spectrum
m-THPC	meso-tetrahydroxy-phenyl chlorine
mTOR	mammalian target of rapamycin
NMIBC	non-muscle invasive bladder cancer
PCI	photochemical internalization
PBG	porphobilinogen
PDD	photodetection
PDT	photodynamic therapy
PpIX	protoporphyrin IX
PROTO	proto-porphyrin
PS	photosensitizer
RIP	ribosome-inactivating protein
ROS	reactive oxygen species
SCC	squamous cell carcinoma
TNM	tumor, node, metastasis
$TPCS_{2a}$	tetraphenylchlorin disulfonated
TPPS	tetraphenyl porphine sulfonate
$TPPS_{2a}$	tetraphenylporphine disulfonated
TURBT	transurethral resection of bladder tumors
VEGF	vascular endothelial growth factor

Background and introduction

1. Photodynamic therapy

Photodynamic therapy (PDT) is an effective treatment modality involving light and a photosensitizer used in conjunction with molecular oxygen to elicit cell death [1]. PDT is based on a two-stage process. The first stage is the selective accumulation of a photosensitizer in tumor cells in the absence of light. In the second stage, the photosensitizer is activated by light of the appropriate wavelength and intensity. Activated photosensitizer evokes responses in the tumor cells by reacting with molecular oxygen to produce reactive oxygen species (ROS). Subsequently, these ROS interact with cellular constituents causing biochemical disruption to the cell and induction of cell death in the mode of apoptosis, necrosis or autophagy. ROS produced by PDT can also cause direct cytotoxicity, destruction of tumor vasculature and induction of acute inflammatory response that further lead to activation of an immune response [2,3,4].

1.1 Photodynamic therapy (PDT) in medicine

De Rosa *et al.* and Juzeniene *et al.* have summarised the early history of PDT in several reviews [5,6,7]. The first attempts to use PDT to treat tumors and skin diseases were performed at the beginning of the twentieth century in Munich by the group of professor von Tappeiner. The discovery of oxygen-dependent photodynamic action was described and favorable results were reported using a number of dyes such as eosin and fluorescein [8]. However, there was no long-term follow-up, probably because of the advent of ionizing radiation in cancer therapy, until the application of hematoporphyrin derivative (HpD) for PDT in 1980s. Hematoporphyrin (Hp) was found to have a tumor-localizing ability in a variety of human malignancies. The purification of Hp led to HpD which contains several porphyrin monomers, dimers and oligomers. Dougherty and his co-workers partly purified HpD by removing the monomers [9,10,11]. The resulting product was called Photofrin (Porfimer sodium) which is still the most widely used photosensitizer for clinical PDT. This pioneering work established the modern era of PDT [5,12].

Hans Fischer, who was awarded the Nobel Prize for his work on porphyrins, first reported in 1925 that uroporphyrin had similar phototoxicity as Hp although it is more water soluble than Hp [13]. PDT using 5-aminolevulinic acid (ALA, a precursor to heme synthesis) started in 1987 [14,15], when several investigators reported preferential

accumulation of porphyrins and porphyrin precursors in neoplastic tissue induced by exogenous ALA [5,6]. However, protoporphyrin IX (PpIX) was observed to be converted into heme and/or cleared from the body rapidly after systemic administration due to natural clearance mechanisms, which was problematic for practical use [5,6] . It was in 1990 that Kennedy and Pottier established successful clinical ALA-PDT by topical administration in the treatment of human skin tumors [16]. Since then, endogenously stimulated formation of PpIX has been one of the fastest developing areas in PDT and photodynamic detection (PDD) [5,6].

On the other hand, tetraphenyl porphine sulfonate (TPPS) and aluminum phthalocyanin sulfonates (AlPcS) were introduced in PDT with a better tumor-localizing ability than HpD. Moreover, they could be produced with different numbers of sulfonate groups, ranging from 1 to 4, attached to the aromatic ring structure resulting in different water solubilities, specific tumor uptake, tissue penetration and quantum yield. The sub-cellular localisation of TPPS and AlPcS were observed in lysosome in 1989 [17]. Upon exposure to sub-lethal light, lysosomes were disrupted leading to leakage of the contents of the lysosomes into the cytosol by photochemical reactions [18,19,20,21,22]. The properties of the PSs were also used to release therapeutic molecules trapped by endosomes and lysosomes, termed in 1999 as photochemical internalization (PCI) [23]. Currently, a number of extremely promising applications of PCI to enhance the effect of therapeutic molecules have been proposed and demonstrated, as described in several papers (see recent reviews [6,24,25,26,27]).

1.2 Photosensitizers in PDT

PDT requires selective uptake and prolonged retention of a photosensitizer (PS) in diseased tissue, tracked by irradiation with a particular wavelength [2,28]. The PS is a natural or synthetic chemical compound that has the ability to absorb a photon of visible light and then transfers most of the absorbed energy to molecular oxygen nearby, inducing a series of photochemical reactions to produce lethal toxic agents, ROS. The physical-chemical properties of the PS are very important for the efficacy of PDT. The uptake and subcellular localization of the PS is dependent upon its chemical structure and physical nature of the PS, and the way it is administrated [29]. Different PSs will target different cellular compartments including mitochondria, lysosomes, endoplasmic reticulum (ER) and Golgi apparatus, cytosol and plasmatic membrane, or combinations of these sites. But most PSs tend not to accumulate in nuclei, as reviewed by Sanabria *et al.* [30].

The most important feature of a PS is selectivity, which means the capability of the PS to be taken up and retained in the tumor but not in normal tissue, thus leading to restricted photo-induced damage in surrounding tissue. The selective tumor uptake of the PS is probably due to differences in the physiology between tumors and normal tissues, as described in reviews by Juzeniene *et al.* and Plaetzer *et al.* [5,31]. Compared with normal tissue, tumors have a low pH which protonates PSs to become more lipophilic as they enter tumors via the blood supply, leading to preferential accumulation. Also, tumors contain many macrophages that can ingest and trap PSs, tumors have more low-density lipoprotein (LDL) receptors on the surface which favor the binding of lipophilic PSs, tumors have a leaky microvasculature providing high vascular permeability of the PSs and poor lymphatic drainage favoring retention of PSs, and tumors often have a larger interstitial space and a large amount of newly synthesized collagen which can help the uptake of PSs [5,31]. In addition, coupling of PSs to tumor-specific antibodies or other carriers can enhance the selectivity of a PS [32,33].

Finding a suitable PS is crucial for improving the efficacy of PDT. Some of the ideal characteristics of a good PS include chemical purity, easy synthesis from readily available materials, ability to be enriched in target tissue such as tumor, short half-life and rapid elimination from normal tissue to avoid prolonged photosensitization, absorption of light at a sufficiently long wavelength (within a range of 600-850 nm) so that light penetration in tissue is as deep as possible, and ability to produce a large amount of cytotoxic products upon light activation (high quantum yields), as described in reviews [2,34]. An ideal PS should not be toxic at typical doses in the absence of light. Most importantly, the PS should not cause mutagenic effects [35,36]. Finally, a short interval between administration of the drug and peak accumulation in the target tissue is required to establish a safe, low cost and reproducible clinical PDT protocol [35]. In addition to these characteristics, a PS should have reasonable stability to be useful in PDT. It should be stable enough to avoid degradation processes (photobleaching) during treatment, but some photobleaching tendency can be an advantage as it shortens the duration of general photosensitivity after PDT [34].

Most PSs used in PDT are porphyrins or porphyrin-related compounds. During the past 20 years, synthetic availability of PSs has expanded enormously. A great number of potential PSs for PDT have been developed [34], but only a few have been approved for therapy in humans (Table 1) [5,36,37,38,39].

Table 1. A selection of currently available photosensitizers/prodrugs in clinical PDT [38,39].

Photosensitizer (prodrug)	**Chemical name and class**	**Subcellular localization**	**(Potential) indications**
Photofrin (porfimer sodium)	Hematoporphyrin derivative (HpD) , porphyrin	Golgi apparatus, plasma membrane	Superficial bladder cancer, gastric, cervical, esophageal, lung and endobronchial cancer.
Levulan	5-aminolevulinic acid (ALA), endogenous PpIX, porphyrin	Mitochondria, cytosolic membranes, cytosol	Basal cell carcinoma, Actinic keratosis, Bowen's disease, head and neck cancer, superficial bladder cancer, esophageal
Metvix	Methyl ALA (MAL) , endogenous PpIX, porphyrin	See above	Basal cell carcinoma, Actinic keratosis
Hexvix	Hexyl ALA (HAL), endogenous PpIX, porphyrin	See above	Diagnosis of bladder cancer
Visudyne (Vertiporfin)	Benzoporphyrin derivative monoacid ring A, porphyrin	Mitochondria, ER	Basal cell carcinoma, age-related macular degeneration, choroidal neovascularization
Foscan (Temoporfin)	Meso-tetrahydroxy-phenyl chlorine (m-THPC), chlorin	Mitochondrial, ER	Head and neck cancer, gastric and prostate, pulmonary, gastrointestinal cancer
Photochlor	Hexylether derivative of pyroheophorbide (HPPH), chlorin	Mitochondria, lysosome	Basal cell carcinoma, esophageal cancer, and head and neck cancer
Photosens	Aluminum Phthalocyanine (AlPc), Dye	Mitochondria	Head and neck cancer, lung and gastrointestinal cancers
NPe6	Mono-L-aspartyl chlorin e6, chlorin	Lysosome, endosome	Early lung cancer, cutaneous lesions, ophthalmic lesions

1.3 Light

Each PS has a unique wavelength and intensity of light required for successful activation. Therefore, light dose required to achieve sufficient therapeutic effect is dependent on the PS used and on the optical properties of the tissue [34]. The light sources available for PDT belong to three major groups: broad spectrum lamps, diode lamps and lasers, as summarized by Issa *et al.* [2]. The introduction of lasers equipped with optical fibers revolutionized photosensitization and expanded its applicability in

medicine, enabling the endoscopic delivery of light to almost every part of the human body [35]. In the case of tumors located within body cavities (e.g., bladder), light targeting is achieved through purposely manufactured, linear or spherical diffusive fiber tips [29,40].

In addition to the accumulation of PS in tumor tissue, the specificity of PDT is also based on limiting the application of light to the target tissue. The penetration depth of light through the tissue depends upon the characteristics of the tissue and on the wavelength of the light [41,42]. The light penetration is limited by optical scattering within the tissue, the absorption by endogenous chromophores, and the absorption of light by the PS itself (self-shielding) [35,43]. The most important natural chromophores in tissue are water, oxyhemoglobin (HbO_2) and deoxyhemoglobin, melanin and cytochromes. The absorption spectra of these molecules define the optical window for PDT in tissue (Figure 1). The optical window of living tissue is between 600 nm (above the absorption of heme) and 850 nm (for sufficient generation of the triplet state) where tissue penetration is quite high and quantum yield is sufficient for singlet oxygen production [36,44]. However, the oxygen concentration changes during PDT because of vessel damage and consumption of oxygen leading to a change of the penetration spectrum [5,45].

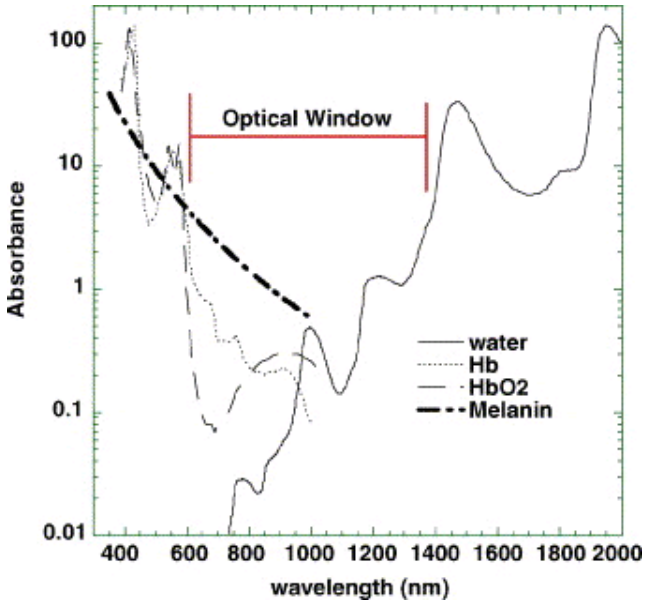

Figure 1. Optical window in tissue. The important tissue chromophores (oxy- and deoxyl-hemoglobinand melanin) have high absorption bands at wavelengths shorter than 600 nm. Water begins to absorb significantly at wavelengths greater than 1300 nm. This figure is reproduced from reference [44] with permission from Elsevier.

For clinical applications, the optimal light source is determined by several factors such as PS properties, disease, equipment cost and size; together with the delivery pattern of the light including total light dose, light exposure time, fluence rate and fractionation mode [46]. Light absorption leads to heat generation in tissue [47,48]. During PDT, the light intensity should be kept at a fluence rate of less than 150 mW/cm^2 by which photochemical reactions can be triggered without hyperthermia [46,49].

The ideal light source in cutaneous PDT should be well absorbed by the PS, achieve a desirable penetration depth to reach target, be of adequate fluence and duration to drive PDT reaction, be rapid to administer, with minimal discomfort, and with minimal side effects including erythema, crusting and dyspigmentation [46]. Currently used light sources, such as pump dye lasers, diode lasers, lamps with appropriate optical filters and light-emitting diodes (LED), achieve some of these objectives, but often with significant side effects [3,50,51,52].

1.4 Mechanism of action

The process starts with absorption of light by the photosensitizer (PS) at its excitation wavelength, resulting in excitation from its ground state (S_0) to its first short-lived excited singlet state (S_1) (Figure 2). The photosensitizer can return to S_0 by emitting the absorbed energy in a radiative process of fluorescence or a non-radiative process of internal conversion. This fluorescing property can be used to evaluate the intracellular localizing of the PS and treatment effects on tumor cells, or utilized for cancer diagnosis [28,37]. Another route for deactivation of S_1 is to convert to the first long-lived excited triplet state (T_1) in a non-radiative process of intersystem crossing. T_1 is the source of the photosensitizing effect. In the absence of other interacting molecules, the excited photosensitizer can return to S_0 from T_1 by emitting the rest of absorbed energy as phosphorescence (Figure 3) [37]. Or, it can react with neighboring molecules (e.g., molecular oxygen ($^3O_2$) or electron-rich substrates) leading to the production of ROS via two competing pathways, called type I and type II photochemical reaction [53,54]. Both reactions can take place simultaneously and the balance between the two reactions is determined by the surrounding substrates, the concentration of oxygen and the PS itself [36,55].

Type I reactions involve electron or hydrogen-atom abstraction by the excited T_1 photosensitizer from the substrate molecules to produce substrate radicals, which after reaction with molecular oxygen can lead to cytotoxic ROS including superoxide anion ($\cdot O_2^-$), hydroxyl radical ($\cdot OH$), and hydrogen peroxide (H_2O_2). *Type II reaction* involves energy transfer from the excited T_1 photosensitizer to ground-state (S_0) molecular

oxygen. This transfer produces molecular oxygen in its first excited singlet state (S_1) which is a powerful cytotoxic species. For most PSs employed in PDT, the Type II reaction is the dominant process [36,53]. In both reactions, the sensitizer returns to its S_0 state and can repeat the process. Thus, it can produce a continuous high level of ROS as long as there is light exposure. However, ROS can also attack the PS molecules, which become chemically modified or degraded leading to photobleaching of the PS [36].

PS (photosensitizer) + *hv* → $^1PS^*$ (excited singlet state) → $^3PS^*$ (excited triplet state)

Type I reactions:

$$^3PS^* + O_2 \rightarrow {\bullet}PS^+ + {\bullet}O_2^-$$
$$^1PS^* + O_2 \rightarrow PS + {\bullet}O_2^- \xrightarrow{^3O_2} {}^1O_2, {\bullet}O_2^-, H_2O_2, {\bullet}OH, {\bullet}O_2$$

$$^3PS^* + \text{Substrate} \rightarrow {\bullet}PS^- + {\bullet}\text{Substrate}^+$$

Type II reactions: $^3PS^* + {}^3O_2 \rightarrow PS + {}^1O_2$

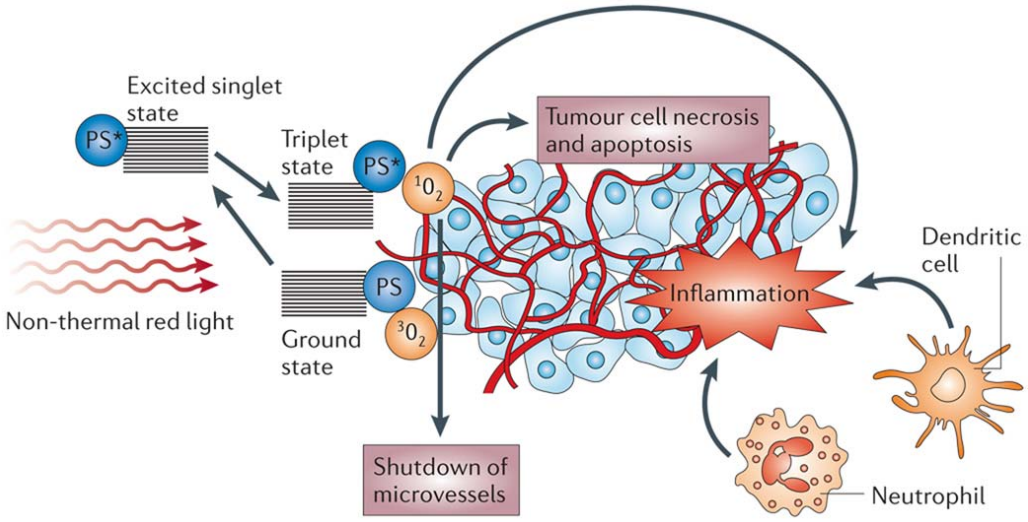

Figure 2. The mechanism of action on tumors in photodynamic therapy. The photosensitizer (PS) is excited by light to a triplet state (PS*). The PS triplet transfers energy to ground-state triplet oxygen and molecules nearby, which produces reactive singlet oxygen ($^1O_2$) and other reactive oxygen species (ROS). ROS can directly kill tumor cells by the induction of necrosis, apoptosis and/or autophagy, can cause destruction of tumor vasculature and produces an acute inflammatory response. This figure is reproduced from reference [4] with permission from Nature Publishing Group.

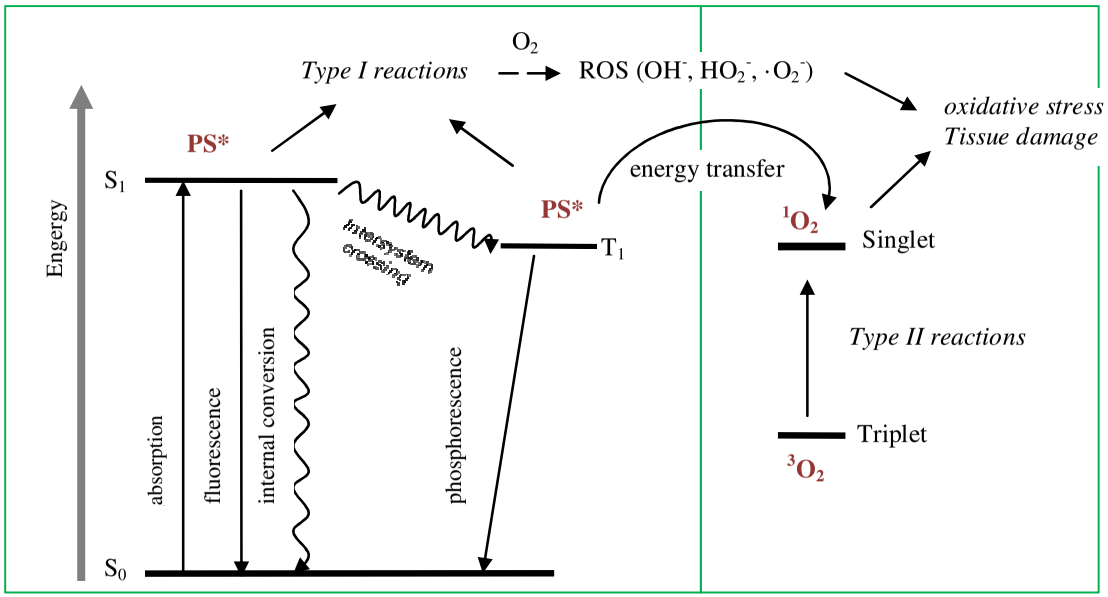

Figure 3. Modified Jablonski diagram. After activating by light, the photosensitizer (PS) is excited from its ground state (S_0) to the excited singlet state (S_1). The excited PS (PS^*) can return to S_0 by emitting fluorescence or internal conversion; or convert to the excited triplet state (T_1) by intersystem crossing and then return to S_0 by emitting the rest of absorbed energy as phosphorescence; or react with neighboring molecules at state (S_1) or state (T_1) leading to the production of ROS via two competing pathways (type I and type II).

The mechanism of action is clearly linked to the site where the PS is located, and the damaged area lies essentially within the tissue that has been exposed to light. This is due to the fact that the lifetime of the main active photoproduct, singlet oxygen, is short in cells, less than 0.05 μs. Thus, singlet oxygen can diffuse less than 0.02 μm from the site of production [5,56]. Action of PDT can cause various damages of cellular organelles, such as mitochondria, lysosomes, cell membrane and microtubules, depending on the subcellular location of PS, which is a key factor for the outcome of PDT, in addition to the determination of the photodamage site [5]. For instance, damages to cell membranes may reduce the metastatic potential of surviving tumor cells, damages to microtubules lead to accumulation of cells in mitosis and subsequently to death [5], and damages to lysosomes result in release of lysosomal enzymes, including endonucleases, proteases and hydralyses, into the cytosol in bioactive form which may induce either necrosis, apoptosis, or autophagy depending on the photo-oxidative level [57]. Since the cell nucleus is not a favorable accumulation site for most of the PSs, and due to the short lifetime of singlet oxygen, DNA damage caused by redistribution and/or relocation of PS after PDT is limited, resulting in low genotoxic potential [35,56]. Such damages will trigger cell survival or cell death signaling pathways.

PDT causes not only direct destruction on tumor cells, but has also effect on tumor stroma [58]. Damage of the stroma may lead to destruction of surviving tumor cells, inhibition of tumor growth, delay of regression and cures, thus enhance the therapeutic effect of PDT [30,59]. The stroma is composed of extracellular matrix (ECM), vasculature and different cellular components including immune cells, fibroblasts and endothelial cells [30]. ECM is a dynamic and complex array of glycoproteins, collagens, glycosaminoglycans and proteoglycans secreted by the cells. PDT produces changes in the components of the ECM (such as damages in proteins and lipids), enhancing cell death by its secondary effect on tumor cells. Also, the cross-links of the collagen matrix produced by PDT reduce the migration of the malignant and stromal cells. The cell adhesion is also altered after PDT, by ECM injury or direct damage in the adhesion proteins (damage to cell membrane) [30].

ROS produced by PDT have been shown to destroy tumors by multifactorial mechanisms (Figure 2), as summarized in recent reviews [4,28]. Illumination and ROS production causes the shutdown of vessels and subsequently deprives the tumor of oxygen and nutrients. This is because endothelial cells of the vascular systems in tumor cells can concentrate PS. Upon illumination, PS in vasculature creates the photodynamic reactions causing tumor ischemia because of irreversible damage to tumor blood supply. In contrast, the surrounding normal vasculature in the non-tumorous region may facilitate PS clearance [28]. The photodamage to the tumor vasculature has a marked contributing effect in PDT evoking the development of

vascular target PDT, such as the treatment of age-related macular degeneration (AMD) and prostate cancer [60,61].

PDT has a significant effect on the immune system, which can be either immunostimulatory or immunosuppressive, which have been described in reviews by Castano *et al.* and Sanabria *et al.* [4,30] and in papers referenced there. Antitumor immunity response is triggered by a series of events after PDT in which inflammatory response is considered to be an important initial step. Dying cells produce danger signals such as heat shock proteins and transcription factors which further induce the expression of cytokines, adhesion and co-stimulatory molecules, and immunologically important genes. The release of vasoactive mediators (e.g. histamine and serotonin) from damaged vasculature increases the permeability of blood vessels. Immune cells and inflammatory mediators are activated. Altogether, antitumor effect is enhanced after PDT by immunostimulation [4,30]. Furthermore, cancer vaccines using *in vitro* PDT-treated cells or lysates take advantage of the immunostimulatory effects, and PDT-generated vaccines have been shown to be tumor-specific [62,63,64,65].

1.5 Cell death induced by PDT

PDT results in a sequence of photochemical processes in photosensitized cells. Cellular oxidative stress occurs when antioxidant mechanisms are overloaded due to high levels of ROS. This leads to cell death by apoptosis, autophagy or necrosis, and those are post-transcriptional events that occur within a few hours after the treatment [12,66,67,68,69]. All kinds of cellular responses may be provoked in a strict dose-dependent manner, i.e. a transition from survival, over autophagy and apoptosis to necrosis depending on the applied PS concentration or light dose (termed photodynamic dose in this thesis) [66]. High light doses trigger necrotic pathways which may have implications for immune response. Low light doses allow for apoptosis and less inflammation and immune response [28,70]. Besides PDT dose, the mode of cell death also depends on PS properties and cell type [71]. Damage to organelles by PDT has been summarized in a review by Juzeniene *et al.* [5]. PS localized in mitochondria or ER generally promotes apoptosis. PS located in lysosomes can induce either necrosis or apoptosis, while in the plasma membrane it will initiate either rescue responses, apoptosis, or necrosis [5].

Recent evidence indicates that autophagy may be induced by PDT as an attempt to repair and survive photo-damaged organelles, and that this can be switched to a cell death signal if this initial response fails [37,72]. Autophagy offers protection from the photodamage at low PDT dose by enhancing survival for some cells, serving as a pro-

survival response via the recycling of damaged organelles, but can serve as an alternate death mode when the PDT dose is increased [73].

1.6 PDT resistance

Similar to drug resistance, there may also be induction of resistance to PDT, which recently has been reviewed by Casas *et al.* and Snabria *et al.* [30,73]. The mechanisms of resistance linked to the PS may be shared with general mechanisms of drug resistance, for instance different cellular uptake and efflux rates of the PS. The structure properties of the PS which determines its subcellular location is believed to be an essential factor in the development of resistance [73]. Under oxidative stress induced by PDT, an increased inactivation of ROS can occur via antioxidant enzymes (e.g. glutathione, superoxide dismutases) and up-regulation of heat shock proteins (HSPs) leading to cell survival by photo-damage repair [73,74,75]. Both oxidative stress and hypoxia induce autophagy [76,77]. The autophagy-lysosomal system represents a major protective mechanism for the clearance of ROS-damaged organelles and irreversibly oxidized cytosolic proteins by recycling proteins and cellular components, and contributes to tumor progression [30,78].

PDT effect on tumor vasculature in combination with oxygen consumption by photoreactions can induce tissue hypoxia. This may limit the PDT efficacy because tumor hypoxia can enhance survival and tumor progression by induction of autophagy to overcome nutrient deprivation, to escape their hostile environment, or to induce changes in the proteome and genome of neoplastic cells [30,73].

It is important to study the mechanisms of PDT resistance to maximize therapeutic outcome by developing new modalities, such as PDT in combination with surgery, chemotherapy, immunotherapy, or radiotherapy, and new strategies, such as increased oxygen supply (arterial flow focalization) and therapeutic inhibition of autophagy [3,73,79,80].

1.7 Applications of PDT

PDT is either used as a single or combined therapy, or as an adjunct to conventional therapies. The main advantages of PDT over conventional therapies include good site-specificity to the tumor, cosmetic outcomes in dermatological PDT, minimal invasion and systemic toxicity (except for skin photosensitivity), few secondary effects, the possibility to treat multiple lesions simultaneously, and to use repetitive cycles of

treatments, as described in reviews [30,35] and their references. PDT offers the remarkable advantage of stimulating an immune response in most cases [30]. Moreover, PDT is also effective in the treatment of chemo- and radio-resistant tumors, and there is very low potential for gene mutagenesis from the clinically approved PS [3].

The clinical approvals for PDT include curative treatment of early or superficial cancers and palliative treatment of more advanced disease, as summarized by Norum *et al.* [27]. Originally used to treat individual malignances, current clinical PDT is often applied in dermatology and ophthalmology. The main applications consist of some types of pre-malignant and malignant diseases such as age-related macular degeneration (AMD), head and neck cancer, basal cell carcinomas (BCCs), squamous cell carcinomas (SCCs), actinic keratosis (AK), Bowen's disease, psoriasis, cutaneous T-cell lymphoma, acne and photo-rejuvenation of wrinkles. PDT is also applied in a number of other diseases such as superficial bladder cancer, prostate cancer, Barrett's oesophagus, early lung cancer, brain cancers, early gastrointestinal cancer, bile duct cancer, cervical and vaginal (see the review by Norum *et al.* [27] and references therein). Moreover, several PSs (Photofrin, temoporfin, verteporfin) have been licensed for use in PDT for the treatment of some advanced cancers including advanced bronchial carcinoma, oesophageal carcinoma, advanced head and neck cancer, and AMD with pathological myopia [27].

PDT is ideal for treating some superficial and early cancers. However, for palliative treatment with the purpose of symptom relief and local control, PDT has not achieved sustained local tumor control for most applied indications due to its limitations [27]. The most important limitation is the treatment side effects represented by residual and prolonged photosensitivity (systemic administration) or pain (topical administration). This may be why most PSs have not been approved for diagnostic purposes [3]. Limitation of efficient light penetration in human tissue restricts PDT effect mostly to the tumor surface, and this may cause tumor relapse from more deeply located parts [30]. The PDT protocol remains largely empirical because of the limitation of light dosimetry which is required to be optimized for every patient [3]. Therefore research has focused on the understanding of the fundamental mechanisms of PDT in a view of chemistry, physics, biology, and medicine. With the development of novel PSs and PS delivery system, and the improvement of light sources, PDT efficacy can certainly be improved [3,81,82,83].

2. ALA-based PDT

2.1 5-aminolevulinic acid (ALA) and its derivatives methyl and hexyl ALA

ALA, the methyl ester (MAL), or the hexyl ester (HAL) serve as a biological precursor to produce excess amount of photosensitizing PpIX (Figure 4) via heme biosynthetic pathway, which is the basis for ALA-based PDT [84,85].

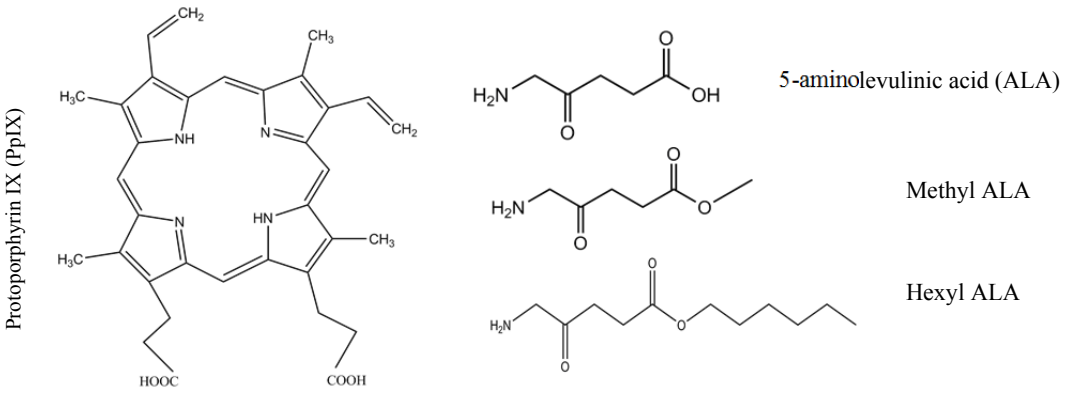

Figure 4. Structure of Protoporphyrin IX (PpIX), 5-aminolevulinic acid (ALA), methyl- and hexyl ALA

ALA is hydrophilic, and in mammalian cells it is taken up mainly by active transport mechanisms. This system requires energy, it depends on pH and temperature, and it is saturable and slow, being only slightly accelerated in tumor cells [2,86]. The low transport rate of ALA through the plasma membrane is the only limitation to the accumulation of PpIX in the treated cells. Therefore, high doses of ALA must be administered and only superficially located lesions can be treated because of the poor penetration. In an attempt to overcome the poor bioavailablility of ALA when using topical administration, a number of esterified ALA derivatives have been examined [84,85].

MAL is more lipophilic than ALA and is taken up by active mechanisms mainly through transporters of non-polar amino acids. Most importantly, MAL is transported both by active mechanisms and by passive diffusion through the membrane. The plurality and efficiency of these mechanisms determine the enhanced penetration of MAL in comparison to ALA, and the difference is even more significant in malignant cells. Soon after cell penetration, MAL is rapidly demethylated to free ALA which is then incorporated into heme biosynthesis [2,86]. MAL (Metvix) was approved in EU for the treatment of basal cell carcinoma (BCC) and actinic keratosis (AK) ten years after ALA was first approved in USA in 1991 for the treatment of AK (Table 1).

HAL is a hexyl ester of ALA. Because of the high lipophilicity of HAL, it has been shown that these molecules were about 50-100 times more efficient than ALA when inducing cellular porphyrin formation (mainly PpIX) with a high selectivity [87,88,89]. The exogenous HAL molecules enter into the cell membrane via passive diffusion. Soon after cell penetration, HAL is converted to free ALA by esterase and incorporated into the heme biosynthesis. HAL (Hexvix) was registered in EU in 2005 for the diagnosis of bladder cancer [90].

2.2 Cellular uptake of the prodrugs

In contrast to HAL, both ALA and MAL are not sufficiently lipophilic to penetrate efficiently through lipid membranes [84,88,91], although MAL can show slight uptake by passive diffusion through the membrane. Thus, various transporter systems are involved in the uptake of ALA and MAL. Studies have indicated that active cellular uptake of ALA is via γ-aminobutyric acid (GABA) transporters (GATs) in mamma cells [91,92,93,94,95]. However, the uptake of MAL is shown to be cell type dependent, either via non-polar amino acid transporters, GATs, or other amino acid transporters [91,93,94,95]. Moreover, ALA is shown to be more potent for PpIX generation than MAL [89,94] due to a faster cellular uptake of ALA, possible due to higher substrate affinity to GATs, and a rate-limitation of MAL conversion to ALA by esterase [94,96].

2.3 PpIX selective accumulation

PpIX is a member of the porphyrin derivatives. Porphyrins are a class of tetrapyrroles consisting of a highly conjugated, heterocyclic macrocycle and may also contain a central metallic atom such as ferrous iron (Heme), cobalt (Vitamin B_{12}) or magnesium (Chlorophyll). Porphyrins are essential for the biological activity of all living organisms. Porphyrins absorb most efficiently at 410 nm, along with four smaller peaks near 510, 540 and 635 nm, due to their highly conjugated skeleton (Figure 4), allowing for irradiation from multiple light sources (e.g. blue and red light) with diverse spectral yields [97]. Earlier research on the biochemistry of porphyria diseases showed that porphyrins can be endogenously produced via heme biosynthesis [98,99]. Exogenous administration of ALA in PDT results in preferential accumulation of PpIX in abnormal cells [16,100,101,102,103]. In addition to therapeutic use, the fluorescence of PpIX is applied for visualization of location and diagnosis of tumors [104,105,106,107].

The heme biosynthetic pathway comprises of eight enzymes, four in mitochondria and four in cytosol. The process starts in the mitochondria with the condensation of succinyl CoA and glycine to form ALA, catalyzed by ALA synthase. The next four steps take place in the cytosol. Two ALA molecules are condensed to form the monopyrrole porphobilinogen (PBG) by ALA deaminase (ALAD) and then four molecules of PBG are converted by PBG deaminase into the cyclic tetrapyrrole uroporphyringen III. Uroporphyrinogen decarboxylase then removes four acetic acid carboxyl groups to form coproporphyrinogen (COPRO) III. The last three steps occur in the mitochondria and involve modifications to the tetrapyrrole side chains of COPRO III and proto-porphyrin (PROTO) III by the oxidases. Finally iron is inserted into the center of protoporphyrin IX (PpIX) by ferrochelatase (Figure 5) [108,109,110].

The heme biosynthesis pathway is normally so tightly regulated that the concentrations of intermediates are below the threshold of photosensitization. There are two rate-limiting steps in normal heme biosynthetic process: 1) synthesis of ALA catalyzed by the enzyme ALAD, which is regulated through negative feedback by heme, and 2) conversion of PpIX to heme by the enzyme ferrochelatase. Incubating cells with excess exogenous ALA, MAL or HAL bypasses the first rate-limiting step, causing accumulation of PpIX. Thus, the rate of production from MAL and HAL is instead limited by enzyme activity of the conversion [111].

In addition to the differences with respect to physiological properties between tumors and normal tissues as mentioned in section 1.2, tumor selectivity of PpIX is based on decreased ferrochelatase activity and increased PBG deaminase activity in some malignant cells [112,113,114,115,116]. Other factors, such as uptake of the pro-drug ALA or its esters, esterase activity of the conversion of ALA esters to ALA, limited availability of ferrous iron due to the higher tumor proliferative activity, state of differentiation, mitochondrial content and cell type, *etc*. also play an important role in this process [102,117,118,119]. Intracellular localization of the PpIX is also considered as a factor that affects the PpIX accumulation. If an excess of PpIX is synthesized, it can diffuse from the mitochondria into ER, lysosomes and the plasma membrane [14,86,120,121,122]. But the accumulation is transient, because PpIX clearance is mostly complete by elimination within 24-48 hours, shortening the period of cutaneous photosensitivity [123].

During PDT many molecules of PpIX are destroyed by reacting with the excited singlet oxygen [124]. However, radical attack leads to modification of side groups and/or the molecular skeleton of the PS. Photo-modification of PpIX typically creates chlorines which are more effective PSs than PpIX [36].

Figure 5. Scheme of ALA, MAL, and HAL incorporation to the heme biosynthetic pathway in mammal cells. Exogenous MAL or HAL is converted into free ALA by esterase in the cytosol before incorporating to the heme biosynthetic pathway. The first rate-limiting step of ALA synthesis regulated by negative feedback of heme is bypassed in the condition of exogenous prodrugs MAL or HAL, but regulated instead by esterase activity of hydrolysis. Low ferrochelatase activity and elevated PBG deaminase activity can result in high PpIX accumulation in some malignant cells [111,115,125].

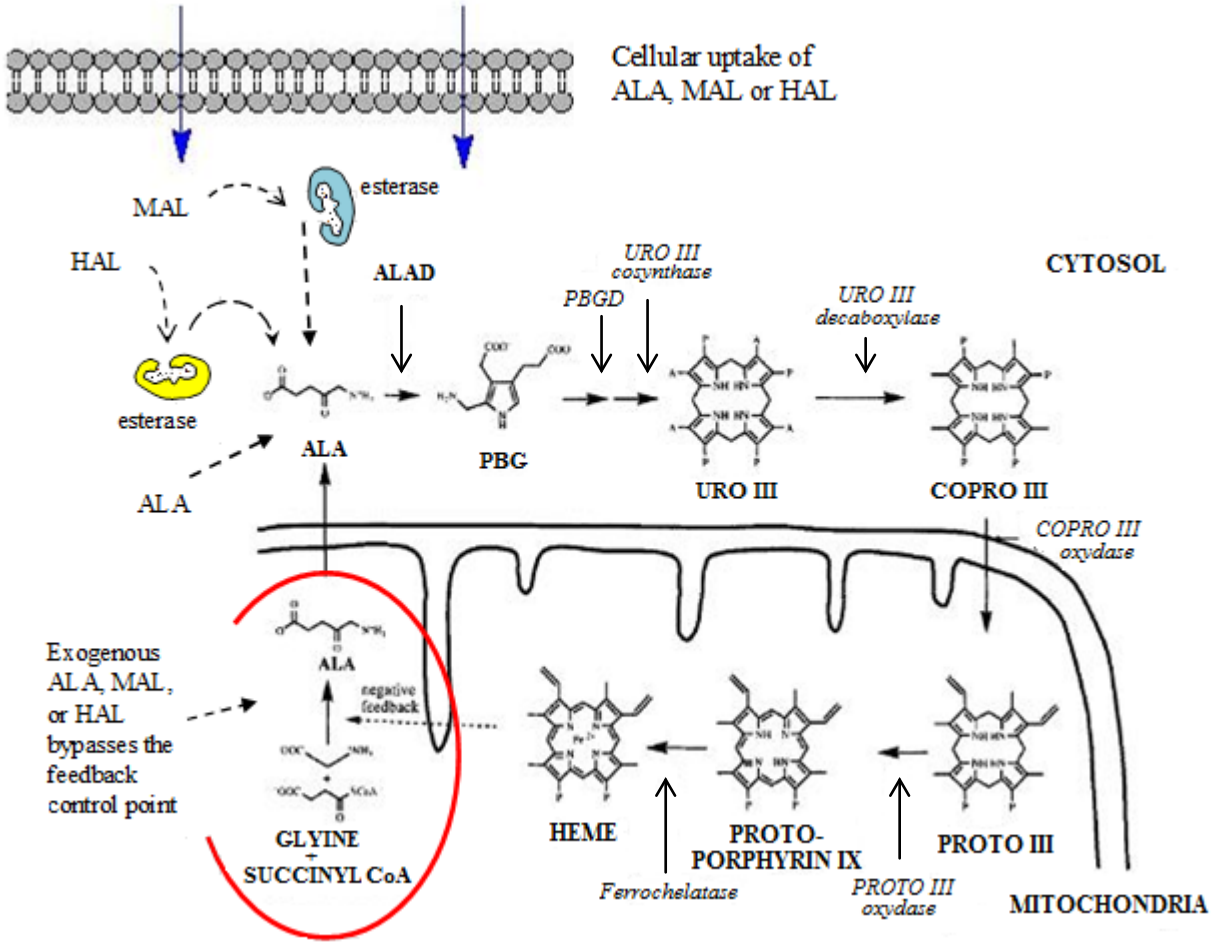

2.4 Cellular responses to ALA-based PDT

PpIX is synthesized in the mitochondria and redistributes into the cytosol and membrane-rich organelles, e.g. ER and cell membrane, and reactive oxygen species (ROS) are produced at these sites. Cellular antioxidant mechanisms are apparently overloaded by high levels of ROS and radicals. This leads to ROS-induced protein modifications and dysfunction, and eventually affects pathways resulting in cell death [126]. The most thoroughly characterized oxidative modifications of proteins subsequent to PDT are irreversible and non-enzymatic carbonylation and oxidation of thiol groups [127,128]. At the molecular level, genes and their products can be either up-regulated or down-regulated after PDT. A strongly altered gene expression is found after ALA-PDT, and this includes immediate early genes and genes involved in cell proliferation, stress responses, apoptosis and cell adhesion, showing that PDT triggers a complicated cellular response involving several biological pathways [129,130,131,132,133,134].

2.5 Clinic applications and future perspectives

ALA-based PDT is widely used in various pre-malignant and malignant cutaneous diseases in many countries. Topical application of ALA and its esters results in consistent PpIX uptake in the applied region. ALA-induced PpIX can accumulate in abnormal tissue at 2-10 fold higher concentration compared to normal tissue [135]. However, with ALA and MAL only superficial lesions can be treated [84,136]. Therefore, improving tissue and depth penetration via various formulations and carriers of the prodrugs is an area of active research [137]. In recent years, a novel modality of ablative fractional laser has been developed for promoting drug delivery via skin by creating microscopic vertical channels in tissue [138]. The ablative fractional lasers have been used in animal models to facilitate intracutaneous uptake and distribution of topical MAL deeper into skin layers [139,140]. When blue light is employed, the penetration depth is only several millimeters [141] which is now utilized to treat non-malignant skin pathologies such as inflammatory dermatoses, psoriasis, acne and warts, infectious cutaneous diseases caused by microbes [142,143].

The earliest and most frequently used light sources in PDT for cutaneous diseases have been non-coherent broad-spectrum light sources in the red and blue wavelengths to activate porphyrins administered either systemically or topically [46,50]. The use of intense pulsed light (IPL) for PDT is promising because it spans wavelengths from the blue to the infrared range, thereby exciting PpIX along many of its successive absorption peaks [144,145]. Although lasers provide the ability to select a specific wavelength, in order to achieve higher irradiances and maximize penetration depth, they

are not suitable alternatives for cutaneous PDT because they are expensive, less reliable and portable, and give small illuminative area in the skin surface [46,146].

ALA may have a role in other applications in surgical oncology based on its ability to discriminate neoplastic tissue from adjacent normal tissue [107,147,148]. A number of efforts have been made to explore potential clinic applications of ALA-based PDT in non-cutaneous solid malignancies such as breast, bladder, ovarian, lung, gastrointestinal, head and neck cancers. However, further large studies are required to optimize the protocols and improve treatment efficacy [147]. Besides diagnostic purposes PpIX fluorescence images can be utilized either for a directed biopsy sampling or as an aid during surgery [5,149].

In contrast to skin photosensitivity as a main limiting factor of PDT with systemic PSs, pain is an important limiting factor for topical ALA-based PDT. In some cases pain is so severe that the treatment is discontinued [150,151]. In some clinical studies MAL is proposed to induce less pain than ALA [151,152,153]. But no significant differences in pain scores were observed between ALA- and MAL-PDT for actinic keratosis based on a clinic study of 600 patients [154]. Although the mechanism of pain has not been fully elucidated, several studies have suggested that it may be due to the uptake of ALA via GABA transporters into the mitochondria-rich sensory neurons and hence high-level accumulation of PpIX [155,156] which further induces nerve stimulation through tissue damage induced by ROS upon irradiation [155,157]. Current pain-reducing strategies include interrupted illumination, cooling of the affected area and local anesthesia [158,159].

3. Photochemical internalization

The rapid development of PDT includes many interesting perspectives. The most appealing one appears to the discovery and development of new PSs, which may progressively improve the efficacy and specificity of a particular therapy. However, the focus of the invention of PSs is not only on PDT itself. Another important field of study is the delivery technology known as photochemical internalization (PCI), which can efficiently release therapeutics accumulated in endosomes and lysosomes, by which the efficacy of some conventional therapies can be enhanced, with reduced side effects that are limited to the illuminated area.

3.1 Background of photochemical internalization (PCI)

In the PCI technology a membrane-embedded photosensitizer is used together with a therapeutic macromolecule by endocytic delivery, a process known as endocytosis [23,160]. The endocytic pathway involves internalization of molecules from the plasma membrane and recycling them back to the surface or sorting them to degradation. In endocytosis, the cell engulfs extracellular substances, forms an intracellular bud by invagination of a portion of plasma membrane, and further forms an intracellular membrane-bounded vesicle, an endosome, by membrane fusion, containing the ingested substances. In general, molecules taken up by endocytosis are rapidly sorted, processed and directed to other organelles or to be subjected to enzymatic degradation in lysosomes [161]. In this way, cells can take up substances that do not readily pass the plasma membrane. The therapeutic macromolecules for PCI generally refer to oligonucleotides, peptides, protein toxins, chemotherapeutic agent and polymers whose sizes are normally larger than 1k Dalton, and bio-availabilities are usually limited by the membrane barrier when used as traditional drugs (step 3 in Figure 6, the process without light exposure (dark)) [25,162,163].

Lysosomes are dynamic membrane-bound organelles containing a large number of acidic hydrolases which can directly contribute to cell death through lysosomal destabilization and enzyme leakage into the cytoplasm [161]. Compelling evidences have shown that lysosomes can fuse with late endosomes, the plasma membrane, phagosomes and autophagosomes. Kissing events (kiss-and-run) and direct fusion with late endosomes are the means by which endocytosed macromolecules are delivered to lysosomes. The hybrid organelle fused by endosome and lysosome is the site of degradation of endocytosed macromolecules. Lysosomes are re-formed from the hybrid organelle by a maturation process [164,165]. As degradation of macromolecules in lysosomes after uptake by endocytosis is a major limitation for the therapeutic efficacy of the macromolecules, PCI has been established to liberate macromolecules trapped by the endocytic pathway before degradation by lysosomal hydrolases (Figure 6, the PCI process). This function of PCI has been demonstrated by a number of *in vitro* and *in vivo* studies [166,167].

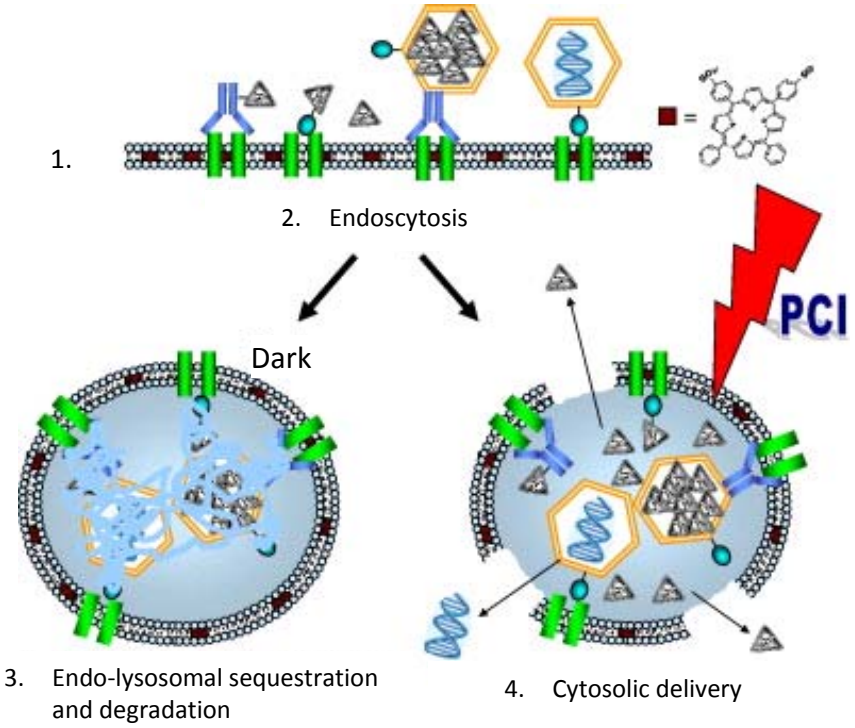

Figure 6. Endolysosomal escape of therapeutics by photochemical internalization. (1) An amphiphilic photosensitizer (■) and a drug (▲) bind to the plasma membrane after administration. To increase the uptake, the therapeutics are usually bound to targeting moieties (such as antibody or growth factor ligand); (2) The photosensitizer and the drug enter into the cell via endocytosis and co-localize in the endolysosomal compartments; (3) Without light exposure (dark), the enclosed drug is eventually hydrolyzed by lysosomal enzymes; While with light exposure (4) (PCI), the photosensitizer is activated leading to production of reactive oxygen species (mainly singlet oxygen) which further oxidizes the membrane. The free drug enters into the cytosol after the rupture of membrane, without degradation by the lysosomal enzymes. This figure is reproduced from reference [25] with permission from Elsevier.

The selection of PSs for PCI is based on the property of membrane-localization at endocytic vesicles. The reason is simply to limit the photodamage to the vesicular membrane, thereby minimizing the possible destruction of the enclosed macromolecules in the lumen compartment. Thus, amphiphilic PSs are ideal for PCI [19]. Currently the most common PSs are porphyrins and chlorins, which have two favorable features with respect to PCI [168]. One feature is the possibility to modify the chemical structure at different loci and with various levels of complexity. The insertion of two polar substituents (e.g. sulphonate groups) on two adjacent rings of the macrocycle makes the PS an amphiphilic species. Another feature is the presence of absorption bands in the

600-850 nm wavelength region, corresponding to maximal light penetration into mammalian tissue [168]. Compared to porphyrins, chlorins exhibit a high extinction coefficient and an absorption peak in the far red waveband and a rapid, high and selective accumulation in the target tissue [86]. To date, $TPPS_{2a}$ (disulfonated meso-tetraphenylporphine) [169,170,171], $TPCS_{2a}$ (disulfonated meso-tetraphenyl chlorin) [169,170,171,172,173] and $AlPcS_{2a}$ (disulfonated aluminum phthalocyanine) [22,174] are the most efficient amphiphilic PSs for PCI, with two sulfonate groups on adjacent phenyl/phthalate rings (Figure 7). They primarily localize in the membranes of endocytic vesicles with their hydrophobic part inserted into the membrane and redistribute in the cytosol after irradiation [22,172,173,174,175,176]. It is of importance that these three amphiphilic PSs are not substrates to the ATP-binding cassette transporter ABCG2 [177].

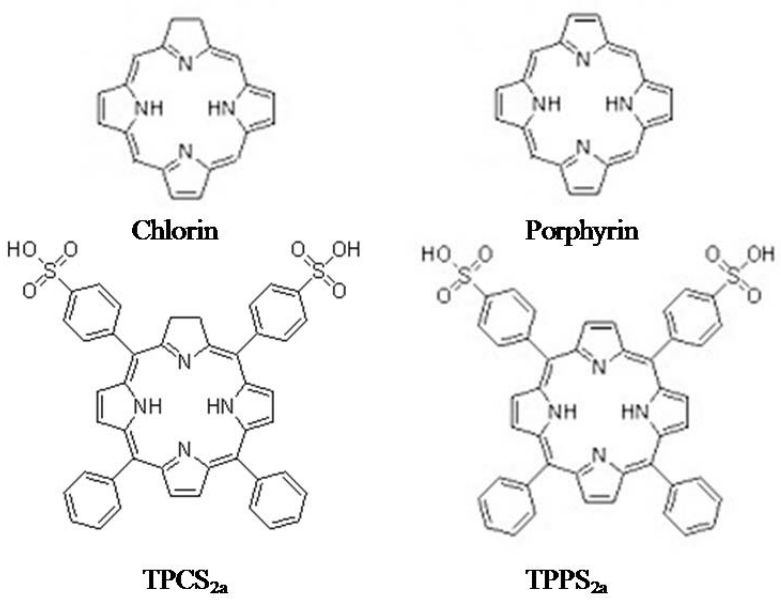

Figure 7. Structures of chlorin, porphyrin, disulfonated meso-tetraphenyl chlorin ($TPCS_{2a}$), and disulfonated meso-tetraphenylporphine ($TPPS_{2a}$).

3.2 Mechanism of action

PCI is based on a three-stage process. The first stage is the selective accumulation of a photosensitizer in the tumor in the absence of light. The second stage is the accumulation of a therapeutic macromolecule in the tumor in the absence of light. In the last stage, the PS is activated by light of the appropriate wavelength and intensity [23]. Another three-stage process has also been suggested in which stage 2 and 3 is

exchanged. In this process, the macromolecules can leak out immediately from the newly formed endosome once it is fused with the photochemically damaged endocytic or lysosomal membrane [178]. However, this alternative process will not be further discussed in this thesis. The ability to release the content of the endosomal/lysosomal vesicles is a fourth novel effect in addition to PDT effects of direct cytotoxicity, vascular damage and activation of immune system [27,179]. The process of clinical application of the PCI technique is shown in Figure 8.

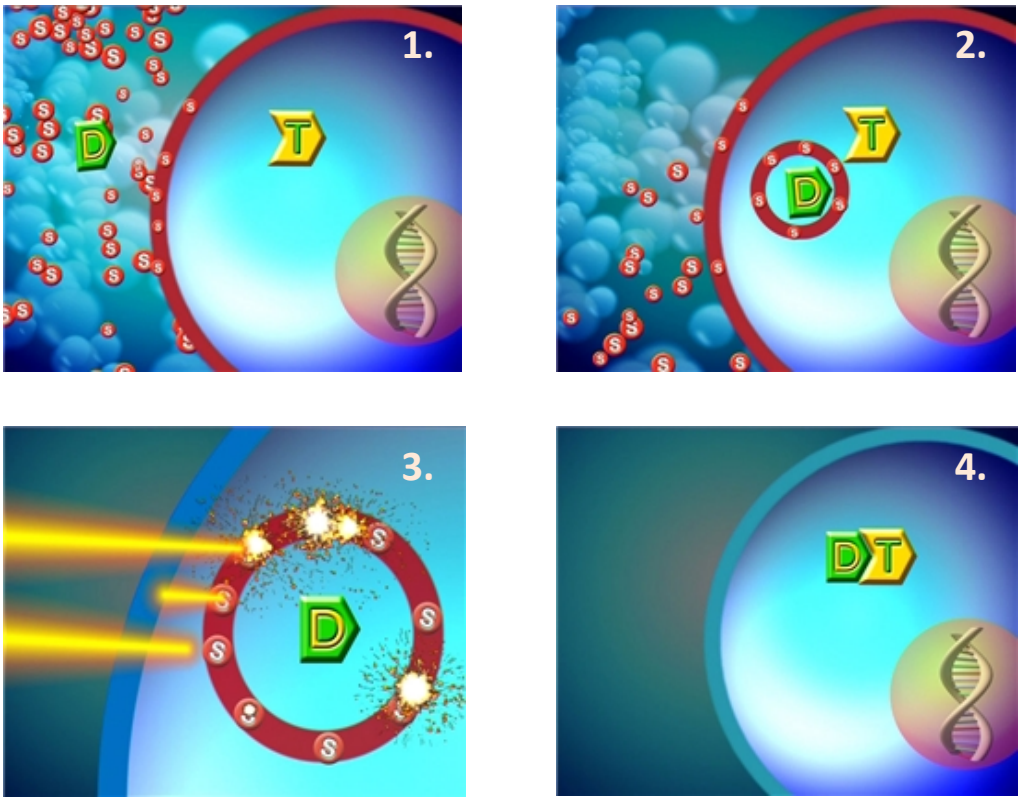

Figure 8. The process of the photochemical internalization technique in clinical applications (A-D). (1) The photosensitizer (S) and the drug (D) are systemically or locally administered into the body and transported or distributed to the target cell containing the therapeutic target molecule (T); (2) The photosensitizer and the drug are taken up by the target cell via endocytosis, but encapsulated in an endosome with photosensitizer localized in the membrane; (3) Illumination activates the photosensitizer and triggers photoreactions in the membrane of the endosome leading to the membrane rupture and then the drug release; (4) The drug molecule can now bind to its intracellular therapeutic target initiating a therapeutic response. This figure is reproduced from http://pcibiotech.no/content/basics-pci with the permission from PCI Biotech AS, Norway.

In the same way as for PDT, the process starts with the activation of the photosensitizer by light, but under PCI conditions the photochemical reactions (Type I and II) are limited to the membrane where the activated PS is located [22]. Singlet oxygen causes mainly membrane damage by oxidizing amino acids including tryptophan, cysteine, histidine, methionine, phenylalanine and maybe guanine, unsaturated fatty acids and cholesterol [180]. Destruction of membrane constitutions results in membrane rupture and the liberation of the trapped macromolecules into the cytosol. The macromolecules exert their pharmacological actions after reaching their target sites [22].

It has been reported that $TPPS_{2a}$-PDT (associated with PCI) has effects on MAPK signaling pathway in NuTu-19 and WiDr cell lines [181]. Both extracellular signal-regulated kinase (ERK) and p38 are activated immediately after PDT in these two cell lines. However, c-Jun NH_2 terminal kinase (JNK) is only activated transiently in NuTu-19 cells. Using selective inhibitors, p38 is shown to serve as a death signal, whereas JNK is a survival one. On contrast, the activation of ERK is not observed to have any influences on cellular response to the PDT-induced cytotoxity [181]. The epidermal growth factor receptor (EGFR) in NuTu-19 cells and mammalian target of rapamycin (mTOR) in WiDr cells are also targets of $TPPS_{2a}$-PDT and $AlPcS_{2a}$-PDT respectively [182,183,184].

In PCI it has been found that a large fraction of lysosomes may be ruptured without inducing significant cell death. This may be partly due to photochemical inactivation of the lysosomal hydrolases and to the action of their cytosolic inhibitors. On the other hand, upon illumination lysosomal contents can be released without losing their biological activity before degradation by lysosomal hydrolases [21]. It has been shown that endosomal photodamage induced by low photodynamic dose (including light dose and PS dose) can lead to impaired membrane trafficking processes without disrupting endosomes. As the photodynamic dose is increased endosomes are disrupted, triggering apoptosis. Necrosis occurs when the photodynamic dose is increased to even higher level [185]. Therefore, the photodynamic dose required for PCI is much lower (sub-lethal) than the ones required for PDT modality.

3.3 Perspectives of PCI

Endocytosis is obligatory for PCI, but the environment of the endocytic vesicles may limit how much the therapeutic effect can be enhanced by PCI [27]. The hydrolases contained in the vesicles may degrade the endocytosed macromolecules. The PCI-generated ROS may inactivate the nearby therapeutic macromolecules by oxidative reactions [27]. And the endocytic rate is cell type-dependent [161]. Nevertheless, the

outcomes of PCI with various macromolecules have revealed a synergetic effect. This indicates that photochemical inactivation of therapeutic macromolecules may be of marginal importance. The findings as described below have highlighted the potential clinical benefits of PCI [25].

3.3.1 PCI for protein toxin and immunotoxin

Ribosome-inactivating proteins (RIPs) are a group of protein toxins which inhibit protein synthesis. Among them, type I RIPs including gelonin and saporin have limited ability to enter the cells. It has been documented that PCI enhances the inhibitive effect of gelonin and saporin under selective PCI conditions [23,173,186,187]. To increase the uptake and specificity of protein toxins, both antibody-conjugated gelonin and saporin (immunotoxin) using antigens such as human epidermal growth factor receptor 2 (HER2), vascular endothelial growth factor (VEGF) and epidermal growth factor (EGF) have been developed for PCI [26,79,188,189,190,191,192,193,194,195]. The efficacy and selectivity of these combinations of PCI indicate a benefit for cancer therapies in preclinical studies and clinical trials [26].

3.3.2 PCI for chemotherapy and multidrug resistance

Many highly effective chemotherapeutic agents are large and water soluble and therefore do not easily penetrate plasma membranes, but are actively transported into cells by endocytosis [196]. PCI of several chemotherapeutic agents including bleomycin, doxorubicin, and mitoxantrone have been documented with significant effect [197,198,199,200,201] and with the ability to reverse any multiple drug resistance to the chemotherapeutic agents under selective conditions [198,202].

3.3.3 PCI for gene delivery

The lack of efficient delivery systems is one of the main problems of gene therapy. Various delivery agents have been evaluated in PCI to mediate gene transfection [203,204]. It was found that PCI enhanced transfection using polycationic vectors (such as polylysine or polyethylenimine) and adenoviral vectors [205,206,207].

3.3.4 PCI for other macromolecules and therapies

A number of studies have also demonstrated that PCI represents an efficient delivery system for the release of other macromolecules such as peptide horseradish peroxidase [21,23], siRNA and peptide nucleic acids [208,209,210,211,212].

3.3.5 Combination strategies of PCI

Local recurrences are a major problem after inadequate surgery in cancer treatment. In order to explore the PCI effect on the remaining tumor cells after inadequate surgical resection, Norum *et al*. [213] used an infiltrative human fibrosarcoma in nude mice to test the effect of bleomycin, PDT, and PCI with bleomycin. Bleomycin was shown to significantly delay tumor regrowth after surgery, and this inhibition was further improved by PCI. The results indicate that PCI of bleomycin may be an efficient intra-operative technique as an adjunct to surgery in cancer treatment [213]. PCI of bleomycin in combination with radiotherapy was also explored using a human soft tissue sarcoma in nude mice (TAX-1 tumor model) by the same research group [214]. The results indicate that radiotherapy in combination with PCI of bleomycin may reduce the total radiation dose necessary to obtain local tumor control by appropriate protocols.

3.4 Differences between PCI and PDT

As a technology for enhancing drug delivery, for instant chemotherapeutic macromolecules, PCI differs from conventional combination strategies of PDT. Although the treatment using PCI with chemotherapeutics is very similar to the combination of PDT and chemotherapy, photodynamic dose of PCI is sub-lethal with the main purpose to promote the cellular internalization of therapeutic molecules. The cell killing effect therefore results predominantly from the chemotherapeutics and not the photodynamic treatment. This is essential in PCI since the technique is designed to favor the delivery of a therapeutic macromolecule without inactivating the molecule or lethally damaging the cell. This is of particularly importance for the delivery of molecules which are not intended to be directly toxic to a cell, such as genes and siRNA [215].

It has been documented in several *in vivo* studies that PCI of therapeutic macromolecules increases both the necrotic depth and the fraction of complete remissions in treated tissue [179,186,216]. PCI has the potential to reduce the administered dose of chemotherapeutic agents, and hence the dose-dependent side effects. PCI may also reverse resistance to drugs such as bleomycin and doxorubincin [198].

4. Bladder cancer

4.1 An introduction to bladder cancer

The bladder consists of three layers: a mucous layer of epithelial cells (urothelium), the underlying submucosa, and the outer muscular layer. A newly diagnosed bladder cancer is usually found in the epithelial lining and has high tendency to grow through the submucosa into the muscular layer, and then invade surrounding tissues and the lymph nodes, resulting in metastasis at last. Classification of bladder cancer by anatomic disease extent, i.e. stage, is important to determine the appropriate treatment strategy and predict outcomes. The most common classification is the TNM system (Table 2) describing tumor growth into the bladder (T), invasion in the lymph nodes (N) and metastasis (M) [217]. Non-muscle invasive bladder cancer (NMIBC), previously called as superficial bladder cancer includes carcinoma *in situ* (CIS, stage Tis), stage Ta and T1 tumors. NMIBC has a high risk of recurrence and a variable risk of progression. Invasive bladder cancer includes stage T2 or T3 tumors, where there is a higher risk that the cancer will spread to other areas of the body than for NMIBC. Advanced bladder cancer includes T4 bladder cancer, cancer in the lymph nodes, or cancer that has spread to another part of the body (Figure 9) [217].

Bladder cancer is one of the most common cancers in the world and causes more than 100 000 deaths every year [218,219]. In Norway bladder cancer has been one of the five most common cancer types for men during the last ten years [220] and in United States it is estimated that 72 570 new cases and 15 210 deaths will be reported in 2013 [221]. Approximately 70-80% of diagnosed bladder cancers worldwide are non-muscular invasive bladder cancer (NMIBC) for which intravesical chemotherapy and/or immunotherapy is used as an adjuvant treatment to the standard transurethral resection [218]. However, significant improvements in preventing disease progression and recurrence have not been obtained [218,219]. On the other hand, systemic therapy is typically reserved for higher stage, muscle-invading, or metastatic diseases [222]. The main risk factors for bladder cancer are cigarette smoking and occupational exposure to toxic chemicals. Age and chronic urinary tract infection are also involved. Due to frequent clinical follow-up, repeated cystoscopies, and often repeated transurethral resections, the treatment for bladder cancer becomes one of the most expensive cases in medical care. [223].

Table 2. Definitions of Tumor, Node, Metastasis (TNM) Staging System of urinary bladder. Used with the permission of the American Joint Committee on Cancer (AJCC), Chicago, Illinois. The original source for this material is the AJCC Cancer Staging Manual, Seventh Edition (2010) published by Springer Science and Business Media LLC, www.springer.com.

Primary Tumor (T)	
TX	Primary tumor cannot be assessed
T0	No evidence of primary tumor
Ta	Non-invasive papillary carcinoma
Tis	Carcinoma *in situ*: "flat tumor"
T1	Tumor invades subepithelial connective tissue
T2	Tumor invades muscularis propria
pT2a	Tumor invades superficial muscularis propria (inner half)
pT2b	Tumor invades deep muscularis propria (outer half)
T3	Tumor invades perivesical tissue
pT3a	Microscopically
pT3b	Macroscopically (extravesical mass)
T4	Tumor invades any of the following: prostatic stroma, seminal vesicles, uterus, vagina, pelvic wall, abdominal wall
T4a	Tumor invades prostatic stroma, uterus, vagina
T4b	Tumor invades pelvic wall, abdominal wall

Regional Lymph Nodes (N)	
Regional lymph nodes include both primary and secondary drainage regions. All other nodes above the aortic bifurcation are considered distant lymph nodes.	
NX	Lymph nodes cannot be assessed
N0	No lymph node metastasis
N1	Single regional lymph node metastasis in the true pelvis (hypogastric, obturator, external iliac, or presacral lymph node)
N2	Multiple regional lymph node metastasis in the true pelvis (hypogastric, obturator, external iliac, or presacral lymph node metastasis)
N3	Lymph node metastasis to the common iliac lymph nodes

Distant metastasis (M)	
M0	No distant metastasis
M1	Distant metastasis

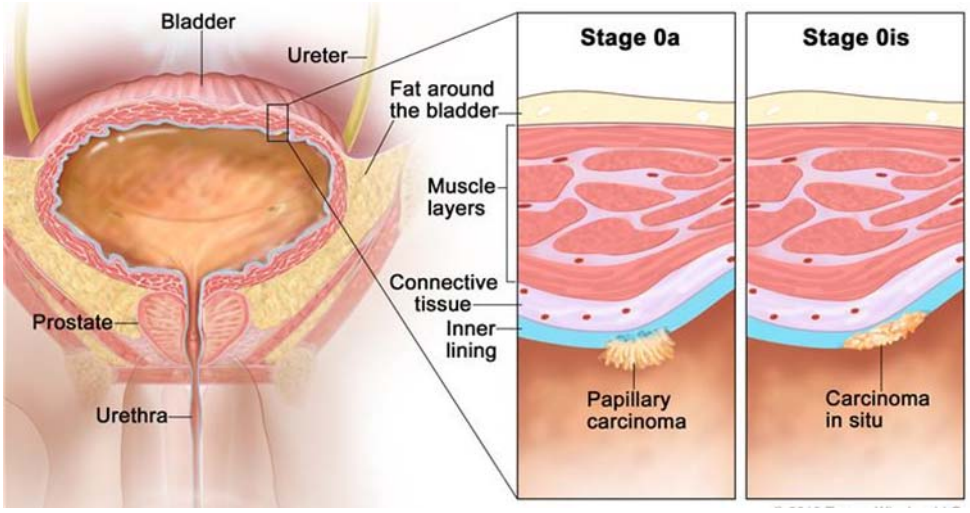

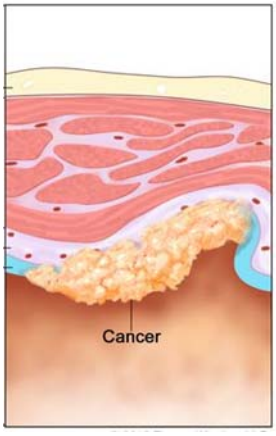

Stage I

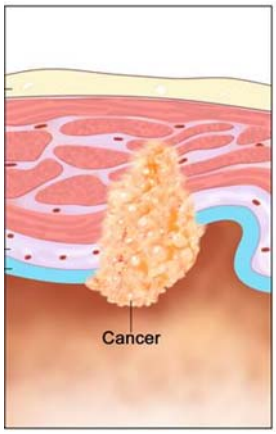

Stage II

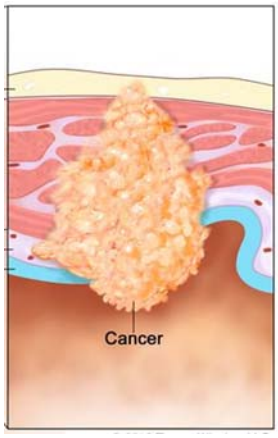

Stage III

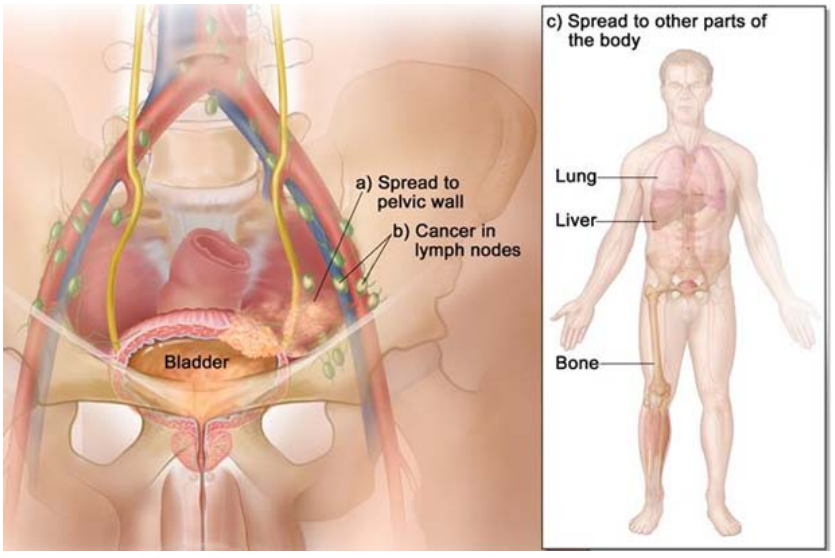

Stage IV

(continued on next page)

Stage	T	N	M
0a	Ta	N0	M0
0is	Tis	N0	M0
I	T1	N0	M0
II	T2a	N0	M0
	T2b	N0	M0
III	T3a	N0	M0
	T3b	N0	M0
	T4a	N0	M0
IV	T4b	N0	M0
	Any T	N1-3	M0
	Any T	Any N	M1

Figure 9. Definitions of anatomic stage/prognostic groups of urinary bladder. Used with the permission of the American Joint Committee on Cancer (AJCC), Chicago, Illinois. The original source for this material is the AJCC Cancer Staging Manual, Seventh Edition (2010) published by Springer Science and Business Media LLC, www.springer.com.

4.2 Treatments for NMIBC

NMIBC is normally removed by surgery during a cystoscopy under general anesthesia. This procedure is known as transurethral resection of bladder tumors (TURBT) which is the first-line treatment. Unfortunately, the high rate of recurrence and progression after TURBT demands the use of adjuvant treatments such as intravesical chemotherapy using mitomycin C (MMC), epirubicin, or doxorubicin [224]. If there is still a risk for development into invasive bladder cancer after the combination of surgery and chemotherapy, then treatment with the bacillus Calmette-Guérin (BCG) vaccine is required. BCG is the most effective use of cancer immunotherapy for preventing recurrence and progression in NMIBC [224,225,226,227]. However, recurrence rates still remain high and progression is not eliminated after BCG. In addition, BCG has some side effects such as bladder irritation, frequency, bleeding, and possibly with flu-like symptoms, joint pain, and skin rash. The main side effect of chemotherapy is bladder irritation and skin rash. Slight chemical cystitis can occur, including dysuria, hematuria, frequency, occasional pyuria or suprapubic pain [228].

To improve the total intravesical drug exposure and hence chemotherapeutic efficacy, various experimental approaches have been evaluated including enhancing the delivery of agents to bladder tissue (e.g. electromotive therapy), enhancing cell membrane permeability (e.g. intravesical hyperthermia), or prolonging the exposure (e.g. bioadhesive) [222]. Electromotive administration (EMDA) of chemotherapy may be applied if progress or recurrence occurs after chemotherapy or BCG as a single treatment. The electrical current applied increases the bladder lining permeability to absorb the chemotherapeutic molecules, thus enhances chemotherapeutic efficacy [229,230]. Another technique, called hyperthermic chemotherapy, is to heat the wall of the bladder with a microwave probe while intravesically administering a chemotherapeutic drug, e.g. MMC, on the purpose of enhancing the uptake [231,232,233,234].

In the future, the perspectives for the treatment for bladder cancer seem to be focused on searching new modalities such as keyhole surgery (laparoscopic or robot cystectomy), multiple chemotherapeutics (e.g. MMC, gemcitabine, doxorubicin, epirubicin, thiotepa, cisplatin, ethoglucid, valrubicin, suramin and their combinations), radiotherapy and immunotherapy, and their optimal combinations [222,235]. Both PDT with potent PSs and PCI with selective chemotherapeutics are of great interest [236,237,238].

4.3 PDT for bladder cancer

NMIBC is potentially well suited for effective treatment by PDT because it is easily accessible for both intravesical instillation and illumination. It is possible to irradiate the whole bladder and thus provide access to multifocal tumors [158,239]. As no difference in light penetration is observed between tumor and normal bladder tissue, the photodynamic response upon diffuse illumination of the bladder will depend on the localization and accumulation of PS within the tumor [240]. PDT can be recommended as a second-line treatment or immediate therapy for patients with tumor recurrence after TURBT, chemotherapy, and/or BCG failure [241,242,243]. It has been shown that bladder PDT is effective in CIS, well-tolerated compared to adjuvant BCG therapy and enhances MMC efficiency as an adjuvant therapy [244].

HpD (photofrin) was first approved for the treatment of NMIBC (superficial bladder cancer) in Canada in 1993. However, HpD itself has several drawbacks, such as contamination with impurities, and relatively low absorbance at 630 nm, where tissue penetration of light is not optimal. PDT for bladder cancer (bladder PDT) with intravenously administered HpD induces long-lasting skin photosensitivity for up to 6-8 weeks. Because of accumulation of HpD in the bladder muscle, fibrosis and permanent

bladder contraction can be observed in some treated patients [245]. In addition, the onset of numerous side effects is sometimes triggered, including urinary frequency, urgency, nocturia, suprapubic pain, and bladder spasm. As a result, the light dose required for activation of HpD will vary largely from patient to patient [5,227,246]. Due to permanent bladder shrinkage induced by severe urgency symptoms and prolonged skin photosensitivity, bladder PDT has progressively been abandoned [237,247], until the introduction of ALA and HAL in bladder diagnosis.

ALA and HAL have been approved for the diagnosis of NMIBC after intravesical instillation. Interestingly, fluorescence guided cystoscopy facilitates a more complete resection and prolongs recurrence-free survival [248]. This has caused regained interest in bladder PDT with intravesical administered PSs, especially to treat CIS. Some efforts have been made to improve ALA-based bladder PDT [103,249,250,251,252,253]. No patients revealed bladder contraction or systemic side effects. However, clinical trials of ALA-based bladder PDT have been extremely sparse, representing only small, single institution series [158,241,254,255,256].

Owing to variable tumor responses and significant side effects such as phototoxicity and bladder contracture, lack of standard protocol, and limited number of appropriate patients, PDT has not become widely accepted as a treatment for human bladder cancer [238,257], demonstrating the need for improved approaches. Currently, a novel PS hypericin, extracted from plants of the *Hypericum genus,* has been developed for the detection of bladder cancer. Compared to white and blue light cystoscopy, hypericin shows minimal side effects and higher specificity and sensitivity [258]. Hypericin-mediated PDT has been tested against bladder cancer *in vitro* showing significantly better photocytotoxicity and selective localization than HpD [259]. Bladder PDT using the new PS Radachlorin® has been shown to be a safe and effective treatment for NMIBC refractory or patients that are intolerant to BCG therapy [244,260].

4.4 PCI for bladder cancer

Very recently, both *in vitro* and *in vivo* studies of the treatment for bladder cancer using PCI combined with the chemotherapeutic agent bleomycin were independently set up by two research groups [236,261]. PCI-enhanced bleomycin effect has been observed in bladder cancer cells that were tested.

In 2005, bleomycin was introduced for PCI. It was found that PCI with bleomycin induced a synergistic inhibition of tumor growth *in vivo* using several tumor models [201]. Later, in 2009, the same group reported that PCI of bleomycin was superior to

PDT and could be used as an adjunct to marginal surgery [179]. A PCI-enhanced bleomycin effect was also documented in malignant gliomas and breast cancer cells [262,263]. These results have shown that PCI has the potential to lower both drug doses and the number of repetitive doses required to achieve sufficient therapeutic effect compared to the single drug dose. Therefore, the toxic side effects of bleomycin can potentially be greatly reduced by using the PCI technique [262]. Altogether, the benefits of PCI with bleomycin encourage further research into bladder cancer treatment.

5. Aims of the study

The use of prodrugs 5-aminolevulinic acid (ALA) and its hexyl ester in bladder diagnosis has stimulated great interest in ALA-PDT clinical trials. However, the number of clinical trials is extremely sparse and PDT has not become widely accepted as a treatment for bladder cancer as yet, demonstrating the need for more studies towards improved strategies.

Based on this purpose, we aimed to:

(1) investigate protein carbonylation, signaling pathways, and biological processes induced/affected by hexyl ALA-PDT, to improve our understanding of biological processes affected by PDT (Paper 1);

(2) study the uptake mechanism of ALA and methyl ALA via the γ-aminobutyric acid (GABA) transporters, searching for a potent pain-reducing strategy for ALA-based PDT (Paper 2);

As a novel drug delivery tool, photochemical internalization (PCI) has the potential to improve the total intravesical therapeutic agent uptake and hence therapeutic efficacy for bladder cancer. Based on this purpose, using a novel photosensitizer $TPCS_{2a}$ (Amphinex®, PCI Biotech AS, Norway), we aimed to:

(3) explore the effect of PCI of the chemotherapeutic agent bleomycin *in vitro* (Paper 3);

(4) establish a research protocol for the photosensitizer $TPCS_{2a}$ in a rat bladder tumor model (Paper 4).

Summary of publications/manuscripts

6. Summary of publications and manuscripts included in the thesis

6.1 Paper 1: Photodynamic therapy with hexyl aminolevulinate induces carbonylation, posttranslational modifications and changed expression of proteins in cell survival and cell death pathways

Yan Baglo, Mirta M. L. Sousa, Geir Slupphaug, Lars Hagen, Sissel Håvåg, Linda Helander, Kamila A. Zub, Hans E. Krokan and Odrun A. Gederaas*

Journal of Photochemical & Photobiological Sciences, 2011

In this study, we examined protein expression levels, post-translational modifications, and protein carbonylation in rat bladder cells (AY-27) after PDT mediated by hexyl 5-aminolevulinic acid (HAL) and blue light (435 nm).

Modern proteomic methods, including immunoprecipitation, two-dimensional difference gel electrophoresis (2D-DIGE), two-dimensional gel electrophoresis (2D-GE), and mass spectrometry (MS), were used in this study (Figure 10). We obtained proteomic maps of AY-27 cells and identified 40 proteins and 10 carbonylated proteins with altered protein expression and/or modification at 2h post-PDT. These proteins were associated with cellular cytoskeleton, transport, oxidative stress response, protein biosynthesis and stability, and DNA repair. The results indicate that HAL-mediated PDT triggers a complex cellular response involving several important biological pathways, such as cell motility, energy metabolism, and signaling pathways for survival and cell death.

This study has extended our understanding of the clinical effects associated with ALA-based PDT, and may pave the way for potential new adjuvant drugs or for targeted use of other treatment modalities.

Remarks:
The work on identification of 40 proteins with altered protein expression (Figure 1-3) was included in the master degree of the candidate. The work on identification of 10 carbonylated proteins and protocol development, classification of 50 identified proteins, pathways affected by PDT, and article writing has only been included in the doctoral degree of the candidate.

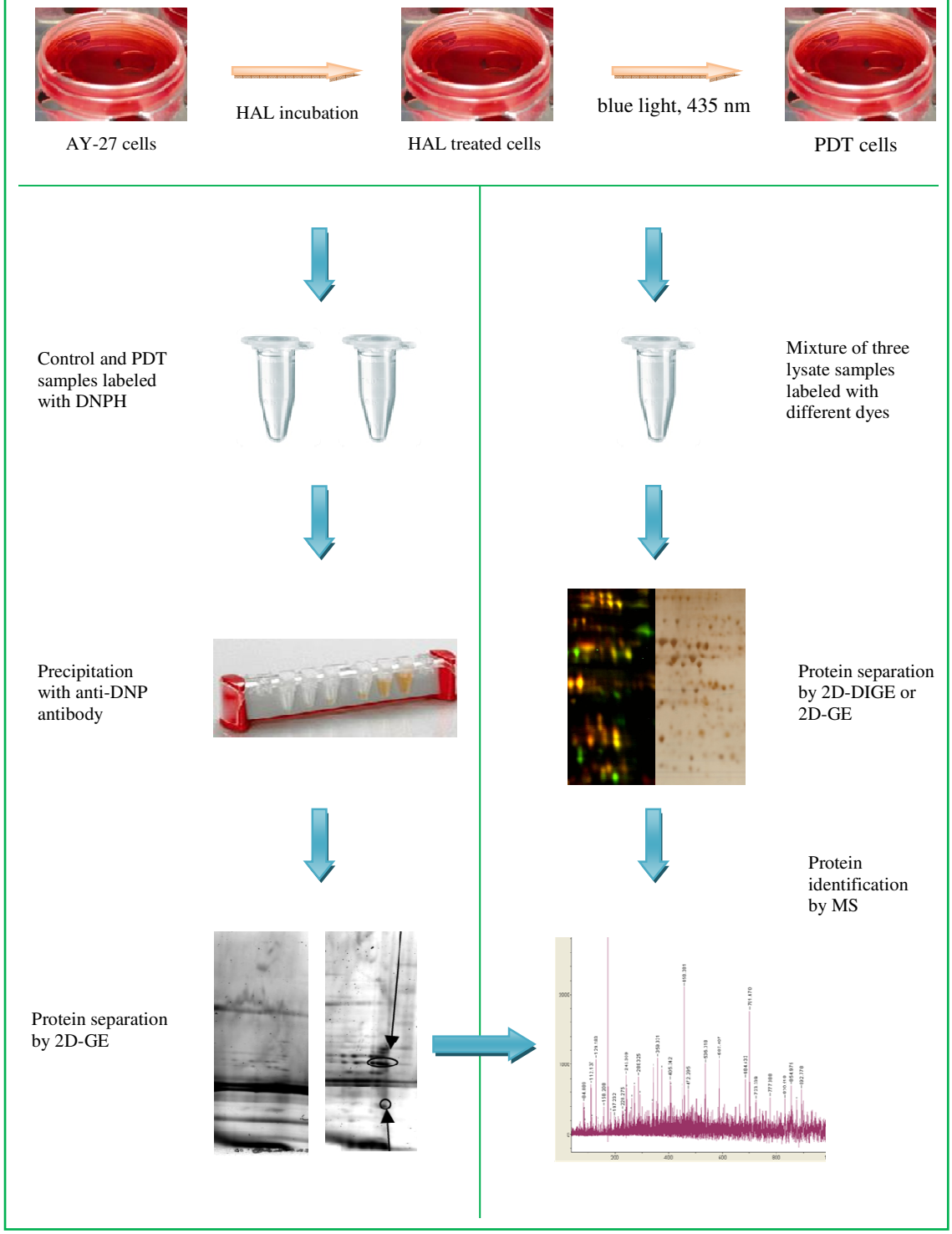

Figure 10. Outline of the experiments of paper 1

6.2 Paper 2: Homology modeling of human γ-butyric acid transporters and the binding of pro-drugs 5- aminolevulinic acid and methyl aminolevulinic acid used in photodynamic therapy

Yan Baglo, Mari Gabrielsen, Ingebrigt Sylte and Odrun A. Gederaas*

Journal of PLOS ONE, 2013

In this study a novel structure-based approach, homology modeling and molecular docking, was employed to investigate the uptake of ALA and MAL via GABA transporters (GATs). We constructed *in silico* models of four human GAT subtypes (GAT-1, GAT-2, GAT-3, and BGT-1) using three x-ray crystal structures of the homologous leucine transporter (LeuT) as templates. The LeuT crystal structures are available in outward-occluded, inward- and outward-open conformations. Homology modeling and docking was performed using ICM software version 3.7 (www.molsoft.com). The alignment was adjusted according to the comprehensive alignment of prokaryotic and eukaryotic NSS transporter sequences published by Beuming *et al*. [264]. After construction, the models were energy refined and quality checked using the programs PROCHECK, ERRAT and VERIFY-3D (http://nihserver.mbi.ucla.edu/SAVES/).

Binding of the native substrate GABA and the possible substrates ALA and MAL was investigated by molecular docking of the ligands into the central putative substrate binding sites in the evaluated outward-occluded GAT models. Electrostatic potentials (ESPs) of the putative substrate translocation pathway of each subtype were calculated using the outward-open and inward-open homology models. The outline of the experiment is show in Figure 11.

Our results suggest that ALA is a substrate of all four GATs and that MAL is a substrate of GAT-2, GAT-3 and BGT-1, based on docking scores and the calculation of the ESPs. Uptake via GATs into peripheral sensory nerve endings may also account for one of the few adverse side effects of ALA-based PDT, namely pain. In addition, the ESP calculations indicate that differences are likely to exist in the entry pathway of the transporters (i.e. in outward-open conformations). Such differences may be used to search for therapeutic inhibitors that selectively target specific GAT subtypes, and this may be used to reduce ALA- and MAL-induced pain.

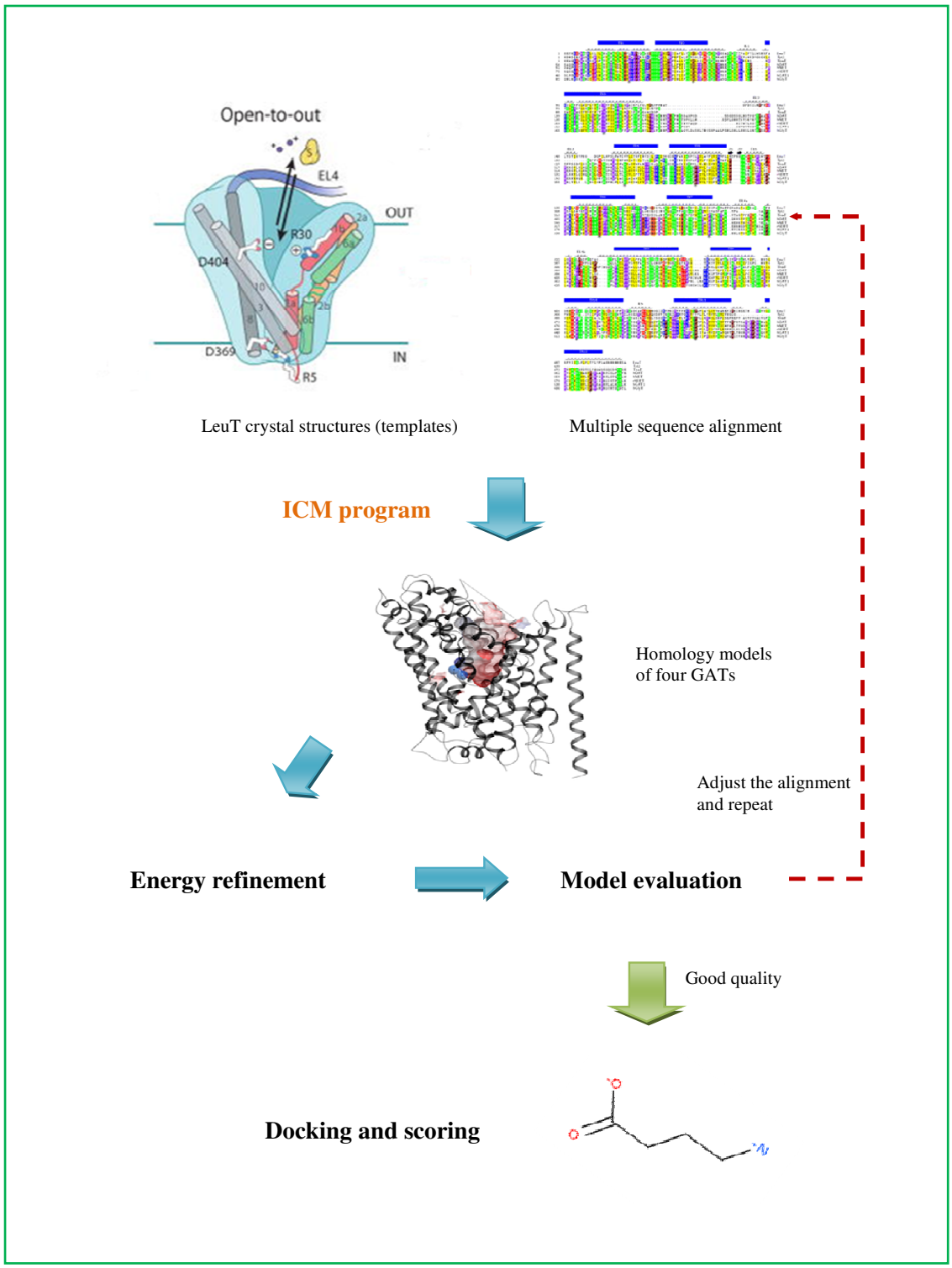

Figure 11. Outline of the experiment of paper 2.

6.3 Paper 3: Enhanced efficacy of bleomycin in bladder cancer cells by photochemical internalization

Yan Baglo*, Lars Hagen, Anders Høgset, Finn Drabløs, Marit Otterlei and Odrun A. Gederaas

Journal of BioMed Research International (submitted)

This work was performed to explore the effect of PCI with bleomycin in bladder cancer cells using the photosensitizer disulfonated tetraphenyl chlorin ($TPCS_{2a}$). Bleomycin is a cytotoxic chemotherapeutic agent widely used in cancer treatment. But its efficacy in bladder cancer is low, possibly due to limited cellular internalization. We investigated cellular sensitivity to photosensitizer uptake, bleomycin and photodynamic dose, and DNA repair capacity by fluorescence measurement, resazurin survival assay, and comet assay, respectively, in three cell lines (Table 3, Figure 12). The results showed that PCI enhanced bleomycin cytotoxicity up to 20% independent of cell type, and elevated bleomycin-induced DNA damage levels in all three cell lines. We further explored two additional strategies to enhance the PCI-bleomycin effect. One strategy was to impair DNA damage responses using the peptide ATX-101. The other was to inhibit activity of bleomycin hydrolase using the protease inhibitor E-64. The results showed that ATX-101 enhanced the PCI-bleomycin efficacy with 14.7%, 30.5%, and 20.7% in A431, T24, and AY-27 cells respectively, whereas E-64 did not have a similar effect.

Table 3. Cellular responses to bleomycin treatment and photodynamic treatment

Cellular response	AY-27	T24	A431
$TPCS_{2a}$ uptake	low	low	high
Sensitivity to light	strong	weak	middle
Sensitivity to bleomycin	low	middle	high
DNA damage repair	high	low	middle
BLMH expression	high	low	low

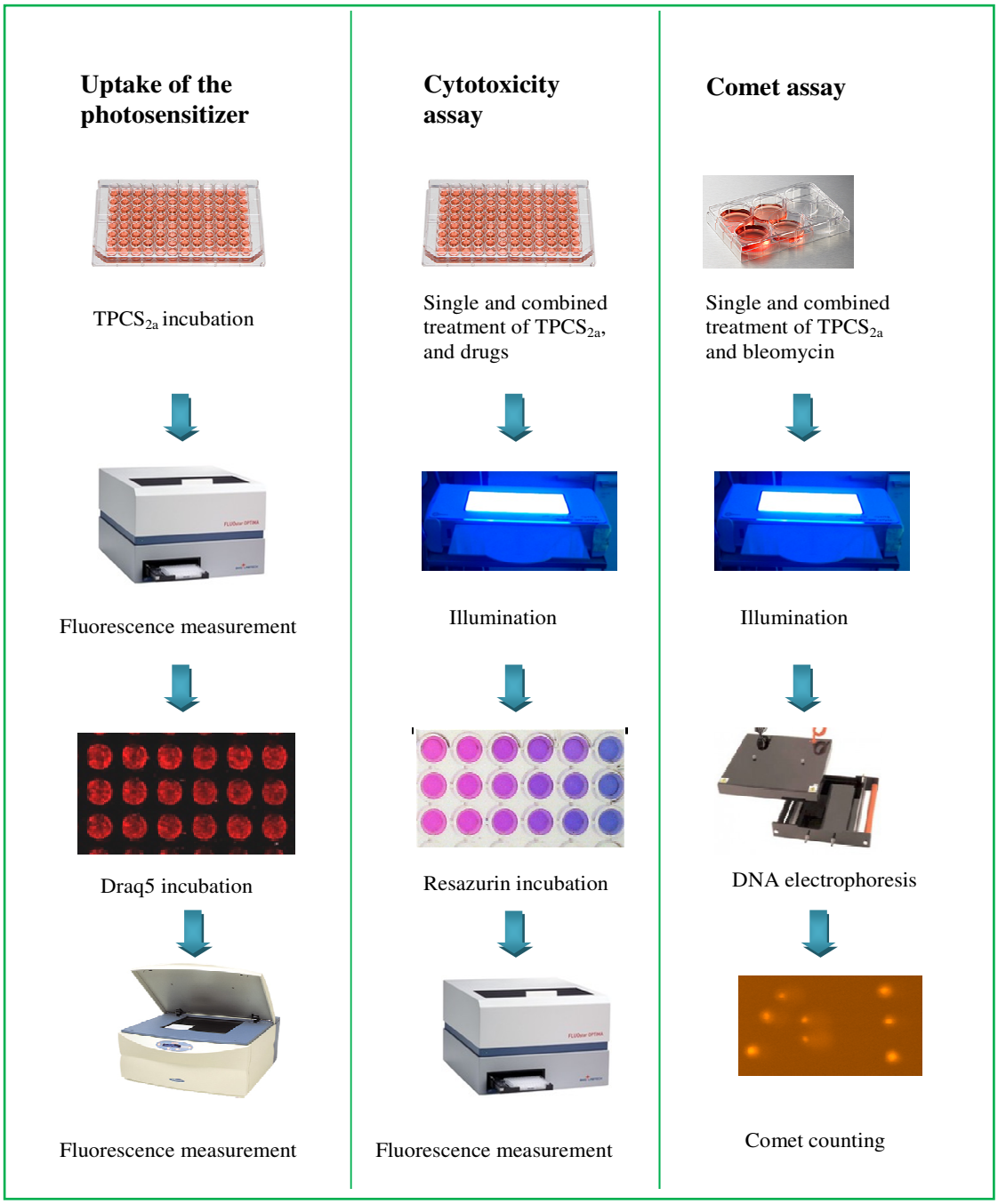

Figure 12. Outline of the main experiments of paper 3.

6.4 Paper 4: Studies of the photosensitizer disulfonated meso-tetraphenyl chlorin in an orthotopic rat bladder tumor model

Yan Baglo*, Qian Peng, Lars Hagen, Kristian Berg, Anders Høgset, Finn Drabløs, and Odrun A. Gederaas

Journal of Photodiagnosis and Photodynamic Therapy (manuscript)

In this study, patterns of uptake, retention and localization of the photosensitizer disulfonated tetraphenyl chlorin ($TPCS_{2a}$) were explored to establish a protocol with $TPCS_{2a}$ in an orthotopic rat bladder tumor model. AY-27 transitional carcinoma cells were intravesically inoculated in rat bladder. Two weeks later, the photosensitizer $TPCS_{2a}$ was intravesically instilled at different concentrations to determine an optimal concentration by *ex vivo* fluorescence measurement. This measurement was performed from bladder inner wall in tumor node(s) after bladder dissection as described by Gederaas *et al.* [261]. With this optimal concentration of $TPCS_{2a}$, bladders were excised at different times to determine an optimal $TPCS_{2a}$-to-light time interval by *ex vivo* fluorescence measurement. The tissue retentive $TPCS_{2a}$ was activated by red light (652 nm, 0.5 J/cm^2) under the presumed optimal protocol determined by fluorescence measurement (3 mg/ml $TPCS_{2a}$ and $TPCS_{2a}$-to-light time interval of 24 h) in the rat bladder tumor model (Figure 13). Necrotic area induced was histologically examined. The results obtained from both fluorescence microscopes and histological examination of the necrotic area showed that the location and penetration of $TPCS_{2a}$ was superficial in the mucosal layer of the bladder wall. The retentive $TPCS_{2a}$ was maximal at 24 h, eliminated thereafter and cleared from the tissue after 72 h.

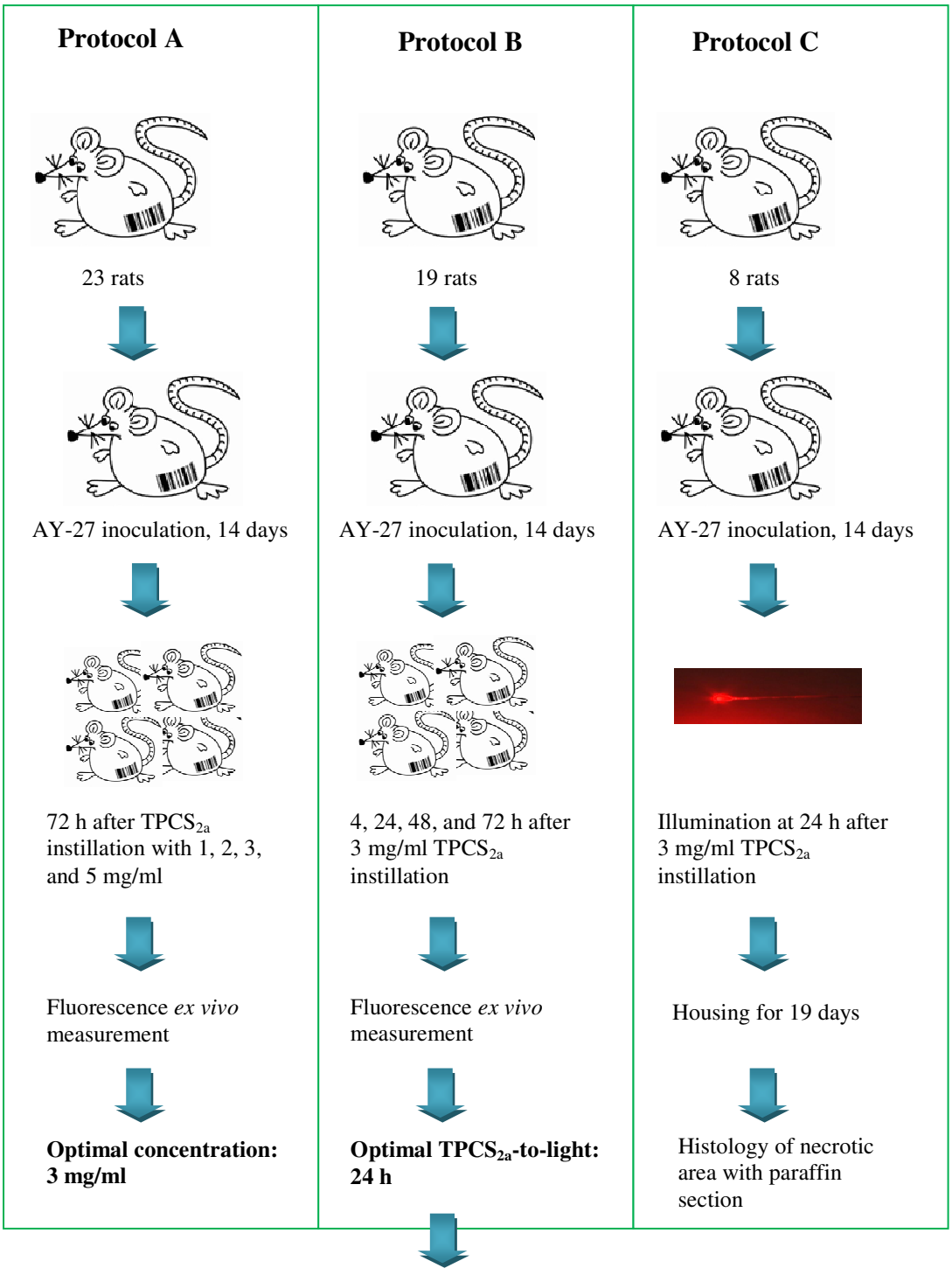

Figure 13. Outline of the experiments of paper 4.

Discussion

This thesis describes preclinical studies of the treatment effects of bladder cancer. This is done at the level of molecules and proteins using photodynamic therapy (PDT) with prodrugs including 5-aminolevulinic acid (ALA) and its esters, and at the level of cells and tissue using photochemical internalization (PCI) of the chemotherapeutic agent bleomycin mediated by the photosensitizer disulfonated tetraphenyl chlorin ($TPCS_{2a}$).

7. PDT for bladder cancer

7.1 Differential protein expression and modifications induced by HAL-PDT

The presence of carbonyl groups is the most widely used marker for oxidative damage to proteins. PDT triggers a sequence of photochemical reactions in photosensitized cells producing high level of reactive oxygen species (ROS) and radicals. Cellular antioxidant mechanisms are apparently overloaded leading to ROS-induced protein modifications and dysfunction, and this eventually affects pathways resulting in cell death [126].

At the molecular level, genes and their products (proteins) have been observed to be either up-regulated or down-regulated after ALA-PDT in human A431 skin cancer cells. This was observed by Verwanger *et al.* and Ruhdorfer *et al*. using cDNA arrays, identifying genes involved in cell proliferation, stress responses, apoptosis and cell adhesion [129,132]. Recently, Demyanenko *et al.* evaluated 112 proteins associated with epigenetic regulation in mouse brain tumor after ALA-PDT, using proteomic antibody microarrays. The PDT alters expression of proteins involved in epigenetic regulation of transcription, histone modification, DNA repair, nuclear protein import, and proliferation [265]. By using modern proteomic methods of 2D-DIGE and MS, we have obtained differential proteomic maps of protein pI-shift induced by HAL-PDT in AY-27 rat bladder cancer cells, and identified 40 proteins from the maps. Further study on the proteins with acidic pI-shift indicated that alternative oxidations such as cysteine sulfinic acid, or secondary enzymatic modifications such as phosphorylation, may be present. In contrast, carbonylation does not mediate a change in pI, which is one of the most used markers for oxidative damage to proteins. Elevation in the total level of protein carbonyls after PDT has previously been documented by Magi *et al.* and Kirdaite *et al.* [266,267]. In order to identify proteins modified by carbonylation after PDT in our study, we developed a protocol of labeling carbonylated proteins with 2,4-dinitrophenyl hydrazine (DNPH) after PDT. Control and PDT samples were derivatized

with DNPH and immunoprecipitated using an anti-DNP antibody prior to separation by 2D-GE and identification by MS. Nine proteins were identify with increased carbonylation and one protein with reduced carbonylation.

We classified the identified proteins by cellular localization demonstrating that the majority of the modified proteins by HAL-PDT were from mitochondria, ER and membranes where the endogenous photosensitizer protoporphyrin IX (PpIX) is synthesized or accumulated. This indicates that these cellular compartments are major targets for HAL-PDT. Although nuclear localization of PpIX has not been observed, we found that several cytoplasmic and nuclear proteins were shown to be affected, likely caused by indirect oxidation or intracellular translocation subsequent to HAL-PDT.

Overall, our results indicate that HAL-mediated PDT triggers a complex cellular response involving several biological pathways. This study has extended our understanding of PDT effects at the protein level. Our findings are relevant for the elucidation of mechanisms modulated by PDT, paving the way to improved clinical PDT efficacy.

The proteomic methods used in this study will not detect proteins at very low concentration, due to the presence of more highly abundant proteins. However, we can use an enrichment strategy with removal of known abundant proteins, or a more specific strategy with immunoprecipitation of a protein of interest from a large amount of lysate. Another suggestion for future work is to repeat the study with a photosensitizer for PCI in order to explore differences between PDT and PCI effects at the protein level.

7.2 The transport of ALA and MAL via human γ-butyric acid transporters

Previous *in vitro* studies have indicated that 5-aminolevulinic acid (ALA) is a substrate for human γ-butyric acid (GABA) transporters (GATs), while its methyl ester MAL is more ambiguous, as this compound seemingly is transported via GAT in some cell types, but not in others [91,92,94,95,268]. Our *in silico* results suggest that ALA is a substrate of all four GATs and that MAL is a substrate of GAT-2, GAT-3 and BGT-1, based on structural analysis of ligand-protein interactions. However, further studies are needed to verify these findings, such as molecular dynamics simulations or wet-lab experiments.

The GATs play an essential role in regulating neurotransmitter signaling and homeostasis by mediating uptake of released GABA from the extracellular space into neurons and glial cells. For ALA-based PDT, the uptake of ALA or MAL via GAT-2,

GAT-3 and BGT-1 (GAT-1 is only found in CNS) into peripheral sensory nerve endings may account for one of the few adverse side effects, namely pain [155,156]. ALA-based PDT in combination with selective inhibitors of the GATs may be an attractive approach to develop pain-reduce strategy and improve the PDT efficacy in the future.

8. PCI for bladder cancer

8.1 PCI enhances bleomycin effect in bladder cancer cells

To improve the total intravesical agent uptake and hence chemotherapeutic efficacy for non-muscle invasive bladder cancer, various experimental approaches have previously been evaluated, including enhancing the agent delivery to bladder tissue using electromotive therapy, and enhancing cell membrane permeability using intravesical hyperthermia [222,269,270]. In this study we employed a novel drug delivery approach consisting of PCI technique in combination with the chemotherapeutic agent bleomycin in rat and human bladder cancer cells (AY-27 and T24 cell lines). Although bleomycin has not shown good clinic efficacy in bladder cancer [271,272,273], we demonstrate that PCI enhances the bleomycin effect *in vitro*, in agreement with a related study reported by Arentsen *et al*. [236]. We further show that PCI elevates bleomycin-induced DNA damage levels in all three cell lines, strongly suggesting that more bleomycin molecules entered the nuclei compared to treatment with bleomycin as a single agent. Thus, the membrane barrier seemed to be bypassed by bleomycin when using the PCI technique.

8.2 Combination strategy of PCI, bleomycin, and an inhibitor of DNA repair

The membrane barrier, degradation by bleomycin hydrolase (BLMH), and elevated DNA repair capacity in cells are considered as main factors towards bleomycin resistance in cells lines with low bleomycin effect [274,275,276]. We demonstrated that a novel peptide drug ATX-101 increases bleomycin efficacy by impairing DNA repair response in treated cells, strongly suggesting that the cellular DNA repair capacity is a crucial factor of bleomycin efficacy. The combination of $TPCS_{2a}$, blue light, bleomycin, and ATX-101 dose used has no or low toxicity, but reaches a promising therapeutic effect in bladder cancer cell lines AY-27 and T24. This shows a potential for reducing possible side effects of bleomycin at high dose in clinical application.

8.3 Studies of $TPCS_{2a}$ in an orthotopic rat bladder tumor model

The photosensitizer $TPCS_{2a}$ displays a superficial distribution pattern in bladder tumor tissue. This may be due to AY-27 cells having low ability to take up the photosensitizer. The retentive $TPCS_{2a}$ is almost cleared from the tumor tissue at 72 hours after instillation. Based on fluorescence measurement of the tissue retentive $TPCS_{2a}$, an optimal $TPCS_{2a}$ protocol has been achieved, including a 24-hour $TPCS_{2a}$-to-light time interval and a dose of 3 mg/ml $TPCS_{2a}$. This protocol will be utilized for further *in vivo* studies of PCI-enhanced therapeutic effects on non-muscle invasive bladder cancer, using a potent chemotherapeutic under an optimal light dose.

As the location and penetration of $TPCS_{2a}$ are shown to be superficial in the rat bladder tumor model, further studies on improvement of tissue penetration of $TPCS_{2a}$ and optimization of light dose are required.

Conclusions

This project has been a preclinical study of PDT/PCI-based treatment effects, with focus on bladder cancer.

1. The state-of-the-art proteomic experiments outlined may be a useful tool for the study of treatment effects on proteins and associated signaling pathways. Our findings provide an overview of biological effects at the protein level after HAL-PDT in rat AY-27 bladder cancer cells, and supplement our understanding of the mechanisms of PDT action.

2. The homology models of GABA transporters (GATs) presented here may provide an important tool for designing potential therapeutic inhibitors for handling treatment effects related to the transporters. For ALA/MAL-PDT, these models may provide future druggability for a pain-reduce strategy based on our findings that ALA/MAL is a potential substrate for the GATs.

3. The observations presented in this thesis indicate that more bleomycin molecules enter the nuclei when using the PCI technique and that the cellular DNA repair capacity is a crucial factor of the PCI-bleomycin efficacy. This study gives basis for a promising combined strategy of PCI-bleomycin and ATX-101 (a peptide inhibitor of DNA repair) in future animal and clinical studies.

4. The orthotopic rat bladder tumor model is a good model for studying enhanced bleomycin treatment of bladder cancer by PCI. This work has developed important parts of a novel and practical protocol for $TPCS_{2a}$-PCI in the animal model. Importantly, the histological findings of superficial distribution of the photosensitizer $TPCS_{2a}$ show a limitation for the approach. The challenge for future study is how to increase the penetration depth of the photosensitizer in tissue.

In summary, this project has developed a highly useful set of tools for studying the effect of PDT and PCI, in particular on bladder cancer, and application of these tools has both generated novel information, and indicated important challenges for future research.

References

[1] T.J. Dougherty, J.E. Kaufman, A. Goldfarb, K.R. Weishaupt, D. Boyle, A. Mittleman, Photoradiation therapy for the treatment of malignant tumors, Cancer Res 38 (1978) 2628-2635.

[2] M.C. Issa, M. Manela-Azulay, Photodynamic therapy: a review of the literature and image documentation, An Bras Dermatol 85 (2010) 501-511.

[3] M. Firczuk, M. Winiarska, A. Szokalska, M. Jodlowska, M. Swiech, K. Bojarczuk, P. Salwa, D. Nowis, Approaches to improve photodynamic therapy of cancer, Front Biosci (Landmark Ed) 16 (2011) 208-224.

[4] A.P. Castano, P. Mroz, M.R. Hamblin, Photodynamic therapy and anti-tumour immunity, Nat Rev Cancer 6 (2006) 535-545.

[5] A. Juzeniene, Q. Peng, J. Moan, Milestones in the development of photodynamic therapy and fluorescence diagnosis, Photochem Photobiol Sci 6 (2007) 1234-1245.

[6] A. Juzeniene, J. Moan, The history of PDT in Norway: Part II. Recent advances in general PDT and ALA-PDT, Photodiagnosis and Photodynamic Therapy 4 (2007) 80-87.

[7] A. De Rosa, D. Naviglio, A. Di Luccia, Advances in Photodynamic Therapy of Cancer, Current Cancer Therapy Reviews 7 (2011) 234-247.

[8] H. von Tappeiner, A. Jesionek, Therapeutische versuche mit fluoreszierenden stoffen, Muench Med Wochenschr 47 (1903) 2042–2044.

[9] T.J. Dougherty, W.R. Potter, K.R. Weishaupt, The structure of the active component of hematoporphyrin derivative, Prog Clin Biol Res 170 (1984) 301-314.

[10] F.H. Figge, G.S. Weiland, L.O. Manganiello, Cancer detection and therapy; affinity of neoplastic, embryonic, and traumatized tissues for porphyrins and metalloporphyrins, Proc Soc Exp Biol Med 68 (1948) 640.

[11] S. Schwartz, Porphyrins and porphyrin precursors in human and experimental porphyria, Fed Proc 14 (1955) 717-722.

[12] T.J. Dougherty, C.J. Gomer, B.W. Henderson, G. Jori, D. Kessel, M. Korbelik, J. Moan, Q. Peng, Photodynamic therapy, J Natl Cancer Inst 90 (1998) 889-905.

[13] H. Fischer, H. Hilmer, F. Lindner, B. Putzer, Chemische befunde bei einem fall von porphyrie (Petry). , Hoppe-Seyler's Z Physiol Chem 150 (1925) 44-101.

[14] Z. Malik, H. Lugaci, Destruction of erythroleukaemic cells by photoactivation of endogenous porphyrins, Br J Cancer 56 (1987) 589-595.

[15] P. Qian, J.F. Evensen, C. Rimington, J. Moan, A comparison of different photosensitizing dyes with respect to uptake C3H-tumors and tissues of mice, Cancer Letters 36 (1987) 1-10.

[16] J.C. Kennedy, R.H. Pottier, D.C. Pross, Photodynamic therapy with endogenous protoporphyrin IX: basic principles and present clinical experience, J Photochem Photobiol B 6 (1990) 143-148.

[17] J. Moan, K. Berg, E. Kvam, A. Western, Z. Malik, A. Ruck, H. Schneckenburger, Intracellular localization of photosensitizers, Ciba Found Symp 146 (1989) 95-107; discussion 107-111.

[18] K. Berg, J.C. Bommer, J.W. Winkelman, J. Moan, Cellular uptake and relative efficiency in cell inactivation by photoactivated sulfonated meso-tetraphenylporphines, Photochem Photobiol 52 (1990) 775-781.
[19] K. Berg, K. Madslien, J.C. Bommer, R. Oftebro, J.W. Winkelman, J. Moan, Light induced relocalization of sulfonated meso-tetraphenylporphines in NHIK 3025 cells and effects of dose fractionation, Photochem Photobiol 53 (1991) 203-210.
[20] Q. Peng, G.W. Farrants, K. Madslien, J.C. Bommer, J. Moan, H.E. Danielsen, J.M. Nesland, Subcellular localization, redistribution and photobleaching of sulfonated aluminum phthalocyanines in a human melanoma cell line, Int J Cancer 49 (1991) 290-295.
[21] K. Berg, J. Moan, Lysosomes as photochemical targets, Int J Cancer 59 (1994) 814-822.
[22] J. Moan, K. Berg, H. Anholt, K. Madslien, Sulfonated aluminium phthalocyanines as sensitizers for photochemotherapy. Effects of small light doses on localization, dye fluorescence and photosensitivity in V79 cells, Int J Cancer 58 (1994) 865-870.
[23] K. Berg, P.K. Selbo, L. Prasmickaite, T.E. Tjelle, K. Sandvig, J. Moan, G. Gaudernack, O. Fodstad, S. Kjolsrud, H. Anholt, G.H. Rodal, S.K. Rodal, A. Hogset, Photochemical internalization: a novel technology for delivery of macromolecules into cytosol, Cancer Res 59 (1999) 1180-1183.
[24] S.L. Boe, E. Hovig, Enhancing nucleic acid delivery by photochemical internalization, Ther Deliv 4 (2013) 1125-1140.
[25] P.K. Selbo, A. Weyergang, A. Hogset, O.J. Norum, M.B. Berstad, M. Vikdal, K. Berg, Photochemical internalization provides time- and space-controlled endolysosomal escape of therapeutic molecules, J Control Release 148 (2010) 2-12.
[26] A. Weyergang, P.K. Selbo, M.E. Berstad, M. Bostad, K. Berg, Photochemical internalization of tumor-targeted protein toxins, Lasers Surg Med 43 (2011) 721-733.
[27] O.J. Norum, P.K. Selbo, A. Weyergang, K.E. Giercksky, K. Berg, Photochemical internalization (PCI) in cancer therapy: from bench towards bedside medicine, J Photochem Photobiol B 96 (2009) 83-92.
[28] R.R. Allison, K. Moghissi, Photodynamic Therapy (PDT): PDT Mechanisms, Clin Endosc 46 (2013) 24-29.
[29] G. Palumbo, Photodynamic therapy and cancer: a brief sightseeing tour, Expert Opin Drug Deliv 4 (2007) 131-148.
[30] L. Milla Sanabria, M.E. Rodriguez, I.S. Cogno, N.B. Rumie Vittar, M.F. Pansa, M.J. Lamberti, V.A. Rivarola, Direct and indirect photodynamic therapy effects on the cellular and molecular components of the tumor microenvironment, Biochim Biophys Acta 1835 (2013) 36-45.
[31] K. Plaetzer, B. Krammer, J. Berlanda, F. Berr, T. Kiesslich, Photophysics and photochemistry of photodynamic therapy: fundamental aspects, Lasers in Medical Science 24 (2009) 259-268.
[32] E. Reddi, Role of delivery vehicles for photosensitizers in the photodynamic therapy of tumours, J Photochem Photobiol B 37 (1997) 189-195.

[33] G.A. van Dongen, G.W. Visser, M.B. Vrouenraets, Photosensitizer-antibody conjugates for detection and therapy of cancer, Adv Drug Deliv Rev 56 (2004) 31-52.
[34] E.S. Nyman, P.H. Hynninen, Research advances in the use of tetrapyrrolic photosensitizers for photodynamic therapy, J Photochem Photobiol B 73 (2004) 1-28.
[35] Z. Luksiene, Photodynamic therapy: mechanism of action and ways to improve the efficiency of treatment, Medicina (Kaunas) 39 (2003) 1137-1150.
[36] K. Plaetzer, B. Krammer, J. Berlanda, F. Berr, T. Kiesslich, Photophysics and photochemistry of photodynamic therapy: fundamental aspects, Lasers Med Sci 24 (2009) 259-268.
[37] E. Buytaert, M. Dewaele, P. Agostinis, Molecular effectors of multiple cell death pathways initiated by photodynamic therapy, Biochim Biophys Acta 1776 (2007) 86-107.
[38] R.R. Allison, G.H. Downie, R. Cuenca, X.-H. Hu, C.J.H. Childs, C.H. Sibata, Photosensitizers in clinical PDT, Photodiagnosis and Photodynamic Therapy 1 (2004) 27-42.
[39] X. Zheng, J. Morgan, S.K. Pandey, Y. Chen, E. Tracy, H. Baumann, J.R. Missert, C. Batt, J. Jackson, D.A. Bellnier, B.W. Henderson, R.K. Pandey, Conjugation of 2-(1'-hexyloxyethyl)-2-devinylpyropheophorbide-a (HPPH) to carbohydrates changes its subcellular distribution and enhances photodynamic activity in vivo, J Med Chem 52 (2009) 4306-4318.
[40] M.C. Gemert, W.-F. Cheong, A.J. Welch, W. Star, Light delivery for whole-bladder photodynamic therapy, Lasers in Medical Science 2 (1987) 273-284.
[41] A.E. Profio, D.R. Doiron, Dosimetry considerations in phototherapy, Med Phys 8 (1981) 190-196.
[42] H. Barr, S.G. Bown, N. Krasner, P.B. Boulos, Photodynamic therapy for colorectal disease, Int J Colorectal Dis 4 (1989) 15-19.
[43] A.L. Major, G.S. Rose, L.O. Svaasand, F. Ludicke, A. Campana, M.J. van Gemert, Intraperitoneal photodynamic therapy in the Fischer 344 rat using 5-aminolevulinic acid and violet laser light: a toxicity study, J Photochem Photobiol B 66 (2002) 107-114.
[44] A.P. Castano, T.N. Demidova, M.R. Hamblin, Mechanisms in photodynamic therapy: part one—photosensitizers, photochemistry and cellular localization, Photodiagnosis and Photodynamic Therapy 1 (2004) 279-293.
[45] S. Mitra, T.H. Foster, Carbogen breathing significantly enhances the penetration of red light in murine tumours in vivo, Phys Med Biol 49 (2004) 1891-1904.
[46] M. Alexiades-Armenakas, Laser-mediated photodynamic therapy, Clin Dermatol 24 (2006) 16-25.
[47] L. Svaasand, C. Gomer, E. Morinelli, On the physical rationale of laser induced hyperthermia, Lasers in Medical Science 5 (1990) 121-128.
[48] B.W. Henderson, S.M. Waldow, W.R. Potter, T.J. Dougherty, Interaction of photodynamic therapy and hyperthermia: tumor response and cell survival studies after treatment of mice in vivo, Cancer Res 45 (1985) 6071-6077.
[49] L.O. Svaasand, Photodynamic and photohyperthermic response of malignant tumors, Med Phys 12 (1985) 455-461.

[50] M.R. Alexiades-Armenakas, R.G. Geronemus, Laser-mediated photodynamic therapy of actinic keratoses, Arch Dermatol 139 (2003) 1313-1320.
[51] M. Alexiades-Armenakas, Long-pulsed dye laser-mediated photodynamic therapy combined with topical therapy for mild to severe comedonal, inflammatory, or cystic acne, J Drugs Dermatol 5 (2006) 45-55.
[52] L. Brancaleon, H. Moseley, Laser and non-laser light sources for photodynamic therapy, Lasers Med Sci 17 (2002) 173-186.
[53] C. Foote, Definition of Type I and Type II photosensitised oxidation., Photochem Photobiol 54 (1991) 659.
[54] M. Ochsner, Photophysical and photobiological processes in the photodynamic therapy of tumours, J Photochem Photobiol B 39 (1997) 1-18.
[55] S.A. Gorman, S.B. Brown, J. Griffiths, An overview of synthetic approaches to porphyrin, phthalocyanine, and phenothiazine photosensitizers for photodynamic therapy, J Environ Pathol Toxicol Oncol 25 (2006) 79-108.
[56] J. Moan, K. Berg, The photodegradation of porphyrins in cells can be used to estimate the lifetime of singlet oxygen, Photochem Photobiol 53 (1991) 549-553.
[57] U.T. Brunk, H. Dalen, K. Roberg, H.B. Hellquist, Photo-oxidative disruption of lysosomal membranes causes apoptosis of cultured human fibroblasts, Free Radic Biol Med 23 (1997) 616-626.
[58] Q. Peng, J.M. Nesland, Effects of photodynamic therapy on tumor stroma, Ultrastruct Pathol 28 (2004) 333-340.
[59] J. Zhang, J. Liu, Tumor stroma as targets for cancer therapy, Pharmacol Ther 137 (2013) 200-215.
[60] A.R. Azzouzi, E. Barret, C.M. Moore, A. Villers, C. Allen, A. Scherz, G. Muir, M. de Wildt, N.J. Barber, S. Lebdai, M. Emberton, TOOKAD((R)) Soluble vascular-targeted photodynamic (VTP) therapy: determination of optimal treatment conditions and assessment of effects in patients with localised prostate cancer, BJU Int 112 (2013) 766-774.
[61] R. Wormald, J. Evans, L. Smeeth, K. Henshaw, Photodynamic therapy for neovascular age-related macular degeneration, Cochrane Database Syst Rev (2007) Cd002030.
[62] M. Korbelik, J. Sun, Photodynamic therapy-generated vaccine for cancer therapy, Cancer Immunol Immunother 55 (2006) 900-909.
[63] M. Korbelik, Cancer vaccines generated by photodynamic therapy, Photochem Photobiol Sci 10 (2011) 664-669.
[64] S.O. Gollnick, L. Vaughan, B.W. Henderson, Generation of effective antitumor vaccines using photodynamic therapy, Cancer Res 62 (2002) 1604-1608.
[65] M. Hakerud, Y. Waeckerle-Men, P.K. Selbo, T.M. Kundig, A. Hogset, P. Johansen, Intradermal photosensitisation facilitates stimulation of MHC class-I restricted CD8 T-cell responses of co-administered antigen, J Control Release 174C (2013) 143-150.
[66] K. Plaetzer, M. Pichler, D. Neureiter, N. Tortik, T. Kiesslich, Apoptosis in cancer cells induced by photodynamic treatment – a methodological approach, Journal of Porphyrins and Phthalocyanines 17 (2013) 197-209.
[67] D. Kessel, M.G. Vicente, J.J. Reiners, Jr., Initiation of apoptosis and autophagy by photodynamic therapy, Autophagy 2 (2006) 289-290.

[68] Y. Luo, D. Kessel, Initiation of apoptosis versus necrosis by photodynamic therapy with chloroaluminum phthalocyanine, Photochem Photobiol 66 (1997) 479-483.
[69] D. Kessel, J.J. Reiners, Jr., Apoptosis and autophagy after mitochondrial or endoplasmic reticulum photodamage, Photochem Photobiol 83 (2007) 1024-1028.
[70] J.O. Yoo, Y.C. Lim, Y.M. Kim, K.S. Ha, Differential cytotoxic responses to low- and high-dose photodynamic therapy in human gastric and bladder cancer cells, J Cell Biochem 112 (2011) 3061-3071.
[71] C.J. Gomer, M. Luna, A. Ferrario, S. Wong, A.M. Fisher, N. Rucker, Cellular targets and molecular responses associated with photodynamic therapy, J Clin Laser Med Surg 14 (1996) 315-321.
[72] L. Li, G. Ishdorj, S.B. Gibson, Reactive oxygen species regulation of autophagy in cancer: implications for cancer treatment, Free Radic Biol Med 53 (2012) 1399-1410.
[73] A. Casas, G. Di Venosa, T. Hasan, B. Al, Mechanisms of resistance to photodynamic therapy, Curr Med Chem 18 (2011) 2486-2515.
[74] B.W. Henderson, A.C. Miller, Effects of scavengers of reactive oxygen and radical species on cell survival following photodynamic treatment in vitro: comparison to ionizing radiation, Radiat Res 108 (1986) 196-205.
[75] C.J. Gomer, S.W. Ryter, A. Ferrario, N. Rucker, S. Wong, A.M. Fisher, Photodynamic therapy-mediated oxidative stress can induce expression of heat shock proteins, Cancer Res 56 (1996) 2355-2360.
[76] C.J. Schofield, P.J. Ratcliffe, Signalling hypoxia by HIF hydroxylases, Biochem Biophys Res Commun 338 (2005) 617-626.
[77] X.H. Ma, S. Piao, D. Wang, Q.W. McAfee, K.L. Nathanson, J.J. Lum, L.Z. Li, R.K. Amaravadi, Measurements of tumor cell autophagy predict invasiveness, resistance to chemotherapy, and survival in melanoma, Clin Cancer Res 17 (2011) 3478-3489.
[78] M. Valko, C.J. Rhodes, J. Moncol, M. Izakovic, M. Mazur, Free radicals, metals and antioxidants in oxidative stress-induced cancer, Chem Biol Interact 160 (2006) 1-40.
[79] A. Weyergang, P.K. Selbo, K. Berg, Sustained ERK [corrected] inhibition by EGFR targeting therapies is a predictive factor for synergistic cytotoxicity with PDT as neoadjuvant therapy, Biochim Biophys Acta 1830 (2013) 2659-2670.
[80] C.E. Olsen, K. Berg, P.K. Selbo, A. Weyergang, Circumvention of resistance to photodynamic therapy in doxorubicin-resistant sarcoma by photochemical internalization of gelonin, Free Radic Biol Med 65C (2013) 1300-1309.
[81] M.R. Saboktakin, R.M. Tabatabaee, The novel polymeric systems for photodynamic therapy technique, Int J Biol Macromol 65c (2014) 398-414.
[82] U. Sunar, Monitoring photodynamic therapy of head and neck malignancies with optical spectroscopies, World J Clin Cases 1 (2013) 96-105.
[83] S. Pervaiz, M. Olivo, Art and science of photodynamic therapy, Clin Exp Pharmacol Physiol 33 (2006) 551-556.
[84] M. Wachowska, A. Muchowicz, M. Firczuk, M. Gabrysiak, M. Winiarska, M. Wańczyk, K. Bojarczuk, J. Golab, Aminolevulinic Acid (ALA) as a Prodrug in Photodynamic Therapy of Cancer, Molecules 16 (2011) 4140-4164.

[85] A. Godal, N.O. Nilsen, J. Klaveness, J.E. Branden, J.M. Nesland, Q. Peng, New derivatives of 5-aminolevulinic acid for photodynamic therapy: chemical synthesis and porphyrin production in in vitro and in vivo biological systems, J Environ Pathol Toxicol Oncol 25 (2006) 109-126.
[86] P.G. Calzavara-Pinton, M. Venturini, R. Sala, Photodynamic therapy: update 2006. Part 1: Photochemistry and photobiology, J Eur Acad Dermatol Venereol 21 (2007) 293-302.
[87] A. Marti, P. Jichlinski, N. Lange, J.P. Ballini, L. Guillou, H.J. Leisinger, P. Kucera, Comparison of aminolevulinic acid and hexylester aminolevulinate induced protoporphyrin IX distribution in human bladder cancer, J Urol 170 (2003) 428-432.
[88] D.I. Morrow, P.A. McCarron, A.D. Woolfson, P. Juzenas, A. Juzeniene, V. Iani, J. Moan, R.F. Donnelly, Hexyl aminolaevulinate is a more effective topical photosensitiser precursor than methyl aminolaevulinate and 5-aminolaevulinic acids when applied in equimolar doses, J Pharm Sci 99 (2010) 3486-3498.
[89] J.M. Gaullier, K. Berg, Q. Peng, H. Anholt, P.K. Selbo, L.W. Ma, J. Moan, Use of 5-aminolevulinic acid esters to improve photodynamic therapy on cells in culture, Cancer Res 57 (1997) 1481-1486.
[90] L.B. Josefsen, R.W. Boyle, Photodynamic therapy and the development of metal-based photosensitisers, Met Based Drugs 2008 (2008) 276109.
[91] R. Schulten, B. Novak, B. Schmitz, H. Lubbert, Comparison of the uptake of 5-aminolevulinic acid and its methyl ester in keratinocytes and skin, Naunyn Schmiedebergs Arch Pharmacol 385 (2012) 969-979.
[92] E. Rud, O. Gederaas, A. Hogset, K. Berg, 5-aminolevulinic acid, but not 5-aminolevulinic acid esters, is transported into adenocarcinoma cells by system BETA transporters, Photochem Photobiol 71 (2000) 640-647.
[93] O.A. Gederaas, A. Holroyd, S.B. Brown, D. Vernon, J. Moan, K. Berg, 5-Aminolaevulinic acid methyl ester transport on amino acid carriers in a human colon adenocarcinoma cell line, Photochem Photobiol 73 (2001) 164-169.
[94] B. Novak, R. Schulten, H. Lubbert, delta-Aminolevulinic acid and its methyl ester induce the formation of Protoporphyrin IX in cultured sensory neurones, Naunyn Schmiedebergs Arch Pharmacol 384 (2011) 583-602.
[95] L. Rodriguez, A. Batlle, G. Di Venosa, S. Battah, P. Dobbin, A.J. Macrobert, A. Casas, Mechanisms of 5-aminolevulinic acid ester uptake in mammalian cells, Br J Pharmacol 147 (2006) 825-833.
[96] Y. Baglo, M. Gabrielsen, I. Sylte, O.A. Gederaas, Homology modeling of human gamma-butyric acid transporters and the binding of pro-drugs 5-aminolevulinic acid and methyl aminolevulinic acid used in photodynamic therapy, PLoS One 8 (2013) e65200.
[97] A.E. O'Connor, W.M. Gallagher, A.T. Byrne, Porphyrin and nonporphyrin photosensitizers in oncology: preclinical and clinical advances in photodynamic therapy, Photochem Photobiol 85 (2009) 1053-1074.
[98] M.R. Moore, P.B. Disler, Chemistry and biochemistry of the porphyrins and porphyrias, Clin Dermatol 3 (1985) 7-23.
[99] A. Neuberger, J.J. Scott, L. Shuster, Synthesis and metabolism of some substances related to delta -aminolaevulic acid, Biochem J 64 (1956) 137-145.

[100] N. Navone, R.E. Frisardi, A. Batlle, C. Polo, Porphyrin biosynthesis in human breast cancer. Preliminary mimetic in vitro studies., Med Sci Res. 16 (1988) 61-62.
[101] J.C. Kennedy, S.L. Marcus, R.H. Pottier, Photodynamic therapy (PDT) and photodiagnosis (PD) using endogenous photosensitization induced by 5-aminolevulinic acid (ALA): mechanisms and clinical results, J Clin Laser Med Surg 14 (1996) 289-304.
[102] Q. Peng, K. Berg, J. Moan, M. Kongshaug, J.M. Nesland, 5-Aminolevulinic acid-based photodynamic therapy: principles and experimental research, Photochem Photobiol 65 (1997) 235-251.
[103] E.L. Larsen, L.L. Randeberg, O.A. Gederaas, C.J. Arum, A. Hjelde, C.M. Zhao, D. Chen, H.E. Krokan, L.O. Svaasand, Monitoring of hexyl 5-aminolevulinate-induced photodynamic therapy in rat bladder cancer by optical spectroscopy, J Biomed Opt 13 (2008) 044031.
[104] H. Messmann, 5-Aminolevulinic acid-induced protoporphyrin IX for the detection of gastrointestinal dysplasia, Gastrointest Endosc Clin N Am 10 (2000) 497-512.
[105] R.M. Szeimies, M. Landthaler, Photodynamic therapy and fluorescence diagnosis of skin cancers, Recent Results Cancer Res 160 (2002) 240-245.
[106] J.E. Frampton, G.L. Plosker, Hexyl aminolevulinate: in the detection of bladder cancer, Drugs 66 (2006) 571-578; discussion 579-580.
[107] A. Nabavi, H. Thurm, B. Zountsas, T. Pietsch, H. Lanfermann, U. Pichlmeier, M. Mehdorn, Five-aminolevulinic acid for fluorescence-guided resection of recurrent malignant gliomas: a phase ii study, Neurosurgery 65 (2009) 1070-1076; discussion 1076-1077.
[108] S. Collaud, A. Juzeniene, J. Moan, N. Lange, On the selectivity of 5-aminolevulinic acid-induced protoporphyrin IX formation, Curr Med Chem Anticancer Agents 4 (2004) 301-316.
[109] E. Rossi, K.A. Costin, P. Garcia-Webb, Ferrochelatase activity in human lymphocytes, as quantified by a new high-performance liquid-chromatographic method, Clin Chem 34 (1988) 2481-2485.
[110] R.S. Ajioka, J.D. Phillips, J.P. Kushner, Biosynthesis of heme in mammals, Biochim Biophys Acta 1763 (2006) 723-736.
[111] G. Di Venosa, H. Fukuda, A. Batlle, A. Macrobert, A. Casas, Photodynamic therapy: regulation of porphyrin synthesis and hydrolysis from ALA esters, J Photochem Photobiol B 83 (2006) 129-136.
[112] N. Schoenfeld, O. Epstein, M. Lahav, R. Mamet, M. Shaklai, A. Atsmon, The heme biosynthetic pathway in lymphocytes of patients with malignant lymphoproliferative disorders, Cancer Lett 43 (1988) 43-48.
[113] N. Schoenfeld, R. Mamet, O. Epstein, M. Lahav, Y. Lurie, A. Atsmon, The heme biosynthetic pathway in the regenerating rat liver. The relation between enzymes of heme synthesis and growth, Eur J Biochem 166 (1987) 663-666.
[114] M.A. Sari, J.P. Battioni, D. Mansuy, J.B. Le Pecq, Mode of interaction and apparent binding constants of meso-tetraaryl porphyrins bearing between one and four positive charges with DNA, Biochem Biophys Res Commun 141 (1986) 643-649.

[115] M. Lahav, O. Epstein, N. Schoenfeld, M. Shaklai, A. Atsmon, Increased porphobilinogen deaminase activity in patients with malignant lymphoproliferative diseases. A helpful diagnostic test, JAMA 257 (1987) 39-42.
[116] S.L. Gibson, D.J. Cupriks, J.J. Havens, M.L. Nguyen, R. Hilf, A regulatory role for porphobilinogen deaminase (PBGD) in delta-aminolaevulinic acid (delta-ALA)-induced photosensitization?, Br J Cancer 77 (1998) 235-242.
[117] K. Inoue, T. Karashima, M. Kamada, T. Shuin, A. Kurabayashi, M. Furihata, H. Fujita, K. Utsumi, J. Sasaki, Regulation of 5-aminolevulinic acid-mediated protoporphyrin IX accumulation in human urothelial carcinomas, Pathobiology 76 (2009) 303-314.
[118] C. Fuchs, R. Riesenberg, J. Siegert, R. Baumgartner, H-dependent formation of 5-aminolaevulinic acid-induced protoporphyrin IX in fibrosarcoma cells, J Photochem Photobiol B 40 (1997) 49-54.
[119] B. Ortel, N. Chen, J. Brissette, G.P. Dotto, E. Maytin, T. Hasan, Differentiation-specific increase in ALA-induced protoporphyrin IX accumulation in primary mouse keratinocytes, Br J Cancer 77 (1998) 1744-1751.
[120] B. Krammer, K. Uberriegler, In-vitro investigation of ALA-induced protoporphyrin IX, J Photochem Photobiol B 36 (1996) 121-126.
[121] Z. Malik, M. Dishi, Y. Garini, Fourier transform multipixel spectroscopy and spectral imaging of protoporphyrin in single melanoma cells, Photochem Photobiol 63 (1996) 608-614.
[122] J.M. Gaullier, M. Geze, R. Santus, T. Sa e Melo, J.C. Maziere, M. Bazin, P. Morliere, L. Dubertret, Subcellular localization of and photosensitization by protoporphyrin IXhuman keratinocytes and fibroblasts cultivated with 5-aminolevulinic acid, Photochem Photobiol 62 (1995) 114-122.
[123] R. Sroka, R. Baumgartner, A. Buser, C. Ell, D. Jocham, E. Unsoeld, Laser assisted detection of endogenous porphyrins in malignant disease, , SPIE Proceedings of physiological monitoring and early detection diagnostic methods, Bellingham, Washington 1641 (1992) 99-106.
[124] K. Konig, H. Schneckenburger, A. Ruck, R. Steiner, In vivo photoproduct formation during PDT with ALA-induced endogenous porphyrins, J Photochem Photobiol B 18 (1993) 287-290.
[125] N. Fotinos, M.A. Campo, F. Popowycz, R. Gurny, N. Lange, 5-Aminolevulinic acid derivatives in photomedicine: Characteristics, application and perspectives, Photochem Photobiol 82 (2006) 994-1015.
[126] K. England, T.G. Cotter, Direct oxidative modifications of signalling proteins in mammalian cells and their effects on apoptosis, Redox Rep 10 (2005) 237-245.
[127] E.R. Stadtman, R.L. Levine, Protein oxidation, Ann N Y Acad Sci 899 (2000) 191-208.
[128] I. Dalle-Donne, M. Carini, M. Orioli, G. Vistoli, L. Regazzoni, G. Colombo, R. Rossi, A. Milzani, G. Aldini, Protein carbonylation: 2,4-dinitrophenylhydrazine reacts with both aldehydes/ketones and sulfenic acids, Free Radic Biol Med 46 (2009) 1411-1419.
[129] T. Verwanger, R. Sanovic, F. Aberger, A.M. Frischauf, B. Krammer, Gene expression pattern following photodynamic treatment of the carcinoma cell line A-431 analysed by cDNA arrays, Int J Oncol 21 (2002) 1353-1359.

[130] T. Verwanger, G. Schnitzhofer, B. Krammer, Expression kinetics of the (proto) oncogenes c-myc and bcl-2 following photodynamic treatment of normal and transformed human fibroblasts with 5-aminolaevulinic acid-stimulated endogenous protoporphyrin IX, J Photochem Photobiol B 45 (1998) 131-135.
[131] L.O. Klotz, C. Fritsch, K. Briviba, N. Tsacmacidis, F. Schliess, H. Sies, Activation of JNK and p38 but not ERK MAP kinases in human skin cells by 5-aminolevulinate-photodynamic therapy, Cancer Res 58 (1998) 4297-4300.
[132] S. Ruhdorfer, R. Sanovic, V. Sander, B. Krammer, T. Verwanger, Gene expression profiling of the human carcinoma cell line A-431 after 5-aminolevulinic acid-based photodynamic treatment, Int J Oncol 30 (2007) 1253-1262.
[133] K. Kuzelova, D. Grebenova, M. Pluskalova, I. Marinov, Z. Hrkal, Early apoptotic features of K562 cell death induced by 5-aminolaevulinic acid-based photodynamic therapy, J Photochem Photobiol B 73 (2004) 67-78.
[134] D. Grebenova, K. Kuzelova, K. Smetana, M. Pluskalova, H. Cajthamlova, I. Marinov, O. Fuchs, J. Soucek, P. Jarolim, Z. Hrkal, Mitochondrial and endoplasmic reticulum stress-induced apoptotic pathways are activated by 5-aminolevulinic acid-based photodynamic therapy in HL60 leukemia cells, J Photochem Photobiol B 69 (2003) 71-85.
[135] S.N. Datta, C.S. Loh, A.J. MacRobert, S.D. Whatley, P.N. Matthews, Quantitative studies of the kinetics of 5-aminolaevulinic acid-induced fluorescence in bladder transitional cell carcinoma, Br J Cancer 78 (1998) 1113-1118.
[136] Q. Peng, A.M. Soler, T. Warloe, J.M. Nesland, K.E. Giercksky, Selective distribution of porphyrins in skin thick basal cell carcinoma after topical application of methyl 5-aminolevulinate, J Photochem Photobiol B 62 (2001) 140-145.
[137] R. Musiol, M. Serda, J. Polanski, Prodrugs in photodynamic anticancer therapy, Curr Pharm Des 17 (2011) 3548-3559.
[138] N. Saedi, H.R. Jalian, A. Petelin, C. Zachary, Fractionation: past, present, future, Semin Cutan Med Surg 31 (2012) 105-109.
[139] C.S. Haak, W.A. Farinelli, J. Tam, A.G. Doukas, R.R. Anderson, M. Haedersdal, Fractional laser-assisted delivery of methyl aminolevulinate: Impact of laser channel depth and incubation time, Lasers Surg Med 44 (2012) 787-795.
[140] M. Haedersdal, J. Katsnelson, F.H. Sakamoto, W.A. Farinelli, A.G. Doukas, J. Tam, R.R. Anderson, Enhanced uptake and photoactivation of topical methyl aminolevulinate after fractional CO2 laser pretreatment, Lasers Surg Med 43 (2011) 804-813.
[141] P. Mroz, A. Yaroslavsky, G.B. Kharkwal, M.R. Hamblin, Cell death pathways in photodynamic therapy of cancer, Cancers (Basel) 3 (2011) 2516-2539.
[142] F. Harris, L. Pierpoint, Photodynamic therapy based on 5-aminolevulinic acid and its use as an antimicrobial agent, Med Res Rev 32 (2012) 1292-1327.
[143] R.M. Szeimies, M. Landthaler, S. Karrer, Non-oncologic indications for ALA-PDT, J Dermatolog Treat 13 Suppl 1 (2002) S13-18.
[144] G. Yang, L.F. Xiang, M.H. Gold, 5-Aminolevulinic Acid-based Photodynamic Intense Pulsed Light Therapy Shows Better Effects in the Treatment of Skin

Photoaging in Asian Skin: A Prospective, Single-blinded, Controlled Trial, J Clin Aesthet Dermatol 3 (2010) 40-43.
[145] J.S. Dover, A.C. Bhatia, B. Stewart, K.A. Arndt, Topical 5-aminolevulinic acid combined with intense pulsed light in the treatment of photoaging, Arch Dermatol 141 (2005) 1247-1252.
[146] C. Clark, A. Bryden, R. Dawe, H. Moseley, J. Ferguson, S.H. Ibbotson, Topical 5-aminolaevulinic acid photodynamic therapy for cutaneous lesions: outcome and comparison of light sources, Photodermatol Photoimmunol Photomed 19 (2003) 134-141.
[147] B. Nokes, M. Apel, C. Jones, G. Brown, J.E. Lang, Aminolevulinic acid (ALA): photodynamic detection and potential therapeutic applications, J Surg Res 181 (2013) 262-271.
[148] N.S. van den Berg, F.W. van Leeuwen, H.G. van der Poel, Fluorescence guidance in urologic surgery, Curr Opin Urol 22 (2012) 109-120.
[149] M.J. Colditz, R.L. Jeffree, Aminolevulinic acid (ALA)-protoporphyrin IX fluorescence guided tumour resection. Part 1: Clinical, radiological and pathological studies, J Clin Neurosci 19 (2012) 1471-1474.
[150] S. Grapengiesser, M. Ericson, F. Gudmundsson, O. Larko, A. Rosen, A.M. Wennberg, Pain caused by photodynamic therapy of skin cancer, Clin Exp Dermatol 27 (2002) 493-497.
[151] A. Kasche, S. Luderschmidt, J. Ring, R. Hein, Photodynamic therapy induces less pain in patients treated with methyl aminolevulinate compared to aminolevulinic acid, J Drugs Dermatol 5 (2006) 353-356.
[152] F.J. Moloney, P. Collins, Randomized, double-blind, prospective study to compare topical 5-aminolaevulinic acid methylester with topical 5-aminolaevulinic acid photodynamic therapy for extensive scalp actinic keratosis, Br J Dermatol 157 (2007) 87-91.
[153] J.M. Steinbauer, S. Schreml, P. Babilas, F. Zeman, S. Karrer, M. Landthaler, R.M. Szeimies, Topical photodynamic therapy with porphyrin precursors--assessment of treatment-associated pain in a retrospective study, Photochem Photobiol Sci 8 (2009) 1111-1116.
[154] T. Dirschka, P. Radny, R. Dominicus, H. Mensing, H. Bruning, L. Jenne, L. Karl, M. Sebastian, C. Oster-Schmidt, W. Klovekorn, U. Reinhold, M. Tanner, D. Grone, M. Deichmann, M. Simon, F. Hubinger, G. Hofbauer, G. Krahn-Senftleben, F. Borrosch, K. Reich, C. Berking, P. Wolf, P. Lehmann, M. Moers-Carpi, H. Honigsmann, K. Wernicke-Panten, C. Helwig, M. Foguet, B. Schmitz, H. Lubbert, R.M. Szeimies, A.-C.S. Group, Photodynamic therapy with BF-200 ALA for the treatment of actinic keratosis: results of a multicentre, randomized, observer-blind phase III study in comparison with a registered methyl-5-aminolaevulinate cream and placebo, Br J Dermatol 166 (2012) 137-146.
[155] P. Gholam, T. Weberschock, K. Denk, A. Enk, Treatment with 5-aminolaevulinic acid methylester is less painful than treatment with 5-aminolaevulinic acid nanoemulsion in topical photodynamic therapy for actinic keratosis, Dermatology 222 (2011) 358-362.
[156] S.M. Wu, Q.G. Ren, M.O. Zhou, Q. Peng, J.Y. Chen, Protoporphyrin IX production and its photodynamic effects on glioma cells, neuroblastoma cells and

normal cerebellar granule cells in vitro with 5-aminolevulinic acid and its hexylester, Cancer Lett 200 (2003) 123-131.
[157] C.A. Morton, K.E. McKenna, L.E. Rhodes, G. British Association of Dermatologists Therapy, S. Audit, G. the British Photodermatology, Guidelines for topical photodynamic therapy: update, Br J Dermatol 159 (2008) 1245-1266.
[158] D.C. Shackley, C. Briggs, A. Gilhooley, C. Whitehurst, K.J. O'Flynn, C.D. Betts, J.V. Moore, N.W. Clarke, Photodynamic therapy for superficial bladder cancer under local anaesthetic, BJU Int 89 (2002) 665-670.
[159] J. Pagliaro, T. Elliott, M. Bulsara, C. King, C. Vinciullo, Cold air analgesia in photodynamic therapy of basal cell carcinomas and Bowen's disease: an effective addition to treatment: a pilot study, Dermatol Surg 30 (2004) 63-66.
[160] K. Berg, M. Folini, L. Prasmickaite, P.K. Selbo, A. Bonsted, B.O. Engesaeter, N. Zaffaroni, A. Weyergang, A. Dietze, G.M. Maelandsmo, E. Wagner, O.J. Norum, A. Hogset, Photochemical internalization: a new tool for drug delivery, Curr Pharm Biotechnol 8 (2007) 362-372.
[161] S. Mukherjee, R.N. Ghosh, F.R. Maxfield, Endocytosis, Physiol Rev 77 (1997) 759-803.
[162] L.M. Bareford, P.W. Swaan, Endocytic mechanisms for targeted drug delivery, Adv Drug Deliv Rev 59 (2007) 748-758.
[163] Y.W. Cho, J.D. Kim, K. Park, Polycation gene delivery systems: escape from endosomes to cytosol, J Pharm Pharmacol 55 (2003) 721-734.
[164] T. Yamashima, S. Oikawa, The role of lysosomal rupture in neuronal death, Prog Neurobiol 89 (2009) 343-358.
[165] J.P. Luzio, P.R. Pryor, N.A. Bright, Lysosomes: fusion and function, Nat Rev Mol Cell Biol 8 (2007) 622-632.
[166] A. Dietze, P.K. Selbo, L. Prasmickaite, A. Weyergang, A. Bonsted, B. Engesaeter, A. Hogset, K. Berg, Photochemical internalization (PCI): a new modality for light activation of endocytosed therapeuticals, J Environ Pathol Toxicol Oncol 25 (2006) 521-536.
[167] J. Woodhams, P.J. Lou, P.K. Selbo, A. Mosse, D. Oukrif, A. MacRobert, M. Novelli, Q. Peng, K. Berg, S.G. Bown, Intracellular re-localisation by photochemical internalisation enhances the cytotoxic effect of gelonin--quantitative studies in normal rat liver, J Control Release 142 (2010) 347-353.
[168] G. Jori, Tumour photosensitizers: approaches to enhance the selectivity and efficiency of photodynamic therapy, J Photochem Photobiol B 36 (1996) 87-93.
[169] M. Lilletvedt, H.H. Tonnesen, A. Hogset, L. Nardo, S. Kristensen, Physicochemical characterization of the photosensitizers TPCS2a and TPPS2a 1. Spectroscopic evaluation of drug--solvent interactions, Pharmazie 65 (2010) 588-595.
[170] M. Lilletvedt, H.H. Tonnesen, A. Hogset, S.A. Sande, S. Kristensen, Evaluation of physicochemical properties and aggregation of the photosensitizers TPCS2a and TPPS2a in aqueous media, Pharmazie 66 (2011) 325-333.
[171] L. Nardo, S. Kristensen, H.H. Tonnesen, A. Hogset, M. Lilletvedt, Solubilization of the photosensitizers TPCS(2a) and TPPS(2a) in aqueous media evaluated by time-resolved fluorescence analysis, Pharmazie 67 (2012) 598-600.

[172] K. Berg, S. Nordstrand, P.K. Selbo, D.T. Tran, E. Angell-Petersen, A. Hogset, Disulfonated tetraphenyl chlorin (TPCS2a), a novel photosensitizer developed for clinical utilization of photochemical internalization, Photochem Photobiol Sci 10 (2011) 1637-1651.
[173] J.T. Wang, K. Berg, A. Hogset, S.G. Bown, A.J. Macrobert, Photophysical and photobiological properties of a sulfonated chlorin photosensitiser TPCS(2a) for photochemical internalisation (PCI), Photochem Photobiol Sci 12 (2013) 519-526.
[174] S. Bonneau, C. Vever-Bizet, H. Mojzisova, D. Brault, Tetrapyrrole-photosensitizers vectorization and plasma LDL: a physico-chemical approach, Int J Pharm 344 (2007) 78-87.
[175] K. Berg, A. Western, J.C. Bommer, J. Moan, Intracellular localization of sulfonated meso-tetraphenylporphines in a human carcinoma cell line, Photochem Photobiol 52 (1990) 481-487.
[176] P.K. Selbo, M.G. Rosenblum, L.H. Cheung, W. Zhang, K. Berg, Multi-modality therapeutics with potent anti-tumor effects: photochemical internalization enhances delivery of the fusion toxin scFvMEL/rGel, PLoS One 4 (2009) e6691.
[177] P.K. Selbo, A. Weyergang, M.S. Eng, M. Bostad, G.M. Maelandsmo, A. Hogset, K. Berg, Strongly amphiphilic photosensitizers are not substrates of the cancer stem cell marker ABCG2 and provides specific and efficient light-triggered drug delivery of an EGFR-targeted cytotoxic drug, J Control Release 159 (2012) 197-203.
[178] L. Prasmickaite, A. Hogset, P.K. Selbo, B.O. Engesaeter, M. Hellum, K. Berg, Photochemical disruption of endocytic vesicles before delivery of drugs: a new strategy for cancer therapy, Br J Cancer 86 (2002) 652-657.
[179] O.J. Norum, J.V. Gaustad, E. Angell-Petersen, E.K. Rofstad, Q. Peng, K.E. Giercksky, K. Berg, Photochemical internalization of bleomycin is superior to photodynamic therapy due to the therapeutic effect in the tumor periphery, Photochem Photobiol 85 (2009) 740-749.
[180] K. Berg, P.K. Selbo, A. Weyergang, A. Dietze, L. Prasmickaite, A. Bonsted, B.O. Engesaeter, E. Angell-Petersen, T. Warloe, N. Frandsen, A. Hogset, Porphyrin-related photosensitizers for cancer imaging and therapeutic applications, J Microsc 218 (2005) 133-147.
[181] A. Weyergang, O. Kaalhus, K. Berg, Photodynamic therapy with an endocytically located photosensitizer cause a rapid activation of the mitogen-activated protein kinases extracellular signal-regulated kinase, p38, and c-Jun NH2 terminal kinase with opposing effects on cell survival, Mol Cancer Ther 7 (2008) 1740-1750.
[182] A. Weyergang, P.K. Selbo, K. Berg, Y1068 phosphorylation is the most sensitive target of disulfonated tetraphenylporphyrin-based photodynamic therapy on epidermal growth factor receptor, Biochem Pharmacol 74 (2007) 226-235.
[183] A. Weyergang, K. Berg, O. Kaalhus, Q. Peng, P.K. Selbo, Photodynamic therapy targets the mTOR signaling network in vitro and in vivo, Mol Pharm 6 (2009) 255-264.
[184] A. Weyergang, O. Kaalhus, K. Berg, Photodynamic targeting of EGFR does not predict the treatment outcome in combination with the EGFR tyrosine kinase inhibitor Tyrphostin AG1478, Photochem Photobiol Sci 7 (2008) 1032-1040.

[185] M. Andrzejak, M. Santiago, D. Kessel, Effects of endosomal photodamage on membrane recycling and endocytosis, Photochem Photobiol 87 (2011) 699-706.
[186] P.K. Selbo, G. Sivam, O. Fodstad, K. Sandvig, K. Berg, In vivo documentation of photochemical internalization, a novel approach to site specific cancer therapy, Int J Cancer 92 (2001) 761-766.
[187] P.K. Selbo, K. Sandvig, V. Kirveliene, K. Berg, Release of gelonin from endosomes and lysosomes to cytosol by photochemical internalization, Biochim Biophys Acta 1475 (2000) 307-313.
[188] W.L. Yip, A. Weyergang, K. Berg, H.H. Tonnesen, P.K. Selbo, Targeted delivery and enhanced cytotoxicity of cetuximab-saporin by photochemical internalization in EGFR-positive cancer cells, Mol Pharm 4 (2007) 241-251.
[189] A. Weyergang, P.K. Selbo, K. Berg, Photochemically stimulated drug delivery increases the cytotoxicity and specificity of EGF-saporin, J Control Release 111 (2006) 165-173.
[190] E.W. Stratford, M. Bostad, R. Castro, E. Skarpen, K. Berg, A. Hogset, O. Myklebost, P.K. Selbo, Photochemical internalization of CD133-targeting immunotoxins efficiently depletes sarcoma cells with stem-like properties and reduces tumorigenicity, Biochim Biophys Acta 1830 (2013) 4235-4243.
[191] M. Bostad, K. Berg, A. Hogset, E. Skarpen, H. Stenmark, P.K. Selbo, Photochemical internalization (PCI) of immunotoxins targeting CD133 is specific and highly potent at femtomolar levels in cells with cancer stem cell properties, J Control Release 168 (2013) 317-326.
[192] A. Bolognesi, P.L. Tazzari, F. Olivieri, L. Polito, R. Lemoli, A. Terenzi, L. Pasqualucci, B. Falini, F. Stirpe, Evaluation of immunotoxins containing single-chain ribosome-inactivating proteins and an anti-CD22 monoclonal antibody (OM124): in vitro and in vivo studies, Br J Haematol 101 (1998) 179-188.
[193] P.S. Lai, C.L. Pai, C.L. Peng, M.J. Shieh, K. Berg, P.J. Lou, Enhanced cytotoxicity of saporin by polyamidoamine dendrimer conjugation and photochemical internalization, J Biomed Mater Res A 87 (2008) 147-155.
[194] P.K. Selbo, G. Sivam, O. Fodstad, K. Sandvig, K. Berg, Photochemical internalisation increases the cytotoxic effect of the immunotoxin MOC31-gelonin, Int J Cancer 87 (2000) 853-859.
[195] M.B. Berstad, A. Weyergang, K. Berg, Photochemical internalization (PCI) of HER2-targeted toxins: synergy is dependent on the treatment sequence, Biochim Biophys Acta 1820 (2012) 1849-1858.
[196] A. Zaniboni, S. Prabhu, R.A. Audisio, Chemotherapy and anaesthetic drugs: too little is known, Lancet Oncol 6 (2005) 176-181.
[197] H. Hirschberg, M.J. Zhang, H.M. Gach, F.A. Uzal, Q. Peng, C.H. Sun, D. Chighvinadze, S.J. Madsen, Targeted delivery of bleomycin to the brain using photo-chemical internalization of Clostridium perfringens epsilon prototoxin, J Neurooncol 95 (2009) 317-329.
[198] P.J. Lou, P.S. Lai, M.J. Shieh, A.J. Macrobert, K. Berg, S.G. Bown, Reversal of doxorubicin resistance in breast cancer cells by photochemical internalization, Int J Cancer 119 (2006) 2692-2698.
[199] P.S. Lai, P.J. Lou, C.L. Peng, C.L. Pai, W.N. Yen, M.Y. Huang, T.H. Young, M.J. Shieh, Doxorubicin delivery by polyamidoamine dendrimer conjugation and

photochemical internalization for cancer therapy, J Control Release 122 (2007) 39-46.
[200] D.K. Adigbli, D.G. Wilson, N. Farooqui, E. Sousi, P. Risley, I. Taylor, A.J. Macrobert, M. Loizidou, Photochemical internalisation of chemotherapy potentiates killing of multidrug-resistant breast and bladder cancer cells, Br J Cancer 97 (2007) 502-512.
[201] K. Berg, A. Dietze, O. Kaalhus, A. Hogset, Site-specific drug delivery by photochemical internalization enhances the antitumor effect of bleomycin, Clin Cancer Res 11 (2005) 8476-8485.
[202] P.K. Selbo, A. Weyergang, A. Bonsted, S.G. Bown, K. Berg, Photochemical internalization of therapeutic macromolecular agents: a novel strategy to kill multidrug-resistant cancer cells, J Pharmacol Exp Ther 319 (2006) 604-612.
[203] K. Berg, M. Berstad, L. Prasmickaite, A. Weyergang, P.K. Selbo, I. Hedfors, A. Hogset, Photochemical internalization: a new tool for gene and oligonucleotide delivery, Top Curr Chem 296 (2010) 251-281.
[204] A. Hogset, L. Prasmickaite, P.K. Selbo, M. Hellum, B.O. Engesaeter, A. Bonsted, K. Berg, Photochemical internalisation in drug and gene delivery, Adv Drug Deliv Rev 56 (2004) 95-115.
[205] A. Hogset, L. Prasmickaite, M. Hellum, B.O. Engesaeter, V.M. Olsen, T.E. Tjelle, C.J. Wheeler, K. Berg, Photochemical transfection: a technology for efficient light-directed gene delivery, Somat Cell Mol Genet 27 (2002) 97-113.
[206] A. Bonsted, B.O. Engesaeter, A. Hogset, G.M. Maelandsmo, L. Prasmickaite, O. Kaalhus, K. Berg, Transgene expression is increased by photochemically mediated transduction of polycation-complexed adenoviruses, Gene Ther 11 (2004) 152-160.
[207] A. Hogset, L. Prasmickaite, T.E. Tjelle, K. Berg, Photochemical transfection: a new technology for light-induced, site-directed gene delivery, Hum Gene Ther 11 (2000) 869-880.
[208] M. Folini, R. Bandiera, E. Millo, P. Gandellini, G. Sozzi, P. Gasparini, N. Longoni, M. Binda, M.G. Daidone, K. Berg, N. Zaffaroni, Photochemically enhanced delivery of a cell-penetrating peptide nucleic acid conjugate targeting human telomerase reverse transcriptase: effects on telomere status and proliferative potential of human prostate cancer cells, Cell Prolif 40 (2007) 905-920.
[209] M. Folini, K. Berg, E. Millo, R. Villa, L. Prasmickaite, M.G. Daidone, U. Benatti, N. Zaffaroni, Photochemical internalization of a peptide nucleic acid targeting the catalytic subunit of human telomerase, Cancer Res 63 (2003) 3490-3494.
[210] T. Shiraishi, P.E. Nielsen, Photochemically enhanced cellular delivery of cell penetrating peptide-PNA conjugates, FEBS Lett 580 (2006) 1451-1456.
[211] M. Pooga, U. Langel, Targeting of cancer-related proteins with PNA oligomers, Curr Cancer Drug Targets 1 (2001) 231-239.
[212] S. Boe, A.S. Longva, E. Hovig, Photochemically induced gene silencing using small interfering RNA molecules in combination with lipid carriers, Oligonucleotides 17 (2007) 166-173.

[213] O.J. Norum, K.E. Giercksky, K. Berg, Photochemical internalization as an adjunct to marginal surgery in a human sarcoma model, Photochem Photobiol Sci 8 (2009) 758-762.
[214] O.J. Norum, O.S. Bruland, L. Gorunova, K. Berg, Photochemical internalization of bleomycin before external-beam radiotherapy improves locoregional control in a human sarcoma model, Int J Radiat Oncol Biol Phys 75 (2009) 878-885.
[215] D.K. Adigbli, A.J. MacRobert, Photochemical internalisation: the journey from basic scientific concept to the threshold of clinical application, Curr Opin Pharmacol 12 (2012) 434-438.
[216] A. Dietze, Q. Peng, P.K. Selbo, O. Kaalhus, C. Muller, S. Bown, K. Berg, Enhanced photodynamic destruction of a transplantable fibrosarcoma using photochemical internalisation of gelonin, Br J Cancer 92 (2005) 2004-2009.
[217] S.B. Edge, D.R. Byrd, C.C. Compton, A.G. Fritz, F.L. Greene, A. Trotti, eds., Urinary bladder. In: AJCC Cancer Staging Manual. 7th ed., Springer, New York, NY., 2010.
[218] M.C. Hall, S.S. Chang, G. Dalbagni, R.S. Pruthi, J.D. Seigne, E.C. Skinner, J.S. Wolf, Jr., P.F. Schellhammer, Guideline for the management of nonmuscle invasive bladder cancer (stages Ta, T1, and Tis): 2007 update, J Urol 178 (2007) 2314-2330.
[219] T.R. Griffiths, C. on behalf of Action on Bladder, Current perspectives in bladder cancer management, Int J Clin Pract (2012).
[220] I.K. Larsen, B. Sæther, B. Aagnes, Cancer in Norway 2010, Institute of population-based cancer research, Norway, 2012.
[221] National Cancer Institute, Bladder Cancer, the National Institutes of Health, USA, 2013.
[222] Z. Shen, T. Shen, M.G. Wientjes, M.A. O'Donnell, J.L. Au, Intravesical treatments of bladder cancer: review, Pharm Res 25 (2008) 1500-1510.
[223] S. Sharma, P. Ksheersagar, P. Sharma, Diagnosis and treatment of bladder cancer, Am Fam Physician 80 (2009) 717-723.
[224] G. Cheung, A. Sahai, M. Billia, P. Dasgupta, M.S. Khan, Recent advances in the diagnosis and treatment of bladder cancer, BMC Med 11 (2013) 13.
[225] P. Bassi, BCG (Bacillus of Calmette Guerin) therapy of high-risk superficial bladder cancer, Surg Oncol 11 (2002) 77-83.
[226] U.O. Nseyo, D.L. Lamm, Therapy of superficial bladder cancer, Semin Oncol 23 (1996) 598-604.
[227] E. Schenkman, D.L. Lamm, Superficial bladder cancer therapy, ScientificWorldJournal 4 Suppl 1 (2004) 387-399.
[228] C. Bolenz, Y. Cao, M.F. Arancibia, L. Trojan, P. Alken, M.S. Michel, Intravesical mitomycin C for superficial transitional cell carcinoma, Expert Rev Anticancer Ther 6 (2006) 1273-1282.
[229] S.M. Di Stasi, A. Giannantoni, A. Giurioli, M. Valenti, G. Zampa, L. Storti, F. Attisani, A. De Carolis, G. Capelli, G. Vespasiani, R.L. Stephen, Sequential BCG and electromotive mitomycin versus BCG alone for high-risk superficial bladder cancer: a randomised controlled trial, Lancet Oncol 7 (2006) 43-51.

[230] Y. Kubota, T. Nakada, H. Yanai, K. Itoh, I. Sasagawa, K. Kawai, Histological evaluation of the effects of electropermeabilization after administration of bleomycin on bladder cancer in the rat, Eur Urol 34 (1998) 372-376.
[231] B. Moskovitz, G. Meyer, A. Kravtzov, M. Gross, A. Kastin, K. Biton, O. Nativ, Thermo-chemotherapy for intermediate or high-risk recurrent superficial bladder cancer patients, Ann Oncol 16 (2005) 585-589.
[232] R. Colombo, L.F. Da Pozzo, A. Salonia, P. Rigatti, Z. Leib, J. Baniel, E. Caldarera, M. Pavone-Macaluso, Multicentric study comparing intravesical chemotherapy alone and with local microwave hyperthermia for prophylaxis of recurrence of superficial transitional cell carcinoma, J Clin Oncol 21 (2003) 4270-4276.
[233] R. Colombo, A. Salonia, L.F. Da Pozzo, R. Naspro, M. Freschi, R. Paroni, M. Pavone-Macaluso, P. Rigatti, Combination of intravesical chemotherapy and hyperthermia for the treatment of superficial bladder cancer: preliminary clinical experience, Crit Rev Oncol Hematol 47 (2003) 127-139.
[234] A.G. van der Heijden, L.A. Kiemeney, O.N. Gofrit, O. Nativ, A. Sidi, Z. Leib, R. Colombo, R. Naspro, M. Pavone, J. Baniel, F. Hasner, J.A. Witjes, Preliminary European results of local microwave hyperthermia and chemotherapy treatment in intermediate or high risk superficial transitional cell carcinoma of the bladder, Eur Urol 46 (2004) 65-71; discussion 71-62.
[235] R.S. Svatek, A.M. Kamat, C.P. Dinney, Novel therapeutics for patients with non-muscle-invasive bladder cancer, Expert Rev Anticancer Ther 9 (2009) 807-813.
[236] H.C. Arentsen, J. Falke, A. Hogset, E. Oosterwijk, J. Alfred Witjes, The effect of photochemical internalization of bleomycin in the treatment of urothelial carcinoma of the bladder: An in vitro study, Urol Oncol (2013).
[237] P. Jichlinski, Photodynamic applications in superficial bladder cancer: facts and hopes!, J Environ Pathol Toxicol Oncol 25 (2006) 441-451.
[238] J.H. Pinthus, A. Bogaards, R. Weersink, B.C. Wilson, J. Trachtenberg, Photodynamic therapy for urological malignancies: past to current approaches, J Urol 175 (2006) 1201-1207.
[239] M.A. D'Hallewin, L. Baert, J.P. Marijnissen, W.M. Star, Whole bladder wall photodynamic therapy with in situ light dosimetry for carcinoma in situ of the bladder, J Urol 148 (1992) 1152-1155.
[240] D.C. Shackley, C. Whitehurst, J.V. Moore, N.J. George, C.D. Betts, N.W. Clarke, Light penetration in bladder tissue: implications for the intravesical photodynamic therapy of bladder tumours, BJU Int 86 (2000) 638-643.
[241] A.P. Berger, H. Steiner, A. Stenzl, T. Akkad, G. Bartsch, L. Holtl, Photodynamic therapy with intravesical instillation of 5-aminolevulinic acid for patients with recurrent superficial bladder cancer: a single-center study, Urology 61 (2003) 338-341.
[242] R. Waidelich, H. Stepp, R. Baumgartner, E. Weninger, A. Hofstetter, M. Kriegmair, Clinical experience with 5-aminolevulinic acid and photodynamic therapy for refractory superficial bladder cancer, J Urol 165 (2001) 1904-1907.
[243] U.O. Nseyo, Photodynamic therapy in the management of bladder cancer, J Clin Laser Med Surg 14 (1996) 271-280.

[244] J.Y. Lee, R.R. Diaz, K.S. Cho, M.S. Lim, J.S. Chung, W.T. Kim, W.S. Ham, Y.D. Choi, Efficacy and safety of photodynamic therapy for recurrent, high grade nonmuscle invasive bladder cancer refractory or intolerant to bacille Calmette-Guerin immunotherapy, J Urol 190 (2013) 1192-1199.
[245] U.O. Nseyo, B. Shumaker, E.A. Klein, K. Sutherland, Photodynamic therapy using porfimer sodium as an alternative to cystectomy in patients with refractory transitional cell carcinoma in situ of the bladder. Bladder Photofrin Study Group, J Urol 160 (1998) 39-44.
[246] U.O. Nseyo, T.J. Dougherty, D.G. Boyle, W.R. Potter, R. Wolf, R. Huben, J.E. Pontes, Whole bladder photodynamic therapy for transitional cell carcinoma of bladder, Urology 26 (1985) 274-280.
[247] M.A. D'Hallewin, L. Baert, Long-term results of whole bladder wall photodynamic therapy for carcinoma in situ of the bladder, Urology 45 (1995) 763-767.
[248] B. Geavlete, R. Multescu, D. Georgescu, M. Jecu, F. Stanescu, P. Geavlete, Treatment changes and long-term recurrence rates after hexaminolevulinate (HAL) fluorescence cystoscopy: does it really make a difference in patients with non-muscle-invasive bladder cancer (NMIBC)?, BJU Int 109 (2012) 549-556.
[249] A. Francois, A. Salvadori, A. Bressenot, L. Bezdetnaya, F. Guillemin, M.A. D'Hallewin, How to avoid local side effects of bladder photodynamic therapy: impact of the fluence rate, J Urol 190 (2013) 731-736.
[250] S. El Khatib, J. Didelon, A. Leroux, L. Bezdetnaya, D. Notter, M. D'Hallewin, Kinetics, biodistribution and therapeutic efficacy of hexylester 5-aminolevulinate induced photodynamic therapy in an orthotopic rat bladder tumor model, J Urol 172 (2004) 2013-2017.
[251] S. Berrahmoune, N. Fotinos, L. Bezdetnaya, N. Lange, J.C. Guedenet, F. Guillemin, M.A. D'Hallewin, Analysis of differential PDT effect in rat bladder tumor models according to concentrations of intravesical hexyl-aminolevulinate, Photochem Photobiol Sci 7 (2008) 1018-1024.
[252] M.J. Bader, H. Stepp, W. Beyer, T. Pongratz, R. Sroka, M. Kriegmair, D. Zaak, M. Welschof, D. Tilki, C.G. Stief, R. Waidelich, Photodynamic therapy of bladder cancer - a phase I study using hexaminolevulinate (HAL), Urol Oncol 31 (2013) 1178-1183.
[253] S. Gronlund-Pakkanen, J. Wahlfors, K. Makinen, T.M. Pakkanen, M. Talja, M. Ala-Opas, E. Alhava, R.B. Moore, The fluorescence biodistribution and kinetics of aminolevulinic acid induced protoporphyrin IX in the bladder of a rat model with orthotopic urothelial carcinoma, J Urol 167 (2002) 1848-1853.
[254] R. Waidelich, W. Beyer, R. Knuchel, H. Stepp, R. Baumgartner, J. Schroder, A. Hofstetter, M. Kriegmair, Whole bladder photodynamic therapy with 5-aminolevulinic acid using a white light source, Urology 61 (2003) 332-337.
[255] R.J. Skyrme, A.J. French, S.N. Datta, R. Allman, M.D. Mason, P.N. Matthews, A phase-1 study of sequential mitomycin C and 5-aminolaevulinic acid-mediated photodynamic therapy in recurrent superficial bladder carcinoma, BJU Int 95 (2005) 1206-1210.

[256] M. Kriegmair, R. Baumgartner, W. Lumper, R. Waidelich, A. Hofstetter, Early clinical experience with 5-aminolevulinic acid for the photodynamic therapy of superficial bladder cancer, Br J Urol 77 (1996) 667-671.
[257] P. Jichlinski, H.J. Leisinger, Photodynamic therapy in superficial bladder cancer: past, present and future, Urol Res 29 (2001) 396-405.
[258] T. Kiesslich, B. Krammer, K. Plaetzer, Cellular mechanisms and prospective applications of hypericin in photodynamic therapy, Curr Med Chem 13 (2006) 2189-2204.
[259] N.E. Stavropoulos, A. Kim, U.U. Nseyo, I. Tsimaris, T.D. Chung, T.A. Miller, M. Redlak, U.O. Nseyo, D. Skalkos, Hypericum perforatum L. extract - novel photosensitizer against human bladder cancer cells, J Photochem Photobiol B 84 (2006) 64-69.
[260] L.S. Lee, P.S. Thong, M. Olivo, W.W. Chin, B. Ramaswamy, K.W. Kho, P.L. Lim, W.K. Lau, Chlorin e6-polyvinylpyrrolidone mediated photodynamic therapy--A potential bladder sparing option for high risk non-muscle invasive bladder cancer, Photodiagnosis Photodyn Ther 7 (2010) 213-220.
[261] O.A. Gederaas, A. Hjelde, L.O. Svaasand, A. Johnsson, K. Berg, R. Manandhar, C. Shrestha, D. Skare, I.K. Ekroll, A. Hogset, Photochemical internalization of bladder cancer-development of an orthotopic in vivo model (in preparation, 2014).
[262] M.S. Mathews, J.W. Blickenstaff, E.C. Shih, G. Zamora, V. Vo, C.H. Sun, H. Hirschberg, S.J. Madsen, Photochemical internalization of bleomycin for glioma treatment, J Biomed Opt 17 (2012) 058001.
[263] M.S. Mathews, V. Vo, E.C. Shih, G. Zamora, C.H. Sun, S.J. Madsen, H. Hirschberg, Photochemical internalization-mediated delivery of chemotherapeutic agents in human breast tumor cell lines, J Environ Pathol Toxicol Oncol 31 (2012) 49-59.
[264] T. Beuming, L. Shi, J.A. Javitch, H. Weinstein, A comprehensive structure-based alignment of prokaryotic and eukaryotic neurotransmitter/Na+ symporters (NSS) aids in the use of the LeuT structure to probe NSS structure and function, Mol Pharmacol 70 (2006) 1630-1642.
[265] S.V. Demyanenko, A.B. Uzdensky, S.A. Sharifulina, T.O. Lapteva, L.P. Polyakova, PDT-induced epigenetic changes in the mouse cerebral cortex: A protein microarray study, Biochim Biophys Acta 1840 (2014) 262-270.
[266] B. Magi, A. Ettorre, S. Liberatori, L. Bini, M. Andreassi, S. Frosali, P. Neri, V. Pallini, A. Di Stefano, Selectivity of protein carbonylation in the apoptotic response to oxidative stress associated with photodynamic therapy: a cell biochemical and proteomic investigation, Cell Death Differ 11 (2004) 842-852.
[267] G. Kirdaite, N. Lange, N. Busso, H. Van Den Bergh, P. Kucera, A. So, Protoporphyrin IX photodynamic therapy for synovitis, Arthritis Rheum 46 (2002) 1371-1378.
[268] O.A. Gederaas, J.W. Lagerberg, O. Brekke, K. Berg, T.M. Dubbelman, 5-aminolevulinic acid induced lipid peroxidation after light exposure on human colon carcinoma cells and effects of alpha-tocopherol treatment, Cancer Lett 159 (2000) 23-32.

[269] H.C. Arentsen, J. Falke, A. Hogset, E. Oosterwijk, J. Alfred Witjes, The effect of photochemical internalization of bleomycin in the treatment of urothelial carcinoma of the bladder: An in vitro study, Urol Oncol 32 (2014) 49 e1-6.
[270] Y. Baglo, L. Hagen, A. Hogset, F. Drablos, M. Otterlei, O.A. Gederaas, Enhanced efficacy of bleomycin in bladder cancer cells by photochemical internalization (mansucript ID: PP-ART-11-2013-050409 submitted Jan. 2014), Photochem Photobiol Sci (2014).
[271] R.B. Bracken, D.E. Johnson, L. Rodriquez, M.L. Samuels, A. Ayala, Treatment of multiple superficial tumors of bladder with intravesical bleomycin, Urology 9 (1977) 161-163.
[272] A.G. Turner, K.R. Durrant, J.S. Malpas, A trial of bleomycin versus adriamycin in advanced carcinoma of the bladder, Br J Urol 51 (1979) 121-124.
[273] N. Gad-el-Mawla, R. Hamsa, E. Chevlen, J.L. Ziegler, Phase II trial of bleomycin in bilharzial bladder cancer, Cancer Treat Rep 62 (1978) 1109-1110.
[274] D.R. Schwartz, G.E. Homanics, D.G. Hoyt, E. Klein, J. Abernethy, J.S. Lazo, The neutral cysteine protease bleomycin hydrolase is essential for epidermal integrity and bleomycin resistance, Proc Natl Acad Sci U S A 96 (1999) 4680-4685.
[275] J. Chen, J. Stubbe, Bleomycins: towards better therapeutics, Nat Rev Cancer 5 (2005) 102-112.
[276] S.M. Sebti, J.P. Jani, J.S. Mistry, E. Gorelik, J.S. Lazo, Metabolic inactivation: a mechanism of human tumor resistance to bleomycin, Cancer Res 51 (1991) 227-232.

Paper 1

Photochemical & Photobiological Sciences

View Online
Dynamic Article Links

Cite this: DOI: 10.1039/c0pp00369g

www.rsc.org/pps

PAPER

Photodynamic therapy with hexyl aminolevulinate induces carbonylation, posttranslational modifications and changed expression of proteins in cell survival and cell death pathways

Yan Baglo, Mirta M. L. Sousa, Geir Slupphaug, Lars Hagen, Sissel Håvåg, Linda Helander, Kamila A. Zub, Hans E. Krokan and Odrun A. Gederaas*

Received 8th December 2010, Accepted 3rd March 2011
DOI: 10.1039/c0pp00369g

Published on 30 March 2011 on http://pubs.rsc.org | doi:10.1039/C0PP00369G
Downloaded by RSC Internal on 26 May 2011

Photodynamic therapy (PDT) using blue light and the potent precursor for protoporphyrin IX, hexyl aminolevulinate (HAL), has been shown to induce apoptosis and necrosis in cancer cells, but the mechanism remains obscure. In the present study, we examined protein carbonylation, expression levels and post-translational modifications in rat bladder cells (AY-27) after PDT with HAL. Altered levels of expression and/or post-translational modifications induced by PDT were observed for numerous proteins, including proteins required for cell mobility, energy supply, cell survival and cell death pathways, by using two-dimensional difference gel electrophoresis (2D-DIGE) and mass spectrometry (MS). Moreover, 10 carbonylated proteins associated with cytoskeleton, transport, oxidative stress response, protein biosynthesis and stability, and DNA repair were identified using immunoprecipitation, two-dimensional gel electrophoresis and MS. Overall, the results indicate that HAL-mediated PDT triggers a complex cellular response involving several biological pathways. Our findings may account for the elucidation of mechanisms modulated by PDT, paving the way to improve clinic PDT-efficacy.

1. Introduction

5-Aminolevulinic acid (ALA) is an endogenous precursor for protoporphyrin IX (PpIX) formed *via* the heme biosynthetic pathway. It has been shown that certain tumor cells have a large capacity to synthesize the photosensitizer PpIX in mitochondria when exposed to adequate concentrations of exogenous ALA because of low activity of ferrochelatase and elevated porphobilinogen deaminase.[1] Hexyl aminolevulinate (HAL) is an ester of ALA that is effectively converted into free ALA by esterases in cytosol before entering into the heme biosynthetic pathway.[2,3] The uptake mechanisms of ALA and ALA methyl ester have been extensively studied in human colon carcinoma cells (WiDr).[4–6]

In recent years, a number of studies on HAL-mediated PDT have been conducted. The improved penetration of HAL due to its high lipophilicity was demonstrated by comparison of distribution of ALA, whilst kinetics and intracellular localization of HAL-induced PpIX were investigated in human and rat bladder cancers *in vivo* and several human cancer cell lines.[7–18] The effect of illumination was examined in rat ovarian cancer and porcine bladder mucosa.[19,20] Moreover, tissue response to HAL-PDT was monitored in rat bladder. The results revealed a clear treatment response *in vivo* including decreased tissue oxygenation and PpIX photobleaching.[21] Later, PpIX photobleaching was proven to be a useful tool to predict the tissue response to HAL-PDT.[22] A clinical study comprising 24 patients demonstrated that HAL-PDT was a non-invasive, repeatable procedure for cervical intraepithelial neoplasia and no severe side effects were encountered.[23] Mechanisms of cell killing in PDT remain obscure, but are most likely complex and apparently involve both caspase-dependent and -independent apoptotic pathways.[24–26]

PDT results in a sequence of photochemical processes in photosensitized cells. Cellular antioxidant mechanisms are apparently overloaded by high levels of reactive oxygen species (ROS) and radicals. This leads to ROS-induced protein modifications and dysfunction, and eventually affects pathways resulting in cell death.[27] The most thoroughly characterized oxidative modifications of proteins subsequent to PDT are irreversible and non-enzymatic carbonylation and oxidation of thiol groups.[28,29] Magi *et al.* found that a specific set of proteins, including structural proteins and chaperones, were carbonylated and their results supported the concept that oxidative damage to proteins was selectively induced by PDT with Purpurin-18.[30]

The aim of the present study was to identify proteins with altered expression levels and/or altered post-translational status 2 h subsequent to HAL-mediated PDT in rat bladder cancer cells (AY-27), using 2D difference gel electrophoresis (2D-DIGE) and mass spectrometry (MS). To detect protein carbonylation and altered expression in less abundant proteins, carbonylated proteins were labeled with 2,4-dinitrophenyl hydrazine (DNPH)

Department of Cancer Research and Molecular Medicine, Norwegian University of Science and Technology, N-7491, Trondheim, Norway. E-mail: odrun.gederaas@ntnu.no; Fax: +4772576400; Tel: +4772573015

View Online

Published on 30 March 2011 on http://pubs.rsc.org | doi:10.1039/C0PP00369G
Downloaded by RSC Internal on 26 May 2011

and immunoprecipitated with anti-DNP antibody prior to 2D-GE and MS.[31,32]

2. Materials and methods

2.1 Cell culture and HAL-mediated light treatment

Rat bladder cancer cells (AY-27) were maintained in RPMI-1640 culture medium (BioWhittaker) supplemented with 5% L-glutamine, 1% penicillin/streptomycin, 0.1% fungizone and 10% fetal bovine serum (FBS) in a humidified atmosphere of 95% air and 5% CO_2 at 37 °C.

About 3.5×10^6 cells were seeded per Petri dish (diameter: 10 cm) and cultured for one day. Subsequent to wash cells with PBS twice, RPMI-1640 culture medium (FBS-free) containing 10 μM HAL (PhotoCure AS, Norway) was added to cells and kept in the dark for 3.5 h. The medium was then replaced with PBS, and the cells were exposed to blue light (435 nm) for 35 s (0.45 J cm^{-2}, Lumi Source, PCI Biotech AS, Norway). Subsequent to 2 h incubation in the dark in FBS-free medium, cells were harvested by scraping in ice-cold PBS and centrifuged (450 g, 5 min, 4 °C).

Three groups of cell samples were analyzed in parallel: HAL; cells incubated with HAL only. PDT; cells treated with blue light after HAL incubation, and controls; without any treatment, neither HAL incubation nor light exposure.

This protocol was chosen based on our earlier unpublished results that the HAL-incubation time (3–3.5 h) gave a stable production of PpIX inside the AY-27 cancer cells and light treatment at the same experimental conditions led to about LD_{80} close to clinic target.

2.2 Protein extraction

Cell pellets were resuspended in 0.3× packed cell volume (PCV) of buffer I (10 mM Tris-HCl pH 8.0, 200 mM KCl, 1 mM DTT, 1% phosphatase inhibitor cocktail 1 and 2 (Sigma), 2% Complete protease inhibitor cocktail (Roche) and mixed with a volume of buffer II (10 mM Tris-HCl pH 8.0, 200 mM KCl, 2 mM EDTA, 40% glycerol, 0.5% NP40, 1 mM DTT and phosphatase- and protease inhibitors as above) corresponding to the combined volumes of the pellet and buffer I. The mixture was incubated on a roller (45 min, 4 °C) and sonicated (2 min, dark) using Branson Sonifier250 (output 2, duty cycle 20). Subsequent to centrifugation (10 min, 16100 g, 4 °C) supernatants (control, HAL and PDT) were collected and protein concentrations were determined using the Bio-Rad protein assay (BioRad Laboratories, USA).

2.3 Two dimensional difference gel electrophoresis (2D-DIGE)

Protein lysates (Control, HAL and PDT), 50 μg of each, were diluted in 2× lysis buffer (7 M urea, 4% CHAPS, 30 mM Tris, 2 M thiourea pH 8–8.5) and labelled with a specific CyDye (Cy2, Cy3 and Cy5, respectively), according to manufacturer's instructions (GE Healthcare). The reaction was quenched by adding 10 mM lysine (1 μl) following incubation for 10 min on ice in the dark. Each labelled protein sample was diluted 2-fold with 2× sample buffer (7 M urea, 4% CHAPS, 30 mM Tris, 130 mM DTT) and incubated on ice for 10 min. The three protein samples were mixed together and 1× sample buffer was added to reach a final volume of 450 μl. Then, 1% IPG buffer pH 3–11 (GE Healthcare) was added to the sample and rehydrated overnight into an IPGstrip (pH 3–11, 24 cm). Isoelectric focusing (IEF) was carried out according to the manufacturer's instructions (GE Heathcare). For the second dimension, strip was first incubated with equilibration stock buffer (50 M Tris-HCl pH 8.8, 6 M urea, 30% glycerol and 2% SDS) containing 1% DTT for 15 min and then with the equilibration stock buffer containing 2.5% iodoacetamide for 15 min under agitation at room temperature. The equilibrated strip was sealed on top of a 10% polyacrylamide gel using colorless liquid agarose. The electrophoresis was run overnight using Ettan DALT electrophoresis system (400 V, 20 mA, 2 W/gel, 20 °C).

Spots were visualized using the Typhoon™ Trio Imager (GE Healthcare) at wavelengths of 520 nm, 580 nm and 620 nm. Images were analyzed using DeCyder™ 2D software, which provides a 3D view of each protein spot. The spots are plotted as peaks that represent directly both the distribution (peak area) of the spot in the gel and its amount (peak volume). The relative peak volumes of protein spots were used to calculate the volume ratio of protein spots pairs (Cy3 and Cy5). Changes in volume ratio of protein spots pairs were used to determine proteins differentially expressed due to PDT treatment. Proteins of interest were then selected using DeCyder™ 2D software and picked using Ettan Spot Picker.

2.4 Two dimensional gel electrophoresis (2D-GE)

The HAL and PDT lysates (300 μg of each) were mixed together and DeStreak rehydration solution (GE Healthcare) was added to reach a final volume of 450 μl. The IPGstrip (pH 3–11, 24 cm) was rehydrated and protein separation by IEF and SDS-PAGE was performed as described above.

After 2D-GE separation, the gel was stained with silver according to the protocol established by Shevchenko[33] with minor modifications. Spots of interest were excised manually.

2.5 Protein identification by mass spectrometry (MS)

Protein spots were in-gel digested with trypsin as described by Shevchenko.[33] Peptides were extracted from the gel and desalted using StageTIP.[34] The eluted peptides were mixed with HCCA (α-cyano-4-hydroxycinnamic acid) matrix (7 g l^{-1} in 50% Acetonitrile, 50% ethanol) and loaded onto a MALDI-plate. Peptide mass fingerprints and MS/MS spectra were obtained using an Ultraflex III MALDI-TOF/TOF instrument (BRUKER Daltonics GmbH, Germany). Protein identification was performed by MSDB database searches using the Mascot software (Matrix Science).

2.6 Carbonylated protein labeling with 2,4-dinitrophenyl hydrazine (DNPH)

Protein lysates (1.5 mg each) were diluted (1 : 1) with 10% SDS and incubated for 5 min prior to addition of an equal volume of 10 mM DNPH in 10% TFA and further incubation for 30 min at room temperature under rotation. Reactions were stopped and the products (DNP-protein) precipitated by adding 2 volumes of 20% ice-cold trichloroacetic acid (TCA) and incubation on ice for 45 min. Precipitated DNP-proteins were pelleted (20 min, 5900 *g*, 4 °C), and pellets were washed three times with acetone (5 min, 4500 g, 4 °C) and resuspended in 600 μl of a 1 : 1 mixture of buffer I and II.

 This journal is © The Royal Society of Chemistry and Owner Societies 2011

View Online

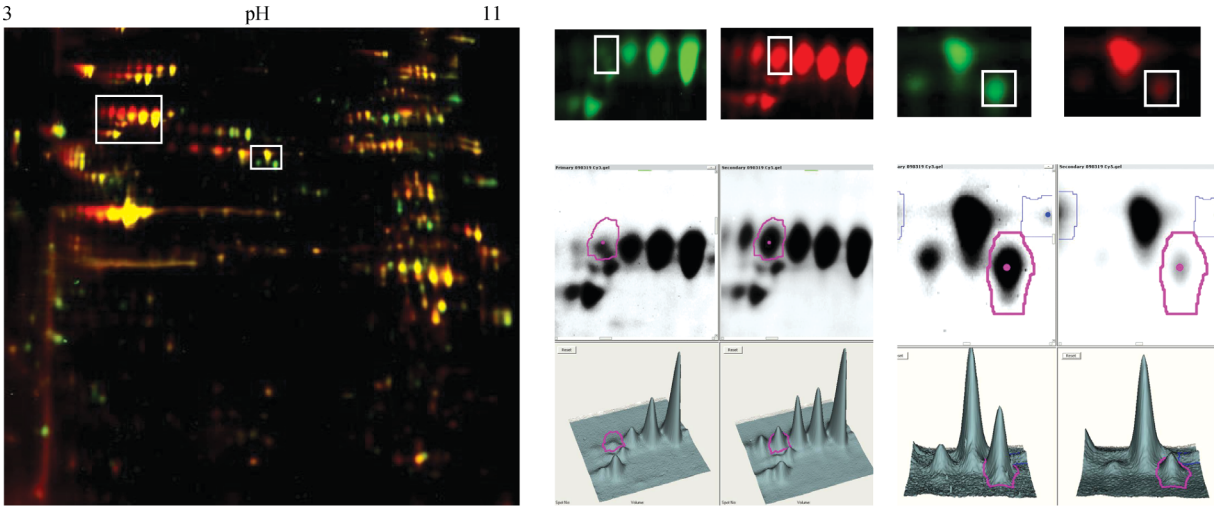

(A) Proteomic map (B) Spot with lower Cy3/Cy5 ratio (C) Spot with higher Cy3/Cy5 ratio

Fig. 1 Proteomic map of HAL and PDT lysate samples of AY-27 cells. (A) Proteins under-expressed (green spots) or over-expressed (red spots) in the PDT sample (HAL and light treatment) compared to control (only HAL treatment); (B) spot with lower Cy3/Cy5 ratio (DeCyder analysis) shown as red in the proteomic map was up-regulated in the PDT sample. This spot together with other 3 spots to the right were identified as heat shock protein 60 kDa later by MS indicating pI-shift.; (C) Spot with higher Cy3/Cy5 ratio shown as green in the proteomic map was down-regulated in the PDT sample.

Published on 30 March 2011 on http://pubs.rsc.org | doi:10.1039/C0PP00369G
Downloaded by RSC Internal on 26 May 2011

2.7 Immunoprecipitation using anti-DNP antibody

Anti-DNP antibodies were covalently coupled to paramagnetic Dynabeads protein A beads according to the manufacturer's protocol (Dynal). DNP-labelled protein samples were incubated with crosslinked beads (150 µl) overnight at 4 °C with constant agitation. The beads were washed three times with 10 mM Tris-HCl (pH 8.3), 50 mM KCl (pH 8.3) and DNP-proteins eluted with 1× Novex LDS loading buffer (13 µl, Invitrogen) and the beads were further incubated overnight in 1× sample buffer (117 µl). The combined eluates were then subjected to 2D-GE using 7 cm IPGstrip (pH 3–11) and a 4–12% gradient NuPAGE gel (Invitrogen). The gel was stained with Krypton protein stain according to the manufacturer's protocol (Pierce, USA) and the spots were visualized using a Typhoon scanner (GE Healthcare).

3. Results and discussion

3.1 PDT treatment causes marked changes in protein expression and apparent post-translational modification status

Alterations in the apparent post-translational modification (PTM) status of proteins two hours subsequent to HAL alone or HAL/PDT treatment of rat bladder cancer cells (AY-27) were monitored in three parallel experiments using 2D-DIGE. Since our primary objective was to identify altered migration of proteins that could indicate differential PTM status, a Cy2-labelled internal control was not included in the experiments. Nevertheless, a marked difference in the overall expression level of several proteins was evident from the Cy3/Cy5 ratios. Moreover, the proteomic maps obtained from the parallel experiments were very similar, indicating that the procedure is highly reproducible. A representative proteomic map of HAL and PDT lysate samples is shown in Fig. 1 (a), in which clear red spots represent up-regulated proteins (Fig. 1, b) and clear green spots represent down-regulated proteins (Fig. 1, c) in the PDT-treated cells as compared to cells treated with HAL only. Yellow spots represent proteins expressed at similar level in both samples. The 2D-DIGE image clearly demonstrates that additional exposure of the HAL-treated cells to blue light causes a striking change in the expression of some proteins. Moreover, several proteins exhibited apparently different migration in the 2D-gel, typically in the form of species having an acidic pI-shift (Fig. 1, b). Such acidic shifts might be the result of enzymatic modifications mediating gain of negative charge by, for example, phosphorylation, or loss of positive charge by, for example, acetylation. However, shifts towards the acidic side may also result from non-enzymatic oxidative modifications, such as oxidation of cysteine to cysteine sulfenic- or sulfinic acid.

In order to increase protein concentration and enhance protein identification in MS analysis, a 2D-GE was run with higher amount of both HAL and PDT lysate samples (Fig. 2), and proteins were excised from the silver-stained gel using the 2D-DIGE gels as reference. A total of 40 proteins were identified and assigned in the 2D-DIGE gel (Fig. 3). Among these, 15 proteins were markedly up-/down-regulated or displayed modified post-translational status, as suggested by their altered migration. As shown in Table 1, heterogeneous nuclear ribonucleoprotein (hnRNP) L and pre-mRNA-processing factor 19 were markedly up-regulated, while pyruvate kinase isozymes M1/M2, vimentin, and tubulin alpha-1 chain were markedly down-regulated. The remaining 10 proteins displayed acidic pI-shifts, as illustrated for HSP60 (Fig. 1, b).

Apparent down-regulation of vimentin could be a consequence of vimentin cross-linking resulting from carbonylation. This has previously been observed in A549 cells subsequent to acrolein-induced carbonylation,[35] and would mediate a loss of vimentin monomers in 1D-GE and 2D-GE gels. Interestingly, several of the most abundant cytoskeletal and chaperone proteins such as β-actin, protein disulfide-isomerase A6 and A3, HSP70/90 and

View Online

Published on 30 March 2011 on http://pubs.rsc.org | doi:10.1039/C0PP00369G
Downloaded by RSC Internal on 26 May 2011

Table 1 Proteins and biological processes/pathways in AY-27 cells affected by HAL-mediated PDT, based on the 24 proteins subject to post-translational modification and differential expression, analyzed using Uniprot and PANTHER software (www.pantherdb.org)

Gene ID	Name of protein	Cellular location	PDT response[a]	Main molecular function	Main biological process/pathway	Reference
P11980	pyruvate kinase isozymes M1/M2	cytosol	D	carbohydrate kinase	glycolysis/pyruvate metabolism	
P68370	tubulin alpha-1A chain	microtubule	D	tubulin	intracellular protein traffic, cell structure and motility, cell cycle, developmental process, *etc.*	30,37,38
P31000	vimentin	nucleus, cytoplasm	D	structural protein	ectoderm development; cell structure	35,39
Q5U1Y5	hnRNP L[b]	nucleus	U	ribosomal protein	mRNA splicing	
Q9JMJ4	pre-mRNA-processing factor 19	nucleus	U	RNA-binding protein	mRNA splicing	
Q63081	protein disulfide isomerase (PDI) A6	ER	P	other isomerase	disulfide-isomerase reaction	43,52
P11598	PDI A3 (p58)	ER	P	isomerase	disulfide-isomerase reaction	43,52
P11884	aldehyde dehydrogenase	mitochondria	P	dehydrogenase	phenylethylamine degradation (carbon metabolism)	
Q66HD0	endoplasmin (GRP94, HSP90)	ER	P	chaperone	protein folding, stress response	43–46,50,51
P63039	60kDa heat shock protein (HSP60)	mitochondria	P	chaperonin	protein folding	30,43–47,49–51
P10719	F1-ATPase beta chain	mitochondria	P	other ion channel, hydrogen transporter, ATP synthase; hydrolase	purine metabolism, electron transport (ATP synthesis)	
Q6P136	hyou1 protein	cytosol	P	chaperone	stress response	
P48721	stress-70 protein (GRP75)	mitochondria	P	chaperone	protein folding; Stress response (apoptosis signaling pathway)	43–46
P14659	heat shock cognate 71kDa protein (HSP70)	cytosol, organelles	P	chaperone	protein folding; Stress response (apoptosis signaling pathway)	30,43–46,48–51
P60711	β-actin	cytoplasm	C, P, U	actin and actin related protein	transport; cytokinesis; cell structure, *etc.*	30–40
P15178	aspartyl-tRNA synthetase	cytoplasm	C, U	aminoacyl-tRNA synthetase	protein biosynthesis	
P02563	myosin-6 heavy chain	cytoplasm	C, U	motor protein, muscle protein	muscle contraction/development, (Wnt signaling pathway, cytokine signaling pathway, *etc*)	

 This journal is © The Royal Society of Chemistry and Owner Societies 2011

View Online

Table 1 *(Contd.)*

Gene ID	Name of protein	Cellular location	PDT response[a]	Main molecular function	Main biological process/pathway	Reference
P32089	tricarboxylate transport protein (TCC)	mitochondria, membrane	C, U	mitochondrial carrier protein	small molecule transport	
A7VJC2	hnRNP A2/B1	nucleus, cytoplasm	C, U	ribonucleoprotein	mRNA splicing	
P04256	hnRNP A1	nucleus, cytoplasm	C, U	ribonucleoprotein	mRNA splicing, mRNA transport	
Q7TP52	carboxymethylene-butenolidase homolog	cytoplasm	C, U	hydrolase; other miscellaneous function protein	carbohydrate metabolism	
Q5M7T9	threonine synthase-like 2	cytosol	C, U	synthase	threonine biosynthesis; vitamin B6 metabolism	
P54758	ephrin type-A receptor 6	membrane	C, U	tyrosine protein kinase, receptor; transferase	protein phosphorylation; cell proliferation and differentiation; receptor protein tyrosine kinase signaling pathway	
Q06226	serum and glucocorticoid -regulated kinase (sgk1)	ER, nucleus, cytoplasm	C, D	kinase activity	Protein phosphorylation; Inhibition of apoptosis; Other homeostasis activities and intracellular signaling cascade	

[a] D: down-regulated; U: up-regulated; P: pI-shift; C: carbonylated. [b] hnRNP: heterogeneous nuclear ribonucleoprotein.

Published on 30 March 2011 on http://pubs.rsc.org | doi:10.1039/C0PP00369G
Downloaded by RSC Internal on 26 May 2011

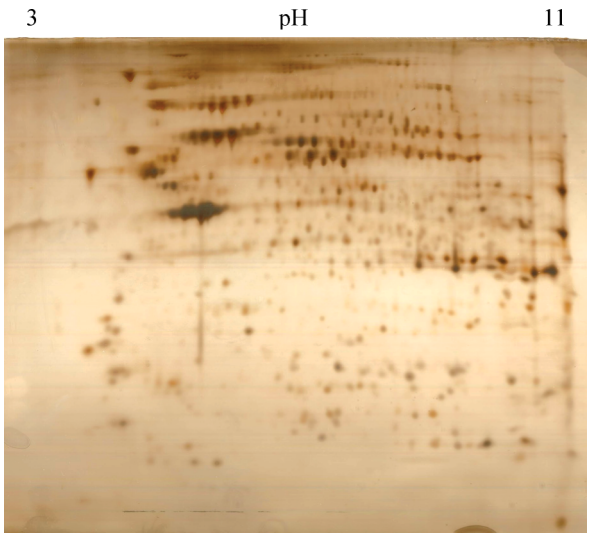

Fig. 2 Silver-stained gel. HAL and PDT lysate samples (300 μg of each) of AY-27 cells were mixed and subjected to IEF in a 24 cm IPGstrip pH 3–11 and separated in a 10% polyacrylamide gel. Proteins selected from the DIGE reference gel were excised from the silver stained gel for MS identification.

Grp75 all display marked acidic pI-shifts after HAL-mediated PDT. It is tempting to speculate that these abundant proteins may be quantitatively dominating targets for direct oxidative attack within the cell during HAL-mediated PDT, and that the observed pI-shifts may represent such covalent modifications that are not reversed by the reducing conditions employed during 2D-DIGE. Cysteine sulfonic acid is such an irreversible modification, whereas cysteine sulfenic acid and reaction products thereof such as glutathioylations, are reversible,[36] and would most likely have been reverted during the procedure of two dimensional gel-electrophoresis. Moreover, carbonylation should not mediate pI shifts since they do not introduce charge differences in the proteins. An alternative explanation would be that these proteins, at least in part, are modified enzymatically as part of the oxidative stress response. At least the protein disulfide isomerases, β-actin, HSP70/90 may become phosphorylated as a consequence of various forms of cellular stress, and for the chaperone group of protein this apparently is part of a regulatory mechanism modulating the substrate specificity.

Damage to several structural proteins induced by PDT was previously reported using other cell lines and photosensitizers. Moor *et al.* and Lee *et al.* stated that cellular structures having high sensitizer and a high oxygen concentration would be preferentially damaged upon illumination.[37,38] Belichenko *et al.* investigated the role of vimentin in apoptosis after PDT with the silicon phthalocyanine Pc4 in human Jurkat T cells and found that the full-length vimentin confers resistance to nuclear apoptosis.[39]

View Online

Published on 30 March 2011 on http://pubs.rsc.org | doi:10.1039/C0PP00369G
Downloaded by RSC Internal on 26 May 2011

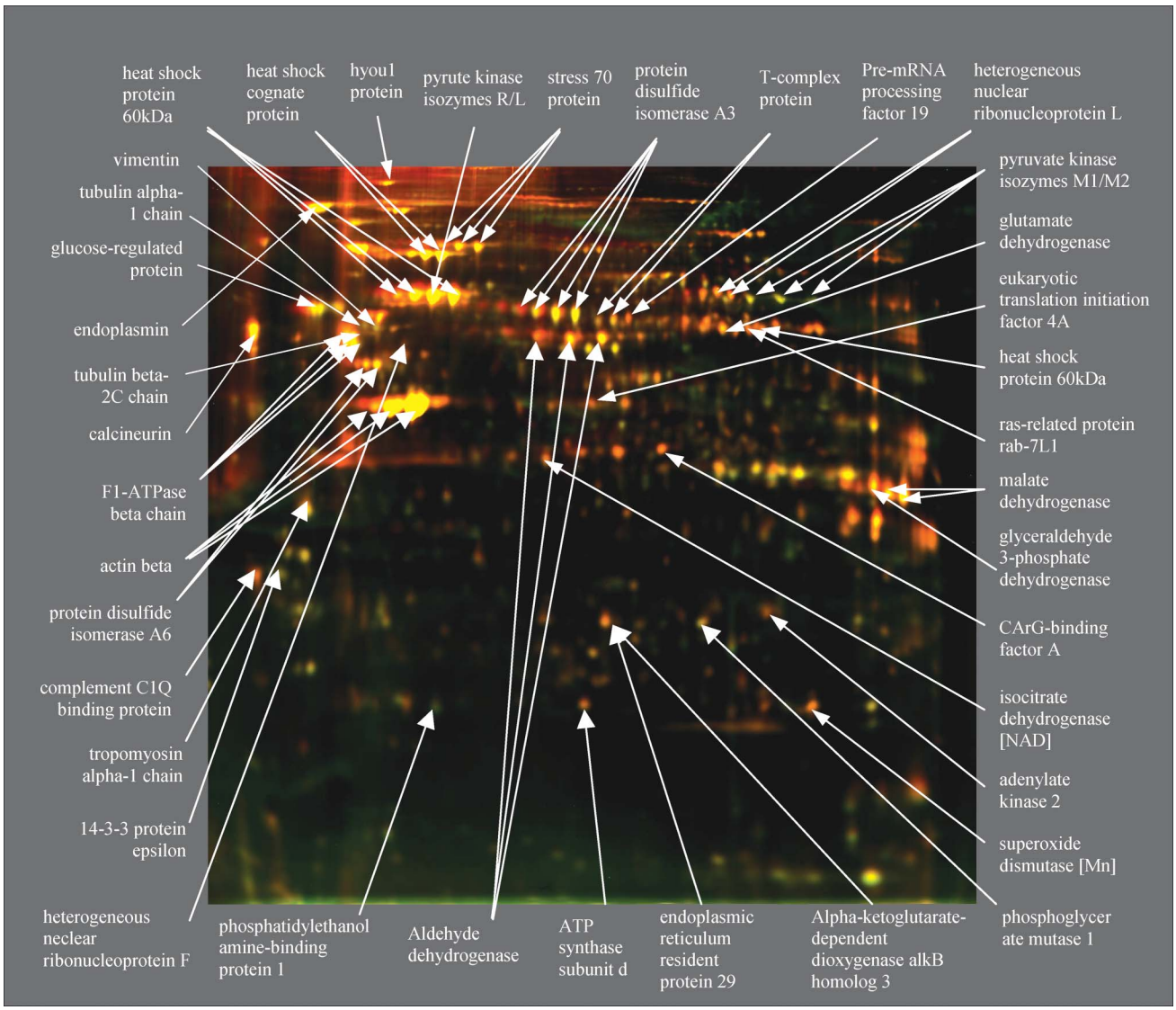

Fig. 3 Mapping of 40 identified proteins in AY-27 cells (DIGE, 10% polyacrylamide gel). Protein spots of interest were picked from both 2D-DIGE gels and silver stained 2D-GE gels and identified by MALDI-TOF/TOF (Ultraflex III, BRUKER Daltonics GmbH, Germany).

Later, Tsaytler *et al.* concluded that more structural proteins were oxidatively modified in human epidermoid carcinoma cells A431 after Pc4-PDT,[40] and Magi *et al.* described that tubulin α-1 chain and β-actin were modified *via* carbonylation after PDT with Purpurin-18 in human HL60 cells.[30]

It has been demonstrated that some cell lines can respond to photodynamic damage by initiating a rescue response[41,42] to induce expression of stress proteins containing a number of heat shock proteins (HSPs) and glucose-regulated proteins (GRPs).[43–46] The contribution by HSP60 increased the resistance to Photofrin-mediated PDT in human colon cancer cell line (HT29),[47] while HSP70 was demonstrated to inhibit apoptosis mediated by PDT with either dihematoporphyrin ether or Purpurin-18 in human leukemia cells (HL60).[48] Elevated expression of both HSP60 and HSP70 after ALA-PDT was observed in several human cell lines by Yanase *et al.*,[49] and these proteins were carbonylated during Purpurin-18 mediated PDT, as reported by Magi *et al.*[30] Moreover, it has been demonstrated that the amounts of HSP60, HSP70 and GRP94 (endoplasmin, HSP90) increased at the cell surface, contributing to enhanced immune responses in mouse tumor cells (SCCVII) after Photofrin-mediated PDT.[50,51] Our results show that several rescue/stress proteins were modified in the rat cell line AY-27 after HAL-PDT, including HSP60, HSP70, GRP94, GRP75 and hyou1 protein. These proteins have important chaperone functions in the cell and apparently may shield the cells from oxidative damage. Interestingly, Magi *et al.*[30] hypothesized that cellular chaperones may actually bind to oxidized proteins and that a protein-protein radical transfer can occur from oxidized proteins to chaperones. Thus, certain chaperones trying to reduce the toxic effect of oxidative stress are themselves oxidized.

Among proteins involved in energy metabolism, pI-shift was observed for hyou1 protein and F1-ATPase beta chain. Additionally, pyruvate kinase isozymes M1/M2 were shown to be down-regulated. These modifications might contribute to energy insufficiency and cell death by inhibiting the hypoxia responses.

 This journal is © The Royal Society of Chemistry and Owner Societies 2011

View Online

Published on 30 March 2011 on http://pubs.rsc.org | doi:10.1039/C0PP00369G
Downloaded by RSC Internal on 26 May 2011

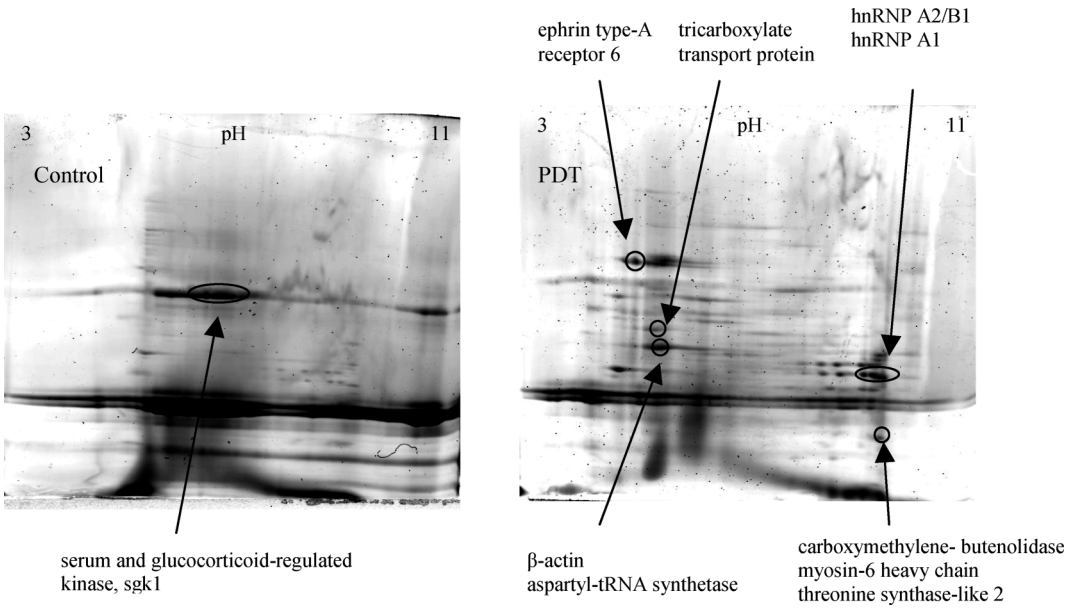

Fig. 4 Mapping of carbonylated proteins of AY-27 cells 2 h subsequent to HAL-mediated PDT. Nine up-regulated proteins are shown in PDT sample (right) and one down-regulated is shown in Control sample (left). Each sample (1.5 mg) was labeled with 10mM DNPH in 10% TFA and immunoprecipited with 150 µl cross-linked protein A beads with anti-DNP antibodies before 2D-GE separation. Protein spots of interest were excised from krypton-gels and 10 carbonylated proteins were identified by MALDI-TOF/TOF.

Moreover, the modifications on the rescue/stress proteins might lose their protective effect against oxidative stress triggering the suicide mechanism after PDT.

Three proteins associated with Ca^{2+} signaling pathways were shown to be affected by ALA-PDT,[43,52] including calreticulin precursor, protein disulfide isomerase (p55) and protein disulfide isomerase A3 (p58).[43] In our study, although protein p58, p55 and calcineurin subunit B have been identified, only p58 was confirmed to be modified by showing a pI-shift. More experiments are required to identify possible HAL-PDT effects on this signaling pathway.

3.2 Detection of carbonylated proteins

The most widely used marker for oxidative damage to proteins is the presence of carbonyl groups. Carbonyls can be introduced into proteins either by direct oxidation of Pro, Arg, Lys, and Thr side chains or by Michael addition reactions with products of lipid peroxidation or glycol-oxidation. Elevation in the total level of protein carbonyls has been documented after PDT, but the identities of the proteins modified by carbonylation or other types of oxidation remain largely incompletely understood. Since carbonylation, in contrast to oxidation of cysteine to cysteine sulfonic or sulfinic acid, do not mediate a change in pI, control and PDT samples were derivatized with DNPH and immunoprecipitated using an anti-DNP antibody prior to separation by 2D-GE. By using this experimental outline we were able to identify 9 proteins with increased carbonylation and, surprisingly, one protein with reduced carbonylation (Fig. 4).

According to our results, β-actin was confirmed to be carbonylated after HAL-PDT, in agreement with results after PDT with Purpurin-18 in HL60.[30] However, carbonylation is apparently not the only modification induced in β-actin by HAL-PDT. The pI-shift towards the acidic side indicates that alternative oxidations such as cysteine sulfinic acid, or secondary enzymatic modifications such as phosphorylation, may be present.

Moreover, protein hnRNP A1 and hnRNP A2/B1 were confirmed to be up-regulated and oxidized. Together with pre-mRNA processing factor 19 and hnRNP L (Table 1), four up-regulated proteins in our results are related to DNA-repair, pre-mRNA processing and mRNA splicing. These results may suggest that transcription, translation or stability may have been increased in response to protein and DNA damages under oxidative stress induced by HAL-mediated PDT.

Interestingly, mitochondrial tricarboxylate carrier protein (TCC) and serum and glucocorticoid-regulated kinase 1 (sgk1) were found to display altered expression or modification after PDT. Both of them are supposed to play a key role in oxidative stress conditions in rat brain.[53,54] Our results demonstrate that both proteins were carbonylated. TCC was up-regulated, while sgk1 was down-regulated already at 2 h post-PDT.

3.3 Proteins, pathways and processes affected by HAL-PDT

ROS-induced modifications may change protein functions, thereby affecting biological processes and signaling pathways.[27] A total of more than 200 post-translational modifications have been identified.[55] Furthermore, increasing evidence suggests that many proteins carry multiple and distinct modifications. These may in some cases antagonize or synergize each other, with important biological consequences.[55] Thus, the PANTHER classification system was used to gain information of potential affected biological processes after HAL-PDT. Clearly, the complex responses indicate that no single mechanism can be responsible for the effects of HAL-PDT (Table 1).

In AY-27 cells the endogenous photosensitizer PpIX is synthesized and accumulated in mitochondria, and moves to other membrane-rich organelles when a certain concentration

View Online

Published on 30 March 2011 on http://pubs.rsc.org | doi:10.1039/C0PP00369G
Downloaded by RSC Internal on 26 May 2011

is reached.[1] Classification of proteins by cellular localization (Table 1) demonstrates that the majority of the modified proteins by HAL-PDT were from mitochondria, ER and membranes. However, in the study of Pc4-PDT,[40] the majority of affected proteins were cytosolic, likely reflecting a somewhat different cellular targeting of PpIX and Pc4.[56] So far, nuclear localization of PpIX has not been observed. Nevertheless, several cytoplasmic and nuclear proteins were shown to be affected in our study, likely caused by indirect oxidation or intracellular translocation subsequent to HAL-mediated PDT.

4. Conclusions

Our results demonstrate that a number of proteins in AY-27 cells are differentially expressed or chemically or enzymatically modified after HAL-mediated PDT, thus most likely affecting important processes, such as cell motility, energy metabolism, and signaling pathways for survival and cell death. The results support previous studies employing other photosensitizers,[30,40] in that numerous cellular pathways are likely to be affected by PDT. The majority of proteins identified subsequent to 2D-DIGE displayed acidic pI-shifts, indicating altered phosphorylation status or oxidative thiol modifications. Notably, these proteins mainly belong to the mitochondrial/ER molecular chaperones and stress proteins, indicating that these cellular compartments are major targets for HAL-mediated PDT. These results have extended our understanding of the clinic effects associated with ALA-PDT, and may pave the way for potential new adjuvant drugs. Our further studies are, however, warranted to elucidate to what degree these modifications are associated with the apoptotic signaling events induced by HAL-PDT. By better understanding mechanisms of PDT-mediated cytotoxicity in AY-27 bladder cancer cells, we aim at improving efficacy of PDT in the *in vivo* rat model[21] and ultimately in treatment of human bladder. This may also pave the way for targeted use of other treatment modalities, such as siRNA and photochemical internalization (PCI).[57]

Acknowledgements

We are grateful to our colleague Kristian Wollen Steen for his excellent laboratory assistance; to Photocure ASA and PCI Biotech AS (Oslo, Norway) for HAL (Hexvix®) and Lamp resource supply; to the FUGE Proteomics Laboratory at NTNU (Trondheim, Norway), and to Professor Steven H. Selman (Medical College of Ohio, USA) for AY-27 cell line supply.

References

1 N. Schoenfeld, O. Epstein, M. Lahav, R. Mamet, M. Shaklai and A. Atsmon, The heme biosynthetic pathway in lymphocytes of patients with malignant lymphoproliferative disorders, *Cancer Lett.*, 1988, **43**(1–2), 43–8.
2 J. Kloek, W. Akkermans and G. M. Beijersbergen van Henegouwen, Derivatives of 5-aminolevulinic acid for photodynamic therapy: enzymatic conversion into protoporphyrin, *Photochem. Photobiol.*, 1998, **67**(1), 150–4.
3 G. Di Venosa, H. Fukuda, A. Batlle, A. Macrobert and A. Casas, Photodynamic therapy: regulation of porphyrin synthesis and hydrolysis from ALA esters, *J. Photochem. Photobiol., B*, 2006, **83**(2), 129–36.
4 E. Rud, O. Gederaas, A. Hogset and K. Berg, 5-aminolevulinic acid, but not 5-aminolevulinic acid esters, is transported into adenocarcinoma cells by system BETA transporters, *Photochem. Photobiol.*, 2000, **71**(5), 640–7.
5 O. A. Gederaas, A. Holroyd, S. B. Brown, D. Vernon, J. Moan and K. Berg, 5-Aminolaevulinic acid methyl ester transport on amino acid carriers in a human colon adenocarcinoma cell line, *Photochem. Photobiol.*, 2001, **73**(2), 164–9.
6 O. A. Gederaas *Biological mechanisms involved in 5-aminovulinic acid based photodynamic therapy*, PhD thesis, NTNU and The Norwegian Radium Hospital, 2000.
7 N. Dognitz, D. Salomon, M. Zellweger, J. P. Ballini, T. Gabrecht and N. Lange, *et al.*, Comparison of ALA- and ALA hexyl-ester-induced PpIX depth distribution in human skin carcinoma, *J. Photochem. Photobiol., B*, 2008, **93**(3), 140–8.
8 A. Marti, P. Jichlinski, N. Lange, J. P. Ballini, L. Guillou and H. J. Leisinger *et al.*, Comparison of aminolevulinic acid and hexylester aminolevulinate induced protoporphyrin IX distribution in human bladder cancer, *J. Urol.*, 2003, **170**(2), 428–32.
9 A. Juzeniene, K. P. Nielsen, L. Zhao, G. A. Ryzhikov, M. S. Biryulina and J. J. Stamnes *et al.*, Changes in human skin after topical PDT with hexyl aminolevulinate, *Photodiagn. Photodyn. Ther.*, 2008, **5**(3), 176–81.
10 R. W. Wu, E. S. Chu, C. M. Yow and J. Y. Chen, Photodynamic effects on nasopharyngeal carcinoma (NPC) cells with 5-aminolevulinic acid or its hexyl ester, *Cancer Lett.*, 2006, **242**(1), 112–9.
11 S. M. WU, Q. G. Ren, M. O. Zhou and Y. Wei, Photodynamic Effects of 5-Aminolevulinic Acid and Its Hexylester on Several Cell Lines, *Acta Biochim. Biophys. Sin.*, 2003, **35**(7), 655–60.
12 A. Casas, C. Perotti, M. Saccoliti, P. Sacca, H. Fukuda and A. M. Batlle, ALA and ALA hexyl ester in free and liposomal formulations for the photosensitisation of tumour organ cultures, *Br. J. Cancer*, 2002, **86**(5), 837–42.
13 S. Berrahmoune, N. Fotinos, L. Bezdetnaya, N. Lange, J. C. Guedenet and F. Guillemin *et al.*, Analysis of differential PDT effect in rat bladder tumor models according to concentrations of intravesical hexyl-aminolevulinate, *Photochem. Photobiol. Sci.*, 2008, **7**(9), 1018–24.
14 L. Zhao, K. P. Nielsen, A. Juzeniene, P. Juzenas, V. Lani and L. W. Ma *et al.*, Spectroscopic measurements of photoinduced processes in human skin after topical application of the hexyl ester of 5-aminolevulinic acid, *J. Environ. Pathol. Toxicol. Oncol.*, 2006, **25**(1-2), 307–20.
15 A. Juzeniene, P. Juzenas, L. W. Ma, V. Iani and J. Moan, Topical application of 5-aminolaevulinic acid, methyl 5-aminolaevulinate and hexyl 5-aminolaevulinate on normal human skin, *Br. J. Dermatol.*, 2006, **155**(4), 791–9.
16 V. Zenzen and H. Zankl, Protoporphyrin IX-accumulation in human tumor cells following topical ALA- and h-ALA-application in vivo, *Cancer Lett.*, 2003, **202**(1), 35–42.
17 S. El Khatib, J. Didelon, A. Leroux, L. Bezdetnaya, D. Notter and M. D'Hallewin, Kinetics, biodistribution and therapeutic efficacy of hexylester 5-aminolevulinate induced photodynamic therapy in an orthotopic rat bladder tumor model, *J. Urol.*, 2004, **172**(5), 2013–7.
18 G. Kirdaite, N. Lange, N. Busso, H. Van Den Bergh, P. Kucera and A. So, Protoporphyrin IX photodynamic therapy for synovitis, *Arthritis Rheum.*, 2002, **46**(5), 1371–8.
19 M. Ascencio, J. P. Estevez, M. Delemer, M. O. Farine, P. Collinet and S. Mordon, Comparison of continuous and fractionated illumination during hexaminolaevulinate-photodynamic therapy, *Photodiagn. Photodyn. Ther.*, 2008, **5**(3), 210–6.
20 L. Vaucher, P. Jichlinski, N. Lange, C. Ritter-Schenk, H. van den Bergh and P. Kucera, Hexyl-aminolevulinate-mediated photodynamic therapy: how to spare normal urothelium. An in vitro approach, *Lasers Surg. Med.*, 2007, **39**(1), 67–75.
21 E. L. Larsen, L. L. Randeberg, O. A. Gederaas, C. J. Arum, A. Hjelde and C. M. Zhao *et al.*, Monitoring of hexyl 5-aminolevulinate-induced photodynamic therapy in rat bladder cancer by optical spectroscopy, *J. Biomed. Opt.*, 2008, **13**(4), 044031.
22 M. Ascencio, P. Collinet, M. O. Farine and S. Mordon, Protoporphyrin IX fluorescence photobleaching is a useful tool to predict the response of rat ovarian cancer following hexaminolevulinate photodynamic therapy, *Lasers Surg. Med.*, 2008, **40**(5), 332–41.
23 P. Soergel, X. Wang, H. Stepp, H. Hertel and P. Hillemanns, Photodynamic therapy of cervical intraepithelial neoplasia with hexaminolevulinate, *Lasers Surg. Med.*, 2008, **40**(9), 611–5.
24 S. Shahzidi, T. Stokke, H. Soltani, J. M. Nesland and Q. Peng, Induction of apoptosis by hexaminolevulinate-mediated photodynamic therapy in

 This journal is © The Royal Society of Chemistry and Owner Societies 2011

View Online

human colon carcinoma cell line 320DM, *J. Environ. Pathol. Toxicol. Oncol.*, 2006, **25**(1-2), 159–71.
25 I. E. Furre, M. T. Moller, S. Shahzidi, J. M. Nesland and Q. Peng, Involvement of both caspase-dependent and -independent pathways in apoptotic induction by hexaminolevulinate-mediated photodynamic therapy in human lymphoma cells, *Apoptosis*, 2006, **11**(11), 2031–42.
26 I. E. Furre, S. Shahzidi, Z. Luksiene, M. T. Moller, E. Borgen and J. Morgan *et al.*, Targeting PBR by hexaminolevulinate-mediated photodynamic therapy induces apoptosis through translocation of apoptosis-inducing factor in human leukemia cells, *Cancer Res.*, 2005, **65**(23), 11051–60.
27 K. England and T. G. Cotter, Direct oxidative modifications of signalling proteins in mammalian cells and their effects on apoptosis, *Redox Rep.*, 2005, **10**(5), 237–45.
28 E. R. Stadtman and R. L. Levine, Protein oxidation, *Ann. N. Y. Acad. Sci.*, 2000, **899**, 191–208.
29 I. Dalle-Donne, M. Carini, M. Orioli, G. Vistoli, L. Regazzoni and G. Colombo *et al.*, Protein carbonylation: 2,4-dinitrophenylhydrazine reacts with both aldehydes/ketones and sulfenic acids, *Free Radical Biol. Med.*, 2009, **46**(10), 1411–9.
30 B. Magi, A. Ettorre, S. Liberatori, L. Bini, M. Andreassi and S. Frosali *et al.*, Selectivity of protein carbonylation in the apoptotic response to oxidative stress associated with photodynamic therapy: a cell biochemical and proteomic investigation, *Cell Death Differ.*, 2004, **11**(8), 842–52.
31 T. Reinheckel, S. Korn, S. Mohring, W. Augustin, W. Halangk and L. Schild, Adaptation of protein carbonyl detection to the requirements of proteome analysis demonstrated for hypoxia/reoxygenation in isolated rat liver mitochondria, *Arch. Biochem. Biophys.*, 2000, **376**(1), 59–65.
32 I. V. Kjaersgard and F. Jessen, Two-dimensional gel electrophoresis detection of protein oxidation in fresh and tainted rainbow trout muscle, *J. Agric. Food Chem.*, 2004, **52**(23), 7101–7.
33 A. Shevchenko, M. Wilm, O. Vorm and M. Mann, Mass spectrometric sequencing of proteins silver-stained polyacrylamide gels, *Anal. Chem.*, 1996, **68**(5), 850–8.
34 M. Mann and O. N. Jensen, Proteomic analysis of post-translational modifications, *Nat. Biotechnol.*, 2003, **21**(3), 255–61.
35 P. C. Burcham, A. Raso and C. A. Thompson, Intermediate filament carbonylation during acute acrolein toxicity in A549 lung cells: functional consequences, chaperone redistribution, and protection by bisulfite, *Antioxid. Redox Signaling*, 2010, **12**(3), 337–47.
36 N. L. Reynaert, A. van der Vliet, A. S. Guala, T. McGovern, M. Hristova and C. Pantano *et al.*, Dynamic redox control of NF-kappaB through glutaredoxin-regulated S-glutathionylation of inhibitory kappaB kinase beta, *Proc. Natl. Acad. Sci. U. S. A.*, 2006, **103**(35), 13086–91.
37 A. C. Moor, Signaling pathways in cell death and survival after photodynamic therapy, *J. Photochem. Photobiol., B*, 2000, **57**(1), 1–13.
38 C. Lee, S. S. Wu and L. B. Chen, Photosensitization by 3,3′-dihexyloxacarbocyanine iodide: specific disruption of microtubules and inactivation of organelle motility, *Cancer Res.*, 1995, **55**(10), 2063–9.
39 I. Belichenko, N. Morishima and D. Separovic, Caspase-resistant vimentin suppresses apoptosis after photodynamic treatment with a silicon phthalocyanine in Jurkat cells, *Arch. Biochem. Biophys.*, 2001, **390**(1), 57–63.
40 P. A. Tsaytler, M. COF, D. V. Sakharov, J. Krijgsveld and M. R. Egmond, Immediate protein targets of photodynamic treatment in carcinoma cells, *J. Proteome Res.*, 2008, **7**(9), 3868–78.
41 T. J. Dougherty, C. J. Gomer, B. W. Henderson, G. Jori, D. Kessel and M. Korbelik *et al.*, Photodynamic therapy, *J. Natl. Cancer Inst.*, 1998, **90**(12), 889–905.
42 C. J. Gomer, A. Ferrario, N. Hayashi, N. Rucker, B. C. Szirth and A. L. Murphree, Molecular, cellular, and tissue responses following photodynamic therapy, *Lasers Surg. Med.*, 1988, **8**(5), 450–63.
43 D. Grebenova, P. Halada, J. Stulik, V. Havlicek and Z. Hrkal, Protein changes in HL60 leukemia cells associated with 5-aminolevulinic acid-based photodynamic therapy. Early effects on endoplasmic reticulum chaperones, *Photochem. Photobiol.*, 2000, **72**(1), 16–22.
44 C. J. Gomer, S. W. Ryter, A. Ferrario, N. Rucker, S. Wong and A. M. Fisher, Photodynamic therapy-mediated oxidative stress can induce expression of heat shock proteins, *Cancer Res.*, 1996, **56**(10), 2355–60.
45 C. J. Gomer, A. Ferrario, N. Rucker, S. Wong and A. S. Lee, Glucose regulated protein induction and cellular resistance to oxidative stress mediated by porphyrin photosensitization, *Cancer Res.*, 1991, **51**(24), 6574–9.
46 P. M. Curry and J. G. Levy, Stress protein expression in murine tumor cells following photodynamic therapy with benzoporphyrin derivative, *Photochem. Photobiol.*, 1993, **58**(3), 374–9.
47 J. G. Hanlon, K. Adams, A. J. Rainbow, R. S. Gupta and G. Singh, Induction of Hsp60 by Photofrin-mediated photodynamic therapy, *J. Photochem. Photobiol., B*, 2001, **64**(1), 55–61.
48 M. Nonaka, H. Ikeda and T. Inokuchi, Inhibitory effect of heat shock protein 70 on apoptosis induced by photodynamic therapy in vitro, *Photochem. Photobiol.*, 2004, **79**(1), 94–8.
49 S. Yanase, J. Nomura, Y. Matsumura, K. Nagai, M. Kinoshita and H. Nakanishi *et al.*, Enhancement of the effect of 5-aminolevulinic acid-based photodynamic therapy by simultaneous hyperthermia, *Int. J. Oncol.*, 2005, **27**(1), 193–201.
50 M. Korbelik, J. Sun and I. Cecic, Photodynamic therapy-induced cell surface expression and release of heat shock proteins: relevance for tumor response, *Cancer Res.*, 2005, **65**(3), 1018–26.
51 I. Cecic and M. Korbelik, Deposition of complement proteins on cells treated by photodynamic therapy in vitro, *J. Environ. Pathol. Toxicol. Oncol.*, 2006, **25**(1-2), 189–203.
52 O. A. Gederaas, K. Thorstensen and I. Romslo, The effect of brief illumination on intracellular free calcium concentration in cells with 5-aminolevulinic acid-induced protoporphyrin IX synthesis, *Scand. J. Clin. Lab. Invest.*, 1996, **56**(7), 583–9.
53 A. L. Wadey, H. Muyderman, P. T. Kwek and N. R. Sims, Mitochondrial glutathione uptake: characterization in isolated brain mitochondria and astrocytes in culture, *J. Neurochem.*, 2009, **109**(Suppl 1), 101–8.
54 B. Schoenebeck, V. Bader, X. R. Zhu, B. Schmitz, H. Lubbert and C. C. Stichel, Sgk1, a cell survival response in neurodegenerative diseases, *Mol. Cell. Neurosci.*, 2005, **30**(2), 249–64.
55 N. Khidekel and L. C. Hsieh-Wilson, A 'molecular switchboard'–covalent modifications to proteins and their impact on transcription, *Org. Biomol. Chem.*, 2004, **2**(1), 1–7.
56 M. Lam, N. L. Oleinick and A. L. Nieminen, Photodynamic therapy-induced apoptosis in epidermoid carcinoma cells. Reactive oxygen species and mitochondrial inner membrane permeabilization, *J. Biol. Chem.*, 2001, **276**(50), 47379–86.
57 P. K. Selbo, A. Weyergang, A. Hogset, O. J. Norum, M. B. Berstad, M. Vikdal and K. Berg, Photochemical internalization provides time- and space-controlled endolysosomal escape of therapeutic molecules, *J. Controlled Release*, 2010, **148**(1), 2–12.

Published on 30 March 2011 on http://pubs.rsc.org | doi:10.1039/C0PP00369G
Downloaded by RSC Internal on 26 May 2011

Paper 2

OPEN ACCESS Freely available online

PLOS ONE

Homology Modeling of Human γ-Butyric Acid Transporters and the Binding of Pro-Drugs 5-Aminolevulinic Acid and Methyl Aminolevulinic Acid Used in Photodynamic Therapy

Yan Baglo[1], Mari Gabrielsen[2], Ingebrigt Sylte[2], Odrun A. Gederaas[1]*

1 Department of Cancer Research and Molecular Medicine, Faculty of Medicine, Norwegian University of Science and Technology, Trondheim, Norway, **2** Medical Pharmacology and Toxicology, Department of Medical Biology, Faculty of Health Sciences, University of Tromsø, Tromsø, Norway

Abstract

Photodynamic therapy (PDT) is a safe and effective method currently used in the treatment of skin cancer. In ALA-based PDT, 5-aminolevulinic acid (ALA), or ALA esters, are used as pro-drugs to induce the formation of the potent photosensitizer protoporphyrin IX (PpIX). Activation of PpIX by light causes the formation of reactive oxygen species (ROS) and toxic responses. Studies have indicated that ALA and its methyl ester (MAL) are taken up into the cells via γ-butyric acid (GABA) transporters (GATs). Uptake via GATs into peripheral sensory nerve endings may also account for one of the few adverse side effects of ALA-based PDT, namely pain. In the present study, homology models of the four human GAT subtypes were constructed using three x-ray crystal structures of the homologous leucine transporter (LeuT) as templates. Binding of the native substrate GABA and the possible substrates ALA and MAL was investigated by molecular docking of the ligands into the central putative substrate binding sites in the outward-occluded GAT models. Electrostatic potentials (ESPs) of the putative substrate translocation pathway of each subtype were calculated using the outward-open and inward-open homology models. Our results suggested that ALA is a substrate of all four GATs and that MAL is a substrate of GAT-2, GAT-3 and BGT-1. The ESP calculations indicated that differences likely exist in the entry pathway of the transporters (i.e. in outward-open conformations). Such differences may be exploited for development of inhibitors that selectively target specific GAT subtypes and the homology models may hence provide tools for design of therapeutic inhibitors that can be used to reduce ALA-induced pain.

Citation: Baglo Y, Gabrielsen M, Sylte I, Gederaas OA (2013) Homology Modeling of Human γ-Butyric Acid Transporters and the Binding of Pro-Drugs 5-Aminolevulinic Acid and Methyl Aminolevulinic Acid Used in Photodynamic Therapy. PLoS ONE 8(6): e65200. doi:10.1371/journal.pone.0065200

Editor: Jonathan Wesley Arthur, Children's Medical Research Institute, Australia

Received December 31, 2012; **Accepted** April 23, 2013; **Published** June 7, 2013

Copyright: © 2013 Baglo et al. This is an open-access article distributed under the terms of the Creative Commons Attribution License, which permits unrestricted use, distribution, and reproduction in any medium, provided the original author and source are credited.

Funding: The authors gratefully acknowledge support and training from BioStruct (the Norwegian national graduate school in structural biology). The funders had no role in study design, data collection and analysis, decision to publish, or preparation of the manuscript.

Competing Interests: The authors have declared that no competing interests exist.

* E-mail: odrun.gederaas@ntnu.no

Introduction

Photodynamic therapy (PDT) is an innovative treatment modality for cancer that involves systemic or topical administration of a photosensitizer pro-drug, or the photosensitizer itself, and activation of the photosensitizer by light of appropriate wavelengths, resulting in generation of reactive oxygen species (ROS) and toxic responses [1–3].

One commonly used PDT pro-drug is 5-aminolevulinic acid (ALA). Topical (dermal) administration of ALA or the ALA methyl ester (MAL) (ALA-based PDT) is approved for treatment of non-melanoma skin cancers including superficial basal cell carcinoma (BCC), actinic keratosis (AK), Bowen's disease (BD), and squamous cell carcinoma in situ (SCC) in many countries [2]. In these cancers, ALA-based PDT may also be used in replacement or to reduce the extent of surgery [4]. Furthermore, the use of ALA-based PDT for the treatment of other types of cancer, e.g. in the brain, stomach and bladder, are currently being evaluated in clinical trials [3]. ALA-based PDT may also be used for the treatment of acne, psoriasis, scleroderma, viral warts, photoaging and cutaneous lymphoma [2].

ALA is an endogenous precursor of the potent photosensitizer protoporphyrin IX (PpIX), which is synthesized in the heme biosynthetic pathway of nucleated cells [5]. By administration of exogenous ALA the first rate-limiting step of the heme biosynthetic pathway, which is regulated by negative feedback of heme, is bypassed [6,7]. Studies have furthermore indicated that PpIX accumulates in greater amounts in tumor cells than in normal cells following the administration of exogenous ALA [5]. The main reasons for the selective accumulation in cancer cells are the changes in the activity of two enzymes of the heme biosynthesis pathway, namely increased activity of porphoblinogen deaminase, which catalyzes an early step of the heme biosynthetic pathway, and decreased activity of ferrochelatase, catalyzing the conversion of PpIX to heme in the last step of the biosynthetic pathway [6]. MAL was developed to increase the hydrophobicity and hence skin penetration of the pro-drug. Once inside the cell, intracellular esterases catalyze the cleavage of the ALA esters to ALA, which then enters the heme biosynthetic pathway [7].

Due to the selective accumulation of PpIX in cancer cells, ALA-based PDT does not cause the serious adverse side effects often

seen with conventional chemotherapy. The main limiting factor for successful clinical ALA-based PDT is pain, which in some cases is so severe that the treatment is discontinued [8,9]. Although the mechanism of pain has not fully been elucidated, several studies have suggested that it may be due to nerve stimulation and tissue damage induced by ROS [10,11]. Interestingly, clinical studies have shown that MAL may induce less pain than ALA [9,12,13].

Studies by our group and others have indicated that active cellular uptake of ALA is via γ-aminobutyric acid (GABA) transporters (GATs) [14–18], of which four human subtypes, GAT-1, GAT-2, GAT-3 and BGT-1 (betaine-GABA transporter-1), have been identified [19-22]. The uptake of MAL, however, seems to be cell type dependent [15–17]. In adenocarcinoma WiDr and LM3 cells, studies have indicated that MAL is transported via non-polar amino acid transporters rather than GAT [15,18]. MAL uptake was also recently suggested to be via GATs and other amino acid transporters in rat peripheral DRG sensory neurons [16] and in human A431 and CCD skin cells [17].

The GATs belong to the neurotransmitter/sodium symporter (NSS) transporter family [23] of the solute carrier 6 (SLC6) superfamily [24]. The NSS family members mediate Na^+-dependent uptake of a wide array of substrates, including dopamine (DAT), serotonin (SERT), noradrenaline (NET), glycine (GlyT) and GABA (GATs) [23], using an alternate access mechanism [25,26]. During transport, the substrate binding site, which has a central location midway between the extracellular environment and the cytoplasm, is sequentially exposed to either side of the membrane through permeation pathways [25,26]. Substrate transport thus involves cycling between outward-open, outward-occluded and inward-open conformational states of the transporters.

Only one member of the NSS family, namely the prokaryotic *Aquifex aeolicus* leucine transporter (LeuT), has so far been crystallized. In support of the alternate-access hypothesis, however, the LeuT crystal structures are available in outward-open, outward-occluded and inward-open conformations [27–29]. Co-crystallized with substrates the transporter is stabilized in an outward-occluded state [29]. In contrast, the crystal structure of LeuT in complex with the competitive inhibitor tryptophan (Trp) shows that Trp stabilizes LeuT in an outward-open conformation [29]. The LeuT crystal structures hence suggest that in order for transport to occur, the substrates must be able to induce a conformational change in the transporter from outward-open to outward-occluded.

In this study, homology models of the four human transporters in outward-occluded, outward- and inward-open conformations were constructed using three x-ray crystal structures of LeuT as templates [27–29]. To investigate the binding of GABA, ALA and MAL, the compounds were docked into in the central putative substrate binding sites in the outward-occluded GAT models. Furthermore, the electrostatic potentials (ESPs) of the putative translocation pathways leading from the extracellular environment to the central substrate binding site (termed the 'entry' pathway) and from the central substrate binding site to the cytoplasm (termed the 'exit' pathway) were calculated in the outward- and inward-open homology models, respectively. Our results suggest that whereas ALA most likely is a substrate of all four GAT subtypes, MAL may only be a substrate of GAT-2, GAT-3 and BGT-1. Furthermore, the results suggest that the major differences between the transporter subtypes most likely are located to the entry pathway. This region may hence be the most interesting to study with the aim of obtaining subtype-selective GAT inhibitors.

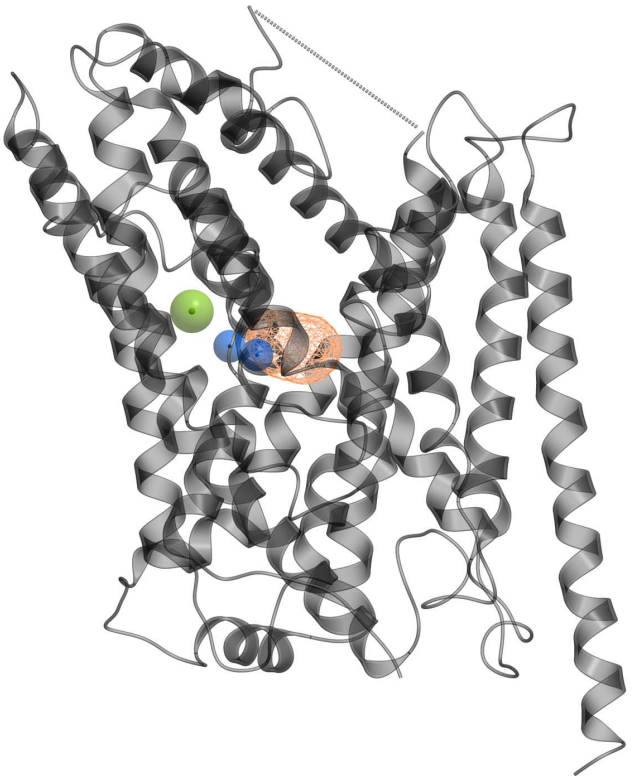

Figure 1. Outward-occluded GAT-2 model. Membrane view of the outward-occluded GAT-2 homology model (grey ribbon representation). Orange wire: the putative substrate binding site detected by ICM PocketFinder; blue spheres: Na1 and Na2 sodium ions; green sphere: chloride ion; dotted line: missing EL2 residues.
doi:10.1371/journal.pone.0065200.g001

Methods

Homology Modeling

The amino acid sequences of GAT-1, GAT-2, GAT-3 and BGT-1 (UniProt accession numbers P30531, Q9NSD5, P48066 and P48065, respectively) [30] were aligned with LeuT using the Internal Coordinate Mechanics (ICM) version 3.7 software [31]. The alignment was adjusted according to the comprehensive alignment of prokaryotic and eukaryotic NSS transporter sequences published by Beuming *et al.* [32] (Figure S1).

Based on the alignment, outward-open GAT models were constructed using the 3F3A LeuT x-ray crystal structure [29] as template, while the outward-occluded and inward-open GAT models were generated based on the 2A65 [27] and 3TT3 [28] crystal structures, respectively. The ICM BuildModel macro was used to construct the models [31]. This macro uses a rigid body approach to transfer the conformation of the structurally conserved regions from the template to the target and constructs the non-conserved loop regions either by *ab initio* modeling (< seven amino acids) or by PDB loop searching (> seven amino acids) [31]. The final models consisted of the twelve TMs and the connecting intra- and extracellular loops, but did not include the N- and C-termini and parts of EL2.

The Na1 and Na2 sodium ions were copied into the outward-open and outward-occluded GAT models from their corresponding LeuT templates as the amino acids coordinating the two sodium ions are highly conserved [32]. Although Rud *et al.* [14] have suggested that three sodium ions are needed for the transmembrane transport of ALA, a Na^+: Cl^- stoichiometry of

Table 1. Central substrate binding site.

GAT-1	GAT-2	GAT-3	BGT-1	Position
Y60	E48	E66	E52	**1.42**
A61	I49	I67	I53	**1.43**
I62	*I*	*I*	*I*	**1.44**
G63	G51	G69	G55	**1.45**
L64	L52	L70	L56	**1.46**
G65	G53	G71	G57	**1.47**
N66	N54	*N*	*N*	**1.48**
L136	L125	L143	L129	**3.46**
Y140	Y129	Y147	Y133	**3.50**
F294	F288	F308	F293	**6.53**
S295	S289	S309	S294	**6.54**
G297	A291	A311	A296	**6.56**
L300	L294	L314	Q299	**6.59**
S396	S390	S410	S395	**8.60**
Q397	*Q*	*Q*	*Q*	**8.61**
C399	V393	V413	*V*	**8.63**
T400	C394	C414	C399	**8.64**
172.2	145.2	161.1	118.6	**Volume (Å^3)**
156	140.4	150.3	121.4	**Area (Å^2)**

Amino acids detected by ICM PocketFinder in the outward-occluded GAT models; in *italics*: amino acids not detected in the respective models.
doi:10.1371/journal.pone.0065200.t001

2:1 was applied in this study due to the lack of positional knowledge of the putative third sodium ion. In addition, a chloride ion was placed in the position corresponding to the carboxylate carbon of LeuT amino acid E290 in the outward-open and outward-occluded models [33,34].

Energy Refinement

The ICM RefineModel macro (default settings) [35] was used to remove possible close contacts between amino acids in the models and to relax the structures. The macro performs 1) side chain sampling using the program module Montecarlo-fast [35], 2) iterative annealing with tethers, and 3) a second side chain sampling. Iterations of Montecarlo-fast consist of a random move followed by local energy minimization and the iteration is either accepted or rejected based on the energy [35].

Structure Quality Check

The programs PROCHECK, ERRAT and VERIFY-3D, available through the Structural Analysis and Verification Server (SAVES, http://nihserver.mbi.ucla.edu/SAVES/), were used to perform structure quality checks of the models before and after the refinement step.

Evaluation of the Outward-occluded Models by Docking

To evaluate whether the outward-occluded GAT models could separate binders from decoys, an evaluation test set containing 17 binders and 170 decoys was established (Figure S2; S3). The 170 decoys were selected using ICM Molcart [31] based on their structural similarities with the binders (Figure S3). The compounds were charge labeled using default ECEPP/3 partial charges [36] before docking.

The ICM PocketFinder macro (default settings) [37] was used to define the central putative substrate binding site of the outward-occluded GAT homology models into which the evaluation test set was docked. The PocketFinder algorithm uses the 3D protein structure to detect possible ligand binding pockets and does not require knowledge about potential ligands [37].

The test set database was docked using the ICM batch docking method and a semi-flexible docking approach in which the transporter, represented as 3D grid potential maps accounting for van der Waals (vdw), electrostatics, hydrophobic and hydrogen bonding interactions, was kept rigid while the ligands were fully

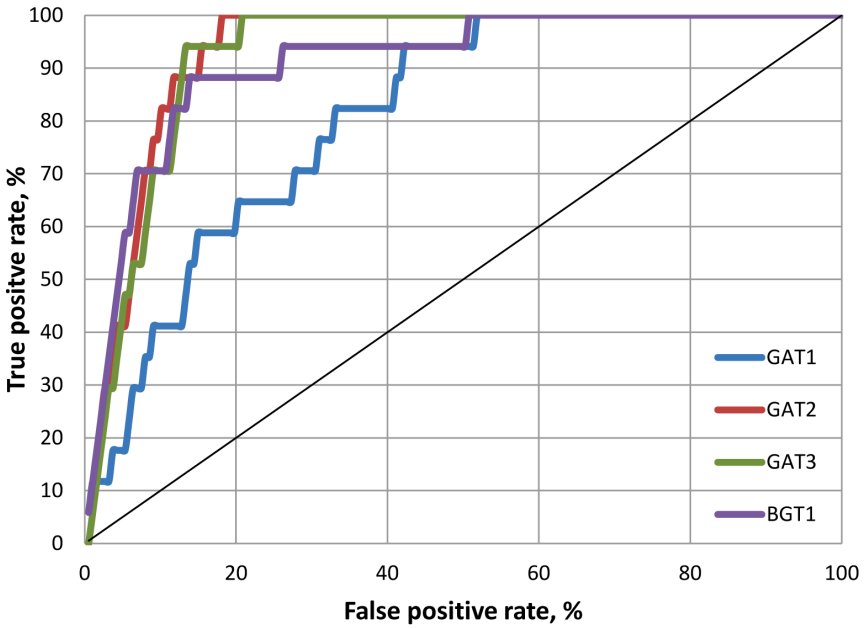

Figure 2. Evaluation docking results. ROC curves obtained from docking of 17 binders and 170 decoys into the central putative substrate binding sites of detected in the outward-occluded GAT models.
doi:10.1371/journal.pone.0065200.g002

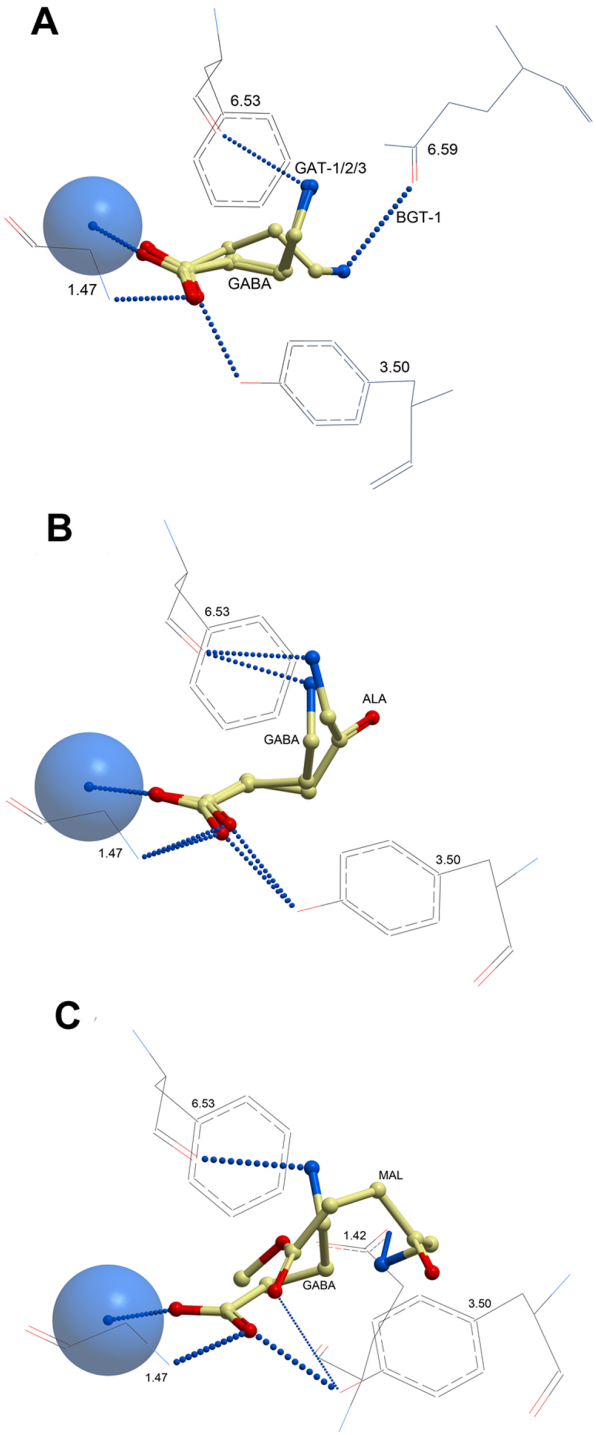

Figure 3. Orientations of GABA, ALA and MAL in the central substrate binding pocket. a) GABA in all four GAT models, b) GABA and ALA in GAT-2, and c) GABA and MAL in GAT-2. Amino acids in positions 1.47 (G), 3.50 (Y) and 6.53 (F) are conserved among the GAT subtypes, whereas the amino acids in positions 1.42 (Y in GAT-1; E in the others) and 6.59 (Q in BGT-1, L in the others) are non-conserved. Intermolecular hydrogen bonds are shown as dotted lines; the thickness of the lines representing the energy of the interaction. Amino acid side chains are shown in wire representation, ligands in yellow xstick representation, and Na1 sodium ion as blue sphere. Color coding of atoms: blue: nitrogen; red: oxygen.
doi:10.1371/journal.pone.0065200.g003

Table 2. Docking scores (kcal/mol) of GABA, ALA and MAL.

Ligand	GAT-1	GAT-2	GAT-3	BGT-1
GABA	−30.12	−28.37	−20.51	−36.14
ALA	−32.10	−23.40	−27.62	−35.77
MAL	7.11	−19.10	−19.72	−19.00

doi:10.1371/journal.pone.0065200.t002

flexible. ICM uses a Monte Carlo global energy optimization algorithm to dock the ligands [31]. Due to the stochastic nature of the docking procedure three parallel docking runs were performed.

The ICM VLS scoring function was used to score the resulting ligand-protein complexes. The scoring function uses steric, entropic, hydrogen bonding, hydrophobic and electrostatic terms to calculate the score and also include a correction term proportional to the number of atoms in the ligand to avoid bias towards larger ligands [38].

Following docking, receiver operating characteristic (ROC) curves for each GAT model were generated using the best scored orientation of each ligand from the three parallel docking simulations, and the normalized 'area under curve' (noAUC) value for each transporter was calculated.

Full-atom Docking Refinement of ALA, MAL and GABA

Following semi-flexible docking of ALA, MAL and GABA, full-atom refinement of the complexes was performed. During the refinement, energy minimization and sampling of the side chain torsional angles of the amino acids within 5 Å of the ligands using ICM biased probability Monte Carlo (BPMC) [31] was performed. To score the complexes following the full-atom refinement, the ICM scanScoreExtrenal macro was used [35].

Electrostatic Potentials (ESPs)

ICM PocketFinder [35] was used to detect the substrate translocation pathways in the outward-open and inward-open GAT models (Table S3; S4). The identified amino acids were selected and the ESPs of the amino acids were calculated using the ICM Rapid Exact-Boundary Electrostatics (REBEL) algorithm with a potential scale value of 5 kcal/e.u. charge units (default values) [31]. The Na1 and Na2 ions (with a charge of +1) were included in the ESP calculations in the outward-open homology model. The ESP of GABA, ALA and MAL were also calculated using the ICM-REBEL [31].

Indexing of Residues

To facilitate comparison of amino acid positions between the four GAT subtypes, a generic numbering scheme developed for the NSS transporters [32,39] is used in this paper. The most conserved residue in each of the twelve TM segments is given the number 50, and the other residues are numbered according to its position relative to this most conserved residue. Hence, a residue with a generic position number lower or higher than 50 indicates that it is located N- or C-terminal to the most conserved residue in the TM helix, respectively. The reference GAT-1 residues are as follows: $W68^{1.50}$, $P96^{2.50}$, $Y140^{3.50}$, $T217^{4.50}$, $P247^{5.50}$, $Q291^{6.50}$, $F339^{7.50}$, $F386^{8.50}$, $Y432^{9.50}$, $Y453^{10.50}$, $P505^{11.50}$, and $P549^{12.50}$ (Table S1).

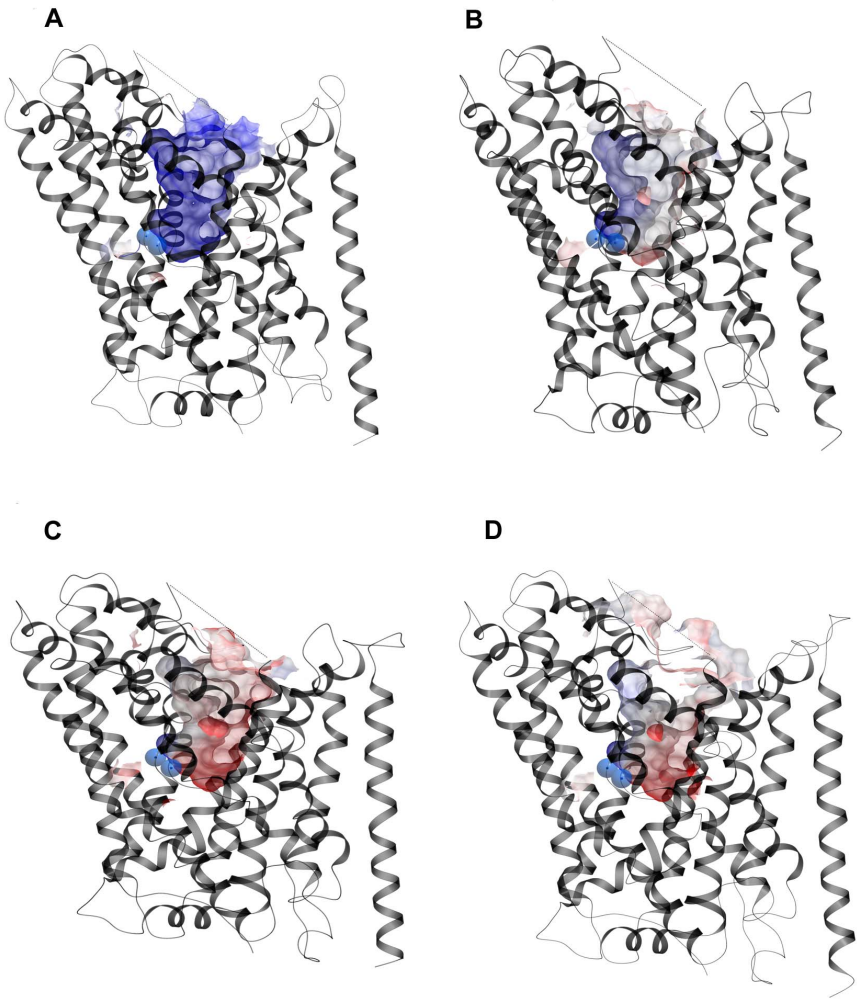

Figure 4. Entry pathway ESPs. ESPs of the entry pathways detected in the outward-open GAT models (grey ribbon representation). a) GAT-1, b) GAT-2, c) GAT-3, and d) BGT-1. Blue spheres: Na1 and Na2 sodium ions. Color coding: red: negative ESP; blue: positive ESP; grey: neutral ESP.
doi:10.1371/journal.pone.0065200.g004

Results

Homology Modeling

In this study, homology models of the four human GATs were constructed in outward-open, outward-occluded and inward-open conformations based on LeuT x-ray crystal structures (PDB id 3F3A, 2A65 and 3TT3, respectively). The stereochemical quality of the homology models both before and after energy refinements were evaluated using the PROCHECK [40], ERRAT [41] and VERIFY 3D [42,43] programs and compared with LeuT template structures (Table S2). The ERRAT scores revealed that some atoms in the unrefined models had overlapping van der Waals surfaces, and these models were hence discarded. For the refined models, the ERRAT scores were similar to that of their corresponding templates and Ramachandran plots provided by the PROCHECK were found to be satisfactory (Table S2). The VERIFY 3D scores were lower for the refined structures than the corresponding LeuT, but acceptable (Table S2). The structure of the outward-occluded GAT-2 homology model is shown in Figure 1.

Evaluation of the Outward-occluded Models by Docking

To further evaluate the outward-occluded models, an evaluation test set containing 17 binders and 170 decoys was docked into the central substrate binding site detected by ICM PocketFinder [35] (Table S3; S4). The compounds included as binders were either substrates or presumed substrates (i.e. compounds that only have been tested in some of the GATs but likely interact with all four transporter subtypes) and small-size inhibitors that presumably bind in the central substrate binding site (Figure S2). The decoys were selected based on their structural similarities with the binders (Figure S3). Specifically, all decoys contained at least one $-COO^-$ or $-SO_3^-$ moiety.

The putative substrate binding site was formed by amino acids in TM 1, 3, 6, and 8 and the majority of the amino acids were conserved among the four GAT subtypes (Table 1). Some interesting differences were also seen between the transporters. For instance, GAT-2, GAT-3 and BGT-1 contained a negatively charged glutamate in position 1.42 which in GAT-1 was an aromatic tyrosine (Table 1). The GAT-1 pocket was identified as the largest of the four (Table 1). With the exception of $L300^{6.59}$, all the identified amino acids have previously been shown by site-directed mutagenesis studies to play roles in the GABA binding and/or transport in GAT-1 [44,45]. The localization of the

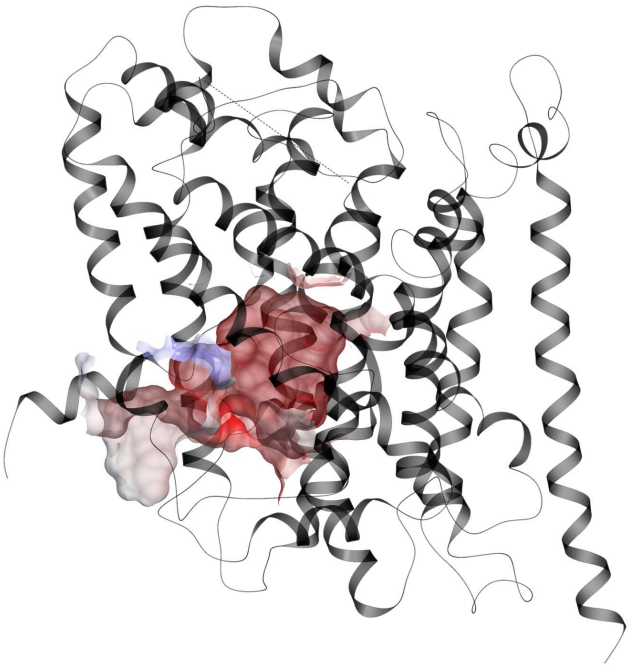

Figure 5. GAT-1 exit pathway ESPs. GAT-1 in grey ribbon representation. Color coding of ESPs as in Figure 4.
doi:10.1371/journal.pone.0065200.g005

putative GAT substrate binding site furthermore corresponded well to the position of the substrate binding site seen in the LeuT crystal structures and also with the results of Dodd and Christie [45]. Dodd and Christie showed that substitutions of the amino acids in positions 1.42, 3.46, 6.56 and 8.64 of the creatine transporter (CRT) to the corresponding GAT-1 amino acids results in the loss of creatine and gain of GABA transport activity [45].

Following docking, ROC curves and noAUC values of each model were obtained (Figure 2). A noAUC value of 100 represents a perfect separation between binders and decoys. The results showed that the GAT-1 model was the least specific with a noAUC value of 68.8, whereas the noAUC values for other three subtypes were excellent (noAUC values of 95.7, 94.0 and 90.4 for GAT-2, GAT-3 and BGT-1, respectively) (Figure 2). Analysis of the docking results in GAT-1 showed that the lower noAUC value obtained for this transporter was due to more decoys rather than fewer substrates being selected. This was not surprising as the GAT-1 model had the largest binding pocket of the four models (Table 1). The evaluation docking hence suggested that the models were acceptable for docking of substrates.

Docking of GABA, ALA and MAL

To study the interaction of PDT pro-drugs ALA and MAL and the native substrate GABA in the GAT models, the ligands were docked into the central putative substrate binding site of the outward-occluded GAT models using a regular semi-flexible docking approach, followed by refinement of the GAT substrate binding site amino acids within 5 Å of the three ligands. The results showed that GABA, ALA and MAL had favorable (i.e. negative) docking scores in all four GATs, except MAL in GAT-1 (Table 2). The orientations of GABA, ALA and MAL in the central substrate binding site can be seen in Figure 3.

The docking results showed that the carboxyl group of GABA coordinated the Na1 ion and formed hydrogen bonds to the side

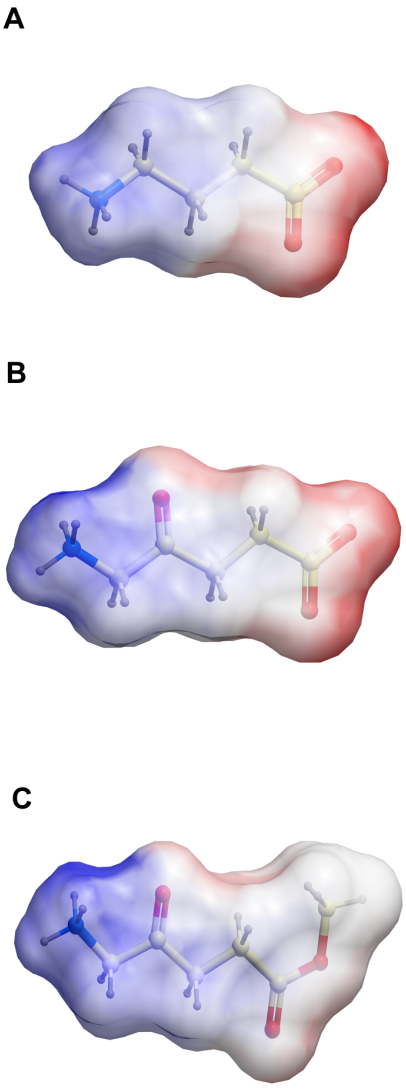

Figure 6. GABA (a), ALA (b) and MAL (c) ESPs. Color coding of ESPs as in Figure 4.
doi:10.1371/journal.pone.0065200.g006

chain hydroxyl group of $Y^{3.50}$ and to the main chain nitrogen atom of $G^{1.47}$ in all four GAT subtypes (Figure 3). The amine moiety of GABA formed a hydrogen bond to the main chain oxygen of $F^{6.53}$ in GAT-1, GAT-2 and GAT-3, whereas it in BGT-1 was involved in a hydrogen bond to the side chain oxygen of $Q^{6.59}$, which is a leucine residue in the other GATs (Table 1).

The GABA orientations are in accordance with the results of docking of GABA in GAT-1, GAT-2 and GAT-3 published by other groups, in which the orientation of the carboxyl moiety of GABA was very similar to the present orientation whereas the localization of the amine moiety was more variable [46–49]. This was not surprising as the same template was used for homology modeling in all studies, and comparison of GABA in the GAT models and Leu in the template structure showed that GABA occupied the same regions of the binding pocket as Leu in the template structure [27] (results not shown).

The carboxyl moiety of ALA had a similar orientation as that of GABA, interacting with Na1, $Y^{3.50}$ and $G^{1.47}$ (Figure 3). Furthermore, like GABA, the amine moiety in ALA was found in two localizations in the transporter models: in GAT-1 and GAT-2 the amine moiety interacted with the backbone oxygen

atom of $F^{6.53}$, whereas it in GAT-3 and BGT-1 the moiety formed an ionic interaction with the side chain of $E^{1.42}$ (which is a tyrosine in GAT-1) (Figure 3).

MAL occupied the same region as GABA and ALA in the GATs (Figure 3). However, as MAL contains an ester moiety whereas GABA and ALA have a carboxylate moiety, MAL was not able to coordinate the Na1 ion (Figure 3). In GAT-1, a hydrogen bond was formed between the ester and amine moieties of the ligand and to the backbone oxygen atom of $F^{6.53}$ (results not shown). In GAT-2, GAT-3 and BGT-1, hydrogen bonds were present between the ester and amine moieties of MAL and between the ester moiety and the side chain hydroxyl of $Y^{3.50}$ (Figure 3). Furthermore, in the latter transporters, the amine moiety of MAL in addition formed ionic interactions with $E^{1.42}$ (Figure 3), while the corresponding amino acid in GAT-1 was tyrosine (Table 1). The ionic interaction with $E^{1.42}$ probably accounted for the relatively high scoring of MAL in GAT-2, GAT-3 and BGT-1 (Table 2).

Electrostatic Potentials (ESP) of Outward- and Inward-open Homology Models

The ESPs of the funnel-shaped entry pathway extending from the extracellular environment to the central substrate binding pocket in the outward-open homology models varied considerably (Figure 4). Whereas the GAT-1 entry pathway and central putative substrate binding site was highly positive in nature, the corresponding areas in GAT-2, GAT-3 and BGT-1 consisted of positive, negative and hydrophobic sub-regions (Figure 4). The major differences between the GAT subtypes in the entry pathway were the amino acids in position 1.42, 6.59 and 8.64, located in the central substrate binding site region, and the amino acids in positions 1.54, EL4 and 10.45, located in the vestibule leading from the extracellular environment to the central substrate binding site (Table S3; S4). In contrast, only minor differences in the ESPs of the exit pathway reaching from the central substrate binding site to the cytoplasm in the inward-open GAT models were observed, and this region was highly negative in all four GAT subtypes (Figure 5). The ligand ESPs indicated that the surface of MAL is more positively charged than that of GABA and ALA which had zwitterionic charge distribution (Figure 6).

Discussion

Whereas studies have suggested that the PDT pro-drug ALA is a GAT substrate [16,17], studies regarding MAL are more ambiguous as this compound seemingly is transported via GAT in some cell types but not in others [15,17]. Molecular insight into the binding interactions of GABA, ALA and MAL in the central substrate binding site of the four GAT subtypes may help shed light on this question.

GABA is the primary inhibitory neurotransmitter in the central nervous system (CNS) and a native substrate for the GATs. The GATs play an essential role in regulating neurotransmitter signaling and homeostasis by mediating uptake of released GABA from the extracellular space into neurons and glial cells. Abnormal levels of GABA can result in inappropriate neural signaling and underlie CNS disorders such as epilepsy, depression, schizophrenia, drug addiction, and acute and chronic pain [50–54]. GAT-1 for instance plays an important role in the treatment of epilepsy being targeted by the antiepileptic tiagabine [55]. The GATs may, however, also play important roles in non-CNS and non-neuronal diseases. In contrast to GAT-1, which is exclusively expressed in the CNS, GAT-2 and BGT-1 are also expressed in the peripheral nervous system (PNS), and has been found in several other tissues, including the kidneys, liver, heart, lungs, and testis [21,22,27,56]. GAT-3 was also recently shown to be expressed in human skin cells [17]. Molecular insight into the structure and function of the GATs is important for an increased understanding of GABAergic neurotransmission and may be important for drug development in several therapeutic areas.

In the present study, the outward-occluded GAT models, in which the central substrate binding site is closed from either side of the membrane, were chosen for docking of the native substrate GABA and the putative substrates ALA and MAL as x-ray crystal structures show that LeuT in the presence of substrates adopts this conformation [29]. Based on the orientations of GABA, ALA and MAL in the substrate binding site, as well as the docking scores, our results suggest that ALA may be a substrate in all four GATs whereas MAL may be a substrate in GAT-2, GAT-3 and BGT-1. However, whether a compound is transported or not via GAT is also dependent on other factors than the ability to bind to and induce the outward-occluded conformation of the transporter. Dodd and Christie have for instance shown that though the creatine transporter activity can be changed from creatine to GABA by substitution of a few amino acids in the central substrate binding site, the substitutions alone are not sufficient for efficient GABA transport [45]. Hence, though the obtained docking orientations and scores suggested that ALA and MAL may be substrates of all or some GAT subtypes, further studies are needed to verify these findings.

The ESPs of the translocation pathways may reveal electrostatic forces involved in substrate binding and translocation and highlight differences between the four GAT subtypes. The ESPs of the putative entry and exit permeation pathways in the outward- and inward-open GAT homology models, respectively, were hence calculated (Figure 4; 5). The x-ray structure of LeuT in complex with the competitive inhibitor tryptophan (Trp) [29] shows that Trp prevents the extracellular gate from closing, hence stabilizing the transporter in a conformation in which the central substrate binding site is accessible from the extracellular environment [29]. The outward-open GAT models constructed based on this LeuT structure were hence used to illustrate the entry pathways. The inward-open LeuT crystal structure was used as a template for modeling the GAT subtypes used to calculate the ESPs of the exit pathway extending from the central substrate binding site to the cytoplasm. In this structure, the extracellular gate has closed, an intracellular vestibule has opened and the Na1 and Na2 sodium binding sites seen in the outward-open and outward-occluded structures have been disrupted [28]. These changes has occurred due to large conformational changes, including reorientation of TMs 1, 2, 5, 6 and 7, hinge bending of the intracellular half of TM1 and occlusion of the extracellular vestibule by EL4 [28].

The ESP calculations indicated that the major differences between the GAT subtypes were located in the outward-open models, hence in the entry pathway region of the transporters (Figure 4). The ligand ESPs also showed that GABA and ALA had a zwitterionic charge distribution, whereas the MAL charge distribution was cationic in nature due to the replacement of the carboxyl moiety found in GABA and ALA with an ester group (Figure 6). The ESPs hence support the notion that MAL may not be a GAT-1 substrate, as the results suggest that the entry pathway of this GAT subtype is highly positive in nature (Figure 4).

The amino acids in the entry region are the first to come in contact with the substrates and hence play crucial roles in ligand recognition and binding. The finding that the major differences between the GAT subtypes are located in this region may be of clinical importance as it has been suggested that the pain often

observed during ALA-based PDT may result from uptake of ALA via GAT-2 and BGT-1 into the mitochondria-rich sensory neurons and hence high-level accumulation of PpIX [11,57]. Current pain-reducing strategies include interrupted illumination, cooling of the affected area and local anesthesia [58,59]; however, in some cases the pain is severe and the treatment is discontinued [8,9]. Exploitation of the differences in the entry pathways to develop inhibitors that can be used to selectively inhibit the uptake of ALA into the sensory neurons may hence be used clinically to reduce ALA-induced pain.

In summary, this study pioneers in structure-based characterization of ALA and MAL transports via the four GABA transporters using the homology modeling approach. Although ALA-based PDT has been used successfully for the treatment of a variety of skin cancers, pain is a limiting factor. ALA-based PDT in combination with selective inhibitors of the GAT may be an attractive approach to develop pain-reduce strategy and improve the PDT efficacy in the future.

Supporting Information

Figure S1 Alignment.
(TIF)

Figure S2 Evaluation test set binder structures.
(TIF)

Figure S3 Evaluation test set decoy structures.
(TIF)

Table S1 NSS numbering scheme.
(DOCX)

Table S2 SAVES results.
(DOCX)

Table S3 Amino acids, entry pathway.
(DOCX)

Table S4 Amino acids, exit pathway. The GAT homology models constructed in this study are available from the authors upon request.
(DOCX)

Acknowledgments

We gratefully acknowledge support and training from BioStruct (the Norwegian national graduate school in structural biology), and thank professor Finn Drabløs (Department of Cancer Research and Molecular Medicine, NTNU) for his professional discussion.

Author Contributions

Conceived and designed the experiments: OAG IS YB MG. Performed the experiments: YB MG. Analyzed the data: YB MG. Contributed reagents/materials/analysis tools: YB MG IS. Wrote the paper: YB MG IS OAG.

References

1. Dougherty TJ (1984) Photodynamic therapy (PDT) of malignant tumors. Crit Rev Oncol Hematol 2: 83–116.
2. Issa MC, Manela-Azulay M (2010) Photodynamic therapy: a review of the literature and image documentation. An Bras Dermatol 85: 501–511.
3. Pottier R, Krammer B, Stepp H, Baumgartner R (2006) Photodynamic therapy with ALA, a clinical handbook: RSC Publishing.
4. Peng Q, Warloe T, Berg K, Moan J, Kongshaug M, et al. (1997) 5-Aminolevulinic acid-based photodynamic therapy. Clinical research and future challenges. Cancer 79: 2282–2308.
5. Scott J (1955) The biosynthesis of porphyrins and porphyrin metabolism. Ciba Foundation symposium Churchill, London: p54.
6. Schoenfeld N, Epstein O, Lahav M, Mamet R, Shaklai M, et al. (1988) The heme biosynthetic pathway in lymphocytes of patients with malignant lymphoproliferative disorders. Cancer Lett 43: 43–48.
7. Di Venosa G, Fukuda H, Batlle A, Macrobert A, Casas A (2006) Photodynamic therapy: regulation of porphyrin synthesis and hydrolysis from ALA esters. J Photochem Photobiol B 83: 129–136.
8. Grapengiesser S, Ericson M, Gudmundsson F, Larko O, Rosen A, et al. (2002) Pain caused by photodynamic therapy of skin cancer. Clin Exp Dermatol 27: 493–497.
9. Kasche A, Luderschmidt S, Ring J, Hein R (2006) Photodynamic therapy induces less pain in patients treated with methyl aminolevulinate compared to aminolevulinic acid. J Drugs Dermatol 5: 353–356.
10. Morton CA, McKenna KE, Rhodes LE (2008) Guidelines for topical photodynamic therapy: update. Br J Dermatol 159: 1245–1266.
11. Gholam P, Weberschock T, Denk K, Enk A (2011) Treatment with 5-aminolaevulinic acid methylester is less painful than treatment with 5-aminolaevulinic acid nanoemulsion in topical photodynamic therapy for actinic keratosis. Dermatology 222: 358–362.
12. Moloney FJ, Collins P (2007) Randomized, double-blind, prospective study to compare topical 5-aminolaevulinic acid methylester with topical 5-aminolaevulinic acid photodynamic therapy for extensive scalp actinic keratosis. Br J Dermatol 157: 87–91.
13. Steinbauer JM, Schreml S, Babilas P, Zeman F, Karrer S, et al. (2009) Topical photodynamic therapy with porphyrin precursors–assessment of treatment-associated pain in a retrospective study. Photochem Photobiol Sci 8: 1111–1116.
14. Rud E, Gederaas O, Hogset A, Berg K (2000) 5-aminolevulinic acid, but not 5-aminolevulinic acid esters, is transported into adenocarcinoma cells by system BETA transporters. Photochem Photobiol 71: 640–647.
15. Gederaas OA, Holroyd A, Brown SB, Vernon D, Moan J, et al. (2001) 5-Aminolaevulinic acid methyl ester transport on amino acid carriers in a human colon adenocarcinoma cell line. Photochem Photobiol 73: 164–169.
16. Novak B, Schulten R, Lubbert H (2011) delta-Aminolevulinic acid and its methyl ester induce the formation of Protoporphyrin IX in cultured sensory neurones. Naunyn Schmiedebergs Arch Pharmacol 384: 583–602.
17. Schulten R, Novak B, Schmitz B, Lubbert H (2012) Comparison of the uptake of 5-aminolevulinic acid and its methyl ester in keratinocytes and skin. Naunyn Schmiedebergs Arch Pharmacol.
18. Rodriguez L, Batlle A, Di Venosa G, Battah S, Dobbin P, et al. (2006) Mechanisms of 5-aminolevulinic acid ester uptake in mammalian cells. Br J Pharmacol 147: 825–833.
19. Nelson H, Mandiyan S, Nelson N (1990) Cloning of the human brain GABA transporter. FEBS Lett 269: 181–184.
20. Borden LA, Dhar TG, Smith KE, Branchek TA, Gluchowski C, et al. (1994) Cloning of the human homologue of the GABA transporter GAT-3 and identification of a novel inhibitor with selectivity for this site. Receptors Channels 2: 207–213.
21. Borden LA, Smith KE, Gustafson EL, Branchek TA, Weinshank RL (1995) Cloning and expression of a betaine/GABA transporter from human brain. J Neurochem 64: 977–984.
22. Christiansen B, Meinild AK, Jensen AA, Brauner-Osborne H (2007) Cloning and characterization of a functional human gamma-aminobutyric acid (GABA) transporter, human GAT-2. J Biol Chem 282: 19331–19341.
23. Saier MH, Jr. (2000) A functional-phylogenetic classification system for transmembrane solute transporters. Microbiol Mol Biol Rev 64: 354–411.
24. Chen NH, Reith ME, Quick MW (2004) Synaptic uptake and beyond: the sodium- and chloride-dependent neurotransmitter transporter family SLC6. Pflugers Arch 447: 519–531.
25. Jardetzky O (1966) Simple allosteric model for membrane pumps. Nature 211: 969–970.
26. Tanford C (1983) Translocation pathway in the catalysis of active transport. Proc Natl Acad Sci U S A 80: 3701–3705.
27. Yamashita A, Singh SK, Kawate T, Jin Y, Gouaux E (2005) Crystal structure of a bacterial homologue of Na+/Cl–dependent neurotransmitter transporters. Nature 437: 215–223.
28. Krishnamurthy H, Gouaux E (2012) X-ray structures of LeuT in substrate-free outward-open and apo inward-open states. Nature 481: 469–474.
29. Singh SK, Piscitelli CL, Yamashita A, Gouaux E (2008) A competitive inhibitor traps LeuT in an open-to-out conformation. Science 322: 1655–1661.
30. Apweiler R, Bairoch A, Wu CH, Barker WC, Boeckmann B, et al. (2004) UniProt: the Universal Protein knowledgebase. Nucleic Acids Res 32: D115–119.
31. Abagyan R, Totrov M, Kuznetsov D (1994) ICM–A new method for protein modeling and design: Applications to docking and structure prediction from the distorted native conformation. Journal of Computational Chemistry 15: 488–506.
32. Beuming T, Shi L, Javitch JA, Weinstein H (2006) A comprehensive structure-based alignment of prokaryotic and eukaryotic neurotransmitter/Na+ symporters (NSS) aids in the use of the LeuT structure to probe NSS structure and function. Mol Pharmacol 70: 1630–1642.

33. Forrest LR, Tavoulari S, Zhang YW, Rudnick G, Honig B (2007) Identification of a chloride ion binding site in Na+/Cl -dependent transporters. Proc Natl Acad Sci U S A 104: 12761–12766.
34. Zomot E, Bendahan A, Quick M, Zhao Y, Javitch JA, et al. (2007) Mechanism of chloride interaction with neurotransmitter:sodium symporters. Nature 449: 726–730.
35. Abagyan R, Totrov M (1994) Biased probability Monte Carlo conformational searches and electrostatic calculations for peptides and proteins. J Mol Biol 235: 983–1002.
36. Nemethy G, Gibson KD, Palmer KA, Yoon CN, Paterlini G, et al. (1992) Energy parameters in polypeptides. 10. Improved geometrical parameters and nonbonded interactions for use in the ECEPP/3 algorithm, with application to proline-containing peptides. J Phys Chem 96: 6472–6484.
37. An J, Totrov M, Abagyan R (2005) Pocketome via comprehensive identification and classification of ligand binding envelopes. Mol Cell Proteomics 4: 752–761.
38. Schapira M, Abagyan R, Totrov M (2003) Nuclear hormone receptor targeted virtual screening. J Med Chem 46: 3045–3059.
39. Goldberg NR, Beuming T, Soyer OS, Goldstein RA, Weinstein H, et al. (2003) Probing conformational changes in neurotransmitter transporters: a structural context. Eur J Pharmacol 479: 3–12.
40. Laskowski RA, Macarthur MW, Moss DS, Thornton JM (1993) PROCHECK: a program to check the stereochemical quality of protein structures. J Appl Cryst 26: 283–291.
41. Colovos C, Yeates TO (1993) Verification of protein structures: patterns of nonbonded atomic interactions. Protein Sci 2: 1511–1519.
42. Bowie JU, Luthy R, Eisenberg D (1991) A method to identify protein sequences that fold into a known three-dimensional structure. Science 253: 164–170.
43. Luthy R, Bowie JU, Eisenberg D (1992) Assessment of protein models with three-dimensional profiles. Nature 356: 83–85.
44. Anderson CM, Kidd PD, Eskandari S (2010) GATMD: gamma-aminobutyric acid transporter mutagenesis database. Database (Oxford) 2010: baq028.
45. Dodd JR, Christie DL (2007) Selective amino acid substitutions convert the creatine transporter to a gamma-aminobutyric acid transporter. J Biol Chem 282: 15528–15533.
46. Skovstrup S, Taboureau O, Brauner-Osborne H, Jorgensen FS (2010) Homology modelling of the GABA transporter and analysis of tiagabine binding. ChemMedChem 5: 986–1000.
47. Wein T, Wanner KT (2010) Generation of a 3D model for human GABA transporter hGAT-1 using molecular modeling and investigation of the binding of GABA. J Mol Model 16: 155–161.
48. Pallo A, Simon A, Bencsura A, Heja L, Kardos J (2009) Substrate-Na+ complex formation: coupling mechanism for gamma-aminobutyrate symporters. Biochem Biophys Res Commun 385: 210–214.
49. Shi L, Quick M, Zhao Y, Weinstein H, Javitch JA (2008) The mechanism of a neurotransmitter:sodium symporter–inward release of Na+ and substrate is triggered by substrate in a second binding site. Mol Cell 30: 667–677.
50. Brambilla P, Perez J, Barale F, Schettini G, Soares JC (2003) GABAergic dysfunction in mood disorders. Mol Psychiatry 8: 721–737, 715.
51. Wong CG, Bottiglieri T, Snead OC, 3rd (2003) GABA, gamma-hydroxybutyric acid, and neurological disease. Ann Neurol 54 Suppl 6: S3–12.
52. Coyle JT (2004) The GABA-glutamate connection in schizophrenia: which is the proximate cause? Biochem Pharmacol 68: 1507–1514.
53. Jasmin L, Wu MV, Ohara PT (2004) GABA puts a stop to pain. Curr Drug Targets CNS Neurol Disord 3: 487–505.
54. Salat K, Kulig K (2011) GABA transporters as targets for new drugs. Future Med Chem 3: 211–222.
55. Sarup A, Larsson OM, Schousboe A (2003) GABA transporters and GABA-transaminase as drug targets. Curr Drug Targets CNS Neurol Disord 2: 269–277.
56. Borden LA, Smith KE, Hartig PR, Branchek TA, Weinshank RL (1992) Molecular heterogeneity of the gamma-aminobutyric acid (GABA) transport system. Cloning of two novel high affinity GABA transporters from rat brain. J Biol Chem 267: 21098–21104.
57. Wu SM, Ren QG, Zhou MO, Peng Q, Chen JY (2003) Protoporphyrin IX production and its photodynamic effects on glioma cells, neuroblastoma cells and normal cerebellar granule cells in vitro with 5-aminolevulinic acid and its hexylester. Cancer Lett 200: 123–131.
58. Shackley DC, Briggs C, Gilhooley A, Whitehurst C, O'Flynn KJ, et al. (2002) Photodynamic therapy for superficial bladder cancer under local anaesthetic. BJU Int 89: 665–670.
59. Pagliaro J, Elliott T, Bulsara M, King C, Vinciullo C (2004) Cold air analgesia in photodynamic therapy of basal cell carcinomas and Bowen's disease: an effective addition to treatment: a pilot study. Dermatol Surg 30: 63–66.

SUPPRORTING INFORMATION

Title:

Homology Modeling of Human γ-Butyric Acid Transporters and the Binding of Pro-drugs 5-Aminolevulinic Acid and Methyl Aminolevulinic Acid used in Photodynamic Therapy

List of figures and tables:

Figure S1

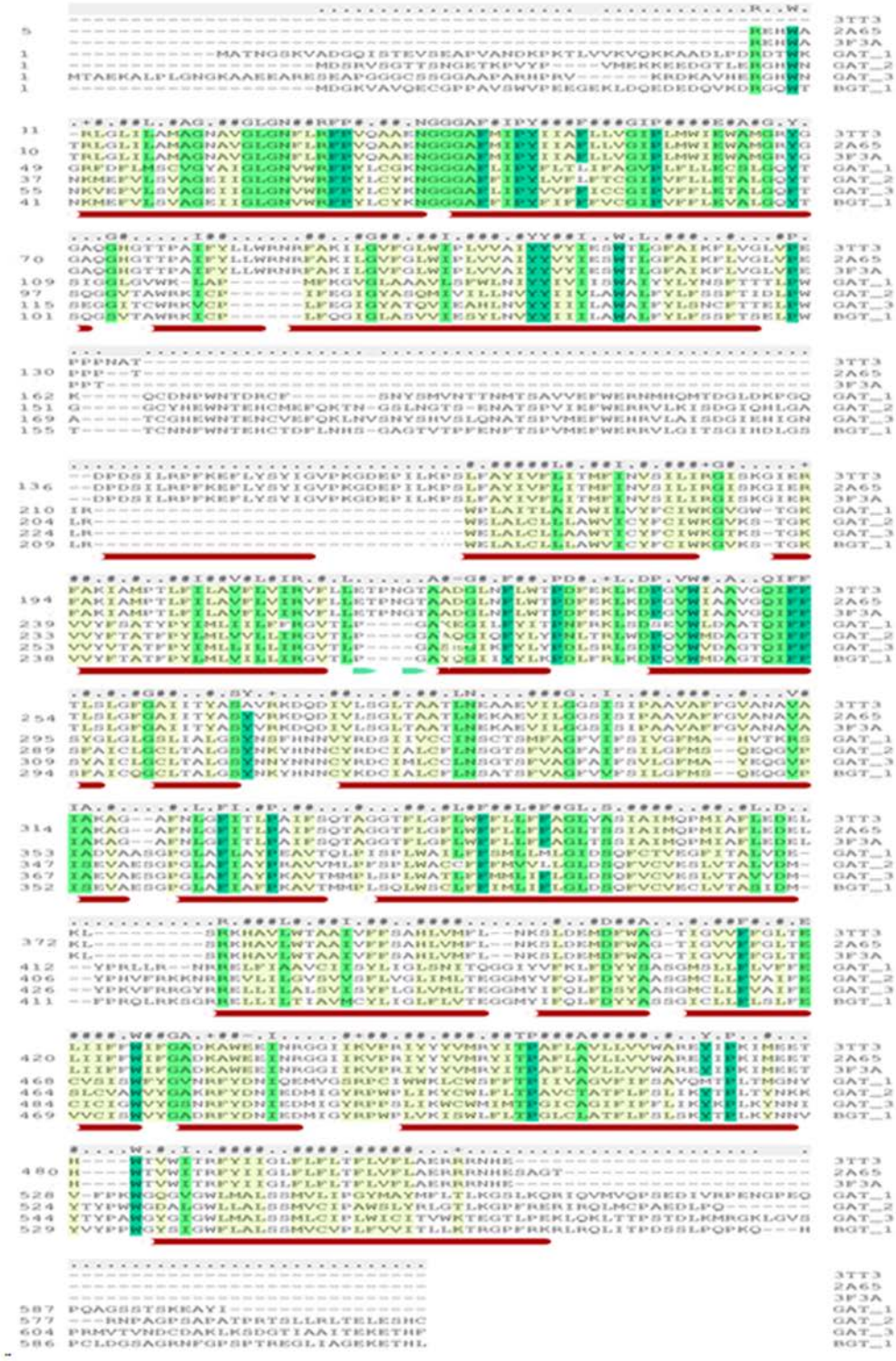

Figure S2

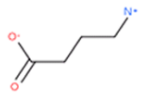

GABA

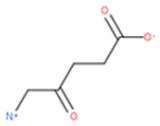

5-ALA

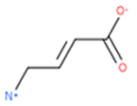

CACA

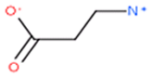

Beta alanine

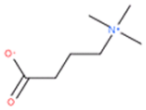

GBB

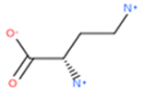

L-DABA

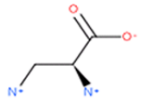

L-DAPA

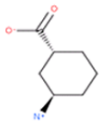

R,R-ACHC

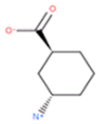

S,S-ACHC

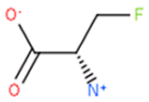

R-fluoro-alanine

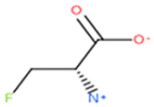

S-fluoro-alanine

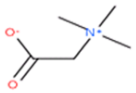

Betaine

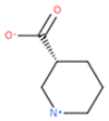

R-nipecotic acid

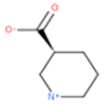

S-nipecotic acid

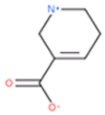

Guvacine

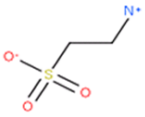

Taurine

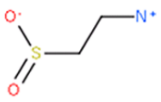

Hypotaurine

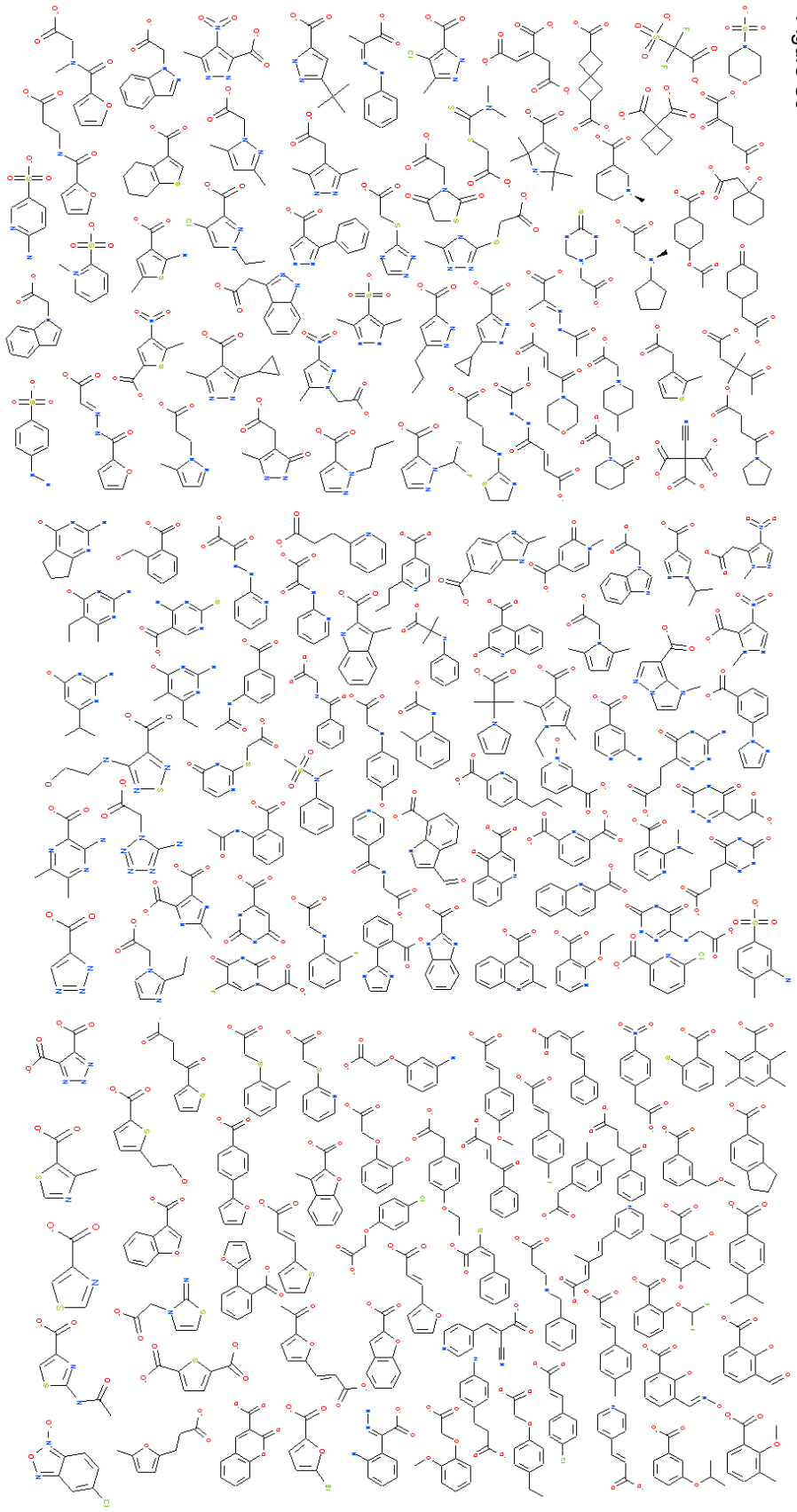

Figure S3

Table S1.

Position	LeuT	GAT-1	GAT-2	GAT-3	BGT-1
1.50	L29	W68	W56	W74	W60
2.50	P57	P96	P84	P102	P88
3.50	Y108	Y140	Y129	Y147	Y133
4.50	V171	T217	C211	C231	C216
5.50	L202	P247	P241	P261	P246
6.50	Q250	Q291	Q285	Q305	Q290
7.50	S298	F339	F333	F353	F338
8.50	F345	F386	F379	F400	F385
9.50	F387	Y432	F428	Y448	Y433
10.50	W406	Y453	Y449	Y469	Y454
11.50	P457	P505	P501	P521	P506
12.50	T498	P549	P546	P566	P551

Table S1. NSS numbering scheme.

Table S2.

	Template	**Template**	**Template**
GAT-1	**2A65**	**3F3A**	**3TT3**
Ramachandran plot	95.3 / 4.7 / 0	94.7 / 5.3 / 0	95.5 / 4.2 / 0.3
Errat	87.931	92.391	86.726
Verify-3D	75.26 %	77.40 %	74.51 %
GAT-2	**2A65**	**3F3A**	**3TT3**
Ramachandran plot	94.2 / 5.5 / 0.3	94.8 / 5.2 / 0	95.5 / 3.9 / 0.6
Errat	92.308	94.828	89.956
Verify-3D	81.55 %	78.86 %	67.02 %
GAT-3	**2A65**	**3F3A**	**3TT3**
Ramachandran plot	94.2 / 5.5 / 0.3	94.7 / 5.3 / 0	94.9 / 4.5 / 0.6
Errat	93.162	87.931	90.749
Verify-3D	79.25 %	79.92 %	71.73 %
BGT-1	**2A65**	**3F3A**	**3TT3**
Ramachandran plot	94.0 / 6.0 / 0	94.8 / 5.2 / 0	94.5 / 4.7 / 0.8
Errat	92.949	93.966	88.210
Verify-3D	83.23 %	78.22 %	67.88 %
LeuT	**2A65**	**3F3A**	**3TT3**
Ramachandran plot	94.5 / 5.5 / 0	94.9 / 5.1 / 0	92.3 / 6.7 / 0
Errat	93.028	94.400	87.889
Verify-3D	93.15 %	90.18 %	90.06 %

Table S2. SAVES results. Ramachandran plot: most favored/additional allowed/generously allowed regions.

Table S5.

GAT-1	GAT-2	GAT-3	BGT-1	Position
Y60	E48	E66	E52	**1.42**
A61	I49	I67	I53	**1.43**
I62	I50	I68	I54	**1.44**
G63	G51	G69	G55	**1.45**
L64	L52	L70	L56	**1.46**
G65	G53	G71	G57	**1.47**
N66	N54	N72	N58	**1.48**
W68	W56	W74	W60	**1.50**
R69	R57	R75	R61	**1.51**
Y72	Y60	R78	R64	**1.54**
L136	L125	L143	L129	**3.46**
Y139	Y128	Y146	Y132	**3.49**
Y140	Y129	Y147	Y133	**3.50**
I143	V132	I150	I136	**3.53**
W146	W135	W153	W139	**3.56**
F294	F288	F308	F293	**6.53**
S295	S289	S309	S294	**6.54**
Y296	F290	Y310	F295	**6.55**
G297	A291	A311	A296	**6.56**
L300	L294	L314	Q299	**6.59**
A357	A351	A371	A356	**EL4**
A358	E352	E372	E358	**EL4**
G360	G354	G374	G361	**EL4**
P361	P355	P375	P362	**EL4**
L363	L357	L377	L364	**EL4**
A364	A358	A378	A365	**EL4**
F365	F359	F379	F366	**EL4**
S396	S390	S410	S395	**8.60**
T400	C394	C414	C399	**8.64**
F447	F443	F463	F448	**10.44**
K448	Q444	Q464	Q449	**10.45**
D451	D447	D467	D452	**10.48**
L460	L456	L476	L461	**10.57**

Table S5. Amino acids of the entry pathway, outward-open models.

Table S6.

GAT-1	GAT-2	GAT-3	BGT-1	Position
S56	S44	S62	S48	1.38
G59	G47	G65	G51	1.41
Y60	E48	E66	E52	1.42
A61	I49	I67	I53	1.43
I62	I50	I68	I54	1.44
G63	G51	G69	G55	1.45
L64	L52	L70	L56	1.46
G65	G53	G71	G57	1.47
N66	N54	N72	N58	1.48
F98	F86	F104	F90	2.48
L136	L125	L143	L129	3.46
Y140	Y129	Y147	Y133	3.50
V240	V234	V254	V239	5.43
Y241	Y235	Y255	Y240	5.44
S243	T237	T257	T242	5.46
A244	A238	A258	A243	5.47
T245	T239	T259	T244	5.48
F294	F288	F308	F293	6.53
S295	S289	S309	S294	6.54
Y296	F290	Y310	F295	6.55
G297	A291	A311	A296	6.56
L300	L294	L314	Q299	6.59
S302	C296	C316	C301	6.61
L303	L297	L317	L302	6.62
L306	L300	L320	L305	6.65
V323	L317	L337	L322	7.34
N327	N321	N341	N326	7.38
M391	L385	F405	F390	8.55
L392	L386	L406	L391	8.56
D395	D389	D409	D394	8.59
S396	S390	S410	S395	8.60
F398	F392	F412	F397	8.62
C399	V393	V413	V398	8.63
T400	C394	C414	C399	8.64

Table S6. Amino acids of the exit pathway, inward-open homology models.

Paper 3

Enhanced efficacy of bleomycin in bladder cancer cells by photochemical internalization

Yan Baglo[1], Lars Hagen[1], Anders Høgset[2], Finn Drabløs[1], Marit Otterlei[1] and Odrun A. Gederaas[1]

1. *Department of Cancer Research and Molecular Medicine, Faculty of Medicine, Norwegian University of Science and Technology, P.O.Box 8905, N-7491 Trondheim, Norway.*
2. *PCI Biotech AS, Strandveien 55, N-1366 Lysaker, Norway*

Correspondence should be addressed to Yan Baglo; yan.baglo@ntnu.no.

Bleomycin is a cytotoxic chemotherapeutic agent widely used in cancer treatment. However, its efficacy in different cancers is low, possibly due to limited cellular internalization. In this study, a novel approach known as photochemical internalization (PCI) was explored to enhance bleomycin delivery in bladder cancer cells (human T24 and rat AY-27), as bladder cancer is a potential indication for use of PCI with bleomycin. The PCI technique was mediated by the amphiphilic photosensitizer disulfonated tetraphenyl chlorin ($TPCS_{2a}$) and blue light (435 nm). Two additional strategies were explored to further enhance the cytotoxicity of bleomycin; a novel peptide drug ATX-101 which is known to impair DNA damage responses, and the protease inhibitor E-64 which may reduce bleomycin degradation by inhibition of bleomycin hydrolase. Our results demonstrate that the PCI technique enhances the bleomycin effect under appropriate conditions, and importantly we show that PCI-bleomycin treatment leads to increased levels of DNA damage supporting that the observed effect is due to increased bleomycin uptake. Impairing the DNA damage responses by ATX-101 further enhances the efficacy of the PCI-bleomycin treatment, while inhibiting the bleomycin hydrolase does not.

1. Introduction

Bladder cancer is one of the most common cancers in the world and causes more than 100 000 deaths every year [1,2]. In Norway bladder cancer has been one of the five most common cancer types for men during the last ten years [3] and in United States it is estimated that 72 570 new cases and 15 210 deaths will be reported in 2013 [4]. Approximately 70-80% of diagnosed bladder cancers worldwide are non-muscular invasive bladder cancer (NMIBC) for which intravesical chemotherapy is used as an adjuvant treatment to the standard transurethral resection [1]. However, significant improvements in preventing disease progression and recurrence have not been obtained [1,2]. Due to high intrinsic cytotoxicity and low myelosuppression and immune-suppression, bleomycin is used in the treatment of cancers such as malignant

lymphomas, testicular carcinomas, and squamous cell carcinomas (see review by Ramotar and Wang [5] and references therein). However, good clinic efficacy has not been found in bladder cancer [6,7,8]. This could be due to low uptake into the cells as bleomycin consists of rather large water-soluble glycopeptidic molecules that are most likely unable to cross cell membranes by passive diffusion, and thus rely on endocytosis and/or transporters [9,10]. Studies have shown that cellular responses to bleomycin are cell type-dependent. In cell lines with low sensitivity to bleomycin, the drug resistance is considered mainly to be due to membrane barrier, degradation by hydrolases in lysosomes or bleomycin hydrolase (BLMH) in the cytosol, elevated DNA repair capacity, and low activity of bleomycin transporters [9,10,11,12,13]. Severe side effects of bleomycin at high dose are therefore limiting its clinical applications [5]. In an effort to overcome the membrane barrier for bleomycin, electro- permeabilization was shown to enhance the efficacy [14,15].

The PCI technology has been developed from photodynamic therapy (PDT) as an efficient drug delivery tool to enhance the effect of several types of therapeutic molecules [16]. In the PCI technology a membrane-embedded photosensitizer is used together with a therapeutic agent by endocytotic delivery [17,18]. The photosensitizers used in PCI, such as meso-tetraphenyl chlorin disulfonate ($TPCS_{2a}$) used in this study, are specially designed as amphiphilic molecules that initially localize to the plasma membrane, but are later incorporated into the endosomal membranes by endocytosis [19,20,21]. When used together with bleomycin, the bleomycin molecules are enclosed in the endocytotic vesicles, and exposure to light leads to endosomal rupture by phototoxic damage and release of bleomycin molecules into the cytosol [22,23]. Side effects often seen in the conventional systemic therapeutic strategies can also be reduced by PCI because the enhanced effect is localized to the area exposed to light [24,25]. Enhanced efficacy of PCI with bleomycin has been documented in several preclinical studies and clinical trials [24,25,26,27,28]. A phase I clinical trial of $TPCS_{2a}$-mediated PCI of bleomycin showed no severe side effects associated with the treatment, and the efficacy and safety of the modality are currently being evaluated in a phase II interventional clinical trial [27,29].

Once inside the nucleus, bleomycin-induce DNA strand breaks are leading to apoptosis, extended cell cycle arrest, mitotic cell death, and increasing risk of chromosome aberrations if not properly repaired [30,31,32]. A novel designed cell-penetrating peptide named ATX-101, containing the AlkB homolog 2 PCNA-interacting motif (APIM), has been shown to enhance cytotoxicity of several chemotherapeutic drugs [33]. The APIM-motif mediate interaction with proliferating cell nuclear antigen (PCNA) in many proteins involved in DNA repair, apoptosis, restart of replication and cell cycle regulation after DNA damage. Impairing the interactions between these proteins and PCNA by ATX-101 impairs the cellular DNA damage responses and thus sensitizes the cells to chemotherapeutic drugs [33,34,35,36,37]. In this study, cytotoxicity of $TPCS_{2a}$-mediated PCI of bleomycin (PCI-bleomycin) was studied in rat bladder cancer cells (AY-27) and human bladder cancer cells (T24) using

the PCI strategy of illumination after bleomycin treatment [38,39]. For all experiments, a human epidermoid carcinoma cell line (A431) was used as reference due to its sensitivity to PCI [40]. Furthermore, we examined the effects of inhibiting the DNA damage response and bleomycin degradation in combination with PCI-bleomycin. The levels of induced DNA damages were investigated using the comet assay. Our results demonstrate that PCI enhances bleomycin efficacy in human and rat bladder cancer cells under optimal conditions. Combination therapy using PCI-bleomycin and ATX-101 further enhanced the observed cytotoxicity.

2. Materials and Methods

2.1 Cell culture

Rat bladder transitional carcinoma cells (AY-27) were maintained in the same RPMI culture medium and conditions as described in our earlier study [41]. Human epidermoid carcinoma cells (A431) and human bladder carcinoma cells (T24) were maintained in Dulbecco's Modified Eagle's Medium (D6429) supplemented with 2 mM L-glutamine, 1% penicillin/streptomycin, 10 mM HEPES, 1 mM natrium pyruvate (Lonza), and 10% (v/v) fetal bovine serum. All medium chemicals were purchased from Sigma except noted.

2.2 Chemicals

$TPCS_{2a}$ (30 mg ml^{-1}, Amphinex®) dissolved in Tween 80 and 50 mM Tris buffer was provided by PCI Biotech AS (Oslo, Norway) and stored at 4 °C in aliquots. The stock was first diluted with 50 mM Tris phosphate buffer (pH 8.5) to 0.06 mg ml^{-1} and further diluted with fresh culture medium immediately before use. All work with $TPCS_{2a}$ was performed under subdued light or light protection.

Bleomycin powder (15000 IU, Baxter, Norway) was dissolved with 0.9% salt water as stock (1000 IU ml^{-1}) and stored at -20 °C in aliquots. Peptide drug ATX-101 (1 mM) was supplied by APIM Therapeutics AS (Trondheim, Norway) and stored at 4 °C in aliquots. Protease inhibitor E-64 powder (Sigma), a known inhibitor of bleomycin hydrolase [42,43], was diluted with de-ionized water as stock (1 mM) and stored at -20 °C in aliquots. Resazurin sodium salt powder (Sigma) was dissolved with PBS to 2.5 mM followed by filtering and sonication under subdued light. Resazurin stock was stored at -20 °C in aliquots. These chemical stocks were further diluted to desired concentrations with fresh culture medium immediately before use.

DRAQ5™ solution (5 mM, BioStatus Limited, UK), a novel DNA-detecting far-red- fluorescing dye [44], was stored at 4 °C under light protection and diluted with PBS (1:10000) under subdued light immediately before use.

2.3 Light source

Blue light with λ_{max} of 435 nm used in this study was available from a LumiSource® lamp (PCI Biotech AS, Norway). The lamp is designed specifically to provide stable and homogenous fluency with an irradiance of 12.9 mW cm^{-2} over a defined illumination area, allowing attached living cells to be illuminated from the bottom of culture dishes or plates. With the light doses used in the PCI experiments, the photosensitizer is not likely to be affected by photobleaching [45].

2.4 Cellular uptake of $TPCS_{2a}$

Cells were seeded out into 96-well plates (6000 cells/well, CytoOne, USA Scientific, Inc). Attached cells were incubated with $TPCS_{2a}$ at a series of concentrations (18 h). Subsequent to removal of $TPCS_{2a}$-medium, fluorescence intensity of cellular accumulated $TPCS_{2a}$ was measured using FLUOStar Omega microplate reader (410 nm/650 nm, BMG Labtech GmbH, Germany). The cells were immediately washed with cold PBS, fixed with fresh 2% paraformaldehyde (150 µl/well, 15 min, on ice, no shaking), and stained with 0.5 µM DRAQ5 (50 µl/well, 20 min, RT, gentle shaking, in the dark). The plates were dried out after washing with cold PBS. Fluorescence intensity of DNA binding DRAQ5 was measured using Odyssey Imager at 700 nm channel according to the user manual (Li-Cor® Infrared imaging system, LI-COR Biosciences, Ltd, UK). Cellular accumulation of $TPCS_{2a}$ was determined by dividing relative fluorescence intensity (normalized with control cells) of $TPCS_{2a}$ with fluorescence intensity of DRAQ5 (DNA content in the same well).

Table 1 Therapeutic drug and light doses (used in Figure 3b and 4b)

Cell line	$TPCS_{2a}$ (µg ml^{-1})	Light (J cm^{-2})	Bleomycin (IU ml^{-1})	ATX-101 (µM)	E-64 (µM)
A431	0.2	0.387	5	5	10
T24	0.2	0.774	5	5	10
AY-27	0.1	0.387	50	5	50

2.5 Resazurin survival assay

Control and treated cells were incubated with resazurin medium (200 µM, 130 µl/well, 2-3 h, 37 °C) under light protection and fluorescence intensity was measured using the FLUOStar Omega microplate reader (544 nm/590 nm). Cell survival fraction was determined after normalization with fluorescence intensity of resazurin medium and control cells.

2.6 Cytotoxicity assays

Cells were seeded out into 96-well plates (6000 cells/well). Attached cells were treated using one of the protocols below:

Protocol A (photodynamic treatment): the cells were incubated with $TPCS_{2a}$ for 18 h. Subsequent to removal of $TPCS_{2a}$-medium, cells were washed with culture medium twice and chased (4 h) in fresh drug-free medium before exposure to blue light at different intervals [26].

Protocol B (drug treatment): the cells were (co-)incubated with drug(s) (bleomycin, ATX-101 or E-64) for 4 h and then washed once with culture medium.

Protocol C (PCI-bleomycin treatment): here protocol B was incorporated into protocol A after $TPCS_{2a}$-treatment. The treated cells were (co-)incubated with bleomycin (and ATX-101/E-64) for 4 h instead of being chased in drug-free medium. The cells were washed once before illumination. Therapeutic drug and light doses used are listed in Table 1.

Finally, cell survival fraction was determined by resazurin survival assay after post-incubation for 48 h. The time point of 48 h was selected based on bleomycin effect measured at each day from 1 to 7 days after bleomycin treatment in theses cell lines (see Figure 1S, Supplementary Information). Cell survival fractions showed the same relative relationship among the three cell lines across the time series. Considering the subsequent studies on bleomycin effects in different combined treatments, cell growth measured at 48 h after bleomycin treatment seemed to be an optimal time point which could show clear differences in treatment effect in all cell lines that were used. Clonogenic assay was also performed in T24 and AY-27 cell lines as method control, showing that T24 had weaker colony forming capacity than AY-27. However, due to possibly misleading results caused by differences in colony forming capacity rather than drug effects, clonogenic assay was not used for the actual study (see Figure 2S, Supplementary Information).

Using protocol C, the cells were washed one additional time compared to protocol A. This could eliminate cellular $TPCS_{2a}$ and thereby reduce the photodynamic cytotoxicity to a small extent in PCI-drug(s) treated cells (see Figure 3S, Supplementary Information). However, this matched the PCI strategy using sub-lethal photodynamic dose.

2.7 Analysis of BLMH expression by Western blot

Protein lysate was extracted from (treated) cells using the same protocol described in our earlier study [41]. Briefly, cell pellet was resuspended in lysis buffer followed by sonication. Protein concentration was determined using Bio-Rad protein assay after centrifugation.

Expression of bleomycin hydrolase (BLMH) was analyzed by 1D Western blot using a standard protocol (Invitrogen). As described [34], protein lysates (100 μg) were

separated on 10% Bis-Tris gel (NuPAGE, Invitrogen) and transferred onto PVDF membrane (Immobilon, Millipore). Proteins were further detected using anti-BLMH primary antibody (ab77111, Abcam), HRP-conjugated rabbit anti-mouse secondary antibody (p0260, Dako Denamark) and anti-PCNA antibody (ab29, Abcam) as loading control. K562 whole cell lysate (30 μg, ab7911, Abcam) was used as positive control of the primary antibody.

2.8 Comet assay

Cells were seeded out into 6-well plates (5×10^4 cells/well, CytoOne). Bleomycin or PCI-bleomycin treated cells were washed with PBS and then detached with accutase (15 min, 37 °C, Sigma) immediately after treatments or after an interval of post-incubation (15 min and 30 min, respectively) in culture medium. DNA damage level was further evaluated using a standard protocol of single cell gel electrophoresis [46,47,48]. As described [48], the cells were resuspended at 37 °C in 1% low-melt agar after centrifugation and loaded on a pre-coated microscope slide which was immediately cooled down on ice. The embedded cells were lysed in fresh cold lysis buffer [48] overnight and then electrophoresed in cold alkaline buffer (pH 13.3). DNA fragments stained with ethidium bromide were visualized in an inverted fluorescence microscope (Zeiss Axiovert 200M, Germany) equipped with a Sony XCD-X700 camera. Several hundreds of comets in each sample were evaluated using Komet 5.5 imaging software (Andor Technology).

3. Results and discussion

3.1 Cellular uptake of $TPCS_{2a}$ and dose responses to blue light and bleomycin

The uptake of $TPCS_{2a}$ to the endosomal membrane is essential for drug delivery. To assess the uptake capacity in the skin cancer cell line A431 and the bladder cancer cell lines T24 and AY-27, fluorescence intensity of cellular $TPCS_{2a}$ was measured and normalized against cell count. The results showed that the uptake was dose-dependent in all three cell lines (Figure 1a). Importantly, a much higher uptake was seen in the skin cancer cell line A431 compared to the bladder cancer cell lines T24 and AY-27 (Figure 1a). The endocytotic rate is cell type dependent [49], and this may account for differences in cellular $TPCS_{2a}$ uptake as seen in the these cell lines.

According to the principle of PCI, the applied doses of both photosensitizer and light (termed photodynamic dose in this paper) are supposed to be sub-lethal, leading mainly to damage to the endosomal/lysosomal membrane. Therefore, we set out to determine the sub-lethal photodynamic doses before evaluating PCI-bleomycin efficacy. No dark toxicity, $TPCS_{2a}$ buffer toxicity (Tween 80 and 50 mM Tris buffer), or light toxicity was observed in any of the cell lines under the experimental conditions (data not shown), thus the cytotoxicity is dependent upon light activation of the $TPCS_{2a}$ molecules. The results showed that T24 cells were resistant to activation by blue light although they had similar $TPCS_{2a}$ uptake as the AY-27 cells that were very light sensitive (Figure 1b). A431 cells, which accumulated more $TPCS_{2a}$ molecules than the two other cell lines, were medium sensitive to light activation (Figure 1b). Light doses that gave low (0-20%) reduction in cell survival in this experiment (Figure 1b, arrows) were selected for the PCI-bleomycin experiments, but in the following experiments a further three times reduction of the $TPCS_{2a}$ concentration was applied in order to further reduce the background cytotoxicity. In summary, these results show that the cell lines accumulate different levels of $TPCS_{2a}$, but that this did not directly correlate with their light sensitivity.

Next, we tested the bleomycin sensitivity of the different cell lines. We treated the cells with bleomycin for 4 hours, and measured the cell growth after 48 hours. A431 was the most, and AY-27 the least sensitive cell line (Figure 1c).

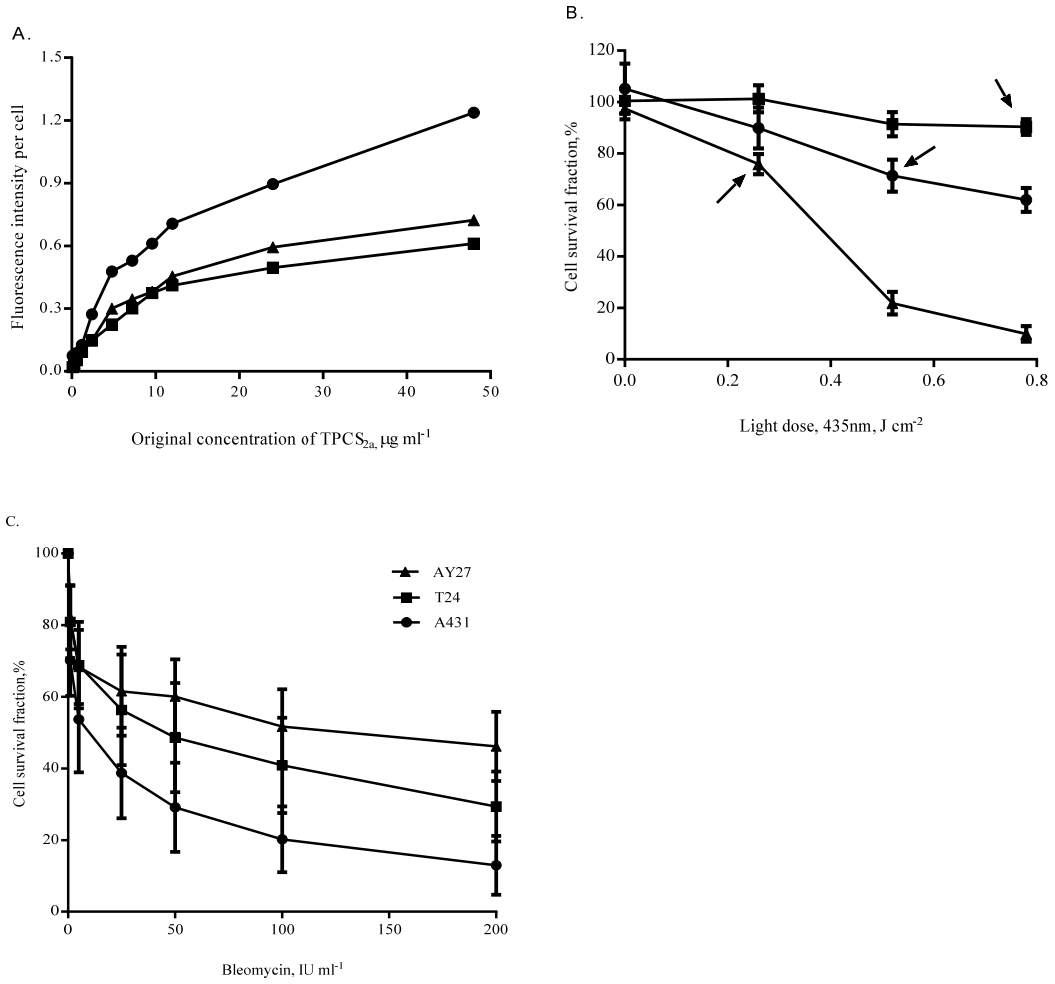

Figure 1. Cellular uptake of $TPCS_{2a}$ is dose-dependent, its cytotoxicity is dependent upon dose of blue light, and bleomycin cytotoxicity is cell type-dependent. (A) Cellular accumulation at increasing concentrations of $TPCS_{2a}$ in A431, T24 and AY-27 cells. After 18 h the $TPCS_{2a}$ fluorescence was normalized to fluorescence intensity per cell by DRAQ5-staining. The data are from one representative experiment out of two (mean of 12 wells). (B) Cytotoxicity of increasing blue light doses (435 nm) in A431, T24 and AY-27 cells exposed to 0.3 µg ml^{-1} $TPCS_{2a}$ for 18 h. The data are from one representative experiment out of three (mean of 24 wells ± SD). Light doses selected for further PCI experiments are shown with arrows. (C) Dose response to bleomycin determined as cell growth after 48 h. A431, T24 and AY-27 cells were treated with different bleomycin doses for 4 h. The data are from one representative experiment out of four (mean from 48 wells ± SD).

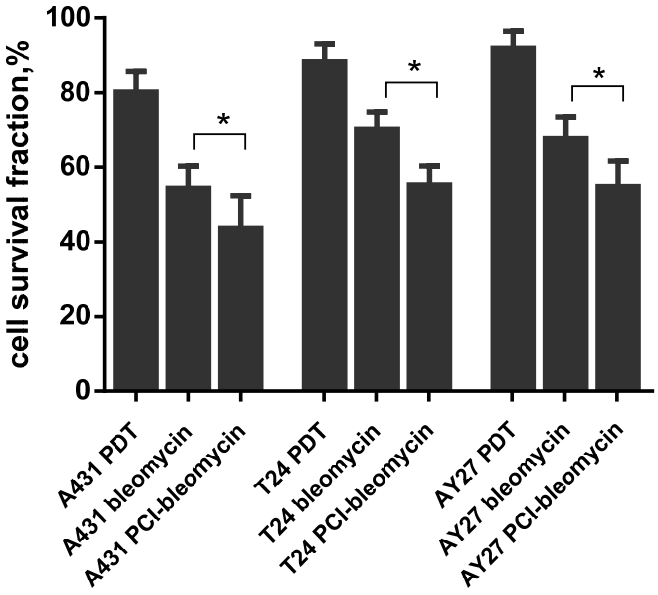

Figure 2. PCI enhances cytotoxic effect of bleomycin in all three cell lines. Cell survival fractions were determined 48 h after incubation with 0.1 μg ml^{-1} $TPCS_{2a}$ for 18 h, 50 IU ml^{-1} bleomycin or fresh medium for 4 h, and illumination (light doses as indicated in Figure 1b) in sequence. The data are from one representative experiment out of three (mean of 24 wells ± SD). P-values were calculated using two-tailed Student's t-test and the values ($p<0.0001$, presented with asterisk) indicated significant differences between bleomycin and PCI-bleomycin treatments.

3.2 The effect of bleomycin is increased in combination with PCI

To determine the efficacy of PCI-bleomycin in the three cell lines, sub-lethal doses of light (see arrows in Figure 1b) and $TPCS_{2a}$ (0.1 μg ml^{-1}) were used. P-values were calculated using two-tailed Student's t-test and the values ($p<0.0001$) indicated that differences in cytotoxicity between bleomycin versus PCI-bleomycin treatment were highly significant. In line with the PCI concept, sub-lethal photodynamic doses were applied. In addition, the PDT effect included in PCI-bleomycin treatment in each cell line was less than its PDT control due to an additional washing (see section 2.6 in Methods). The results showed that bleomycin cytotoxicity was enhanced up to 20% by PCI, independent of cell type (Figure 2). This is likely due to increased uptake of bleomycin in the cells. At the selected conditions, A431 cells were more sensitive than the bladder cancer cells (44% surviving cells versus 55%, respectively, Figure 2). This likely reflects that this cell line had highest uptake of $TPCS_{2a}$ in addition to being the most sensitive towards bleomycin (Figure 1a and 1c). These results are in agreement with recent results reported by Arentsen *et al*. [28].

3.3 Inhibition of bleomycin hydrolase did not increase the cytotoxicity of PCI-bleomycin treatment

Different sensitivity towards bleomycin could be due to differences in uptake of the drug, differences in how the cells process the drug or repair the DNA damages induced by the drug. Bleomycin hydrolase (BLMH) is a cytosolic enzyme which has been shown to inactivate bleomycin before it enters the nucleus, and is thus believed to contribute to bleomycin resistance [11,12,30]. When measuring the BLMH expression in the three cell lines, we found that AY-27 cell line expressed more BLMH than the other two cells lines (almost 2x, Figure 3a). No change in BLMH levels from the BLMH inhibitor E-64 was observed. AY-27 was the most bleomycin-resistant cell line (Figure 1c), also in presence of E-64 (Figure 3b), suggesting that BLMH is not important for the resistance of AY-27 towards bleomycin. The changes in sensitivity towards bleomycin in the other cell lines were also minimal following addition of E-64 (Figure 3b), thus BLMH is most likely not important for bleomycin sensitivity of these cells.

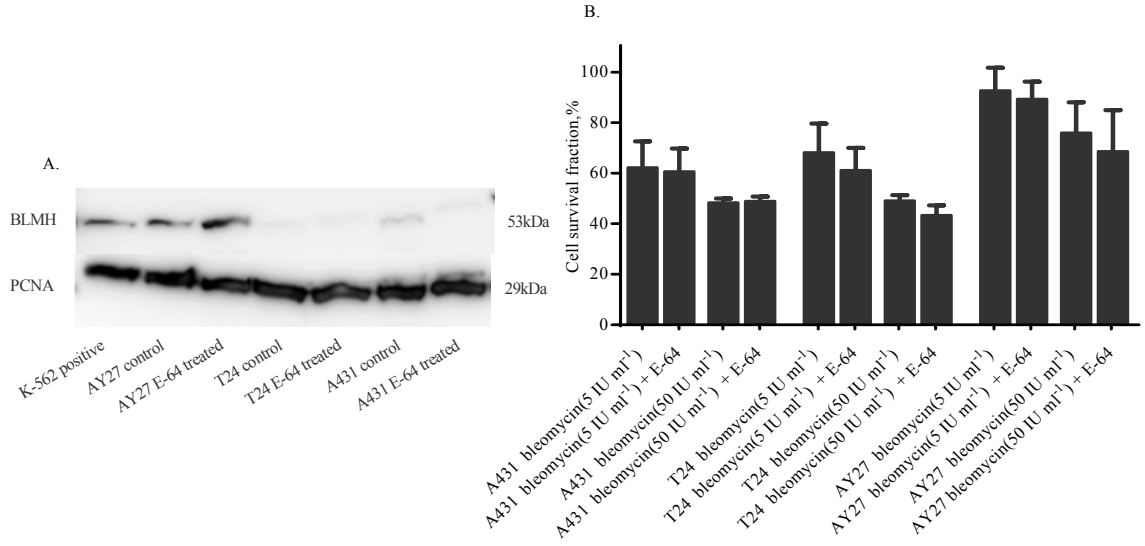

Figure 3. Bleomycin hydrolase is strongly expressed in AY-27 cells but the protease inhibitor E-64 does not sensitize AY-27 to bleomycin. (A) Western blots of BLMH expression in K562 (positive control), A431, T24 and AY-27 cells. E-64 treated cells are included as control. PCNA expression level is used as loading control. The image is from one representative experiment out of three. (B) Bleomycin cytotoxicity at two concentrations (5 and 50 IU ml^{-1}) with and without E-64 treatment (concentrations used are listed in Table 1). Cell survival fractions were determined 48 h after 4 h-treatment of the drug(s). The data are from one representative experiment out of three (mean of 24 wells ± SD).

3.4 Impairing DNA damage responses during PCI-bleomycin treatment increased the efficacy

Bleomycin binds to DNA strands resulting in both single stranded and double stranded DNA breaks. We measured the levels of DNA damage induced by bleomycin alone and by PCI-bleomycin using comet assays. An increase in DNA damage by PCI-bleomycin versus only bleomycin would strongly indicate increased uptake of bleomycin in the cells. We also measured the DNA repair rate in each cell line. Because it takes 15 min to detach cells, the earliest time points for DNA damage evaluation were after 15 min. Cells were left to repair for additional 15 and 30 min (30 and 45 min in total, respectively) (Figure 4a). Statistical analysis was performed using two-tailed Student's t-test. Highly significant differences in DNA damage levels between treatments ($p<0.0001$) are shown with asterisks in Figure 4. Bleomycin-induced DNA damage was observed in all cell lines, but the levels at different time points varied between the cell lines. Bleomycin alone induced more DNA damage and the damage was removed more slowly in T24 and A431 than in AY-27 cells, consistent with the observation that AY-27 was more resistant to bleomycin. Furthermore, the results showed that PCI-bleomycin induced a higher level of DNA damage than bleomycin alone in all three cell lines (Figure 4a), supporting increased import of bleomycin. The highest increase in levels of DNA damage was seen in AY-27 cells, and importantly no reduction in the level of DNA damage could be detected 45 minutes after PCI-bleomycin treatment in this cell line, suggesting that the repair capacity was saturated. The observation that cell survival after 48 hours was 55% (see Figure 2) shows that a large fraction of the cells were eventually repaired, but at later time points.

The novel peptide drug ATX-101 has the potential to reduce several aspects of the cellular defense systems, including DNA repair, and is therefore enhancing the efficacy of several chemotherapeutics [33,34,35]. We tested if ATX-101 could increase the efficacy of PCI-bleomycin, and found that ATX-101 enhanced the PCI-bleomycin efficacy with 14.7%, 30.5%, and 20.7% in A431, T24, and AY-27 cells respectively, showing statistically significant differences (Figure 4b). The cytotoxic effects of the double combinations ATX-101-bleomycin and ATX-101-$TPCS_{2a}$-PDT are similar or lower than PCI-bleomycin, and lower than the triple combination ATX-101-PCI-bleomycin (data not shown). Any PDT effect in these PCI combination treatments was reduced due to one additional washing. The additive effects of ATX-101 were stronger in the bladder cancer cells than in the skin cancer cells under these experimental conditions (Figure 4b). Because the bladder cancer cells were less sensitive towards bleomycin both with regard to cell survival and induction of DNA damage (Figure 1 and 4), these results suggest that the cellular DNA repair capacity is a crucial factor of the efficacy of bleomycin, and therefore also the efficacy of PCI-bleomycin. As expected from the results in Figure 3b, addition of E-64 did not affect PCI-bleomycin efficacy.

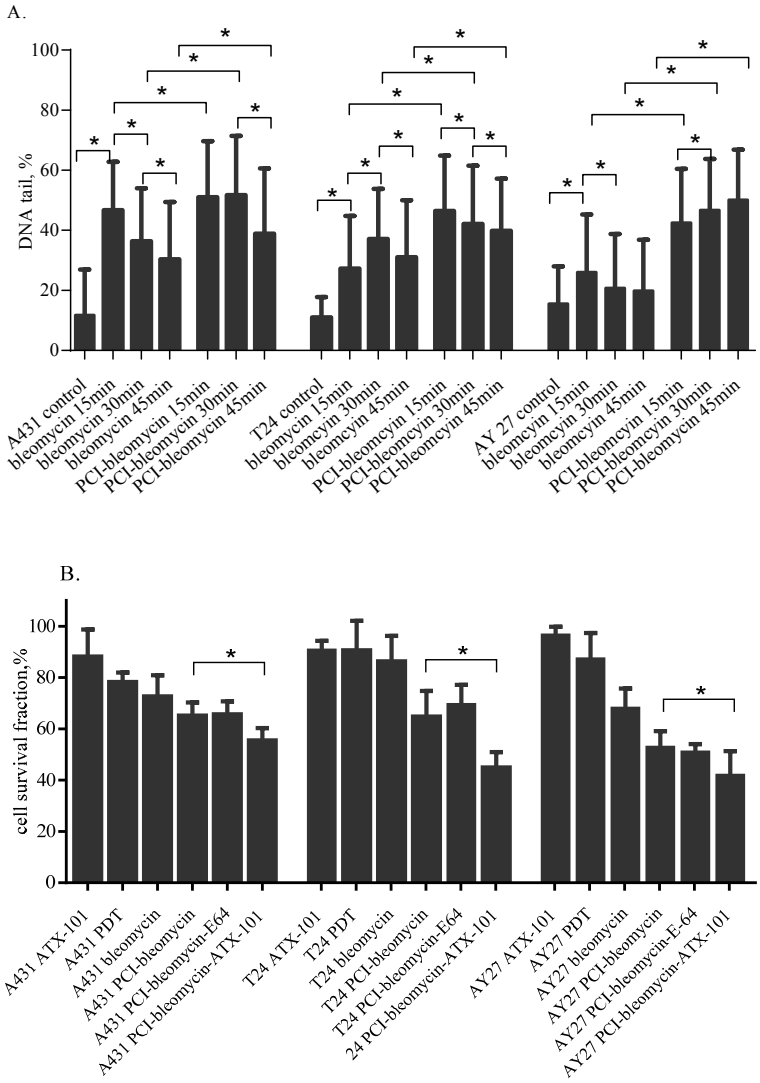

Figure 4. PCI elevates bleomycin-induced DNA damages and ATX-101 enhances PCI-bleomycin cytotoxicity. (A) Bleomycin and PCI-bleomycin induced DNA damages. Comet assay was performed at different intervals after incubation with 0.1 μg ml^{-1} $TPCS_{2a}$ (18 h), 50 IU ml^{-1} bleomycin (4 h), and illumination (light doses as indicated in Figure 1b) in sequence, or with the bleomycin treatment only. The data are from one representative experiment out of two experiments (mean of 500/700 cells ± SD). P-values were calculated using two-tailed Student's t-test and the values ($p<0.0001$, presented with asterisk) indicated that the level of DNA damage between bleomycin treatment and PCI-bleomycin, or between different time intervals of the same treatment, were significant different. (B) Cell growth after treatment with PDT, bleomycin, ATX-101, PCI-bleomycin, and PCI-bleomycin in combination with E-64 or ATX-101. Cell survival fractions were determined 48 h after incubation with $TPCS_{2a}$ (18 h), bleomycin with/without ATX-101/E-64 (4 h), and light exposure in sequence (drug and light doses are shown in Table 1). Any PDT effect in the PCI combination treatments was reduced due to one additional washing (see section 2.6 in Materials and Methods). The data are from one representative experiments out of three (mean of 12/24 wells ± SD). P-values were calculated using Student's t-test and the values ($p<0.0001$, presented with asterisk) indicated that cell growth after bleomycin-bleomycin and PCI-bleomycin-ATX-101 treatment were significantly different.

Conclusions

This is a fundamental study of specific aspects of the PCI technique. Using sub-lethal photodynamic doses, our results show that the cytotoxic effect of bleomycin is enhanced by $TPCS_{2a}$-mediated PCI in the tested bladder cancer cells, although these cell lines show clear differences with respect to sensitivity to photosensitizer uptake, light dose, and DNA repair capacity. We show that the PCI technique elevates bleomycin-induced DNA damage levels in all three cell lines, strongly suggesting that more bleomycin molecules enter the nuclei compared to treatment with bleomycin as a single agent. Thus, the membrane barrier to bleomycin seems to be bypassed by the PCI technique. We have further demonstrated that application of a cocktail of PCI-bleomycin and ATX-101, under condition where individual drug levels have no or low toxicity, reaches a promising therapeutic effect in the human bladder cancer cells T24 which is two-fold stronger than in the reference cell line, the human skin cancer cells A431. Combining PCI-chemotherapy treatments with inhibitors of DNA repair therefore seems to be a promising therapeutic strategy for increased efficacy “on site”.

Conflict of Interests

The authors declare no conflict of interests.

Acknowledgments

The authors would like to thank PCI Biotech AS (Oslo, Norway) for $TPCS_{2a}$ and APIM Therapeutics AS (Trondheim, Norway) for ATX-101 supply. The cell line AY-27 was generously supplied by Professor Steven H. Selman (Medical College of Ohio, Toledo, OH). This study was supported by grants from Liaison Committee between the Central Norway Regional Health Authority and the Norwegian University of Science and Technology (NTNU). We gratefully thank PhD candidate Linda Helander, department engineer Siri Backhe, and senior engineer Nina-Beate Liabakk at our department, and senior engineer Karin Solvang-Garten at Department of Circulation and Medical Imaging (NTNU) for their lab support and discussions. We gratefully thank Scientist Qian Peng (Department of Pathology, the Norwegian Radium Hospital, Oslo) for his excellent professional discussions and suggestions.

References

[1] M.C. Hall, S.S. Chang, G. Dalbagni, R.S. Pruthi, J.D. Seigne, E.C. Skinner, J.S. Wolf, Jr., P.F. Schellhammer, Guideline for the management of nonmuscle invasive bladder cancer (stages Ta, T1, and Tis): 2007 update, J Urol 178 (2007) 2314-2330.

[2] T.R. Griffiths, C. on behalf of Action on Bladder, Current perspectives in bladder cancer management, Int J Clin Pract (2012).

[3] I.K. Larsen, B. Sæther, B. Aagnes, Cancer in Norway 2010, Institute of population-based cancer research, Norway, 2012.

[4] National Cancer Institute, Bladder Cancer, the National Institutes of Health, USA, 2013.

[5] D. Ramotar, H. Wang, Protective mechanisms against the antitumor agent bleomycin: lessons from Saccharomyces cerevisiae, Curr Genet 43 (2003) 213-224.

[6] R.B. Bracken, D.E. Johnson, L. Rodriquez, M.L. Samuels, A. Ayala, Treatment of multiple superficial tumors of bladder with intravesical bleomycin, Urology 9 (1977) 161-163.

[7] A.G. Turner, K.R. Durrant, J.S. Malpas, A trial of bleomycin versus adriamycin in advanced carcinoma of the bladder, Br J Urol 51 (1979) 121-124.

[8] N. Gad-el-Mawla, R. Hamsa, E. Chevlen, J.L. Ziegler, Phase II trial of bleomycin in bilharzial bladder cancer, Cancer Treat Rep 62 (1978) 1109-1110.

[9] G. Pron, N. Mahrour, S. Orlowski, O. Tounekti, B. Poddevin, J. Belehradek, Jr., L.M. Mir, Internalisation of the bleomycin molecules responsible for bleomycin toxicity: a receptor-mediated endocytosis mechanism, Biochem Pharmacol 57 (1999) 45-56.

[10] M. Aouida, R. Poulin, D. Ramotar, The human carnitine transporter SLC22A16 mediates high affinity uptake of the anticancer polyamine analogue bleomycin-A5, J Biol Chem 285 (2010) 6275-6284.

[11] S.M. Sebti, J.P. Jani, J.S. Mistry, E. Gorelik, J.S. Lazo, Metabolic inactivation: a mechanism of human tumor resistance to bleomycin, Cancer Res 51 (1991) 227-232.

[12] D.R. Schwartz, G.E. Homanics, D.G. Hoyt, E. Klein, J. Abernethy, J.S. Lazo, The neutral cysteine protease bleomycin hydrolase is essential for epidermal integrity and bleomycin resistance, Proc Natl Acad Sci U S A 96 (1999) 4680-4685.

[13] L.H. Einhorn, Curing metastatic testicular cancer, Proc Natl Acad Sci U S A 99 (2002) 4592-4595.

[14] Y. Kubota, T. Nakada, H. Yanai, K. Itoh, I. Sasagawa, K. Kawai, Histological evaluation of the effects of electropermeabilization after administration of bleomycin on bladder cancer in the rat, Eur Urol 34 (1998) 372-376.

[15] Y. Kubota, T. Nakada, H. Yanai, H. Kakizaki, I. Sasagawa, M. Watanabe, Electropermeabilization in bladder cancer chemotherapy, Cancer Chemother Pharmacol 39 (1996) 67-70.

[16] T.J. Dougherty, Photodynamic therapy, Photochem Photobiol 58 (1993) 895-900.

[17] K. Berg, M. Folini, L. Prasmickaite, P.K. Selbo, A. Bonsted, B.O. Engesaeter, N. Zaffaroni, A. Weyergang, A. Dietze, G.M. Maelandsmo, E. Wagner, O.J. Norum, A. Hogset, Photochemical internalization: a new tool for drug delivery, Curr Pharm Biotechnol 8 (2007) 362-372.

[18] K. Berg, P.K. Selbo, L. Prasmickaite, T.E. Tjelle, K. Sandvig, J. Moan, G. Gaudernack, O. Fodstad, S. Kjolsrud, H. Anholt, G.H. Rodal, S.K. Rodal, A. Hogset, Photochemical internalization: a novel technology for delivery of macromolecules into cytosol, Cancer Res 59 (1999) 1180-1183.

[19] K. Berg, S. Nordstrand, P.K. Selbo, D.T. Tran, E. Angell-Petersen, A. Hogset, Disulfonated tetraphenyl chlorin (TPCS2a), a novel photosensitizer developed for clinical utilization of photochemical internalization, Photochem Photobiol Sci 10 (2011) 1637-1651.

[20] P.K. Selbo, G. Sivam, O. Fodstad, K. Sandvig, K. Berg, In vivo documentation of photochemical internalization, a novel approach to site specific cancer therapy, Int J Cancer 92 (2001) 761-766.

[21] M. Lilletvedt, H.H. Tonnesen, A. Hogset, L. Nardo, S. Kristensen, Physicochemical characterization of the photosensitizers TPCS2a and TPPS2a 1. Spectroscopic evaluation of drug--solvent interactions, Pharmazie 65 (2010) 588-595.

[22] K. Berg, A. Dietze, O. Kaalhus, A. Hogset, Site-specific drug delivery by photochemical internalization enhances the antitumor effect of bleomycin, Clin Cancer Res 11 (2005) 8476-8485.

[23] K. Berg, P.K. Selbo, L. Prasmickaite, A. Hogset, Photochemical drug and gene delivery, Curr Opin Mol Ther 6 (2004) 279-287.

[24] O.J. Norum, K.E. Giercksky, K. Berg, Photochemical internalization as an adjunct to marginal surgery in a human sarcoma model, Photochem Photobiol Sci 8 (2009) 758-762.

[25] O.J. Norum, J.V. Gaustad, E. Angell-Petersen, E.K. Rofstad, Q. Peng, K.E. Giercksky, K. Berg, Photochemical internalization of bleomycin is superior to photodynamic therapy due to the therapeutic effect in the tumor periphery, Photochem Photobiol 85 (2009) 740-749.

[26] P.K. Selbo, A. Weyergang, A. Hogset, O.J. Norum, M.B. Berstad, M. Vikdal, K. Berg, Photochemical internalization provides time- and space-controlled endolysosomal escape of therapeutic molecules, J Control Release 148 (2010) 2-12.

[27] ClinicalTrials.gov, Safety Study of Amphinex Based Photochemical Internalisation (PCI) of Bleomycin in Patients With Cutaneous Cancer, 2011.

[28] H.C. Arentsen, J. Falke, A. Hogset, E. Oosterwijk, J. Alfred Witjes, The effect of photochemical internalization of bleomycin in the treatment of urothelial carcinoma of the bladder: An in vitro study, Urol Oncol (2013).

[29] ClinicalTrials.gov, A Study to Evaluate the Safety and Efficacy of PC-A11 in Patients With Recurrent Head and Neck Squamous Cell Carcinoma, 2013.

[30] J. Chen, J. Stubbe, Bleomycins: towards better therapeutics, Nat Rev Cancer 5 (2005) 102-112.

[31] O. Tounekti, G. Pron, J. Belehradek, Jr., L.M. Mir, Bleomycin, an apoptosis-mimetic drug that induces two types of cell death depending on the number of molecules internalized, Cancer Res 53 (1993) 5462-5469.

[32] O. Tounekti, A. Kenani, N. Foray, S. Orlowski, L.M. Mir, The ratio of single- to double-strand DNA breaks and their absolute values determine cell death pathway, Br J Cancer 84 (2001) 1272-1279.

[33] R. Muller, K. Misund, T. Holien, S. Bachke, K.M. Gilljam, T.K. Vatsveen, T.B. Ro, E. Bellacchio, A. Sundan, M. Otterlei, Targeting proliferating cell nuclear antigen and its protein interactions induces apoptosis in multiple myeloma cells, PLoS One 8 (2013) e70430.

[34] K.M. Gilljam, E. Feyzi, P.A. Aas, M.M. Sousa, R. Muller, C.B. Vagbo, T.C. Catterall, N.B. Liabakk, G. Slupphaug, F. Drablos, H.E. Krokan, M. Otterlei, Identification of a novel, widespread, and functionally important PCNA-binding motif, J Cell Biol 186 (2009) 645-654.

[35] K.M. Gilljam, R. Muller, N.B. Liabakk, M. Otterlei, Nucleotide excision repair is associated with the replisome and its efficiency depends on a direct interaction between XPA and PCNA, PLoS One 7 (2012) e49199.

[36] A. Ciccia, A.V. Nimonkar, Y. Hu, I. Hajdu, Y.J. Achar, L. Izhar, S.A. Petit, B. Adamson, J.C. Yoon, S.C. Kowalczykowski, D.M. Livingston, L. Haracska, S.J. Elledge, Polyubiquitinated PCNA Recruits the ZRANB3 Translocase to Maintain Genomic Integrity after Replication Stress, Mol Cell 47 (2012) 396-409.

[37] A. Bacquin, C. Pouvelle, N. Siaud, M. Perderiset, S. Salome-Desnoulez, C. Tellier-Lebegue, B. Lopez, J.B. Charbonnier, P.L. Kannouche, The helicase FBH1 is tightly regulated by PCNA via CRL4(Cdt2)-mediated proteolysis in human cells, Nucleic Acids Res 41 (2013) 6501-6513.

[38] L. Prasmickaite, A. Hogset, P.K. Selbo, B.O. Engesaeter, M. Hellum, K. Berg, Photochemical disruption of endocytic vesicles before delivery of drugs: a new strategy for cancer therapy, Br J Cancer 86 (2002) 652-657.

[39] M.B. Berstad, A. Weyergang, K. Berg, Photochemical internalization (PCI) of HER2-targeted toxins: synergy is dependent on the treatment sequence, Biochim Biophys Acta 1820 (2012) 1849-1858.

[40] A. Weyergang, P.K. Selbo, K. Berg, Photochemically stimulated drug delivery increases the cytotoxicity and specificity of EGF-saporin, J Control Release 111 (2006) 165-173.

[41] Y. Baglo, M.M. Sousa, G. Slupphaug, L. Hagen, S. Havag, L. Helander, K.A. Zub, H.E. Krokan, O.A. Gederaas, Photodynamic therapy with hexyl aminolevulinate induces carbonylation, posttranslational modifications and changed expression of proteins in cell survival and cell death pathways, Photochem Photobiol Sci 10 (2011) 1137-1145.

[42] S.K. Sreedharan, C. Verma, L.S. Caves, S.M. Brocklehurst, S.E. Gharbia, H.N. Shah, K. Brocklehurst, Demonstration that 1-trans-epoxysuccinyl-L-leucylamido-(4-guanidino) butane (E-64) is one of the most effective low Mr inhibitors of trypsin-catalysed hydrolysis. Characterization by kinetic analysis and by energy minimization and molecular dynamics simulation of the E-64-beta-trypsin complex, Biochem J 316 (Pt 3) (1996) 777-786.

[43] G. Morris, J.S. Mistry, J.P. Jani, S.M. Sebti, J.S. Lazo, Cysteine proteinase inhibitors and bleomycin-sensitive and -resistant cells, Biochem Pharmacol 41 (1991) 1559-1566.

[44] R. Edward, Red/far-red fluorescing DNA-specific anthraquinones for nucl:cyto segmentation and viability reporting in cell-based assays, Methods Enzymol 505 (2012) 23-45.

[45] J.T. Wang, K. Berg, A. Hogset, S.G. Bown, A.J. Macrobert, Photophysical and photobiological properties of a sulfonated chlorin photosensitiser TPCS(2a) for photochemical internalisation (PCI), Photochem Photobiol Sci 12 (2013) 519-526.

[46] N.P. Singh, M.T. McCoy, R.R. Tice, E.L. Schneider, A simple technique for quantitation of low levels of DNA damage in individual cells, Exp Cell Res 175 (1988) 184-191.

[47] P.L. Olive, J.P. Banath, The comet assay: a method to measure DNA damage in individual cells, Nat Protoc 1 (2006) 23-29.

[48] A. Hanssen-Bauer, K. Solvang-Garten, K.M. Gilljam, K. Torseth, D.M. Wilson, 3rd, M. Akbari, M. Otterlei, The region of XRCC1 which harbours the three most common nonsynonymous polymorphic variants, is essential for the scaffolding function of XRCC1, DNA Repair (Amst) 11 (2012) 357-366.

[49] S. Mukherjee, R.N. Ghosh, F.R. Maxfield, Endocytosis, Physiol Rev 77 (1997) 759-803.

Supplementary Information

Enhanced efficacy of bleomycin in bladder cancer cells by photochemical internalization

Yan Baglo[1], Lars Hagen[1], Anders Høgset[2], Finn Drabløs[1], Marit Otterlei[1] and Odrun A. Gederaas[1]

1. *Department of Cancer Research and Molecular Medicine, Faculty of Medicine, Norwegian University of Science and Technology, P.O.Box 8905, N-7491 Trondheim, Norway.*
2. *PCI Biotech AS, Strandveien 55, N-1366 Lysaker, Norway*

Correspondence should be addressed to Yan Baglo; yan.baglo@ntnu.no.

The results shown in Figure 1S, 2S and 3S are repetitive or supplementary to the figures in the main paper, thus they are presented here as Supplementary Information. These results were used to determine an optimal time point (48 h) and support for the cytotoxicity assays (section 2.6 in Materials and Methods of the main paper).

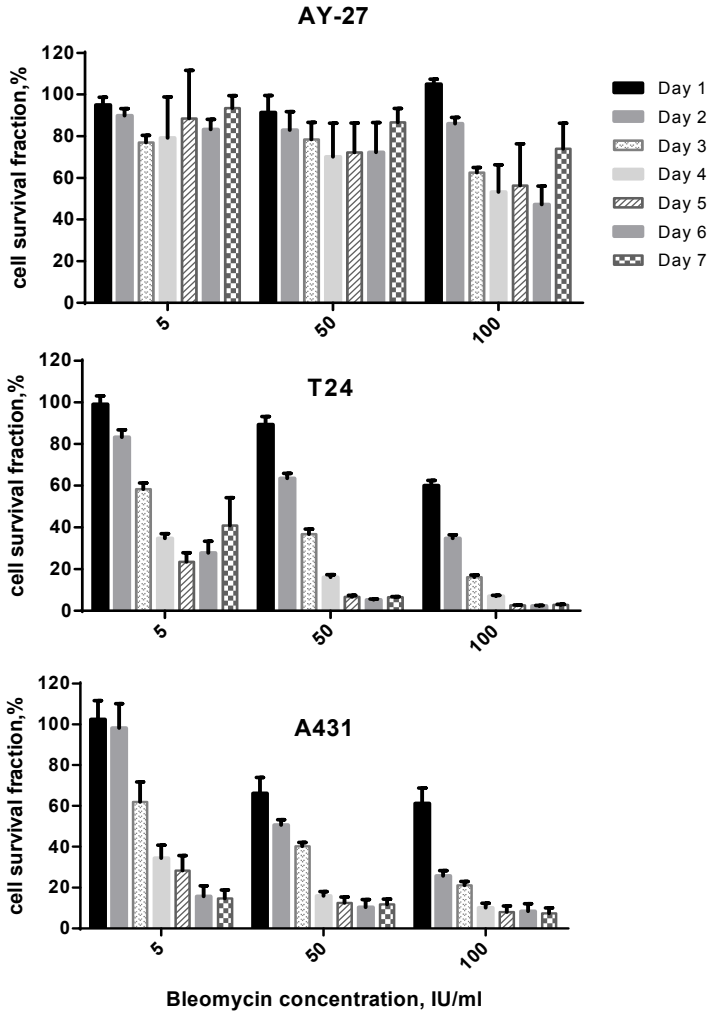

Figure 1S (Supplementary). The long-term bleomycin cytotoxicity in the three cell lines AY-27, T24 and A431. Cells were seeded out into 25 cm^2 culture flasks (1×10^6 cells/flask) and treated with bleomycin (4 h) at indicated concentrations (5, 50, and 100 IU ml^{-1}) after cell attachment. The cells were re-plated into 96-well plates (1000 cells/well) with parallels. Cell survival fraction was determined by resazurin survival assay from the next day until the seventh. The data are from one representative experiments out of two (mean of 12/24 wells ± SD).

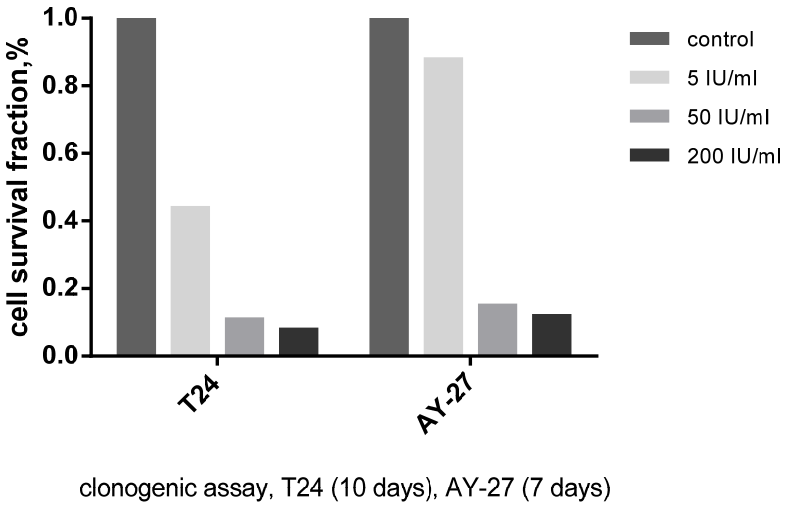

Figure 2S (Supplementary). Cell survival after bleomycin treatment in T24 and AY-27 cell line. Cells were seeded out into 25 cm^2 culture flasks (1×10^6 cells/flask) and treated with bleomycin (4 h) at indicated concentrations (5, 50, and 200 IU ml^{-1}) after cell attachment. The cells were re-plated into petri dishes (100 cells/dish) with parallels. The fraction was determined and calibrated with the amount of colonies using a standard clonogenic assay. The time for colony forming was seven days for AY-27 cells and ten days for T24 cells.

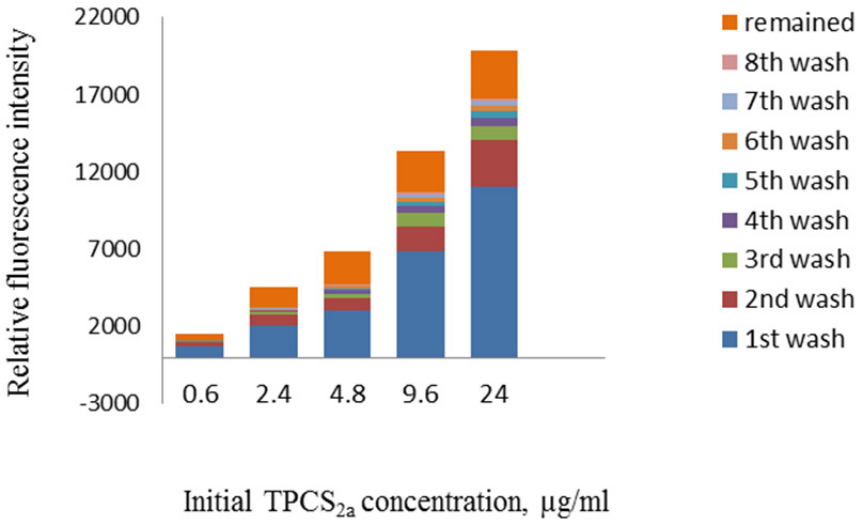

Figure 3S (Supplementary). Elimination of $TPCS_{2a}$ in AY-27 cells. Attached cells in 96-well plate were incubated with $TPCS_{2a}$ (18 h) at different concentrations and washed with culture medium (100 µl/well) at every chase of 10-15 min. Chased medium was moved to a new 96-well plate in the same well position. The amount of released $TPCS_{2a}$ and cellular retention after 8^{th} washing were determined by fluorescence measurement using FLUOStar Omega microplate reader (410 nm/640 nm, ±10 nm).

Paper 4

Manuscript

Studies of the photosensitizer disulfonated meso-tetraphenyl chlorin in an orthotopic rat bladder tumor model

Yan Baglo[a,*], Qian Peng[b], Lars Hagen[a], Kristian Berg[c], Anders Høgset[d], Finn Drabløs[a], Odrun A. Gederaas[a]

a Department of Cancer Research and Molecular Medicine, Faculty of Medicine, Norwegian University of Science and Technology, N-7491 Trondheim, Norway

b Department of Pathology, the Norwegian Radium Hospital, Oslo University Hospital, Montebello, N-0310 Oslo, Norway

c Department of Radiation Biology, the Norwegian Radium Hospital, Oslo University Hospital, Montebello, N-0310 Oslo, Norway

d PCI Biotech AS, Strandveien 55, N-1366 Lysaker, Norway

*Corresponding author:
Yan Baglo
Department of Cancer Research and Molecular Medicine, Faculty of Medicine, NTNU
Postbox 8905, N7491 Trondheim, Norway
Telephone: 0047 72826606 E-mail: yan.baglo@ntnu.no

Summary

Background

Photochemical internalization (PCI) is a novel technology for the release of a therapeutic molecule from endocytic vesicles into the cytosol of a cell. The release of molecules occurs after activation of an endocytic membrane-embedded photosensitizer by light. In this study uptake and localization of the photosensitizer disulfonated tetraphenyl chlorin ($TPCS_{2a}$) were explored to optimize a PCI protocol in an orthotopic rat bladder tumor model.

Methods

Female Fischer F344 rats were intravesically instilled with 0.4×10^6 AY-27 transitional carcinoma cells before allowing tumor growth for 14 days. The photosensitizer $TPCS_{2a}$ was intravesically instilled at different concentrations, and bladders were excised after different time intervals. The retention, penetration, and localization of intratumoral $TPCS_{2a}$ were explored *ex vivo* using fluorescence spectroscopy and fluorescence microscopy to determine an optimal PCI protocol. These results were compared to histological analysis of necrotic areas after activation of intratumoral $TPCS_{2a}$ by red light (652 nm, 0.5 J/cm^2).

Results

A superficial distribution pattern of the photosensitizer $TPCS_{2a}$ was seen in bladder tumor tissue, and $TPCS_{2a}$ was almost cleared from the tumors after 72 hours. The highest retention of $TPCS_{2a}$ was found at 24 hours after instillation when using a concentration of 3 mg/ml.

Conclusion

An optimal PCI protocol was defined for the tumor model, including a 24-hour $TPCS_{2a}$-to-light interval and a dose of 3 mg/ml $TPCS_{2a}$. This protocol will be utilized for the study of PCI-enhanced therapeutic effects on non-muscle invasive bladder cancer, using a potent chemotherapeutic under an optimal light dose.

Keywords

Photochemical internalization; photodynamic therapy; rat orthotopic bladder tumor model; non-muscle invasive bladder cancer; disulfonated meso-tetraphenyl chlorin

Introduction

In Norway, bladder cancer has been one of the five most common cancer types for men during the past decade [1]. Approximately 70-80% of diagnosed bladder cancers worldwide are non-muscular invasive bladder cancer (NMIBC) consisting of carcinoma *in situ*, stage Ta and T1 tumors. NMIBC is normally removed by surgery during a cystoscopy under general anesthesia, known as transurethral resection of bladder tumors (TURBT). Unfortunately, the high rate of recurrence and progression after TURBT means that adjuvant treatments may usually be required, such as intravesical chemotherapy using mitomycin C, epirubicin, or doxorubicin and/or immunotherapy using Bacillus Calmette-Guérin (BCG) vaccine [2,3,4,5]. However, recurrence rates still remain high, and progression is not eliminated after the combined therapies. Side effects including bladder irritation, skin rash, frequency and pain are often seen with the chemo- and immunotherapy [6]. To improve the total intravesical agent uptake and hence chemotherapeutic efficacy, various experimental approaches have been evaluated, including enhancing the agent delivery to bladder tumor tissue using electromotive therapy and photochemical internalization (PCI), enhancing cell membrane permeability using intravesical hyperthermia [7,8,9]. Hexaminolevulinate-guided transurethral resection has been shown to significantly improve detection of Ta and T1 lesions and reduce recurrences [10]. In this study, photochemical internalization (PCI) [11] have been studied *in vivo* to enhance the effect of therapeutic agents for NMIBC.

PCI has been developed from photodynamic therapy (PDT) [12], but is designed to favor the delivery of a therapeutic molecule without inactivating the molecule or lethally damaging the cell. The cell killing effect therefore results predominantly from the therapeutic molecule, rather than the photodynamic treatment [13]. This is of particular importance for the delivery of genes and siRNA [14]. However, PCI is based on the same photochemical principles as PDT. PCI can be looked upon as a three-stage process. The first stage is the selective accumulation of an amphiphilic photosensitizer in the tumor endosomal or lysosomal membranes via endocytosis, in the absence of light. The second stage is the accumulation of a therapeutic molecule in the endocytic vesicles, also in the absence of light. In the last stage, the photosensitizer is activated by light of the appropriate wavelength and intensity. Using a sub-lethal photodynamic dose, activated photosensitizer evokes a response only in the endosomal and lysosomal membranes by reacting with molecular oxygen leading to membrane rupture and release of the molecules [11]. PCI could be combined with different therapeutic macromolecules or molecules with limited ability to penetrate the cell membrane, but PCI has also been shown to enhance therapeutic efficacy of some conventional cytotoxic therapies, with reduced side effects as the therapeutic site is limited to the illuminated area [15,16].

NMIBC is potentially well suited for effective treatment by PDT or PCI because it is easily accessible for both intravesical instillation and illumination. In addition, it is possible to irradiate the whole bladder and hence provide access to multifocal tumors [17]. As no difference in light penetration is observed between tumor and normal bladder tissue, the photodynamic responses upon illumination of the bladder will depend on the localization and accumulation of the photosensitizer within the tumor [18]. In this study, the potent photosensitizer disulfonated tetraphenyl chlorin ($TPCS_{2a}$) was utilized to explore its tissue localization and accumulation in a rat bladder tumor model [19,20,21,22], to establish an optimal protocol for the first stage of PCI.

$TPCS_{2a}$ is an amphiphilic chlorin produced from disulfonate tetraphenyl phorphyrin ($TPPS_{2a}$) [15,23]. The absorption spectrum of $TPCS_{2a}$ has been investigated in organic media and shown to be only slightly affected by the properties of the organic solvents. It is observed that $TPCS_{2a}$ has absorption maximum at 650-653 nm and emission maximum at 654-657 nm in organic solvents [24,25]. As a fluorophore, $TPCS_{2a}$ is found to have stronger light absorption in the red wavelength region and to be more efficient for *in vivo* applications than its corresponding porphyrin $TPPS_{2a}$ [23,24,25,26,27]. $TPCS_{2a}$ was approved for use in clinical studies in 2008, and a phase I clinical trial of $TPCS_{2a}$-mediated PCI of bleomycin in head-and-neck cancer showed no severe side effects associated with the treatment. The efficacy and safety of the modality are currently being evaluated in a phase II clinical intervention trial [28,29]. In animal studies, $TPCS_{2a}$-mediated PCI of the chemotherapeutic agent bleomycin has been investigated as an adjunct to radiotherapy and surgery by Norum *et al*. [30,31], showing that PCI induces synergistic therapeutic effects in a human sarcoma model. PCI is also proposed to have potential competence to bypass the development of drug resistance induced by repeated exposure to therapeutics [15]. Very recently, PCI-enhanced vaccination using $TPCS_{2a}$ was demonstrated to strongly increase stimulation of CD8 T-cell responses preventing tumor growth in a mouse skin tumor model [32]. With rapid development of $TPCS_{2a}$ usage in PCI, it has become of great interest in the possible treatment of bladder cancer [7,8].

Materials and Methods

Cell suspension

Rat bladder transitional carcinoma cells (AY-27) [33] were maintained in the same RPMI-1640 culture medium and conditions as described in our earlier study [34]. Immediately before intravesical inoculation of AY-27 cells into rat bladder, single cell suspension was prepared at a desired density with RPMI-1640 medium supplement with glutamine (5%) and stored on ice until instillation.

Photosensitizer

The photosensitizer $TPCS_{2a}$ (30 mg/ml, Amphinex®) disaggregated in Tween 80 and 50 mM Tris buffer [35] was provided by PCI Biotech AS (Lysaker, Norway) and stored at 4 °C in aliquots. The solution was diluted into desired concentrations with 50 mM phosphate buffer (pH 8.5) for inoculation in rat bladder. For cell incubation, the solution was diluted first with 50 mM Tris buffer (pH 8.5) and then with culture medium immediately before use [8]. All work with $TPCS_{2a}$ was performed under subdued light or light protection.

Animals

Female rats (Fischer inbred F344, 8-10 weeks old, body mass 160-180 grams) were used in all experiments. The animals were housed in standard conditions under conventional pathogen-free microbiological status, as described by Arum *et al.* [21]. Every six rats were housed in a standard cage and fed with standard rat food pellets and tap water. Rat bladder was modeled as a sphere with a volume of 0.3 ml in order to determine volume of a single instillation [20]. All animal experiments were approved by Norwegian National Animal Research Authority (NARA).

Orthotopic bladder tumor model

After weighing of body mass, the rats were numbered, and allocated into control and treated groups according to experimental designs (see later). The tumor model has been described previously [19,20,21]. Briefly, under anesthesia each rat received 0.4×10^6 AY-27 cells intravesically through an 18 gauge plastic cannula after acidic and alkaline conditioning [21]. A standard dose of temgesic for pain relieve was given as required after recovery. The rats were further housed for 14 days allowing tumor growth according to earlier histological investigations by Larsen *et al.* [20]. The tumor stages in this model have been evaluated to be similar to human urinary carcinoma at stage T1-3 WHO grade 3 [21].

Intravesical $TPCS_{2a}$ administration

Each bladder was quickly washed three times with 0.9% salt water through an 18 gauge plastic cannula, while the rat was under anesthesia. Instillation of $TPCS_{2a}$ solution (0.3 ml) at desired concentration was followed by incubation for two hours in the dark, while the rat body was rotated 90 degrees every 30 minutes allowing homogenous uptake of the photosensitizer into the whole bladder. Finally, the rats were housed under light protection until *ex vivo* fluorescent measurement.

Fluorescent intensity measurement

JETI PDT fluorometer (JETI Technische Instrumente GmbH, German) is a miniaturized fiber-optic spectrometer for the detection of fluorescence in the wavelength range of 550 nm to 800 nm, using a single excitation wavelength. A violet LED lamp with a peak wavelength at 405 nm was used for excitation. The instrument is able to measure fluorescence emission from $TPCS_{2a}$, where fluorescence can be excited at 405 nm, and the measurements were performed with an external 200 μm diameter optical fiber. Subsequent to calibration, a series of fluorescence intensity data were collected from 550 nm to 800 nm using the software of the PDT fluorometer (V.1.2).

Each bladder was excised under anesthesia and opened from the urethra. The rats were then sacrificed. After flat fixing the opened bladder upon a cardboard with the mucosal layer exposed, fluorescence measurement was performed from the mucosal layer on at least five random areas by JETI PDT fluorometer. After measurement, the tissue was quickly frozen in liquid nitrogen and stored at -80 °C before sectioning.

Illumination with red light

Intravesical illumination was performed using a laser fiber (BioLitech AG, Germany) coupled to an optometer (P-9710-1/P-9710-2, Gigahertz-Optic GmbH, Germany). The intensity of the laser (652 nm) was measured and controlled with the optometer until light delivery was stable after pre-warming the optometer (30 min) and the laser (15 min). The exposure to the whole bladder wall with red light (652 nm, 0.5 J/cm^2) was performed by inserting the fiber through an 18 gauge plastic cannula after inflating bladder with 0.3 ml salt water.

Frozen sections

Tissue blocks were made with tissue OCT compound (Tissue-Tek®, Sakura Finetek USA) from a piece of frozen bladder and frozen with liquid nitrogen. Tissue frozen sections (5 μm) were cross sectioned through bladder walls under light protection using Leica cryostat (CM3050S, Leica Biosystems Nussloch GmbH, Germany) at -20 °C. The frozen sections were collected to a glass slide and stored at -80 °C until microscope examination or haematoxylin erythrosine saffron (HES) staining using a standard protocol for histological frozen sections.

Tissue paraffin

Bladder tumor tissue was immersed in 4% formaldehyde until paraffin embedding.

After cross sectioning of the tissue through bladder walls, the sections (4 μm) were HES stained in an automatic slide stainer (Tissue-Tek®, PrismaTM, Sakura Finetek USA, Inc.) using a standard protocol for histological paraffin sections.

Intratumoral localization of $TPCS_{2a}$

Localization of $TPCS_{2a}$ in the frozen sections of bladder tumor tissue was visualized using an Olympus IX71 inverted fluorescence microscope (410 nm BP/590 nm LP). Each frozen tumor tissue section was covered with Dako fluorescent mounting medium (Dako Danmark A/S) before being thawed. Images were taken by a CCD camera (XM10), using a 4× objective, and a Cell^P Image visualization software. A neighboring section was HES-stained in the automatic slide stainer using a standard protocol for frozen sections. Histological examination was performed in a microscope (Nikon Eclipse 80i) and images were taken by a digital Sight camera with the NIS-Elements F3.0 software.

Microscopic fluorescence photometry

$TPCS_{2a}$ fluorescence measurements were done by microscopic fluorescence photometry using a microscope (Nikon Eclipse E800) with a 100 W mercury lamp and a highly light-sensitive thermo-electrically cooled charge-coupled device camera (ORCAII-ER, Hamamatsu, Japan). The resolution was 1280×1024 pixels with a dynamic range of 12 bits per pixel. The images were taken with a 4× objective and a filter combination composed of a 380-420 nm excitation filter, a 430 nm beam splitter and a 605±55 nm band-pass emission filter. A rectangular area superimposing the tumor zone from the superficial to deep part was made on each fluorescence image. The fluorescence intensity within the selected area was then quantified as a function of depth of the tumor by an image processing unit (Aqua Cosmos software). In the measurements, each mean value of specific $TPCS_{2a}$ fluorescence intensity was calculated from the pixels at the exact same depth location; the mean values were then plotted as a function of the depth of the tumor by SigmaPlot 10 (Systat Software Inc., CA).

Experimental design

Protocol A. Assessment of tissue $TPCS_{2a}$ at different instilled concentrations

A total of 37 rats were allocated into one of the six groups: (1) control, 4 rats (without any treatments); (2) tumor, 5 rats (inoculated with AY-27 cells only); (3) 1 mg/ml $TPCS_{2a}$, 7 rats; (4) 2 mg/ml $TPCS_{2a}$, 7 rats; (5) 3 mg/ml $TPCS_{2a}$, 7 rats; and (6) 5 mg/ml $TPCS_{2a}$, 7 rats. Groups 2-6 were intravesical inoculated with 4×10^6 AY-27 cells. After housing for 14 days, groups 3-6 received intravesical

instillation of $TPCS_{2a}$ at the noted concentrations and the animals were housed for 72 hours under light protection. In the end, all bladders were excised and fluorescence intensity was measured immediately using a JETI fluorometer. An optimal $TPCS_{2a}$ concentration was chosen from these experiments for the use in protocol B.

Protocol B. Assessment of tissue $TPCS_{2a}$ at different time intervals

Nineteen rats were allocated into one of the six groups: (1) control, 1 rat; (2) tumor, 1 rat; (3) 4 hours retention time, 4 rats; (4) 24 hours retention time, 4 rats; (5) 48 hours retention time, 5 rats; and (6) 72 hours retention time, 4 rats. After establishing tumor in Groups 2-6 (see protocol A), group 3-6 received intravesical instillation of $TPCS_{2a}$ at the optimal concentration (chosen from experiments in protocol A) and the animals were housed for further 4, 24, 48 or 72 hours respectively under light protection. Group 3-5 were excised with bladder at each determined time; while Group 6 and the control groups were excised with bladder at the last experiment day. Fluorescence intensity was measured immediately using the JETI fluorometer. An optimal $TPCS_{2a}$ distribution time in tissue, i.e. $TPCS_{2a}$-to-light time interval, was chosen from these experiments for the use in protocol C.

Protocol C. Assessment of necrotic area when using the optimal $TPCS_{2a}$ concentration and $TPCS_{2a}$-light interval

Eight rats established with bladder tumor (see protocol A) were intravesical instilled with $TPCS_{2a}$ at the optimal concentration (protocol A) and housed for the optimal time (protocol B). Bladders were intravesically exposed to red light (laser, 652 nm, 0.5 J/cm^2) in salt water. Then, all bladders were excised after housing the rats for additional 19 days.

All bladder tumor tissue samples except the photodynamically treated ones were frozen at -80 °C until tissue sectioning for histological analysis and fluorescence microscope in order to explore $TPCS_{2a}$ localization and penetration in the bladder tumor tissue. The photodynamically treated tissue samples were immersed in 4% formaldehyde until paraffin sectioning.

Results

Tumor characteristics in the model

The bladder consists of three layers: the mucous layer of epithelial cells (urothelium), the underlying submucosa, and the outer muscular layer. Bladder tumors were visually present in all inoculated rats (see Table 1). Histology showed that the tumors were multifocal and developed in either stage T1 or T2 with varied tumor size. In Figure 1, bladder histology shows clear tumor characteristics in the model system.

Table 1 Tumor development for each experiment

Experiment	Number of control rats	Number of inoculated rats	Rats with tumor present	Rats without tumor present	Number of dead rats
A	4	33	33	0	0
B	1	18	18	0	0
C	0	8	8	7	1	0

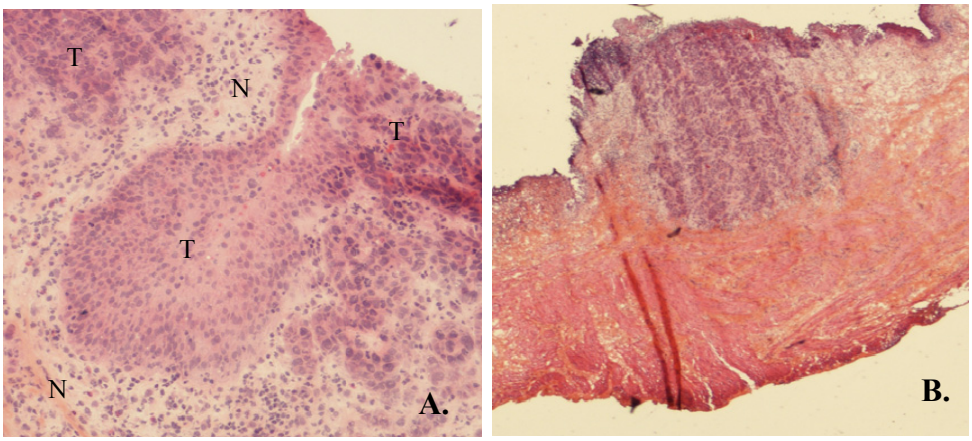

Figure 1. Histology of rat bladder tumors developed for 14 days after intravesical inoculation with AY-27 cells. (A) Normal urothelium (N) and multifocal bladder tumors (T) (1×100). (B) Bladder tumor in stage T2 (1×20). The bladder was inoculated with 0.4×10^6 AY-27 cells. The images were taken in microscope (Nikon Eclipse 80i) using a Digital Sight Camera, showing HES sections (5 µm). The upper part is the mucosal layer and the lower part in image B is the muscular layer of the bladder.

Determination of intratumoral $TPCS_{2a}$ with fluorescence spectroscopy

The amount of retentive $TPCS_{2a}$ in bladder tumor tissue was measured *ex vivo* by a JETI PDT fluorometer. In accordance with absorbance and fluorescence spectra of $TPCS_{2a}$ in organic solvents [24], the molecules of $TPCS_{2a}$ were excited at 405 nm in bladder tumor tissue and maximum fluorescence emission was detected at 654-656 nm, in which a peak at 655 nm was dominant. Fluorescence spectra of $TPCS_{2a}$ obtained from control, tumor control and $TPCS_{2a}$-treated bladder samples in this study are shown in Figure 2, in which only the $TPCS_{2a}$-treated sample presents the typical $TPCS_{2a}$ fluorescence spectrum [24]. Thus, for the data collection in this study, only relative fluorescence intensity (RFI) at the peak of 654-656 nm from the typical $TPCS_{2a}$ spectrum was recorded to present the amount of retentive $TPCS_{2a}$ in the measured tissue, and calibrated to integration time 200 ms of the instrument. For $TPCS_{2a}$-free tissue, such as control and tumor control in Figure 2, the value of RFI was set to zero in subsequent experiments (see Figure 3).

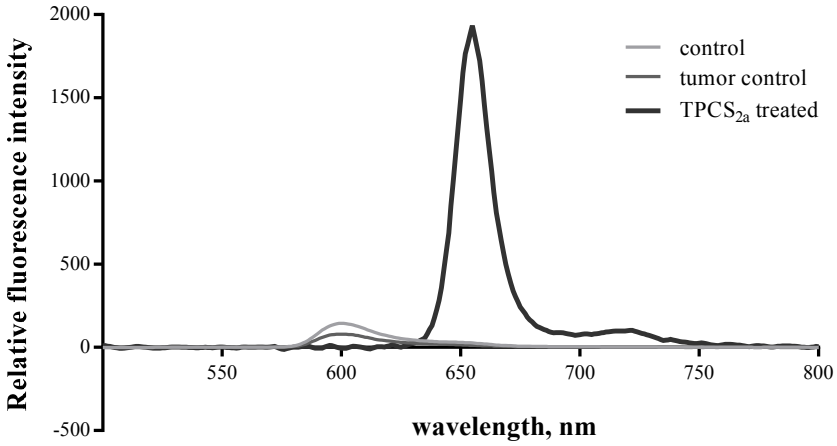

Figure 2. Fluorescence emission spectra of $TPCS_{2a}$ in bladder tumor tissues. Data were obtained from JETI PDT fluorometer at calibrated integration time of 200 ms. Fluorescence of $TPCS_{2a}$ was excited at 405 nm by JETI equipped laser. $TPCS_{2a}$ fluorescence was detected *ex vivo* only from $TPCS_{2a}$-treated bladder tumor tissue, not the controls.

$TPCS_{2a}$ uptake and elimination in tissue

To explore an optimal concentration of $TPCS_{2a}$ and optimal $TPCS_{2a}$-to-light time interval for the PCI protocol in the tumor model, two animal trials were performed (protocol A and B in Methods). The retentive $TPCS_{2a}$ in tumor tissue as measured under different treatment conditions is shown in Figure 3. The photosensitizer retention in bladder tumor tissue was first explored at 72 h after intravesical instillation using four different concentrations of $TPCS_{2a}$ (1, 2, 3 and 5 mg/ml; protocol A in Methods). Means of relative fluorescence intensity (RFI) of $TPCS_{2a}$ were measured and calculated as 1.8, 11.9, 15.7 and 22.8 respectively, with increasing concentration of $TPCS_{2a}$, showing a clear dose-dependency (Figure 3A). One animal with extremely high uptake was observed in the group treated with 5 mg/ml $TPCS_{2a}$. However, significant difference of the mean was neither observed between the groups treated with 2 and 3 mg/ml, nor between the groups treated with 3 and 5 mg/ml $TPCS_{2a}$ (two-tailed unpaired t-test, p value > 0.05). Based on this, 3 mg/ml was chosen for further study on four different retention time intervals (4, 24, 48 and 72 h; protocol B in Methods). Mean of retentive $TPCS_{2a}$ was obtained as 427, 669, 236, and 1.7 RFI respectively with increasing time after administration (Figure 3B). The maximum retentive $TPCS_{2a}$ was seen at 24 h after intravesical instillation, and elimination of $TPCS_{2a}$ occurred thereafter. Tissue $TPCS_{2a}$ was almost cleared after 72 hours (Figure 3B). A time interval of 24 h was therefore chosen for the animal trial using protocol C (see Figure 6).

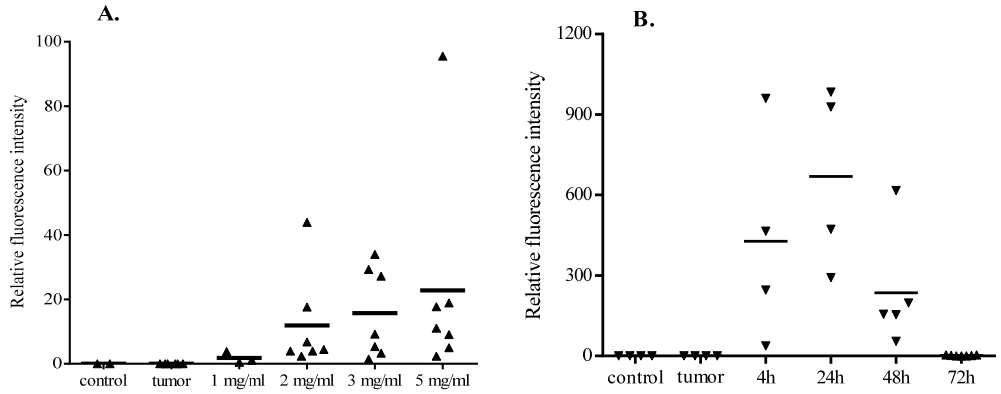

Figure 3. Uptake and retention of $TPCS_{2a}$ in bladder tumor tissues. (A) Relative florescence intensity (RFI) of $TPCS_{2a}$ measured 72 h after intravesical instillation at concentration of 1, 2, 3, and 5 mg/ml respectively (protocol A); (B) RFI of $TPCS_{2a}$ with an originally instilled concentration of 3 mg/ml measured at retention time of 4, 24, 48, and 72 h respectively (protocol B). Data were obtained from a JETI PDT fluorometer at calibrated integration time of 200 ms. Mean RFI of each group is shown as a horizontal line. Please observe the difference in vertical scale between A and B.

Localization of intratumoral $TPCS_{2a}$

To investigate the distribution and localization of $TPCS_{2a}$ in bladder tumor tissue, frozen sections of the tumor samples with strongest RFI from each treated group (Fig. 3B) were selected, together with the control samples, to be investigated by fluorescence microscopy using a 590 nm long-pass emission filter. Frozen sections and their corresponding HES sections from one tumor control and one treated sample (4 h of retention time) are shown in Figure 4. We are showing the fluorescent image of the sample after 4 h retention time, rather than 24 h, which was the optimal $TPCS_{2a}$-to-light interval (Figure 3B), because of weaker fluorescence in the 24 h sample as a result of accidental photobleaching during sample sectioning. However, the sample after 4 h retention time had very similar measured RFI as the sample after 24 h retention time (Figure 3B) and very similar fluorescent distribution pattern. Comparison of the frozen section with its corresponding HES section and the control sample shows that $TPCS_{2a}$ was located in the tumor surface of the mucosal layer, and that the distribution of $TPCS_{2a}$ is superficial (Figure 4C). No fluorescence of $TPCS_{2a}$ was detected in the tumor control sample (Figure 4A). Since the emission filter used is 590 nm long-pass, in order to confirm that the fluorescent compound was likely to be $TPCS_{2a}$ (emission peak at 654-657 nm) [24,25], the neighboring frozen sections from the same samples were examined with a band-pass filter (605 ± 55 nm) in a separate experiment, and the penetration depth was calculated by a semi-quantitative approach (see Figure 5).

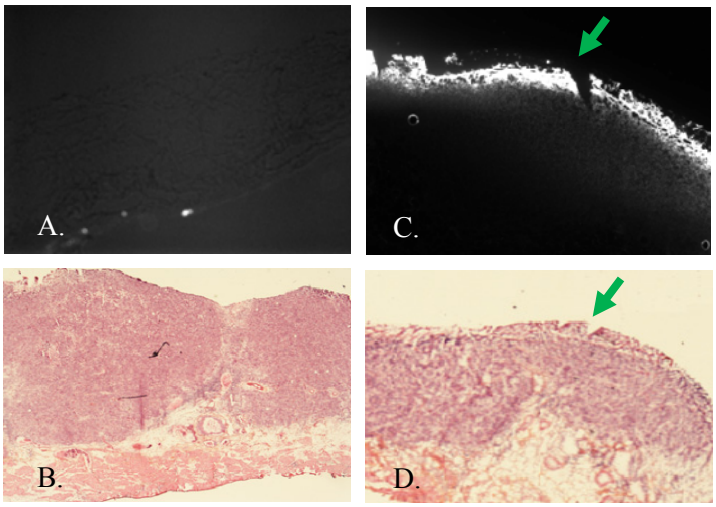

Figure 4. Fluorescence (A, C) and transmission (B, D) microphotographs of bladder tumors taken from a control sample (without $TPCS_{2a}$) (A, B) or from a $TPCS_{2a}$-treated sample (3 mg/ml, 4 h). The fluorescence images of frozen tissue sections (5 µm) were taken from an Olympus IX71 inverted fluorescence microscope (410 nm BP/590 nm LP) using a CCD camera (X10) with a 4× objective; while the transmission images of HES-stained neighboring tissue sections (5 µm,) were taken from a Nikon Eclipse 80i microscope with a digital Sight camera using a 20× objective. The fluorescence images were enlarged to the same scale as the transmission images. The same histological orientation of the fluorescent and transmission images is indicated with the green arrows for the tumor areas (the mucosal layer of the bladder wall).

Penetration of $TPCS_{2a}$

The PCI technology only functions within regions of tumor tissue that contain photosensitizer. It is therefore important to understand how deeply $TPCS_{2a}$ can penetrate into bladder tumor tissue after intravesical instillation. This was investigated using microscopic fluorescence photometry (Figure 5). The mean of $TPCS_{2a}$ fluorescence intensity (see Methods) measured at each distance from the starting point (green arrows) was plotted as a function of tissue depth, confirming that $TPCS_{2a}$ penetration was superficial, less than 0.2 mm (Figure 5F).

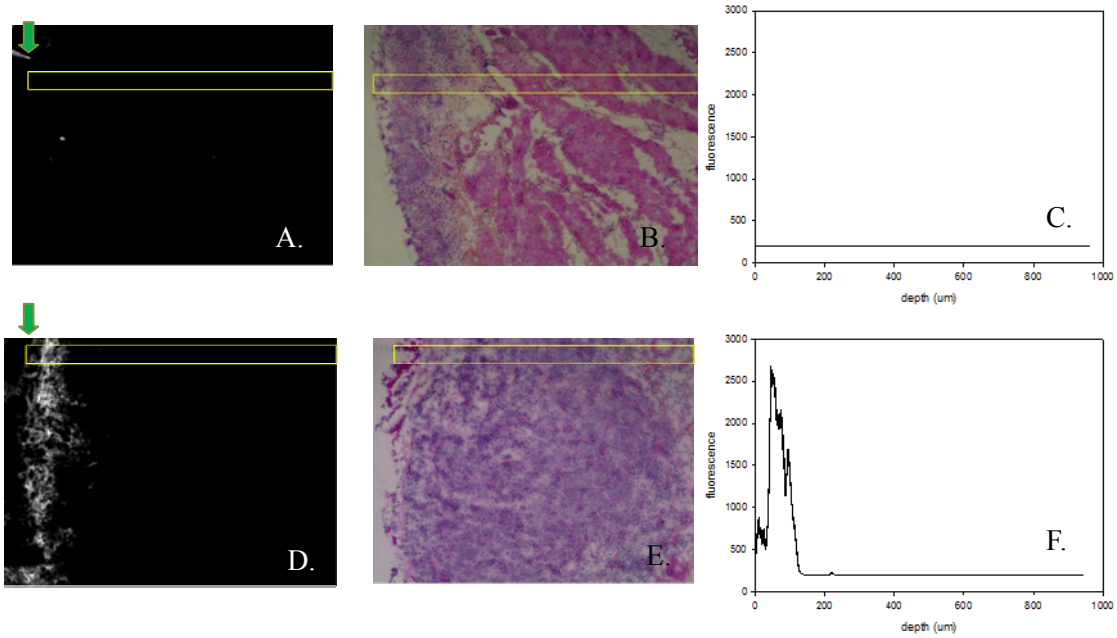

Figure 5. Fluorescence intensity of $TPCS_{2a}$ against the depth of tumor. (A) and (B) are from the neighboring tissue sections of a control sample (without $TPCS_{2a}$); while (D) and (E) are from the neighboring tissue sections of a $TPCS_{2a}$-treated sample (3 mg/ml, 4 h). The fluorescence images of the frozen tissue sections (5 µm, A and D) and transmission images of the HES-stained tissue sections (5 µm, B and E) were taken from the microscope (Nikon Eclipse E800) with a thermo-electrically cooled CCD camera using a 4× objective. The fluorescence intensity of $TPCS_{2a}$ within the rectangular areas was quantified with the software of AquaCosmos and plotted for the control sample (C) and the $TPCS_{2a}$-treated sample (F). The left side of the rectangular areas is the mucosal layer of the bladder wall (i.e. the tumor surface). The graphs of tissue distribution were plotted with the SigmaPlot® 10 software.

Light activation of $TPCS_{2a}$ in tissue

So far the distribution of $TPCS_{2a}$ in tissue has been estimated using fluorescence. It is possible that this underestimates concentrations due to photobleaching occurring during sample sectioning, and due to sensitivity of the instrument used for fluorescence measurement. In order to investigate more precise location and penetration of the photosensitizer under the presumed optimal protocol determined using fluorescence measurements (Figure 3), a third animal trial was performed (Protocol C in Methods). Here the retentive $TPCS_{2a}$ was activated using red light (652 nm, 0.5 J/cm^2). This will cause a limited necrosis, which may be used to estimate the distribution of $TPCS_{2a}$ in tissue. Necrosis was present in 4 rat bladders and one sample is shown in Figure 6. Histology of the sample shows that necrotic lesions (more than 0.5 mm, black arrows) were found at the surface of the mucosal layer of the bladder wall, where $TPCS_{2a}$ was located. The, maximum necrotic thickness was measured to be around 1 mm (Figure 6, blue arrow).

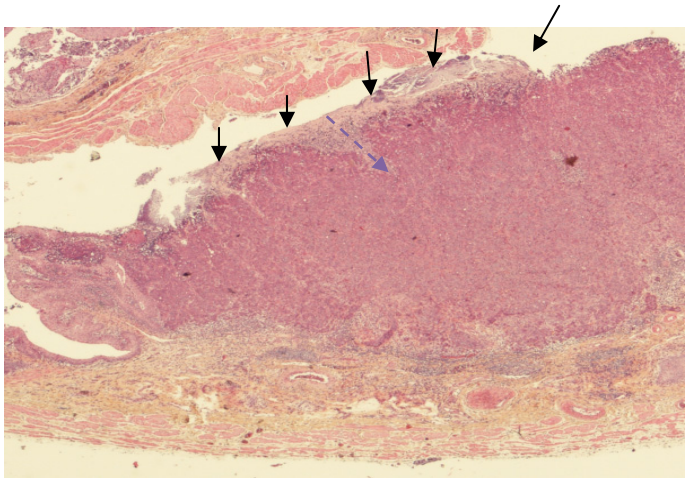

Figure 6. Histology of tumor-bearing bladder sample after intravesical illumination. The photodynamic response was mediated with $TPCS_{2a}$ (3 mg/ml), $TPCS_{2a}$-to-light interval of 24 h, and red light (652 nm, 0.5 J/cm^2). The induced necrotic area is shown to be superficial (pointed to by black arrows) and maximum necrotic thickness is about 1 mm (depth of the blue arrow). The image was taken in a Nikon Eclipse 80i microscope using a Digital Sight Camera (1×20).

Discussion

The PCI technology has been shown to be a potentially effective modality for cancer treatment [13]. However, the technology is complex with action mechanisms involving both photosensitizer, light, and drug. In particular, after choosing a photosensitizer (PS) and light source, the outcome of the PCI modality is additionally influenced by the photosensitizer dose, PS-to-light time interval, light dosimetry, and presence of molecular oxygen [36]. Thus, the evaluation of PCI efficacy requires the modality to be appropriate and optimized. Our previous *in vitro* studies have demonstrated that the AY-27 cell line is very sensitive to both $TPCS_{2a}$ concentration and light dose, and that the photodynamic cytotoxicity depends upon light activation of cellularly accumulated $TPCS_{2a}$ molecules [8]. Our present results show that the retentive $TPCS_{2a}$ concentration in tissue is proportional to the original administered doses (Figure 3A). Because most rats receiving 5 mg/ml $TPCS_{2a}$ showed similar retentive level as groups with 2 or 3 mg/ml, we decided to use 3 mg/ml as an optimal concentration of $TPCS_{2a}$ in this tumor model. It is desirable to do PCI at a low PS concentration to reduce side effects, but going below 3 mg/ml seems to give more cases with very low PS uptake (Figure 3A).

It has been supposed that urine formation may be the main reason for drug elimination in the rat bladder model after intravesical drug instillation. Other mechanisms are also known to be involved, such as removal via blood vessels and possibly molecular degradation [37]. Our results show that the concentration of $TPCS_{2a}$ in tissue reached maximum within 24 hours after intravesical instillation, followed by elimination until clearance from the tissue after 72 hours. Although fluorescence intensity was relative strong at the time interval of 4h, it was not suitable for animal experiment due to limited time for anesthesia. Thus, we decided to use 24 hours as an optimal $TPCS_{2a}$-to-light time interval in the tumor model.

Histological examination showed that the tumors grew from the mucosal layer of bladder wall in a multifocal pattern, and developed to Stage T1 or T2 in the tumor model (Figure 1). Although tumor size was different between rats, the localization and penetration of $TPCS_{2a}$ in tissue was superficial in the mucosal layer as demonstrated by both fluorescence microscopy (Figure 4 and 5) and histological identification of necrotic area (Figure 6). The depth of the necrotic area (at least 0.5 mm) is somewhat deeper than the depth measured by fluorescence (less than 0.2 mm). This may be due to photobleaching, sensitivity of the JETI PDT florometer, and high sensitivity of AY-27 cells to $TPCS_{2a}$ and light dose (our results in another submitted manuscript). However, both methods show that the

affected area is superficial.

In summary, we have established a PCI protocol for the $TPCS_{2a}$ photosensitizer for studies of a rat bladder tumor model. The optimal $TPCS_{2a}$ concentration is 3 mg/ml and optimal time for intravesical illumination for drug release (i.e. $TPCS_{2a}$-to-light interval) is 24 h after $TPCS_{2a}$ instillation. As the location and penetration of $TPCS_{2a}$ are shown to be superficial in the rat bladder tumor model, further studies on improvement of tissue penetration and optimization of light dose are required.

Financial support

This study was mainly supported by grants from the Liaison Committee between the Central Norway Regional Health Authority (HMN) and the Norwegian University of Science and Technology (NTNU). The rats used in the animal experiments were supported by grants from PCI Biotech AS (Norway). Y.B. received a two-month salary in 2009 from PCI Biotech AS (Norway) and The Research Council of Norway (NFR) for performing some of the animal experiments described here.

Acknowledgments

We would like to thank for cooperation from the experimental animal facility and the Core Facilities at the Norwegian University of Science and Technology (NTNU, Trondheim, Norway). We would thank PCI Biotech AS (Norway), not only for financial support, but also for supplying photosensitizer $TPCS_{2a}$ and light sources. We would like to thank Professor Steven H. Selman (Medical College of Ohio, Toledo, OH) who generously supplied the cell line AY-27. We thank associate Professor Anna M. Bofin (Department of Laboratory Medicine, NTNU) for histological training and experimental support, PhD candidate Linda Helander (Department of Cancer Research and Molecular Medicine, NTNU) for her important discussions and Vlada Vasovic (Department of Pathology, the Norwegian Radium Hospital) for his excellent technical assistance.

References

[1] I.K. Larsen, B. Sæther, B. Aagnes, Cancer in Norway 2010 http://www.kreftregisteret.no/no/Generelt/Publikasjoner/Cancer-in-Norway/Cancer-in-Norway-2010/, 2012.

[2] P. Bassi, BCG (Bacillus of Calmette Guerin) therapy of high-risk superficial bladder cancer, Surg Oncol 11 (2002) 77-83.

[3] G. Cheung, A. Sahai, M. Billia, P. Dasgupta, M.S. Khan, Recent advances in the diagnosis and treatment of bladder cancer, BMC Med 11 (2013) 13.

[4] U.O. Nseyo, D.L. Lamm, Therapy of superficial bladder cancer, Semin Oncol 23 (1996) 598-604.

[5] E. Schenkman, D.L. Lamm, Superficial bladder cancer therapy, ScientificWorldJournal 4 Suppl 1 (2004) 387-399.

[6] C. Bolenz, Y. Cao, M.F. Arancibia, L. Trojan, P. Alken, M.S. Michel, Intravesical mitomycin C for superficial transitional cell carcinoma, Expert Rev Anticancer Ther 6 (2006) 1273-1282.

[7] H.C. Arentsen, J. Falke, A. Hogset, E. Oosterwijk, J. Alfred Witjes, The effect of photochemical internalization of bleomycin in the treatment of urothelial carcinoma of the bladder: An in vitro study, Urol Oncol 32 (2014) 49 e41-46.

[8] Y. Baglo, L. Hagen, A. Hogset, F. Drablos, M. Otterlei, O.A. Gederaas, Enhanced efficacy of bleomycin in bladder cancer cells by photochemical internalization (mansucript ID: PP-ART-11-2013-050409 submitted 29-11-2013), Photochem Photobiol Sci (2014).

[9] Z. Shen, T. Shen, M.G. Wientjes, M.A. O'Donnell, J.L. Au, Intravesical treatments of bladder cancer: review, Pharm Res 25 (2008) 1500-1510.

[10] A. Stenzl, M. Burger, Y. Fradet, L.A. Mynderse, M.S. Soloway, J.A. Witjes, M. Kriegmair, A. Karl, Y. Shen, H.B. Grossman, Hexaminolevulinate Guided Fluorescence Cystoscopy Reduces Recurrence in Patients With Nonmuscle Invasive Bladder Cancer, The Journal of Urology 184 (2010) 1907-1914.

[11] K. Berg, P.K. Selbo, L. Prasmickaite, T.E. Tjelle, K. Sandvig, J. Moan, G. Gaudernack, O. Fodstad, S. Kjolsrud, H. Anholt, G.H. Rodal, S.K. Rodal, A. Hogset, Photochemical internalization: a novel technology for delivery of macromolecules into cytosol, Cancer Res 59 (1999) 1180-1183.

[12] T.J. Dougherty, Photodynamic therapy, Photochem Photobiol 58 (1993) 895-900.

[13] K. Berg, M. Folini, L. Prasmickaite, P.K. Selbo, A. Bonsted, B.O. Engesaeter, N. Zaffaroni, A. Weyergang, A. Dietze, G.M. Maelandsmo, E. Wagner, O.J. Norum, A. Hogset, Photochemical internalization: a new tool for drug delivery, Curr Pharm Biotechnol 8 (2007) 362-372.

[14] D.K. Adigbli, A.J. MacRobert, Photochemical internalisation: the journey from basic scientific concept to the threshold of clinical application, Curr Opin Pharmacol 12 (2012) 434-438.

[15] P.K. Selbo, A. Weyergang, A. Hogset, O.J. Norum, M.B. Berstad, M. Vikdal, K. Berg, Photochemical internalization provides time- and space-controlled endolysosomal escape of therapeutic molecules, J Control Release 148 (2010) 2-12.

[16] O.J. Norum, P.K. Selbo, A. Weyergang, K.E. Giercksky, K. Berg, Photochemical internalization (PCI) in cancer therapy: from bench towards bedside medicine, J Photochem Photobiol B 96 (2009) 83-92.

[17] M.A. D'Hallewin, L. Baert, J.P. Marijnissen, W.M. Star, Whole bladder wall photodynamic therapy

with in situ light dosimetry for carcinoma in situ of the bladder, J Urol 148 (1992) 1152-1155.

[18] D.C. Shackley, C. Whitehurst, J.V. Moore, N.J. George, C.D. Betts, N.W. Clarke, Light penetration in bladder tissue: implications for the intravesical photodynamic therapy of bladder tumours, BJU Int 86 (2000) 638-643.

[19] Z. Xiao, T.J. McCallum, K.M. Brown, G.G. Miller, S.B. Halls, I. Parney, R.B. Moore, Characterization of a novel transplantable orthotopic rat bladder transitional cell tumour model, Br J Cancer 81 (1999) 638-646.

[20] E.L. Larsen, L.L. Randeberg, O.A. Gederaas, C.J. Arum, A. Hjelde, C.M. Zhao, D. Chen, H.E. Krokan, L.O. Svaasand, Monitoring of hexyl 5-aminolevulinate-induced photodynamic therapy in rat bladder cancer by optical spectroscopy, J Biomed Opt 13 (2008) 044031.

[21] C.J. Arum, E. Anderssen, K. Tommeras, S. Lundgren, D. Chen, C.M. Zhao, Gene expression profiling and pathway analysis of superficial bladder cancer in rats, Urology 75 (2010) 742-749.

[22] S. El Khatib, S. Berrahmoune, A. Leroux, L. Bezdetnaya, F. Guillemin, M.A. D'Hallewin, A novel orthotopic bladder tumor model with predictable localization of a solitary tumor, Cancer Biol Ther 5 (2006) 1327-1331.

[23] K. Berg, S. Nordstrand, P.K. Selbo, D.T. Tran, E. Angell-Petersen, A. Hogset, Disulfonated tetraphenyl chlorin (TPCS2a), a novel photosensitizer developed for clinical utilization of photochemical internalization, Photochem Photobiol Sci 10 (2011) 1637-1651.

[24] M. Lilletvedt, H.H. Tonnesen, A. Hogset, L. Nardo, S. Kristensen, Physicochemical characterization of the photosensitizers TPCS2a and TPPS2a 1. Spectroscopic evaluation of drug--solvent interactions, Pharmazie 65 (2010) 588-595.

[25] J.T. Wang, K. Berg, A. Hogset, S.G. Bown, A.J. Macrobert, Photophysical and photobiological properties of a sulfonated chlorin photosensitiser TPCS(2a) for photochemical internalisation (PCI), Photochem Photobiol Sci 12 (2013) 519-526.

[26] S. Banfi, E. Caruso, S. Caprioli, L. Mazzagatti, G. Canti, R. Ravizza, M. Gariboldi, E. Monti, Photodynamic effects of porphyrin and chlorin photosensitizers in human colon adenocarcinoma cells, Bioorg Med Chem 12 (2004) 4853-4860.

[27] K. Berg, P.K. Selbo, A. Weyergang, A. Dietze, L. Prasmickaite, A. Bonsted, B.O. Engesaeter, E. Angell-Petersen, T. Warloe, N. Frandsen, A. Hogset, Porphyrin-related photosensitizers for cancer imaging and therapeutic applications, J Microsc 218 (2005) 133-147.

[28] ClinicalTrials.gov, Safety Study of Amphinex Based Photochemical Internalisation (PCI) of Bleomycin in Patients With Cutaneous Cancer http://clinicaltrials.gov/show/NCT00993512.

[29] ClinicalTrials.gov, A Study to Evaluate the Safety and Efficacy of PC-A11 in Patients With Recurrent Head and Neck Squamous Cell Carcinoma http://clinicaltrials.gov/ct2/show/study/NCT01606566.

[30] O.J. Norum, K.E. Giercksky, K. Berg, Photochemical internalization as an adjunct to marginal surgery in a human sarcoma model, Photochem Photobiol Sci 8 (2009) 758-762.

[31] O.J. Norum, O.S. Bruland, L. Gorunova, K. Berg, Photochemical internalization of bleomycin before external-beam radiotherapy improves locoregional control in a human sarcoma model, Int J Radiat Oncol Biol Phys 75 (2009) 878-885.

[32] M. Hakerud, Y. Waeckerle-Men, P.K. Selbo, T.M. Kundig, A. Hogset, P. Johansen, Intradermal photosensitisation facilitates stimulation of MHC class-I restricted CD8 T-cell responses of co-

administered antigen, J Control Release 174C (2013) 143-150.

[33] S.M. Cohen, J.P. Yang, J.B. Jacobs, M. Arai, S. Fukushima, G.H. Friedell, Transplantation and cell culture of rat urinary bladder carcinoma, Invest Urol 19 (1981) 136-141.

[34] Y. Baglo, M.M. Sousa, G. Slupphaug, L. Hagen, S. Havag, L. Helander, K.A. Zub, H.E. Krokan, O.A. Gederaas, Photodynamic therapy with hexyl aminolevulinate induces carbonylation, posttranslational modifications and changed expression of proteins in cell survival and cell death pathways, Photochem Photobiol Sci 10 (2011) 1137-1145.

[35] M. Lilletvedt, G. Smistad, H.H. Tonnesen, A. Hogset, S. Kristensen, Solubilization of the novel anionic amphiphilic photosensitizer TPCS 2a by nonionic Pluronic block copolymers, Eur J Pharm Sci 43 (2011) 180-187.

[36] M. Triesscheijn, P. Baas, J.H. Schellens, F.A. Stewart, Photodynamic therapy in oncology, Oncologist 11 (2006) 1034-1044.

[37] I. Grabnar, M. Bogataj, A. Belic, V. Logar, R. Karba, A. Mrhar, Kinetic model of drug distribution in the urinary bladder wall following intravesical instillation, Int J Pharm 322 (2006) 52-59.